NUREG/CR-5613

Paleoliquefaction Features Along the Atlantic Seaboard

Prepared by D. Amick, R. Gelinas, G. Maurath, R. Cannon, D. Moore, E. Billington, H. Kemppinen

Ebasco Services Incorporated

Prepared for
U.S. Nuclear Regulatory Commission

AVAILABILITY NOTICE

Availability of Reference Materials Cited in NRC Publications

Most documents cited in NRC publications will be available from one of the following sources:

1. The NRC Public Document Room, 2120 L Street, NW, Lower Level, Washington, DC 20555

2. The Superintendent of Documents, U.S. Government Printing Office, P.O. Box 37082, Washington, DC 20013-7082

3. The National Technical Information Service, Springfield, VA 22161

Although the listing that follows represents the majority of documents cited in NRC publications, it is not intended to be exhaustive.

Referenced documents available for inspection and copying for a fee from the NRC Public Document Room include NRC correspondence and internal NRC memoranda; NRC Office of Inspection and Enforcement bulletins, circulars, information notices, inspection and investigation notices; Licensee Event Reports; vendor reports and correspondence; Commission papers; and applicant and licensee documents and correspondence.

The following documents in the NUREG series are available for purchase from the GPO Sales Program: formal NRC staff and contractor reports, NRC-sponsored conference proceedings, and NRC booklets and brochures. Also available are Regulatory Guides, NRC regulations in the *Code of Federal Regulations*, and *Nuclear Regulatory Commission Issuances*.

Documents available from the National Technical Information Service include NUREG series reports and technical reports prepared by other federal agencies and reports prepared by the Atomic Energy Commission, forerunner agency to the Nuclear Regulatory Commission.

Documents available from public and special technical libraries include all open literature items, such as books, journal and periodical articles, and transactions. *Federal Register* notices, federal and state legislation, and congressional reports can usually be obtained from these libraries.

Documents such as theses, dissertations, foreign reports and translations, and non-NRC conference proceedings are available for purchase from the organization sponsoring the publication cited.

Single copies of NRC draft reports are available free, to the extent of supply, upon written request to the Office of Information Resources Management, Distribution Section, U.S. Nuclear Regulatory Commission, Washington, DC 20555.

Copies of industry codes and standards used in a substantive manner in the NRC regulatory process are maintained at the NRC Library, 7920 Norfolk Avenue, Bethesda, Maryland, and are available there for reference use by the public. Codes and standards are usually copyrighted and may be purchased from the originating organization or, if they are American National Standards, from the American National Standards Institute, 1430 Broadway, New York, NY 10018.

DISCLAIMER NOTICE

NUREG/CR-5613
RA

Paleoliquefaction Features Along the Atlantic Seaboard

Manuscript Completed: July 1990
Date Published: October 1990

Prepared by
D. Amick, R. Gelinas, G. Maurath, R. Cannon, D. Moore, E. Billington, H. Kemppinen

Ebasco Services Incorporated
2211 West Meadowview
Greensboro, NC 27407

Prepared for
Division of Engineering
Office of Nuclear Regulatory Research
U.S. Nuclear Regulatory Commission
Washington, DC 20555
NRC FIN D1682

ABSTRACT

The spacial distribution of seismically-induced liquefaction features discovered along the Atlantic seaboard suggests that during the last 2000 to 5000 years large earthquakes within the region may have been restricted exclusively to South Carolina. Paleoliquefaction evidence for six large prehistoric earthquakes was discovered there. At least five of these past events originated in the established Charleston source area - the locale of a magnitude 7+ event in 1886. Within the past two millennia large events may have occurred in coastal South Carolina about every 500 to 600 years. Despite a systematic search, no similar evidence of large prehistoric earthquakes originating outside of South Carolina was found.

EXECUTIVE SUMMARY

This document presents the results of studies carried out by Ebasco Services Incorporated for the United States Nuclear Regulatory Commission under contract NRC-04-86-117. The overall objective of this investigation was to provide information on the spacial and temporal distribution of large prehistoric earthquakes along the Atlantic Seaboard. In turn, these data could then be used in seismic hazard evaluations for the region.

Background

A review of historical seismicity occurring in the eastern United States confirms that the overall level of activity along the Atlantic Seaboard is relatively low, consistent with its intraplate tectonic setting. The Modified Mercalli intensity X Charleston S.C. earthquake of August 31, 1886 stands out as the largest seismic event to occur in this region during historical times. This earthquake resulted in approximately 60 deaths in the meizoseismal area (Dutton, 1889) and caused 5 million dollars (1886 rates) in property damage in the town of Charleston (Bolt, 1978). Its proximity to populated areas made it the most destructive U.S. earthquake of the 19th century. Although nearly identical in magnitude to the 1989 Loma Prieta earthquake which struck northern California, the M_s=7.1 (Nuttli, 1983) Charleston earthquake caused damage over a much larger area.

The potential for similar large events to occur again in Charleston or elsewhere in the eastern U.S. must be assessed to better understand long-term seismic hazard in the region. This task is especially difficult because the 1886 earthquake occurred far from a present plate boundary in a region where no comparable earthquakes had occurred during the historical record. Furthermore, there is no clear evidence of past surface faulting episodes associated with large prehistoric Charleston earthquakes. Consequently, many of the traditional recognition criteria used to assess seismic potential are absent.

Regulatory Framework

Based in part on the opinions expressed by the Atomic Energy Commission (AEC) and the United States Geological Survey (USGS) in the late 1960's and early 1970's, the U.S. Nuclear Regulatory Commission (USNRC) established the regulatory position that seismicity occurring in the Charleston, S.C. area was related to a tectonic structure(s) unique to the epicentral area of the 1886 event. For the purposes of deterministic seismic design considerations, the occurrence of similar large earthquakes along the Atlantic Seaboard outside the Charleston area was not considered a credible occurrence. However, over the past two decades, detailed investigations of the tectonics and seismicity of the southeastern U.S. have failed to conclusively identify the cause and source of the 1886 Charleston earthquake. Consequently, in 1982, the USGS clarified their earlier position on this issue and concluded that based on available data there are other areas along the Atlantic Seaboard that are characterized by tectonic features similar to those identified in the

Charleston region, thus inferring that the potential for events similar to the 1886 earthquake existed outside the Charleston, S.C. area, although with a low probability.

Because of the unresolved questions regarding the cause and source of Eastern U.S. seismicity, the USNRC is actively pursuing alternate probabilistic methods for evaluating the seismic design of critical facilities. These methods take into account the uncertainty in the causative models for large Eastern U.S. earthquakes such as the 1886 event. Critical input to these studies include the definition of seismic source areas, their maximum seismic potential, and the recurrence interval between large earthquakes.

Recent Paleoliquefaction Studies in the Charleston Area

While there was no clear evidence of surface faulting associated with the 1886 earthquake, historical accounts report that strong ground motion associated with this event resulted in the formation of numerous seismically induced liquefaction features over a 1500 square kilometer area (Dutton, 1889). Within the past six years, investigations of liquefaction features have provided significant new information regarding the long-term seismic history of the region. Gohn and others (1984), Obermeier and others (1985, 1986, and 1989), Talwani and Cox (1985), Weems and others (1986), Maurath and Amick (1988), Gelinas and others (1990), and Amick and others (1990) document the existence of liquefaction features that are interpreted to have been caused by the 1886 Charleston earthquake and several similar large prehistoric seismic events. These studies all suggest that prehistoric seismicity has occurred repeatedly within the Charleston epicentral area and that the return period between earthquakes similar to the 1886 event is longer than the historic record.

As noted by Gohn and others (1984), the confirmation that large earthquakes have occurred in the Charleston, S.C. area throughout the Holocene is consistent with the concept of a unique seismotectonic setting at Charleston. However, the results of many worldwide paleoseismic investigations have shown that sources responsible for large prehistoric earthquakes may be aseismic between large rare events. Consequently, the absence of a large damaging earthquake elsewhere along the Atlantic Seaboard over the past several hundred years does not preclude the possibility of such an occurrence in the recent geologic past or the future.

This Study

This study is a phased investigation to determine in a systematic fashion, whether or not seismically induced paleoliquefaction features such as those observed in the Charleston area are present elsewhere in young sediments of the Atlantic Coastal Plain. The discovery of similar liquefaction features in other areas could indicate that large potentially damaging earthquakes have not been restricted to the Charleston area in the recent geologic past. Conversely, if no evidence of similar liquefaction features is found, the uniqueness of the Charleston area in the context of eastern United States seismicity would tend to be confirmed.

Phase 1 of this study centered on documenting the ages and characteristics of "control" liquefaction sites and features located in the Charleston area, and identifying the criteria by which similar sites and features, which may be located elsewhere, could be identified. Phase 2 investigations built on the results of these control studies and centered on the search for seismically induced paleoliquefaction features outside the epicentral area of the 1886 Charleston earthquake.

Characterization of Control Liquefaction Sites

During Phase 1 investigations, a total of 103 probable seismically induced liquefaction sites were identified in the Charleston area. Each of these sites was located on geologic maps, county soil maps, topographic maps, and available remote sensing imagery. In addition, ground penetrating radar was tested at known liquefaction sites to determine if it could be used as a tool to locate and trace liquefaction features.

The results of Phase 1 studies indicate that the great majority of liquefaction sites located in the vicinity of the 1886 Charleston, SC earthquake occur in deposits which are either late Pleistocene or Holocene in age (4,000 to about 240,000 years old). As noted by Obermeier and others (1986), materials older than about 240,000 years were found to be significantly less susceptible to liquefaction than these younger deposits. None of the seismically induced liquefaction sites identified were found in materials older than about 700,000 years. This is probably due to decreased ground water levels in these older deposits, thicker overlying soil profiles and compaction of potential source sands due to natural aging.

Liquefaction features in the Charleston area were found to occur primarily in either beach, back-barrier, or fluvial deposits. However, beach settings were clearly the most favorable depositional environment for the generation and preservation of seismically-induced liquefaction features. Virtually all liquefaction sites for which local stratigraphic information was available were underlain by at least three meters of sand, or by at least three meters of alternating sand, silt, and clay beds. The sands were generally fine to medium grained, well-sorted with silica contents in excess of 95%. The depth to the probable source beds at these liquefaction sites was in virtually every case less than six to seven meters and the ground-water table was characteristically less than one to three meters beneath the present ground surface. Further, most of the liquefaction sites were located in soils classified as sands or silty sands, under the Unified Soil Classification System. Finally, most of the seismically induced liquefaction sites identified on the basis of historical accounts of the 1886 earthquake were located within 40 kilometers of the epicenter of this event.

These studies confirmed that the morphology of the seismically induced liquefaction features can vary significantly. While many factors must play a part in determining the morphology of a particular liquefaction feature, local stratigraphy appeared to play the dominant role. Field observations as well as theoretical considerations suggest that the thickness of the source bed, the presence or absence

of an overlying non-liquefiable cap, and the thickness and cohesiveness of the cap controlled to a great degree the type of liquefaction feature that formed.

As noted by previous investigators, the two most common seismically induced liquefaction features observed during these studies were sand-blow explosion craters and sand vents/fissures. Sand-blow explosion craters formed as a result of the explosive upward movement of pore fluids and liquefied materials and are associated with a concave upwards bowl shaped "crater". They were roughly circular to elliptical in plan view. In section, their most distinguishing characteristics were a central "feeder vent" and two separate clast zones, which form near the bottom and top of the crater as a result of differential settlement following the initial explosive excavation of the crater. This type of liquefaction feature occured almost exclusively where no significant confining layer other than a soil profile was present over liquefiable sands and where the source beds were relatively thick and loose. In the Charleston area this local stratigraphic setting was most commonly found in old beach and near-shore marine depositional environments. Significantly, this type of liquefaction feature was virtually absent in fluvial sites, where thinly bedded silts, sands and clays were common.

In addition, sand vents/fissures were also found in the Charleston area. At almost all locales where sand vents/fissures have been found, a non-liquefiable confining layer or "cap" was present over the source bed of liquefied sands. At some sites the cap appeared to have been transported short distances down slope due to a loss of friction along the boundary between the cap and the underlying sand resulting from the formation of water interlayers. During transport, the cap apparently failed under laterally directed tension, resulting in the ejection of the underlying liquefied sands into tabular fissures in the cap materials. The fissures at these sites were generally oriented normal to the direction of lateral transport. At other sand vent sites, the cap appeared to have been shattered in place due to heaving associated with elevated pore pressures within the underlying water interlayer and/or oscillatory motion between the cap and the underlying liquefied sands. At these sites the cap was often broken in polygons rather than along distinct tabular fissures. In the Charleston area, the local stratigraphic setting most commonly associated with sand vents/fissures were interbedded river terrace or back-barrier deposits. Although liquefiable these deposits were generally thinner and not as loose as materials at locales where explosion craters were found.

Other Observations

A systematic evaluation of remote sensing imagery including black and white, color and infrared photography was also completed during Phase 1. Unfortunately, no consistent recognizable expressions for either liquefaction sites associated with the 1886 earthquake or liquefaction sites associated with older, pre-historic earthquakes was found. With very few exceptions, sands vented during the 1886 earthquake at known liquefaction sites could not be identified. Furthermore, and most importantly from the point of view of finding evidence of prehistoric liquefaction events in other areas of the Atlantic Seaboard, none of the pre-1886

liquefaction structures was found to be associated with recognizable expressions on the available imagery. Low altitude aerial surveys carried out during this study also found no distinct expression associated with known liquefaction sites.

While the Phase 1 evaluation of remote sensing imagery and low altitude aerial reconnaissance studies failed to establish recognition criteria for the identification of liquefaction sites, the morphological evaluation yielded some promising results. About one third of the sites in the Charleston area were found to be associated with characteristic topographic depressions identified on 1:24,000 scale topographic maps. These features were primarily associated with historical liquefaction sites located in beach complexes and take the form of a series of small circular to elliptical depressions along the dune crests. The preferred model for the development of these features suggests that they are indicative of loose, thick sands deposits, which were especially susceptible to liquefaction, when saturated. Consequently, this distinctive morphology could possibly be used to identify areas where thick deposits of loose liquefiable sands are present and/or areas where liquefaction may have occurred in the recent geologic past. Further, field investigations also found that in existing exposures, liquefied sands were often observed to erode faster than the adjacent "host" materials, resulting in a distinctive morphologic expression.

Ground Penetrating Radar

During this study, Ground Penetrating Radar (GPR) was also tested at known liquefaction sites located in the Charleston area, to determine if this technique could be used as a reconnaissance tool in the search for paleoliquefaction features outside the Charleston area. In interbedded depositional settings where an identifiable fine grained "cap" was present over the source sands, GPR anomalies were associated with the known liquefaction features. At these sites the near surface materials were silts and clayey sands, which due to their relatively high conductivities, tend to attenuate the GPR signal. In areas where underlying sands had experienced liquefaction and moved upward resulting in the rupture or disruption of the overlying "cap" a distinctive GPR anomaly was observed. Subsequently, as an additional field test of this technique, GPR data was then collected in several areas where local conditions appeared to be right for liquefaction, but where no liquefaction features had been identified previously. Several potential liquefaction sites in the Charleston area were identified solely on the basis of this reconnaissance GPR survey. Trenches were excavated across several of these GPR anomalies and, in each trench, liquefaction features were observed.

Revised Earthquake Chronology for the Charleston Area

During the study of "control" liquefaction sites located in the Charleston area, samples of organic materials were recovered from within many liquefaction features and subsequently submitted for Carbon-14 age dating. In addition, as part of this study, published radiometric age data for Charleston liquefaction features were also compiled and evaluated. Most of these data have been reported in Obermeier and

others (1985), Talwani and Cox (1985), Weems and others (1986), Weems and others (1988) and Weems and Obermeier (1990).

Collectively the Carbon-14 dating studies conducted by previous investigators and those carried out as part of this study suggest that in addition to liquefaction resulting from the 1886 earthquake, five other earthquakes associated with liquefaction may have occurred near Charleston during Holocene times. Including the 1886 event these are referred to from youngest to oldest as liquefaction episodes **CH-1** through **CH-6**. The inferred age of each Charleston liquefaction episode is shown in Table E-1.

Episodes **CH-1**, **CH-4**, and **CH-5** are strongly supported by the available data and each was documented through the dating of several liquefaction features at two or more liquefaction sites. Episodes **CH-2**, **CH-3**, and **CH-6** are based on reliable information, but due to limited studies, to date, these episodes have been identified at only one liquefaction site located in the Charleston area.

The Search for Evidence of Other Earthquake Sources

The Phase 2 search for paleoliquefaction evidence of other large prehistoric earthquakes originating outside the Charleston area followed two paths. First, reconnaissance level investigations were conducted in the Wilmington, Delaware and Central Virginia areas. Second, a detailed, systematic search of late Quaternary beach and near-shore deposits in Virginia, North Carolina, South Carolina and Georgia was implemented.

Wilmington, Delaware and Central Virginia Search Areas: Along the Atlantic seaboard, intensity VII earthquakes have occurred at two other locales where potentially liquefiable deposits are present (Central Virginia and Wilmington, Delaware). The levels of ground motion resulting in MM intensity VII effects are generally not sufficient to generate liquefaction features (Russ, 1983). However, if the return periods between large rare events are greater than several hundred years, Charleston-like earthquakes may have occurred in these areas prior to colonization. Consequently, reconnaissance searches for paleoliquefaction evidence of prehistoric earthquakes were initiated in both of these areas.

No evidence of liquefaction was found in either the central Virginia or Wilmington, Delaware areas. However, it must be stressed that potentially liquefiable deposits are not pervasive in these areas and existing exposures are somewhat limited, especially within 40 km of the larger historical events. Further, while the results of control studies as well as the work of Obermeier and others (1986) found that beach and near-shore marine deposits are most favorable for the generation and preservation of liquefaction features, most of the potentially liquefiable deposits in the central Virginia area are fluvial in origin, and the sources of those in the Wilmington area are fluvial and estuary. Furthermore, many of the deposits closest to the historical earthquakes are recent overbank deposits that are geologically very young (probably less than several thousand years in age). Given

their age these units could not provide liquefaction data on early to mid Holocene seismicity which could have occurred prior to their deposition. The negative results of our search for liquefaction features in this area must be viewed with these limitations in mind.

Southeastern Atlantic Seaboard Search Area: A detailed search for evidence of prehistoric earthquakes was implemented along the Atlantic seaboard. This search focused on late Quaternary beach and near-shore marine deposits. These units are most similar to the deposits in which, the great majority of liquefaction features in the Charleston area have been identified. Although no large earthquakes (other than the 1886 Charleston event) have been reported along this 1000 km stretch of the Atlantic seaboard, the potential for the generation and preservation of liquefaction evidence of large prehistoric earthquakes is very high. Furthermore, the extent of exposures, such as drainage ditches, sand and gravel quarries and borrow pits, allowed for a fairly uniform search throughout this region, thus increasing the chance of discovering liquefaction features.

Investigations were completed at over 1000 potential liquefaction sites, extending from the margins of the 1886 meizoseismal area southward to the Georgia/Florida state line, and northward to Cape May, New Jersey. With the exception of the Delmarva Peninsula and Cape May areas where exposures are limited, a fairly uniform search has been completed throughout the region.

Although suitable sites were investigated throughout the region, liquefaction features were found almost exclusively in South Carolina (the lone exception discovered during this investigation is located just north of the S.C./N.C. state line). These sites were located well to the south and north of the 1886 meizoseismal area and are referred to as "outliers". At most outliers multiple liquefaction features representing two or more liquefaction episodes were identified.

Detailed studies were conducted at selected northern and southern outliers. Organic samples were collected and analyzed using radiocarbon dating techniques to determine the age of these outlying liquefaction features and to allow for comparison with the ages of paleoliquefaction episodes identified in the Charleston area. The results of radiocarbon age dating are also presented in Table E-1 for the southern and northern outliers.

Based on the ages of organic samples collected from southern outlying liquefaction sites, four liquefaction episodes may have occurred in this area during Holocene times. They are referred to from youngest to oldest as episodes **S-1** through **S-4**. All are thought to be the result of earthquakes originating in the established Charleston source area and provide independent confirmation of Charleston liquefaction episodes **CH-1, CH-2, CH-3,** and either **CH-5** or **CH-6** (Table E-1).

Based on the ages of organic samples collected from the northern outlying liquefaction sites, four liquefaction episodes may have occurred in this area during Holocene times. From youngest to oldest they are referred to as **N-1** through **N-4**.

Liquefaction episodes **N-1** and **N-2** are based on data from the northern outlying liquefaction site which is located closest to the Charleston source area. The ages of the liquefaction features discovered there correlate with, and provide independent confirmation of, Charleston liquefaction episodes **CH-2** and **CH-3**. The age of **N-4** is generally consistent with episodes **CH-5** or **CH-6**, but is only poorly constrained (Table E-1).

While liquefaction episodes **N-1**, **N-2** and **N-4** probably result from earthquakes occurring in the established Charleston source area, liquefaction episode **N-3** has no clear parallel episode in the Charleston epicentral area and the data collected to date suggest that its causative event **may** have originated at another locale. Alternately, the earthquake associated with liquefaction episode **N-3** may have originated near Charleston but it has not yet been identified in the paleoliquefaction record. Additional studies would be needed to confirm the existence of this postulated northern earthquake source.

Earthquake Return Periods and Completeness of Paleoliquefaction Record

The paleoliquefaction data suggest that the **apparent** interval between liquefaction episodes has decreased from as much as 2000 years during mid-Holocene times to about 600 years in more recent times. However, since sea level has been at or near its present level and climatic conditions have been relatively stable over the past 2000 years, the paleoliquefaction record is probably most complete for only this period. The return period between large earthquakes during this time probably is more representative of the overall seismic process acting in the area.

During the period 2000 years before present (YBP) to about 5000 YBP sea level was generally one to four meters below present levels and fluctuated widely. Consequently, the paleoliquefaction record for this time interval probably includes only those earthquakes which occurred during periodic transgressive seas and/or wet climatic periods. Further, before about 5000 YBP the climate in the southeastern United States was drier and sea level was more than four meters lower than present. Such conditions would severely reduce or eliminate the potential for liquefaction and may explain the absence of early Holocene paleoliquefaction features in the paleoliquefaction record.

Magnitudes of Prehistoric Earthquakes

Based on empirical data, the smallest earthquake which could reasonably be expected to generate significant liquefaction features is estimated to be in the magnitude range of m_b 5.8$\pm$.4. Each of the seven earthquakes postulated (**CH-1** to **CH-6**; and **N-3**) would be expected to have exceeded this threshold magnitude. The M_s 7.1 1886 earthquake (**CH-1**) generated liquefaction features over the same general area as episodes **CH-2** and **CH-3**, suggesting that these two older earthquakes were of similar magnitude. At this time, data are inconclusive regarding distribution of liquefaction features associated with older Charleston liquefaction

episodes. This is especially true given that the impact of increases and decreases in liquefaction potential due to climatic and/or other factors is not fully understood.

Implication for Long-Term Seismic Hazard

To date, no conclusive paleoliquefaction evidence of large prehistoric earthquakes originating outside of South Carolina has been found. This finding is consistent with those of Obermeier and others (1989), who concluded on the basis of crater size and number that pre-1886 shaking was strongest in the meizoseismal zone of the 1886 earthquake and is in keeping with the concept of a unique seismotectonic setting at Charleston. However, the return period for the Charleston source area is less than previously established, with large Charleston earthquakes occurring about every 600 years. In addition to the established Charleston source area, paleoseismic data suggest that one additional source within coastal South Carolina **may** have been active within the past several thousand years.

Paleoliquefaction data collected as part of this study suggests that unlike some intraplate earthquake sources, prehistoric seismicity in coastal S.C. may have behaved in a generally time-predictable manner during late Holocene times. The return period between the past four large liquefaction associated earthquakes is about 500 years. Since only about 100 years have elapsed since the 1886 event, the probability of a similar earthquake occurring within the Charleston area over the next several decades is inferred to be low.

While the potential for an earthquake large enough to produce significant liquefaction features is low, the hazard presented by smaller earthquakes both in the Charleston area and elsewhere along the Atlantic Seaboard should not be overlooked. Assuming the earthquake process behaves in a similar time-predictable manner for smaller magnitude events, and that potentially damaging events can occur independant of the rare 1886-like earthquakes, frequency-magnitude relations derived from historical data suggest that the probability of an event similar to the Modified Mercalli intensity VII 1912 Charleston-Summerville earthquake occurring during the next few decades is relatively high (greater than 60%). Although smaller than the 1886 earthquake, such an event could be in the magnitude m_b 5.0 to 6.0 range. Given the low attenuation characteristics of the region such an event would be felt throughout the southeastern U.S. and would be of engineering concern in the epicentral region.

TABLE OF CONTENTS

TABLE OF CONTENTS (Cont'd)

LIST OF TABLES

LIST OF FIGURES

LIST OF FIGURES (Cont'd)

LIST OF FIGURES (Cont'd)

LIST OF FIGURES (Cont'd)

1.0 INTRODUCTION

A review of historical seismicity occurring in the eastern United States confirms that the overall level of activity along the Atlantic Seaboard is relatively low, consistent with its intraplate tectonic setting (Figure 1.1). The Modified Mercalli (MM) intensity X Charleston S.C. earthquake of August 31, 1886 stands out as the largest seismic event to occur in this region during historical times. This earthquake resulted in approximately 60 deaths in the meizoseismal area (Dutton, 1889) and caused 5 million dollars (1886 rates) in property damage in the town of Charleston (Bolt, 1978). Its proximity to populated areas made it the most destructive U.S. earthquake in the 19th century. Although nearly identical in magnitude to the October 17th, 1989 Loma Prieta earthquake which struck northern California, this M_s=7.1 (Nuttli, 1983) earthquake caused damage over a much larger area and was felt as far north as Canada and as far west as the Mississippi River (Figure 1.2).

The potential for similar large events to occur again in Charleston or elsewhere in the eastern U.S. must be assessed to better understand long-term seismic hazard in the region. This task is especially difficult because the 1886 Charleston earthquake occurred far from a present plate boundary in a region where no comparable earthquakes had occurred during the historical record. Furthermore, there is no clear evidence in the Charleston area of past surface faulting episodes associated with large prehistoric earthquakes. Consequently, many of the traditional recognition criteria used by geologists and seismologists to assess seismic potential are absent or potentially misleading.

Over the past two decades, multidisciplinary investigations of the geology, tectonics, and seismicity of the southeastern U.S. have been carried out with the goal of understanding the cause of the 1886 Charleston earthquake. Rankin (1977) and Gohn (1983) provide overviews of some of these studies. Several widely different models have been put forward to explain seismicity in the Charleston area (for a review of these models, see Talwani, 1985 or Dewey, 1985). The cause of this event remains a subject of much debate and no geologic structure has been conclusively identified as its source.

1.1 Studies of Liquefaction in the Charleston Area

Strong ground motion associated with the 1886 event caused secondary deformation in the form of numerous sand expulsion features over a 1500 km^2 area (Figure 1.3). Over the past decade, many investigators including Cox and Talwani (1983), Cox (1984), Gohn and others (1984), Obermeier and others (1985, 1986 and 1987), Talwani and Cox (1985), Gelinas (1986), Weems and others (1986), Maurath and Amick (1988), and Amick and others (1990) have documented the existence of paleoliquefaction features preserved in the geologic record. They interpret these to have been caused by large prehistoric seismic events similar in magnitude to the 1886 earthquake.

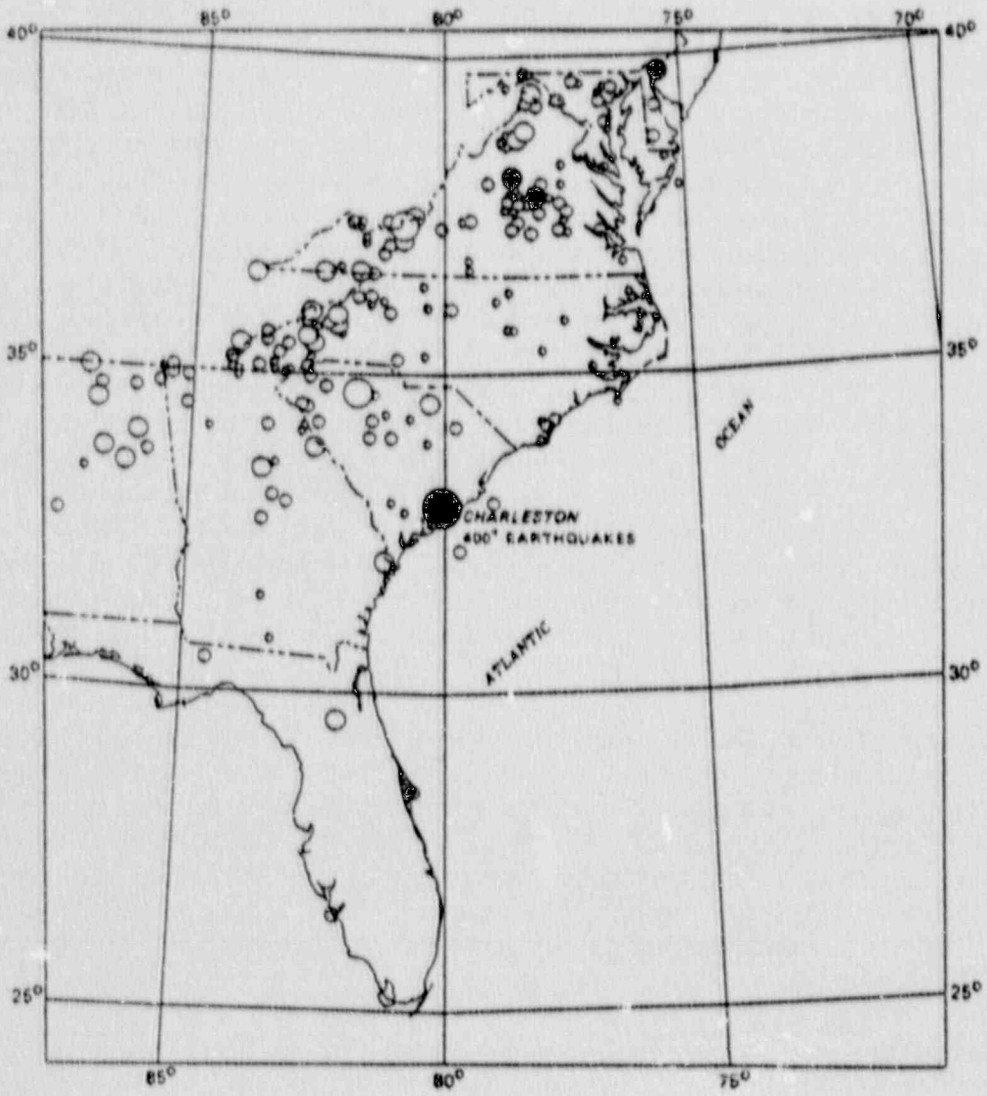

FIGURE 1.1: Distribution of historical seismicity along the Atlantic Seaboard 1754-1970. Symbols scaled to Modified Mercalli intensity with MM VII or greater events occurring in the Charleston, Central Virginia, and Wilmington, Delaware areas represented by solid circles (See discussions in Chapters 8 and 9). Modified from Bollinger (1973).

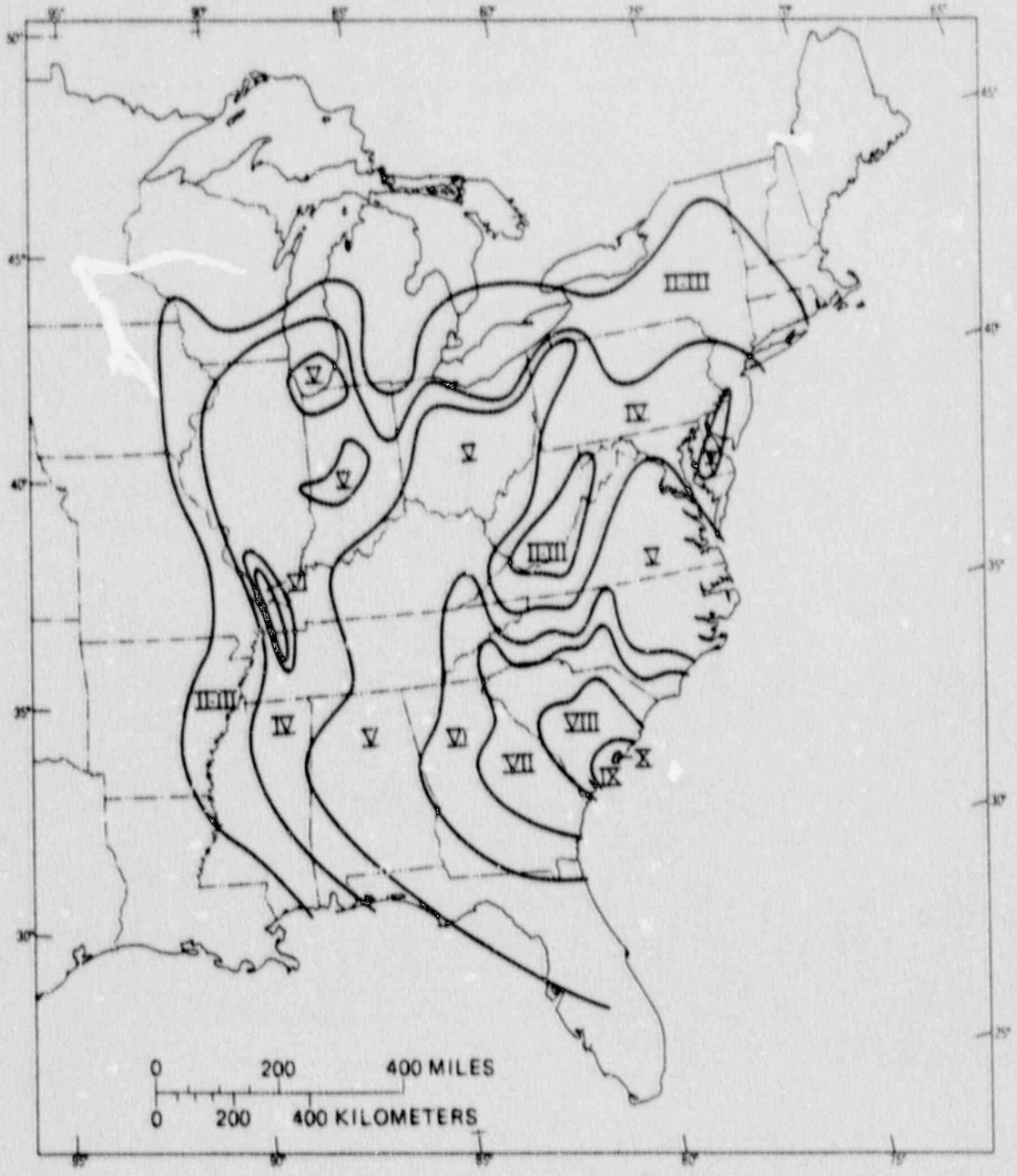

FIGURE 1.2: Isoseismal map for the 1886 Charleston, S.C. earthquake (modified from Bollinger, 1977). Modified Mercalli intensity X levels of ground motion were reported in the epicentral area. Body wave magnitude estimates range from 6.8 to 7.1 (Bollinger, 1977). Nuttli (1983) estimated its surface wave magnitude to be 7.1. Although virtually identical in magnitude to the recent Loma Prieta event, the felt area for this event was an order of magnitude greater (USGS, 1989).

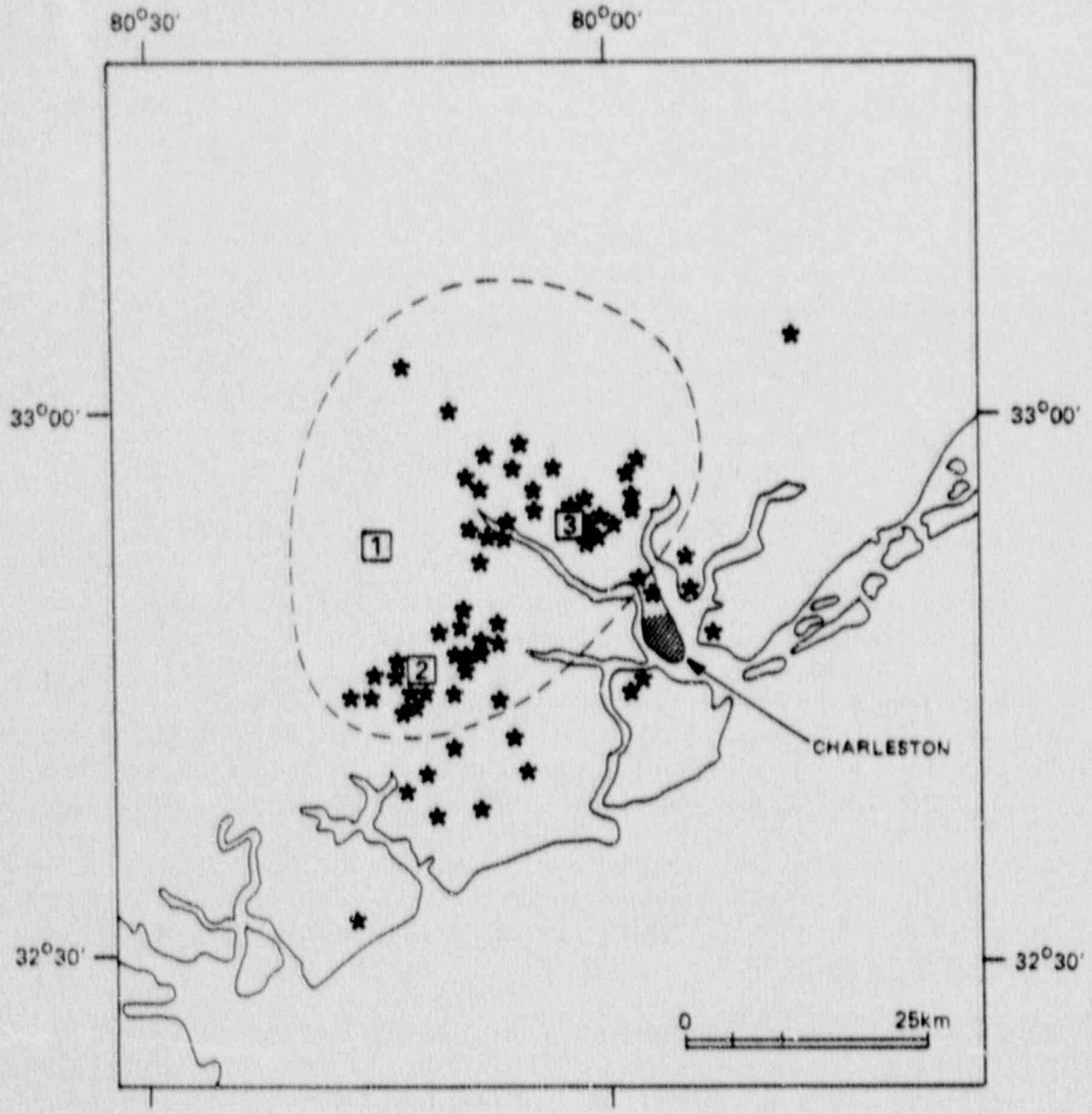

FIGURE 1.3: Distribution of liquefaction sites identified based on the detailed review of historical accounts of the 1886 earthquake. In addition to the sites shown, isolated liquefaction was reported up to about 125 km from Charleston. Primary data sources include Dutton (1889) and Peters and Herrmann (1986). Dashed line identifies the extent of the MM Intensity X meizoseismal area as defined by Bollinger (1977). Site #1 is the Warrens Crossroads locale as reported in Cox (1984). Site #2 is the Hollywood Ditch reported by Gohn and Others (1984) and Talwani and Cox (1985) and Site #3 is the Ten Mile Hill site evaluated during this study.

1.2 Implications of Paleoliquefaction Features

The occurrence of only one large earthquake in the Charleston area over the past three centuries coupled with paleoliquefaction evidence of similar large prehistoric earthquakes strongly suggest that the interval between large earthquakes in this region exceeds the historical record (e.g., Talwani and Cox, 1985). If the return periods for large earthquakes at other locations along the Atlantic seaboard are similar, the absence of large damaging earthquakes in these areas since colonization does not preclude their occurrence in the recent geologic past or in the near future.

This point is reinforced by recent studies tha: have shown that faults responsible for large prehistoric earthquakes may be aseismic between large rare events and that activity may be episodic in nature (Swan, 1990). Therefore the absence of moderate to large earthquakes during historical times and/or the lack of instrumental seismicity in a region does not in and of itself preclude the possible future occurrence of a large earthquake. However, if such events have occurred, paleoliquefaction features like those observed in the Charleston area could also have been preserved in young unconsolidated sediments in the region.

1.3 This Study

This study is designed to determine in a systematic fashion, whether or not seismically induced paleoliquefaction features such as those observed in the Charleston area are present elsewhere in young sediments of the Atlantic Coastal Plain. Initial investigations centered on documenting the characteristics of "control" liquefaction sites and features located in the Charleston area and identifying criteria to guide a regional search for similar features. This aspect of the study is presented in Chapters 2 through 7 augmented by Appendix A.

After completion of these "Control Studies", investigations focused on establishing a revised and updated chronology for large prehistoric earthquakes that have occurred in the Charleston area. This aspect of the study is presented in Chapter 8 augmented by Appendix B.

Using the results of the control studies as a guide, a systematic search for seismically induced paleoliquefaction features outside the epicentral area of the 1886 Charleston earthquake was implemented. The results of this search are presented in Chapters 9 and 10 and the evaluation of the outlying liquefaction features that were discovered during this search is reported in Chapter 11. The significance of these investigations with regard to the identification of earthquake sources and their seismic potential are described in Chapter 12. Implications with respect to long-term seismic hazard in the region are discussed in Chapter 13 and a summary of this study is presented in Chapter 14.

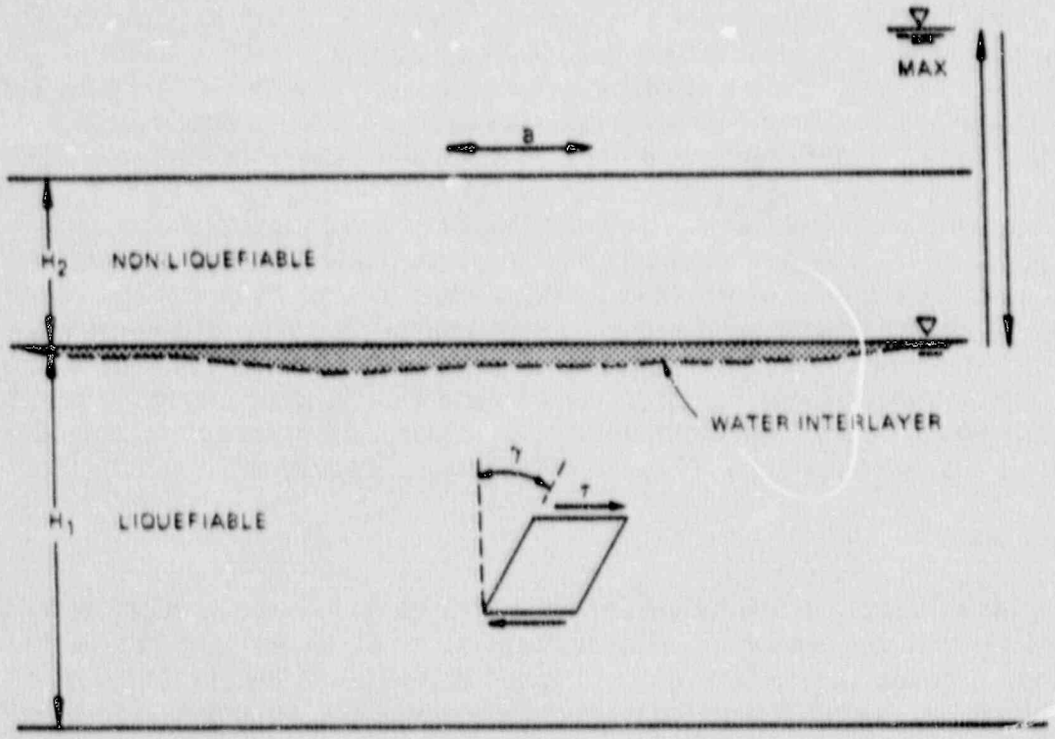

Figure 2.1: Schematic representation of the process of SIL. A liquefiable source bed (H_1) is overlain by a non-liquefiable deposit (H_2). During seismic shaking (a), cyclic shear stress (τ) develops in H_1. The resulting shear strain (γ) causes the reduction in the pore spaces within H_1. In turn, a reduction in pore spaces results in increased pore pressures followed by dewatering of H_1 and the formation of a water interlayer under H_2. As represented by the arrows on the right, the hydrostatic pressures in the water interlayer increases to levels higher than those present before the onset of seismic loading. Note that in the example shown H_2 includes only soils above the local groundwater table. However, H_2 can also include dense non-liquefiable layers present within the saturated zone. Further, if H_2 is relatively impermeable, the local potentiometric surface could actually be above the H_1/H_2 interface.

2.0 LIQUEFACTION

To provide a framework for subsequent discussions this section presents a brief review of seismically induced liquefaction. For more detailed background information on this subject the reader is referred to Youd (1973, 1977, and 1984), Castro (1975), Seed and Idriss (1982) and Dobry and others, 1982).

In simplest terms liquefaction is defined as the transformation of a granular material (usually sand) from a solid state to a fluid state due to an increase in pore-water pressure (Youd, 1973). Liquefaction does not refer to phenomena related exclusively to seismicity. For example, in some stratigraphic and/or topographic settings, a rapid increase in ground water level like that associated with flood conditions or storm surge, could cause liquefaction. The natural settling and compaction of loose saturated sands that are isolated within less permeable stratigraphic units could also cause elevated pore-water pressures which might result in liquefaction. Other non-seismic causes of liquefaction are discussed in Section 6. For clarity, liquefaction which results from cyclic shear strain caused by earthquake ground motions will be referred to as "seismically induced liquefaction" or "SIL".

2.1 Seismically Induced Liquefaction (SIL)

Based on worldwide empirical data (Youd, 1973; Seed and Idriss, 1982), loose materials are more susceptible to SIL than dense materials. High water table conditions also increase SIL potential. Further, as the intensity and duration of strong ground motion increases so does the likelihood of SIL. SIL potential decreases as the percentage of fines increases, and is generally limited to sands or silty sands.

Figure 2.1 provides a schematic representation of the process of SIL which explains many of these observations. In the generic case illustrated, a liquefiable source bed (H_1) is overlain by a non-liquefiable deposit (H_2). During seismic shaking (**a**), cyclic shear stress (τ) develops in H_1. The resulting shear strain (γ) causes the reduction in the pore spaces within the liquefiable unit. In turn, a reduction in pore spaces within H_1 results in increased pore pressures followed by dewatering. Based on laboratory experiments reported by Liu and Qiao (1984), water expelled from pore spaces within H_1 due to increased pore pressures accumulates as interlayers under the more impervious layers (at the H_1/H_2 boundary in our example). As illustrated in Figure 2.1, the hydrostatic pressure in the water interlayer increases to levels higher than those present before the onset of seismic shaking and may exceed the confining stresses.

Whether liquefied materials reach the ground surface, and whether their surface expulsion is relatively passive or explosive, depends on how fast and to what extent the level of pore pressure increases within the water interlayer. In turn, these factors are related to several important factors including: (1) the looseness and thickness of H_1 and how long it is shaken (which control how much water is expelled as a result of seismically induced shear strain); (2) the permeability of H_1 (which controls the

volume of expelled pore water and the time it takes the water to reach the H_1/H_2 interface); and (3) the thickness, cohesiveness, and permeability of H_2 (which determine whether the pore pressures building in the water interlayer are effectively contained, gradually released or build up to "explosive" levels).

2.2 Types of SIL Failure

Worldwide investigations of SIL (Seed, 1968) have led to the identification of three primary types of failure; these include: (1) quick condition failures, (2) lateral spreading landslides, and (3) flow landslides. Of these, flow landslides generally occur on relatively steep slopes, a condition uncommon in the Charleston area and elsewhere along the Atlantic seaboard, and will not be discussed further.

Quick condition SIL generally results from the compaction of thick saturated sands (H_1). Overlying H_2 deposits are often thin and made up of unsaturated loose, non-cohesive sands similar to H_1 beds. Due to the relatively high permeability and non-cohesive nature of H_2, waters expelled from within H_1 during seismic shaking gradually reach the ground surface where the over pressurized conditions are relieved in the form of sand boils and other dewatering features. In most cases, quick condition failures are not explosive and are most often described as bearing capacity failures, such as those observed following the 1964 Niigata, Japan earthquake (Seed, 1968). During this earthquake buildings sank or tilted as a result of the loose bearing capacity in underlying materials.

In contrast, lateral-spreading SIL commonly occurs in interbedded settings where H_2 deposits are fine grain, impermeable, and cohesive. Due to the characteristics of H_2 described above, waters expelled from within H_1 during seismic shaking can not easily reach the ground surface. Uplift pressures develop at the H_1/H_2 boundary and H_2 is broken into blocks and/or flow toward adjacent lower lying areas.

McCulloch and Bonilla (1970) described the flow of unconsolidated sediments during the 1964 Alaskan earthquake and noted many fissures formed parallel to streams. Lateral spreading SIL features were also observed at Van Norman Lake following the 1971 San Fernando earthquakes. They were described as surface cracks oriented parallel to the shore of the lake (Youd, 1973). During failure, the cohesive surface layer (H_2) fractured into large blocks that slid downslope on the underlying liquefied sands. Similar lateral spreading types of SIL features were also reported in studies of the New Madrid area (Obermeier, 1984).

3.0 PREVIOUS SIL INVESTIGATIONS

Historical accounts of the August 31, 1886 Charleston earthquake indicate that SIL features were widespread in the meizoseismal area (Dutton, 1889). In the weeks and months following the 1886 earthquake, Sloan (as reported in Peters and Herrmann, 1986), Dutton (1889), and to a lesser extent McGee (as reported in Peters and Herrmann, 1986) noted the location, effects, and characteristics of many SIL features. Within the past several years, investigators from the United States Geological Survey (USGS) and the University of South Carolina (USC) have conducted SIL investigations in the Charleston area. These 20th century studies found SIL features attributed to the 1886 earthquake and older SIL features, interpreted to have been caused by large prehistoric earthquakes of magnitudes similar to the 1886 event,

3.1 Historical Accounts

As reported by 19th century investigators, the 1886 event produced numerous SIL features over a 1500 km^2 area centered near Charleston (see Figure 1.3). By far the most spectacular SIL features associated with the 1886 earthquake were sand-blow explosion craters. Examples of this type of feature are shown on Figure 3.1. Typical craters within the meizoseismal area were about 0.5 to 1.5 meters deep and up to 3 to 6 meters across. The largest craters reported measured approximately 8 meters in diameter. An extensive ejection blanket of sand (up to 0.7 meters thick) extended for tens of meters outward from many features. At some sites ejected sands were found on tree limbs 6 meters above the ground surface, illustrating the explosive nature of crater development. At other locations reports suggest a much more passive development. While the 1886 mainshock occurred at night, eyewitness accounts indicate that some craters continued to emit sediment-laden waters well into the next day.

In addition to crater-like SIL features, 19th century investigators also report numerous fissures and cracks in the meizoseismal area. While some of these features were described as "dry", many emitted large volumes of water laden with sediment. Fissures as long as 600 meters were reported. Very few photographs of these features are available, perhaps because they were generally less spectacular than the sand-blow explosion craters and were found for the most part along the banks of rivers and streams and in areas of relatively dense vegetation and generally poorer access. A photograph of a large "dry" fissure located along the bank of the Ashley River is presented as Figure 3.2. This site was located near the center of the meizoseismal area of the 1886 event.

Fissures were commonly associated with a series of small craters or "craterlets" along their length. Sloan's description of such a feature follows:

> "Belt of craterlets bearing S80W. Along this ridge many dry cracks have occurred as well as long cracks connecting series of craterlets. We find extending through a field for distance of 700 ft a fissure from 8 to 14 ins in

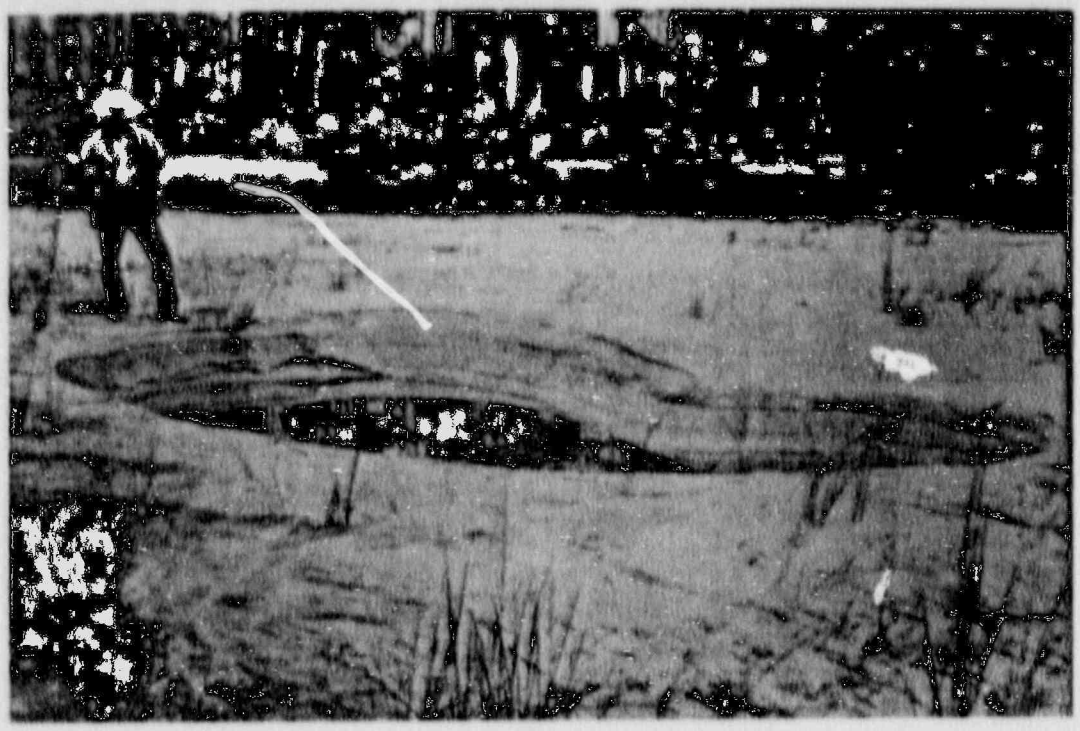

A

B

FIGURE 3.1: Examples of large sand-blow explosion crater associated with the 1886 Charleston, S.C. earthquake. These photographs were taken within a few weeks of the 1886 event and are published in Du'ton (1889). Based on Dutton's accounts, these SIL features were located near Ten Mile Hill (see Figure 1.3). Note the extensive ejection blanket of sand shown in both the foreground and background of both photographs and the dark colored clasts that have fallen into the crater in the lower photo. Within the Charleston, S.C. area this type of SIL feature is found predominantly in beach and near-shore marine deposits (see Chapter 5).

width connecting a series of large craterlets affording liberal quantities of sand. In certain flats these craterlets indicate to have submerged earth 7 inches with water." (From page 59 of Peters and Herrmann, 1986)

The evaluation of accounts provided by 19th century investigators completed as part of this study suggests that many of the fissures and associated craterlets observed following the 1886 event occurred along very gentle slopes adjacent to rivers and streams in the meizoseismal area and were similar to lateral-spreading SIL as described in Chapter 2. Again from Sloan's accounts:

"Crack extends across roadbed and cut, developing within 150 feet several series of cracks ramifying earth for 200 ft in width over a stretch of 700 ft at which point disappears in small stream. Side of hill has evidently vibrated SE & NW with an energy rupturing it from body of hill towards adjacent valley line with which the more pronounced cracks (21 inches in breadth) are parallel - having bearing N 40 E." (From page 23 of Peters and Herrmann, 1986)

"Close inspection revealed fact that there had been a vibratory movement of sufficient energy to have caused entire plastic earth included piling on each side of "draw" to bodily approach channel of stream". "Liberal indications of shortening of distance separating the banks." (From page 63 of Peters and Herrmann, 1986)

3.2 Recent Investigations

Within the past several years, investigators from the United States Geological Survey (USGS) and the University of South Carolina have conducted investigations of SIL features in the Charleston area. The first liquefaction feature found by 20th century investigators was discovered during the summer of 1983 at a SIL site historically attributed to the 1886 earthquake. This site (referred to as the Warrens Crossroads Site; see Site #1 Figure 1.3) was discovered by Cox following discussions with a property owner who knew of a sandy spot on his property where according to his older relatives an 1886 sand blow occurred (Cox, 1984). The excavation of a series of shallow trenches confirmed the presence of a SIL feature (Figure 3.3).

Subsequently, Gohn and others (1984) reported the presence of numerous SIL features in a large drainage ditch located in southern Charleston County (Site #2 Figure 1.3). This site, commonly referred to as the Hollywood Ditch Site, is located near the southwestern extent of the meizoseismal area as reported by Dutton 1889, just north of the town of Hollywood. Obermeier and others (1985), Talwani and Cox (1985), and Weems and others (1986) also reported on age dating investigations of prehistoric liquefaction features at this site. This is the first locale where clear evidence of pre-1886 liquefaction was documented (Figure 3.4). In addition to the Warrens Crossroads and Hollywood Ditch SIL sites, studies by the USGS (Obermeier and others, 1986) identified about a dozen additional SIL locales within the meizoseismal area.

FIGURE: 3.2: An example of large earth fissure associated with the 1886 Charleston earthquake. This photograph was also taken within a few weeks of the 1886 event and was published as plate XIII in Dutton (1889). Although this particular fissure was "dry" and did not appear to vent liquefied sands to the ground surface, historical accounts report that many emitted large volumes of water and sand. This type of liquefaction feature is referred to as a sand vent/fissure. Based on the review of historical accounts of the 1886 earthquake conducted as part of this study as well as the excavation of numerous liquefaction features of this type in the Charleston area, this mode of failure appears to be very similar to lateral spreading landslides as described following large earthquakes in other parts of the world. Within the Charleston, S.C. area this type of liquefaction feature is found predominantly in interbedded deposits, especially fluvial settings (see Chapter 5).

FIGURE 3.3: Sand vent/fissure excavated at the Warren Crossroads SIL site. This photograph provides a cross sectional view of a typical sand vent/fissure (see Figure 3.2 for a plan view) and illustrates the characteristic morphology associated with this type of liquefaction feature. Unlike explosion craters which are circular to elliptical in plan, sand vents/fissures are generally elongated parallel to locale topographic contours. This particular sand vent/fissure was about 5 meters long. In contrast the central vent was only about 30 centimeters wide. Note the lack of a well developed soil profile above thi feature - thought to be indicative of "younger" i.e. 1886 SIL features. Also note the extremely large clasts within the vent and the absence o a small clast zone and a bedded fill sequence.

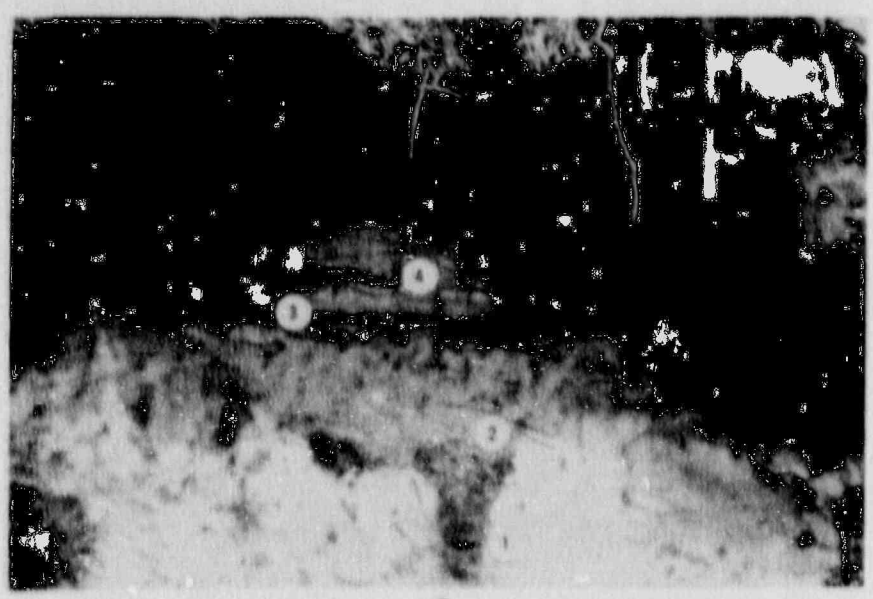

A

B

FIGURE 3.4: Sand-blow explosion craters exposed in a large drainage ditch located near Hollywood, South Carolina. A) Note the handle of a trenching shovel in the upper right for scale. This photograph provides a cross sectional view typical of sand-blow craters (see Figure 3.1 for a plan view). This feature illustrates the characteristic morphology associated with this type of liquefaction feature. The central "vent" is located in the lower center of the photograph and is identified as #1. It is filled with large clasts of the surrounding "host" sand and Bh soil materials, which have "settled" to the bottom of the bowl shaped depression. Above the zone of large clasts is a zone of clean massive sand with relatively few clasts and no distinctive flow structure (#2). Above this layer is a horizontal layer of clean white sand that contains numerous small clasts of Bh material (#3). Above this fine clast zone, extending to within about a foot of the ground surface, are relatively horizontal thin layers of sand and Bh host silty sand material, deposited subsequent to formation of the crater (#4). The well-developed Bh soil horizon above the crater suggests that this liquefaction feature was probably not associated with the 1886 earthquake. (Photograph courtesy of S. Obermeier, from Obermeier and others, 1985). B) Large sand-blow explosion crater exposed in the Hollywood Ditch. Although the crater-like morphology is obvious, many of the internal structures described above are absent.

4.0 CHARACTERIZATION OF LIQUEFACTION SITES

As a first step in establishing the control data set to guide a regional search for paleoliquefaction evidence of large prehistoric earthquakes, a comprehensive catalog of SIL sites located in the Charleston area was prepared. This catalog is based on the detailed review of historical accounts of the 1886 earthquake and 20th century field investigations. Most of the available historical information regarding SIL sites and features associated with the 1886 Charleston earthquake is from the accounts of 19th century investigators which were published primarily in Peters and Herrmann (1986) and Dutton (1889). This information was augmented by the results of recent studies conducted by investigators from the US Geological Survey, other workers from the University of South Carolina and field work conducted as part of this investigation.

4.1 Site Identification

The catalog of SIL sites evaluated includes 63 sites identified based on an evaluation of historical accounts conducted as part of this study, 8 sites identified during field activities conducted as part of this study, and 32 sites identified by other 20th century investigators as reported in Gohn and others (1984), Obermeier and others (1986, 1989), Talwani and Cox (1985), Cox (personal communication, 1987), and Talwani (personal communication, 1987).

A listing of these SIL sites is presented in Table 4-1. A map centered on the Charleston, S.C. area showing the locations of these liquefaction sites is included as Figure 4.1. For the locations of several additional liquefaction sites located outside the boundary of this figure see Figure 1 of Obermeier and others (1989).

4.2 Site Characterization

Each of these SIL sites was located on available geologic maps, county soil maps, topographic maps, and aerial photographs. In addition, as part of these studies field investigations were carried out at 37 sites. These results were used to: (1) characterize broad scale site characteristics, and (2) identify the specific characteristics of the actual SIL features.

Age of Deposits: Based on published information (primarily Colquhoun, 1965 and 1969; McCartan and others, 1984), the age of the host and liquefied materials for each SIL site estimated. The distribution of liquefaction features by age of host materials i ented on Figure 4.2. As shown, 97% of the sites occur in Holocene or mid to late Pleistocene deposits that are less than about 250,000 years in age. Older materials appear to be significantly less susceptible to liquefaction. Further, none of the 103 SIL sites identified are located in deposits that are older than about 750,000 years in age.

These findings demonstrate that in the Charleston area sediments significantly older than Holocene but younger than early Pleistocene are clearly liquefiable. This

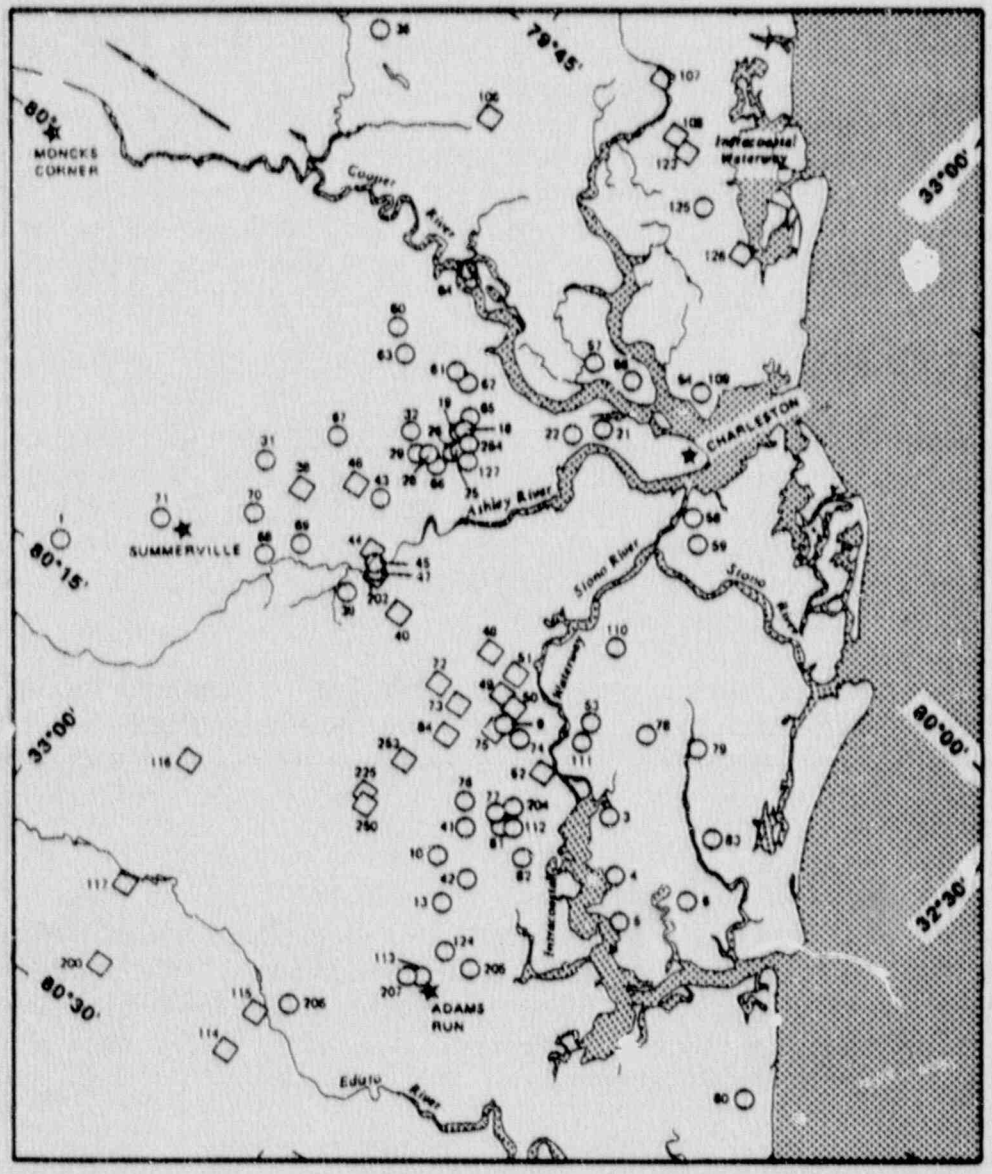

FIGURE 4.1: Map of the Charleston, S.C. area showing the location of SIL sites identified and/or compiled during this study. Numbers correspond to site identifiers presented in Table 4-1. Liquefaction sites identified based on a detailed review of historical accounts of the 1886 earthquake are labeled with single and double digit codes. Liquefaction sites identified by 20th century field studies are noted by three digit codes (100 series from Obermeier and others, 1987; 200 series from this study; 250 series from USC, including Cox and Talwani, personal communication, 1987). Circles identify those sites where the liquefaction features are best described as sand-blow explosion craters. Squares identify those sites where the liquefaction features are best described as sand vents/fissures (see Chapter 5).

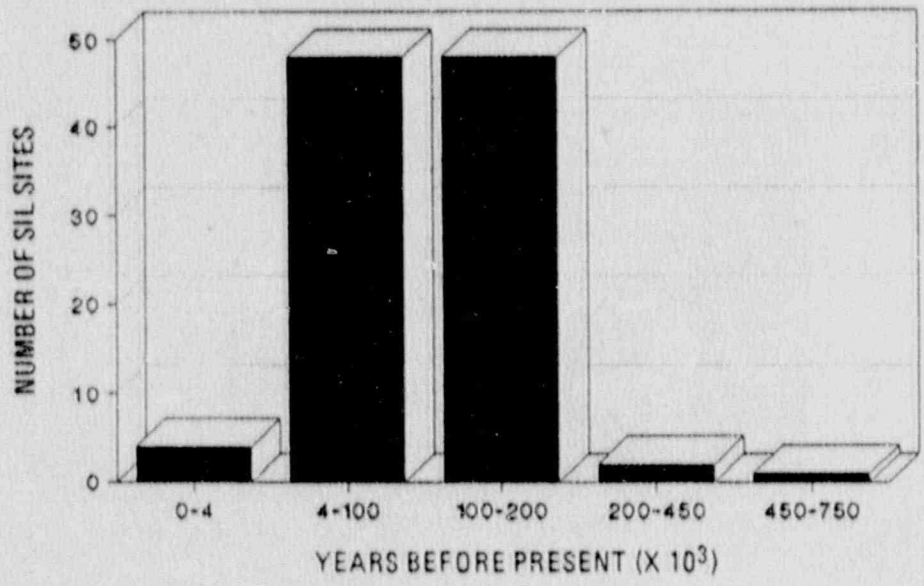

FIGURE 4.2: Distribution of liquefaction features by age of host materials. Most of the SIL sites located in the Charleston area occur in mid to late Pleistocene deposits that are less than about 250,000 years in age. Older materials appear to be significantly less susceptible to liquefaction. None of the 103 SIL sites identified are located in deposits that are older than about 750,000 years in age.

is in contrast to the results of some previous worldwide investigations that have found liquefaction to be restricted primarily to Holocene deposits (for example Youd, 1973). However, it should be noted that laboratory tests have shown the sands that have undergone liquefaction in the Charleston area are composed of at least 95% silica (Cox, 1984, Obermeier and others, 1986). Consequently, the build-up of fines due to the weathering of feldspathic materials to form clay is very limited within these deposits. A higher percentage of fines tend to decrease the liquefaction potential of sand units. The relative lack of fines due to original sediment composition may explain why these "older" mineralogically mature sediments readily experience liquefaction.

Geologic Setting: Each of the SIL sites listed in Table 4-1 was located on available geologic maps. The primary source of geologic data was McCartan and others (1984). This information was augmented by a geomorphic evaluation of each site based on 1:24,000 topographic maps. Site reconnaissance studies were conducted at one third of the sites where the scale of the available geologic maps made it impossible to determine if the site was located within a fluvial setting or in a proximate older marine deposit. Based on published geologic data, field studies, and geomorphic studies, the distribution of liquefaction sites by geologic setting is presented on Figure 4.3.

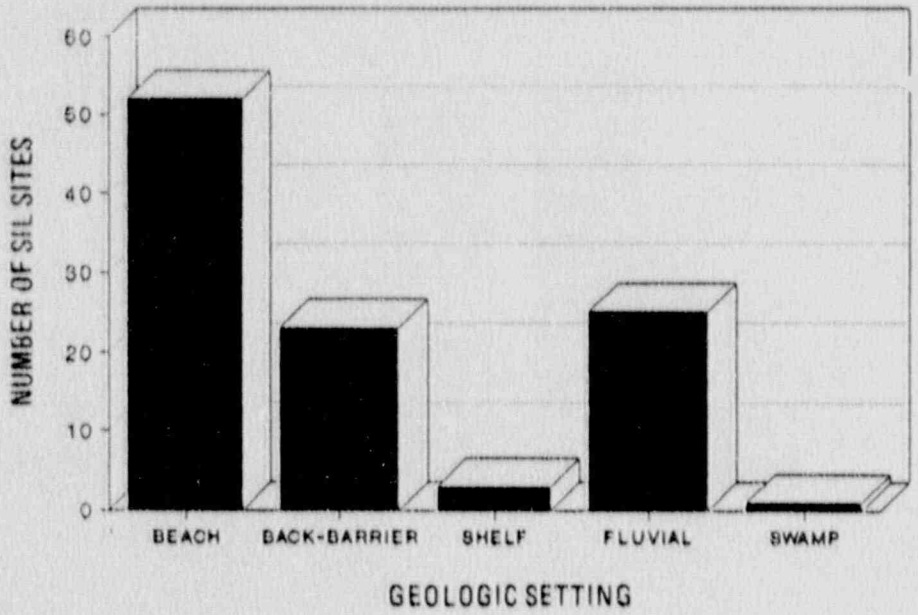

FIGURE 4.3: Distribution of liquefaction sites by geologic setting. Virtually all of the SIL sites identified in the Charleston area are located in beach, backbarrier, or fluvial settings. Of these, half of the sites occur in beach deposits. This observation is not surprising since the looseness, thickness, and relatively high permeability of these units would tend to make them especially prone to liquefaction under seismic loading.

Virtually all of the SIL sites identified in the Charleston area are located in either beach, backbarrier, or fluvial settings. Of these, half of the sites occur in beach ridge deposits. This observation is not surprising since the looseness, thickness, and relatively high permeability of these units would tend to make them especially prone to liquefaction under seismic loading. Morphologically, the beach ridges are located roughly 2-3 meters higher than adjacent land and are formed from a continuous bed of fine-grained sand that in many instances is up to 10 meters thick. A schematic of the typical beach ridge complex is presented in Figure 4.4.

Most of the remaining sites are located in either back barrier (lagoonal) or fluvial (river) deposits. Very few occur in other types of depositional environments. These findings are consistent with the work of Weems and others (1986) and Obermeier and others (1986), who found liquefaction features most commonly along the crests of Mid to Late Pleistocene barrier island complexes in the Charleston area.

Site Stratigraphy and Hydrology: To provide information regarding site stratigraphy the location of each of the SIL sites identified during this study was checked against the locations and logs for 2101 shallow auger holes and 540 water

and test wells in the coastal plain of South Carolina (Colquhoun, 1987). Twenty-six boreholes or wells were identified that are located within a few thousand feet of the identified liquefaction locales. To provide additional data regarding site stratigraphy 14 new continuous split spoon borings where drilled at SIL sites.

Based on these data, all of the SIL sites evaluated were found to be underlain by fine to medium, well-sorted sand, or by interbedded sands, silts and clays. In all but one instance the total thickness of these deposits exceeded three meters. Where clay or silt beds were present they were generally less than one to two meters thick. Conversely, the associated sand beds are typically over one to two meters thick (even thicker in borings located in mid to late Pleistocene beach deposits). The depth of what have been interpreted as probable source sands is, in virtually every instance, less than six to seven meters below the ground surface, and in many instances on the order of only 2 to 3 meters.

All SIL sites are underlain at depth by an impermeable, calcareous, phosphatic clay (Cooper Marl Formation). This formation is present throughout most of the southeastern Coastal Plain of S.C. The depth of this formation was found to vary between four to twenty meters. In all cases the Cooper Marl was below the units that have been interpreted to have experienced liquefaction, and due to its impermeable nature may have acted as a lower "boundary", tending to direct upward increased pore water pressures resulting from seismic loading.

Previous world-wide investigations of SIL have documented the requirement of saturated conditions for liquefaction to occur. In keeping with these studies, the water table was found to be relatively shallow at the great majority of liquefaction sites identified in the Charleston area. At almost all SIL sites the ground-water table is less than three meters below ground surface and probable source sands are indeed saturated. As discussed by Amick and Talwani (1990), where engineering data were available, the presence of loose sands within five meters of the ground surface was documented and the susceptibility of these materials to liquefaction under moderate levels of ground motion was confirmed using the techniques outlined by Seed and Idriss (1982) and Ishakarwa (1985).

Proximity to Historical and Instrumental Seismicity: Each of the SIL sites identified was located with respect to the two epicentra of the 1886 earthquake identified by Dutton and recent instrumentally located earthquakes greater than or equal to magnitude 3 (Tarr and others, 1981). All SIL sites identified on the basis of historical accounts lie within 40 km of an epicentra or instrumentally located magnitude 3 or greater earthquake. The great majority (over 80%) of the sites identified by current investigators are also located within 40 km of an epicentra of the 1886 earthquake or more recently recorded instrumental seismicity.

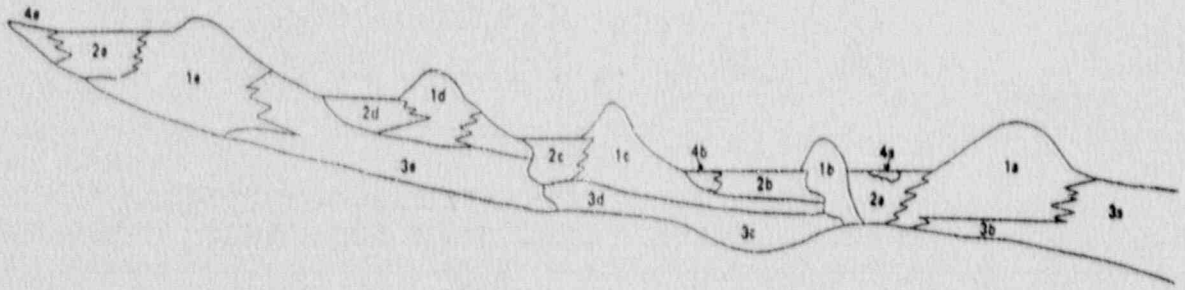

FIGURE 4.4: Schematic representation of several beach ridge systems. Morphologically the beach ridges are located higher than adjacent land and are formed from a continuous bed of medium to fine-grained sand that in many instances is up to 10 meters thick. They are identified with #1 on this figure with "a" being the youngest and "e" being the oldest. Each beach ridge represents a previous sea-level stand that was higher than present sea-levels. Backbarrier deposits (identified as 2) are located landward of each beach ridge. These include estuary deposits and overwash sands. Seaward of each beach ridge are shallow shelf deposits (identified as 3). These generally include silty and shelly sands. Flowing on or incised within the backbarrier deposits are younger fluvial units (identified as 4) which include interbedded sands, silts and clays.

Table 4.1

Listing of Seismically Induced Liquefaction Sites In The Charleston, S.C. Area.

ID	Latitude	Longitude	Primary Feature Type	Age of Event	Depositional Environment	Formation
1	[illegible].0542	80.2358	exp. crater	1886	backbarrier	Wiçomico
3	[illegible].6942	80.1747	exp. crater	1886	beach	Princess Anne
4	32.6713	80.2053	exp. crater	1886	beach	Princess Anne
5	32.6523	80.2310	exp. crater	1886	beach	Princess Anne
6	32.6250	80.1917	exp. crater	1886	shelf	Pamlico/U Talbot
9	32.7772	80.1633	exp. crater	1886	beach	Pamlico/U Talbot
10	32.7617	80.2663	exp. crater	1886	beach	Pamlico/U Talbot
13	32.7455	80.2942	exp. crater	1886	beach	Pamlico/U Talbot
18	32.8937	80.0088	exp. crater	1886	beach	Pamlico/U Talbot
19	32.8992	80.0012	exp. crater	1886	beach	Princess Anne
21	32.8303	79.9525	exp. crater	1886	beach	Princess Anne
22	32.8458	79.9680	exp. crater	1886	beach	Pamlico/U Talbot
25	32.8458	80.0245	exp. crater	1886	beach	Pamlico/U Talbot
26	32.8955	80.0263	exp. crater	1886	beach	Pamlico/U Talbot
28	32.8075	80.0372	exp. crater	1886	beach	Pamlico/U Talbot
29	32.9133	80.0420	exp. crater	1886	backbarrier	Pamlico/U Talbot
31	32.9847	80.1083	exp. crater	1886	beach	Pamlico/U Talbot
32	32.9250	80.0333	exp. crater	1886	backbarrier	Pamlico/U Talbot
36	33.0792	79.8083	exp. crater	1886	backbarrier	Pamlico/U Talbot
38	32.9583	80.1083	vent/fissure	1886	backbarrier	Pamlico/U Talbot
39	32.9000	80.1500	exp. crater	1886	fluvial	Princess Anne
40	32.8667	80.1417	vent/fissure	1886	beach	Pamlico/U Talbot
41	32.7612	80.2433	exp. crater	1886	beach	Pamlico/U Talbot
42	32.7417	80.2667	exp. crater	1886	backbarrier	Pamlico/U Talbot
43	32.9333	80.0833	vent/fissure	1886	fluvial	Princess Anne
44	32.9005	80.1158	vent/fissure	1886	beach	Pamlico/U Talbot
45	32.8947	80.1225	exp. crater	1886	backbarrier	Pamlico/U Talbot
46	32.9167	80.0833	exp. crater	1886	beach	Pamlico/U Talbot
47	32.8917	80.1263	exp. crater	1886	fluvial	Princess Anne
48	32.8072	80.1295	vent/fissure	1886	fluvial	Princess Anne
49	32.7845	80.1487	vent/fissure	1886	fluvial	Princess Anne
50	32.7820	80.1492	vent/fissure	1886	fluvial	Princess Anne
51	32.7863	80.1300	vent/fissure	1886	fluvial	Princess Anne
52	32.7412	80.1797	exp. crater	1886	beach	Princess Anne
53	32.7357	80.1250	exp. crater	1886	beach	Princess Anne
54	32.8000	79.8917	exp. crater	1886	beach	Princess Anne
56	32.8362	79.9125	exp. crater	1886	beach	Princess Anne
57	32.8583	79.9167	exp. crater	1886	beach	Princess Anne
58	32.7542	79.9667	exp. crater	1886	beach	Princess Anne
59	32.7458	79.9792	exp. crater	1886	beach	Princess Anne

Table 4.1 (cont'd)
Listing of Seismically Induced Liquefaction
Sites In The Charleston, S.C. Area.

ID	Latitude	Longitude	Primary Feature Type	Age of Event	Depositional Environment	Formation
60	32.9667	79.9750	exp. crater	1886	backbarrier	Pamlico/U Talbot
61	32.9237	79.9792	exp. crater	1886	beach	Pamlico/U Talbot
62	32.9125	79.9805	exp. crater	1886	beach	Pamlico/U Talbot
63	32.9542	79.9917	exp. crater	1886	backbarrier	Pamlico/U Talbot
64	32.9500	79.9167	exp. crater	1886	backbarrier	Pamlico/U Talbot
65	32.9000	80.0042	exp. crater	1886	beach	Pamlico/U Talbot
66	32.9000	80.0417	exp. crater	1886	beach	Pamlico/U Talbot
67	32.9583	80.0612	exp. crater	1886	backbarrier	Pamlico/U Talbot
68	32.9542	80.1612	exp. crater	1886	backbarrier	Princess Anne
69	32.9388	80.1417	exp. crater	1886	backbarrier	Princess Anne
70	32.9722	80.1417	exp. crater	1886	backbarrier	Pamlico/U Talbot
71	33.0125	80.1833	exp. crater	1886	backbarrier	Wiçomico
72	32.8222	80.1667	vent/fissure	1886	fluvial	Princess Anne
73	32.8069	80.1722	vent/fissure	1886	fluvial	Princess Anne
74	32.7667	80.1667	exp. crater	1886	shelf	Pamlico/U Talbot
75	32.7778	80.1722	vent/fissure	1886	fluvial	Princess Anne
76	32.7708	80.2250	exp. crater	1886	beach	Pamlico/U Talbot
77	32.7500	80.2208	exp. crater	1886	beach	Pamlico/U Talbot
78	32.7042	80.1112	exp. crater	1886	beach	Princess Anne
79	32.6750	80.1000	exp. crater	1886	beach	Princess Anne
80	32.5278	80.2833	exp. crater	1886	beach	Princess Anne
81	32.7417	80.2250	exp. crater	1886	beach	Pamlico/U Talbot
82	32.7222	80.2333	exp. crater	1886	backbarrier	Princess Anne
83	32.6333	80.1458	exp. crater	1886	beach	Princess Anne
84	32.8008	80.1953	vent/fissure	1886	fluvial	Princess Anne
100	33.7438	78.9188	exp. crater	pre-1886	beach	Princess Anne
101	33.4523	79.2243	exp. crater	pre-1886	backbarrier	Pamlico/U Talbot
102	33.4342	79.4430	exp. crater	pre-1886 and 1886	beach	Talbot
103	33.2438	78.4050	vent/fissure	1886	fluvial	Pamlico/U Talbot
104	33.0705	79.5245	vent/fissure	----	beach	Princess Anne
105	32.9967	79.6367	vent/fissure	pre-1886	beach	Princess Anne
106	32.9967	79.8183	vent/fissure	----	backbarrier	Talbot
107	32.8983	79.7558	vent/fissure	----	fluvial	Princess Anne
108	32.8983	79.7558	vent/fissure	----	fluvial	Princess Anne
109	32.8017	79.8917	exp. crater	1886	beach	Princess Anne
110	32.7517	80.0750	exp. crater	1886	beach	Princess Anne
111	32.7383	80.1433	vent/fissure	----	fluvial	Princess Anne
112	32.7417	80.2214	exp. crater	pre-1886 and 1886	beach	Pamlico/U Talbot
113	32.7333	80.3450	exp. crater	1886	beach	Pamlico/U Talbot
114	32.8000	80.4650	vent/fissure	pre-1886	fluvial	Pamlico/U Talbot
115	32.8000	80.4317	vent/fissure	pre-1886	backbarrier	Holocene
116	32.9200	80.3117	vent/fissure	pre-1886 and 1886	swamp	Holocene
117	32.9092	80.4105	vent/fissure	1886	fluvial	Holocene
118	33.0412	80.4513	vent/fissure	----	fluvial	Holocene

Table 4.1 (cont'd)
Listing of Seismically Induced Liquefaction
Sites In The Charleston, S.C. Area.

ID	Latitude	Longitude	Primary Feature Type	Age of Event	Depositional Environment	Formation
119	33.0945	80.6035	vent/fissure	1886	fluvial	Princess Anne
120	33.1300	80.7313	vent/fissure	1886	fluvial	Princess Anne
121	33.2470	80.8263	vent/fissure	1886	fluvial	Princess Anne
122	32.2375	80.8603	exp. crater	pre-1886	beach	Princess Anne
123	32.8908	79.7583	vent/fissure	----	backbarrier	Princess Anne
124	32.7317	80.3217	exp. crater	1886	beach	Pamlico/U Talbot
125	32.8633	79.7850	exp. crater	1886	beach	Princess Anne
126	32.8278	79.7945	vent/fissure	1886	beach	Princess Anne
127	32.8900	80.0250	exp. crater	1886	beach	Pamlico/U Talbot
200	32.8908	80.4672	vent	----	fluvial	Princess Anne
202	32.8930	80.1305	vent/fissure	----	fluvial	Pamlico/U Talbot
204	32.7472	80.2105	exp. crater	1886	shelf	Pamlico/U Talbot
205	32.7145	80.3222	exp. crater	1886	beach	Pamlico/U Talbot
206	32.7886	80.4147	vent/fissure	----	backbarrier	Princess Anne
207	32.7422	80.3514	exp. crater	1886	beach	Pamlico/U Talbot
250	32.8220	80.2662	vent/fissure	1886	backbarrier	Pamlico/U Talbot
253	32.8153	80.2242	undefined	----	beach	Pamlico/U Talbot
254	32.8953	80.0110	exp. crater	1886	beach	Princess Anne
255	32.8217	80.2637	undefined	----	backbarrier	Pamlico/U Talbot

Note: See explanation to Figure 4.1 for key to site identification numbers.

Numbers correspond to site identifiers presented on Figure 4-1. Liquefaction sites identified based on a detailed review of historical accounts of the 1886 earthquake are labeled with single and double digit codes. Liquefaction sites identified by 20th century field studies are noted by three digit codes (100 series from Obermeier and others, 1987; 200 series from this study; 250 series from USC, including Cox and Talwani, personal communication, 1987).

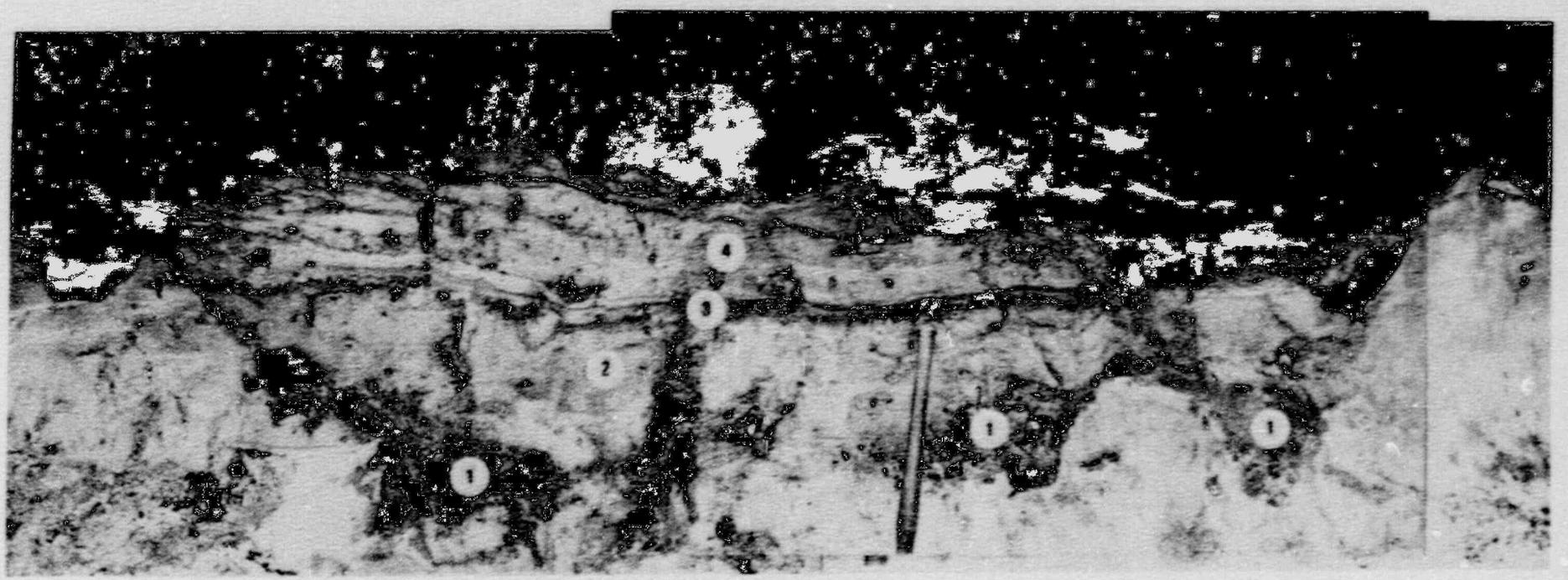

FIGURE 5.1: Cross section of large sand-blow explosion crater discovered during control investigations in the Charleston area (note handle of trenching shovel in right center for scale). This feature is located within several thousand feet of the 1886 crater shown in Figure 3.1 and exhibits the four main characteristics of sand-blow explosion craters discussed by Gohn and others [8]. Three vents or feeder dikes are noted at the base of this feature. They are filled with large clasts of Bh soil. The large clast zones are overlain by a zone of sand which contains scattered clasts and no distinctive flow structure. Above this is a dark subhorizontal layer, approximately 15 cm thick that contains numerous small clasts of Bh material. Above the fine clast zone are shallow dipping thin layers of sand, Bh material, and forest debris deposited subsequent to formation of the crater. Radiocarbon dates of bark and charcoal recovered from the bedded sequence confirm a pre-1886 origin.

5.0 MORPHOLOGY OF LIQUEFACTION FEATURES

In addition to identifying the characteristics of SIL sites located in the Charleston area, the morphology of SIL features also were evaluated. As discussed briefly in Chapter 3, accounts of 19th century investigators suggest two primary types of SIL features. These are referred to as sand-blow explosion craters and sand-vents/fissures. This generally follows the terminology of "explosion craters" and "sand vents" proposed by Obermeier and others (1986).

5.1 Sand-Blow Explosion Craters

Based on historical accounts, the most common SIL features associated with the 1886 earthquake were sand-blow explosion craters (Figure 3.1). Figure 5.1 presents a sectional view of a pre-1886 sand-blow explosion crater discovered during this investigation which is located in the same general area as the 1886 features shown in Figure 3.1.

Following the onset of seismic loading and the development of a water interlayer, four sequential phases have been identified in the development of sand-blow explosion craters: (A) an explosive phase, (B) a flowage phase, (C) a collapse phase, and (D) a filling phase. These were first discussed by Gohn and others (1984) and are based on historical accounts and the internal morphology of exhumed features. This progressive development of a sand-blow explosion crater is illustrated in Figure 5.2A through 5.2D. As shown, two distinct well sorted clast zones are commonly found: (1) a large clast zone near the base of the crater, and (2) a small clast zone located near the top of the crater. Clasts within the large clast zone, are generally 5 to 20 cm in size, and are overlain by a zone of massive to graded sand in which there are relatively few clasts. Above the layer of sands, is the small clast zone which is composed of a horizontal layer of sand containing numerous small (usually less than 2-5 cm in size) clasts. These clasts are usually derived from the original soil profile and often include materials from the A, B, and Bh horizons. Small scale normal faults often cut crater fill materials. Above the fine clast zone, extending to the surface, are thin horizontal to near horizontal layers of sand and silty sand material, deposited subsequent to formation of the sand blow.

It should be noted that Figure 5.1 presents an especially well preserved feature and Figure 5.2 presents an idealized example of a sand-blow explosion crater. Very rarely are all the features described above and illustrated in those figures preserved. For example, while a central vent is shown, this feature is small in cross sectional area when compared to the explosive crater and only rarely were they exposed in near vertical excavations. Most commonly a cross section of the bowl shaped section of the crater was all that could be viewed in trench walls. Further, in many pre-1886 craters bioturbation and weathering associated with soil development had masked or destroyed the uppermost features.

Sand-blow explosion craters were found primarily in beach deposits, and are notably absent in fluvial settings (Figure 5.3). Further, at many of the sand-blow

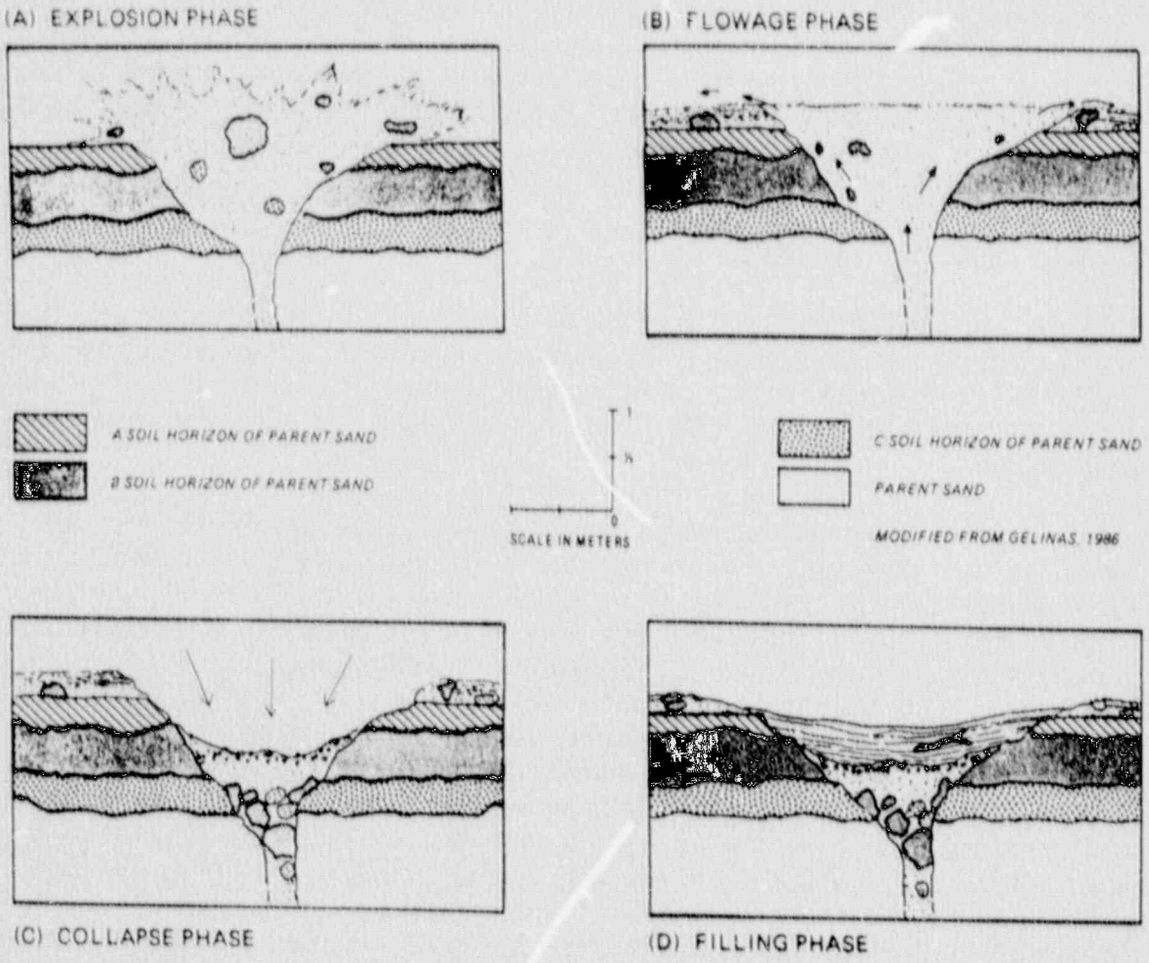

FIGURE 5.2: Schematic representatiot. of the phases in the development of a sand-blow explosion crater proposed by Gohn and others (1984). (A) Explosive Phase - Cyclic seismic loading results in the reduction of void spaces and an associated increase in pore pressures. A water interlayer forms in parent sand with pore pressures great enough to explode and excavate a crater. (B) Flowage Phase - Flow of sand-laden waters continues after ground motion has ceased, and stops only when the pore pressure of the source sands equals the confining pressure. (C) Collapse Phase - Collapse begins when pore-water pressures decrease to nearly the confining pressure of the source sands. During this phase, clasts settle according to size and density, resulting in clast segregation into two zones (the large clast zone near the bottom of the crater and within the central vent and the small clasts zone near the top of the crater). As pore-pressures continue to decrease, upward transport of fine grained material stops and the crater begins to collapse. At this time small-scale dewatering structures may develop as well as local gravitational faulting along the sides of the crater. (D) Filling Phase - Filling of the crater probably takes place in the days, weeks and months following the earthquake, as materials from the crater rim, due to sedimentary and eolian processes eventually fill the crater (modified with permission from Gelinas, 1986).

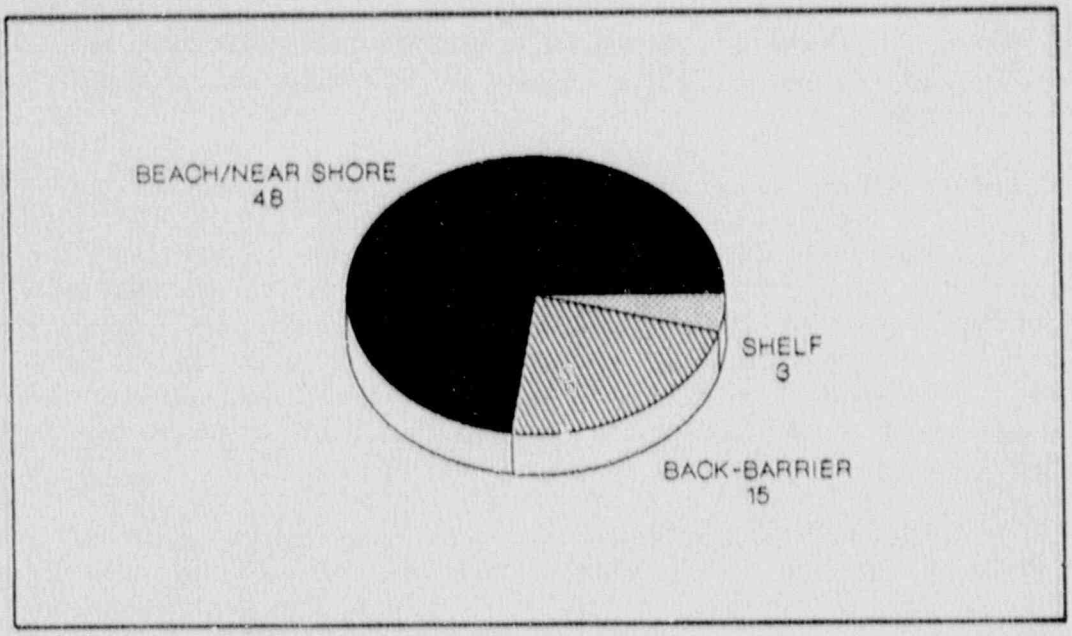

FIGURE 5.3: Distribution of sand-blow explosion craters by depositional environment. They are found primarily in beach deposits, and are notably absent in fluvial settings. The explosive nature of the sand-blow explosion craters and their presence almost exclusively in mid to late Pleistocene beach and near-shore marine deposits is probably due to several factors. Foremost is the fact that mid to late Pleistocene beach deposits (acting as H_1 in Figure 2.1) are thick, loose and permeable.

---

explosion crater sites, especially the beach and near-shore marine locales, no confining layer of non-liquefiable material was present other than unsaturated sands within the soil profile.

The explosive nature of the sand-blow explosion craters and their presence almost exclusively in beach ridge and near-shore marine deposits is probably due to several factors. First, the beach deposits (acting as H_1 in Figure 2.1) are thick, very loose, and permeable. Consequently, the water interlayer which forms during and just after seismic loading can develop very high pressures. Second, based on these studies, the depth to source sands (H_1) in the Charleston area is often only 2 meters and in virtually every locale less than 7 meters. Such a shallow source surely contributes to their explosive nature. Another factor that may contribute is the presence of an impermeable marl below the source bed. This unit may act as a boundary and tend to deflect or channel elevated pore-water pressures to the surface. Further, other than non-cohesive unsaturated sands within the local soil profile, no confining cap is present to inhibit the water interface from reaching the ground surface. However, the much lower permeability of the weathered sands

within the soil profile may prevent the gradual release of elevated pore pressures within the water interlayer and allow them to continue to build until they "explode" to the surface.

5.2 Sand-Vents/Fissures

As previously discussed in Chapter 3, 19th century investigations also report numerous fissures and cracks in the meizoseismal area of the 1886 earthquake. Based on a review of historical accounts, as well as recent field investigations, this type of liquefaction primarily occurred adjacent to rivers and streams in the meizoseismal area. A photograph of a large "dry" fissure located along the bank of the Ashley River was presented previously as Figure 3.2. In this study, this type of liquefaction feature is referred to as a "sand-vent/fissure".

The Warrens Crossroads liquefaction locale described by Cox (1984) is a good example of this type of SIL feature which resulted from the 1886 Charleston earthquake (previously shown in Figure 3.3). It is an elongated fissure five meters in length but less than one meter wide. The orientation of the fissure is generally normal to the local downslope direction, similar to those described in historical accounts of the 1886 event.

At virtually all liquefaction locales where sand-vents/fissures have been found and excavated a cohesive, finer grained, non-liquefiable confining layer or "cap" is present over the source bed of liquefied sands. At some sites the cap appears to have been transported short distances down slope, consistent with a lateral spreading model for formation. During transport, the cap apparently fails under laterally directed tension, resulting in the ejection of the underlying liquefied sands through resulting tabular vent in the cap materials. The long axis of the sand-vents/fissures at these sites are generally oriented normal to the direction of lateral transport.

Several other examples of this type of SIL feature are presented in Figure 5.4. When clasts occur within (H_2) vents/fissures, they are generally large, unsorted, and consist of the fine grained "cap". In contrast to sand-blow explosion craters, small clasts and extensive internal flow structures are generally absent. In addition, small scale structures commonly observed in sand-blow explosion craters and thought to result from compaction associated with dewatering within the crater are also generally absent.

Based on laboratory studies (Chapter 2) and their internal morphology, four sequential phases have been postulated in the development of sand vent/fissure features (Figure 5.5). They include: (A) the development of a water interlayer, (B) lateral flowage, (C) confining cap rupture, and (D) sand extrusion. During cyclic seismic loading pore-water pressures increase in the underlying sand bed causing liquefaction and the development of a water interlayer at the base of the overlying cap. At the contact between the water interlayer and the overlying non-liquefied materials (H_2), pore pressures increase to the point where the non-liquefied cap begins to move laterally in response to local gravitation forces. As the cap is

transported, it begins to break apart, resulting in the formation of tension fractures that are filled by the underlying liquefied sands. As pore-water pressures decrease, the coefficient of friction at the sand/cap boundary increases and lateral spreading ceases. Although downslope mass transport has stopped, the expulsion of sands may continue.

In some cases an infilling phase is also represented in the geologic record. However, when present it is generally much thinner that at sand-blow crater locales, suggesting that the depression at the ground surface resulting from this type of SIL feature is generally shallower. Consequently, the chances for the accumulation of datable organic materials within these types of SIL is greatly reduced.

Although the data are somewhat limited, vents/fissures are, in general, more closely spaced where the cap material is thinner (on the order of several tens of centimeters). At these SIL sites, failure may be more the result of the heaving of the cap due to uplift pressures in the water interlayer than lateral transport. After cap rupture, blocks of soil and cap material rotate and sink as the underlying liquefied sands are extruded onto the ground surface. Further, at these sites the cap is often observed to be broken into polygonal shapes. In plan view, the ejected sands would be expected to coalesce, forming a continuous ejection blanket. In cross section, massive sands with isolated, free-floating polygonal blocks of the cap materials are often observed (Figure 5.6).

At SIL sites where the cap is on the order of a meter or more, typically fewer vents/fissures were observed. In these areas large, monolithic blocks of cap material were transported downslope. In plan view, thicker cap areas would be expected to have ejected sands which form a long, narrow strip. In cross section, thick cap areas are represented by mostly intact confining cap, with only occasional and widely spaced sand vents/fissures. However, unfilled fractures throughout the cap which are thought to be the result of heaving and/or differential oscillatory motion between H_2 (the cap) and H_1 (the underlying liquefied unit) were often observed.

Historical accounts of the 1886 event may provide insight regarding the mechanism responsible for the formation of sand vent/fissure features and the wide variations observed in their morphology. Two examples of Sloan's description of such features follow:

> "We find extending through a field for distance of 700 feet a fissure from 8 to 14 inches in width connecting a series of large craterlets affording liberal quantities of sand." (From page 59 of Peters and Herrmann, 1986)

> "On hillside sloping 30 feet within 400 ft. (where we find valley line indicated by small stream) a two inch crack crosses the roadbed, developing within 150 ft into a perfect network of cracks rupturing the earth over an area 700 ft long with an average breadth of 125 ft into a series of large Earth prisms

separated by fissures varying from a line to 21 inches in breadth, the general direction being parallel to adjacent valley line N40E: which in diverging more to East is entered by belt of cracks which then ceases. The vibration has evidently operated NW-SE rupturing side of hill from body of hill towards valley line." (From page 57 of Peters and Herrmann, 1986)

The first quote probably describes a lateral spreading SIL failure. The second quote also suggests a component of lateral spreading. However, the broad zone of deformation most probably was associated with heaving and associated fracturing due to excessive uplift pressures at the H_1/H_2 interface. Excavations within the materials described above would find broken H_2 (cap) materials surrounded or within mobilized sands. The internal structure of the associated flow mass would very likely resemble the morphology observed at numerous SIL sites,(e.g. at the Warren's Crossroads Site) especially where the cap materials are especially cohesive and relatively thin.

Sand-vents/fissures were noted to occur almost exclusively where a finer grained cohesive confining unit (H_2) lies above liquefiable sands (H_1). As illustrated on Figure 5.7, within the Charleston area this local stratigraphy is most commonly found within backbarrier marine sediments and in interbedded fluvial deposits. This type of liquefaction feature was rare in beach settings, except where a thick soil profile or claypan had developed over the H_1 sand. Their less explosive origin was probably due to the thinner source beds which characterize these depositional environments (which result in less of a build-up in pore pressures within the water interlayer), and the cohesive nature of the overlying cap.

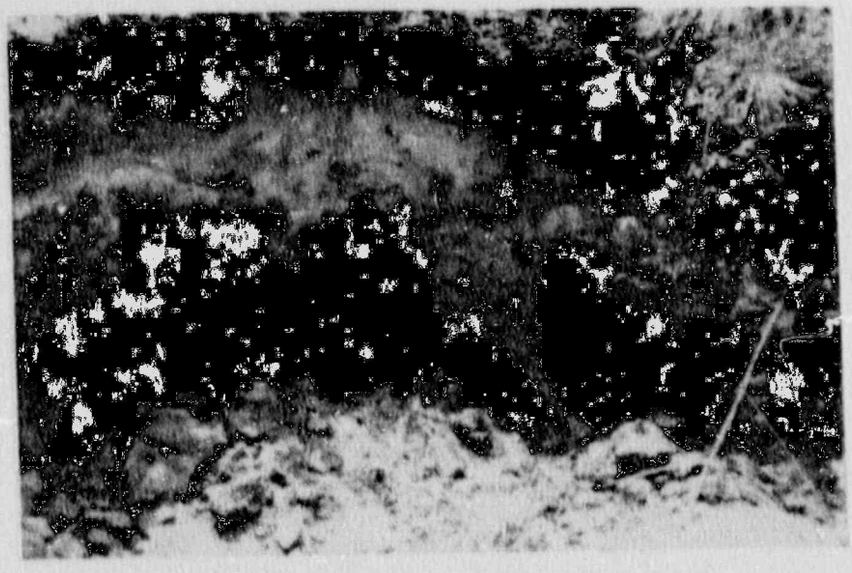

A

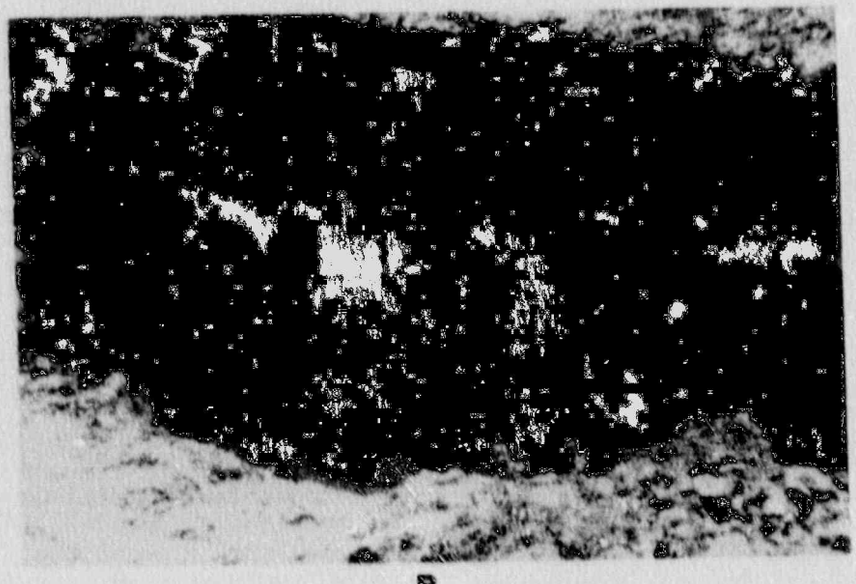

B

FIGURE 5.4: Examples of sand vent/fissure features located on the floodplain of the Edisto river. The Edisto river is located several hundred meters to the east of this site (left side of these photographs). Topography dips gently, approximately 0.07 degrees, towards the river. At this site a layer of gray silty clay approximately 1 m thick acts as H_2 overlying H_1 (a light colored poorly sorted sand). Based on vent orientation and morphology, it is postulated that the confining layer ruptured along fissures parallel to the Edisto river and moved laterally down gradient towards the river as a result of seismic loading. The underlying liquefied sand was simultaneously injected into these fissures aiding lateral spreading.

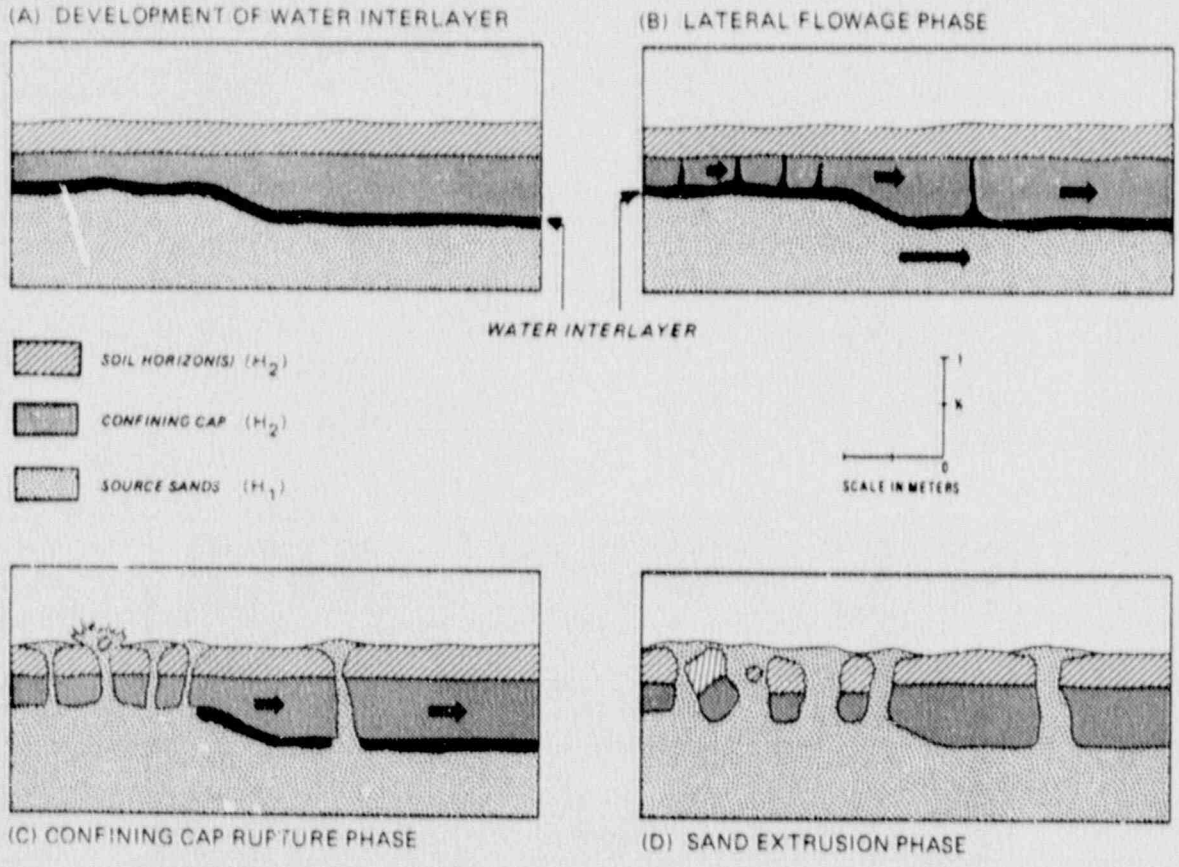

FIGURE 5.5: Schematic representation of the phases in the development of a sand vent/fissure. (A) Development of Water Interlayer - Due to cyclic shear strain and dewatering, a water interlayer forms under a more impervious confining cap. (B) Lateral Flowage Phase - With the liquefaction of underlying sands and the development of a water interlayer, the friction at the contact between H_1 and H_2 is reduced to the point where the non-liquefied cap begins to move laterally in response to local gravitational forces. (C) Confining Cap Rupture Phase - As the cap (H_2) is transported, it begins to break apart, resulting in the formation of tension fractures that are filled by the underlying liquefied sands. Sands begin to vent to the ground surface. As shown in general, vents/fissures are more closely spaced where the cap material is thinner and heaving contributes significantly to the break-up. Where the confining cap is thicker typically fewer vents/fissures are observed. (D) Sand Extrusion Phase - Sands vent to ground surface in greater quantities. With the venting of the sands, pore-water pressures decrease, the coefficient of friction at the sand/cap boundary increases and lateral spreading ceases. Although downslope mass transport has stopped, flow of sand-laden waters continues until the pore pressure of source sands equals the confining pressure.

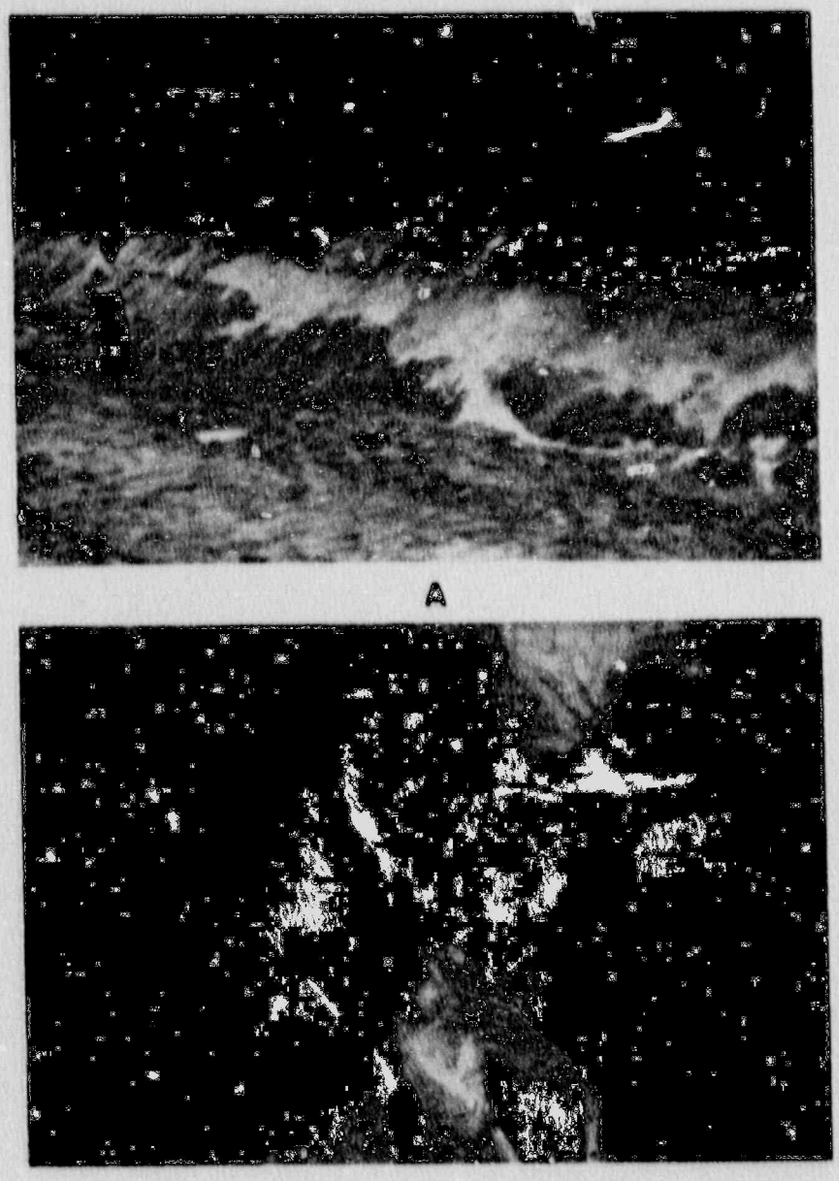

FIGURE 5.6: A) At some SIL sites, failure may be more the result of the heaving of the cap due to uplift pressures in the water interlayer than lateral transport. As the cap ruptures, blocks of soil and cap material rotate and sink as the underlying liquefied sands are extruded onto the ground surface. Further, at these sites the cap is often observed to be broken into polygonal shapes. B) Shows an example of unfilled fractures in the cap which are often found at this type of SIL site. These are thought to be the result of heaving and/or differential oscillatory motion between H_2 (the cap) and H_1 (the underlying liquefied unit).

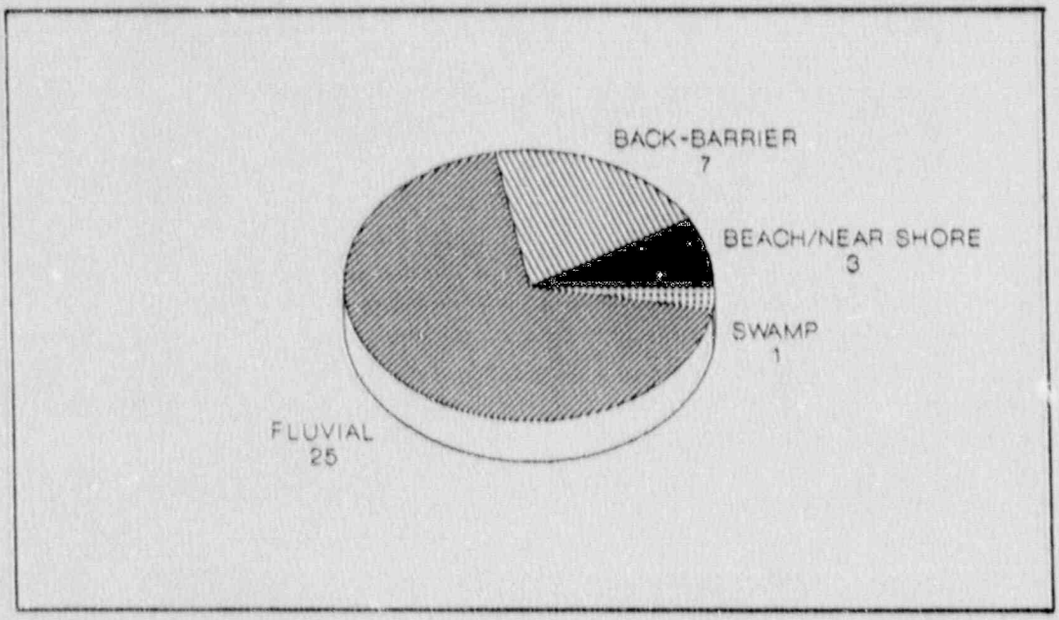

FIGURE 5.7: Distribution of sand vent/fissure features by depositional environment. They are noted to occur almost exclusively where a finer grained cohesive confining unit (H_2) lies above liquefiable sands (H_1). This local stratigraphy is most commonly found within backbarrier marine sediments and in interbedded fluvial deposits. This type of liquefaction feature is rare in beach settings, except where a thick soil profile or claypan has developed over the H_1 sand. Their less explosive origin is probably due to the thinner source beds which characterize these depositional environments (which result in less of a build-up in pore pressures within the water interlayer), and the cohesive nature of the overlying cap.

6.0 PSEUDOLIQUEFACTION FEATURES

Chapters 4 and 5 focused on the characterization of SIL sites and the morphology of SIL features located in the epicentral area of the 1886 earthquake. Equally important in the search for evidence of paleoseismic activity (especially outside the Charleston area) is the ability to distinguish between SIL features and other features that look similar, but are unrelated to past earthquakes (pseudoliquefaction features). This chapter includes a basic discussion of these features and provides several examples of those most likely to be misinterpreted as evidence of past earthquake activity. It is stressed that what is presented here only represents a small sample of the types of pseudoliquefaction features encountered during the course of this study. These brief discussions are not intended to describe and characterize all potential pseudoliquefaction features. Rather, they are designed to make the reader aware of this complexity in the search for evidence of past earthquake activity. For a more extensive discussion of pseudoliquefaction features the reader is referred to Obermeier and others (1986), and Obermeier and others (1990).

Pseudoliquefaction features can resemble both types of the SIL features that have been identified in the Charleston area. However, the presence of distinctive large and small clast zones within sand-blow explosion craters are key recognition criteria that can identify (with a relatively high degree of confidence) these features as SIL features. This is especially true if the local topographic and hydrogeologic settings are not conducive to the development of artesian conditions. Conversely, the morphology and internal structure of sand vent/fissure SIL features are often very similar to the morphology and internal structure of many types of pseudoliquefaction features. Unfortunately, no simple, single set of recognition criteria has been identified which can easily distinguish SIL sand vents/fissures from these other features. Often the strongest evidence for a seismic origin is a match between the grain size of the mobilized sands present in the sand vent/fissure and a source bed present at greater depths. However, even the identification of a source bed at depth does not conclusively prove a seismic origin. For example, the potential for transport of sediments resulting from spring activity, or dewatering of sediments during natural compaction must also be considered.

Due to their striking appearance and relative abundance, geochemical alteration features have a very high potential for misidentification by uninitiated investigators. Figure 6.1 presents a example of a large geochemical pseudoliquefaction feature that could easily be mistaken as evidence of past liquefaction. Note the white sands which appear to have been injected into the surrounding materials. Also note the dark "rind" that is present around the white sands.

During this study, these types of features were found both within the Charleston epicentral area and at numerous other locales along the Atlantic Seaboard. Based on grain size studies, the white sand is identical to the adjacent black "rind" materials and the adjacent "host" sands. Further, no evidence of material transport has been observed. Rather, a chemical process related to ground water flow which result in the bleaching of sands and the development of an adjacent "rind" is the preferred

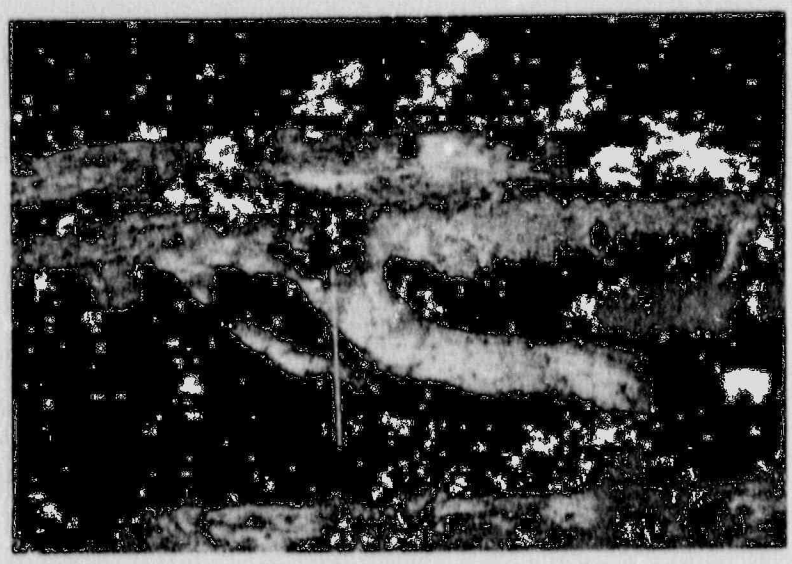

A

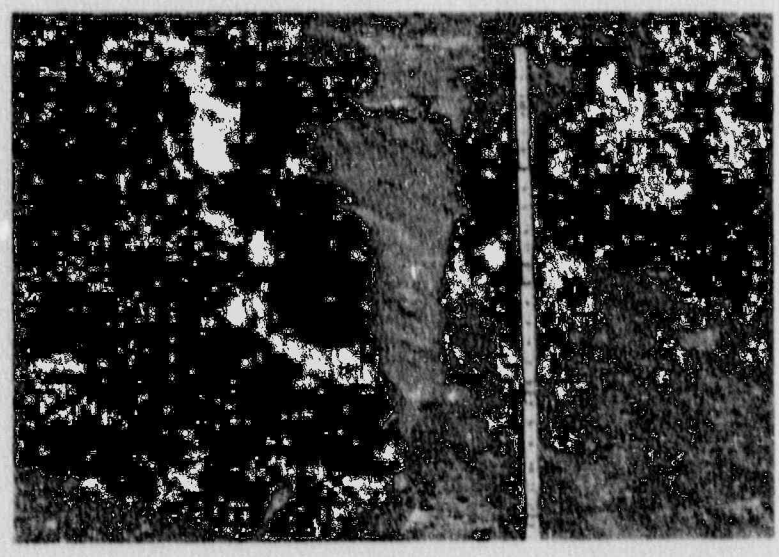

B

Figure 6.1: A) Example of a large pseudoliquefaction feature that could be mistaken as evidence of past liquefaction (hoe in center for scale). Note the white sands which resemble sand vent/fissure SIL features and the apparent "ejection blanket" present at and near the ground surface. Also note the dark "rind" that is present around the white sands. No conclusive evidence of material transport has been observed at any of these locales. A chemical process related to ground water flow resulting in the bleaching of sands and the development of an adjacent "rind" is the preferred model for their origin. B) Example of a small pseudoliquefaction feature that resembles a vent/fissure type SIL feature. At first viewing the color difference suggests that the lighter sands have been transported into the adjacent deposits, a closer inspection clearly shows that the apparent "vent/fissure" does not cut the original bedding. In units where original bedding does not provide such clear marker horizons and the grain size is relatively uniform it would be easy to misinterpret this type of geochemical feature as possible evidence of liquefaction.

model for their origin. Although these features commonly occur in loose sands (and consequently were sometimes located in close proximity to actual SIL features), there is no evidence to suggest that they indicate past earthquake activity.

In addition to this type of pseudoliquefaction feature, numerous other geochemical features which could under some conditions be mistaken for SIL were discovered during this investigation. Figure 6.1 also provides an example where geochemical alteration has resulted in the development of what appears to be a vent/fissure SIL feature. Although the color (and in some instances even the texture) of this type of feature resembles some of the features identified as liquefaction in the Charleston, SC area, in this example shown, the feature clearly does not cut the original bedding. There is no evidence of material transport associated with a liquefaction episode. However, in units where the original bedding does not provide such clear marker horizons and the grain size is relatively uniform it would be easy to misinterpret this type of geochemical feature as possible evidence of liquefaction.

Other types of pseudoliquefaction features discovered during this study include those resulting from biological and mechanical processes. Examples of biological activity that results in pseudoliquefaction features include root casts and infillings as well as infilled animal burrows. Pseudoliquefaction features can also result from mechanical processes such as the infilling of tree throws.

7.0 GEOMORPHIC AND REMOTE SENSING INVESTIGATIONS

In the Charleston area SIL features are not generally associated with an identifiable surface expression, and virtually all prehistoric SIL features identified have been found in existing excavations. As a means to expedite future searches, the morphology of SIL sites/features, aerial photography and ground penetrating radar were evaluated as potential reconnaissance tools.

7.1 Morphology of SIL Sites

At about one-third of the SIL sites studied, unique topographic depressions were noted on 1:24,000 topographic maps. These features were primarily associated with historical SIL sites located along beach ridges and take the form of a series of small circular to elliptical depressions along the crests. Examples are presented in Figure 7.1 and 7.2. The observed depressions are generally less than one meter deep and between 30 to 80 meters across (significantly wider than even the largest 1886 sand-blow explosion crater). When elliptical, the long axes of the features tend to parallel the trend of the beach ridge. These depressions are distinctly different from and should not be confused with "Carolina Bays". In addition, they do not appear to be related to primary sedimentary features, or be the result of local eolian processes. Further, due to their size, these features are not relics of explosion craters. Rather, it is suggested that they are the result of compaction within the sands due to: (1) natural diagenesis, or (2) liquefaction induced compaction at depth within the thick sands. In case 1, this type of morphology could be used to identify areas especially prone to SIL because thick deposits of loose sands are likely present. In case 2, this morphology could be used to define areas of thick sands where SIL may have occurred in the recent geologic past.

7.2 Morphology of SIL Features

In addition to studies using 1:24,000 scale maps, field investigations were conducted to develop recognition criteria for SIL features. With few exceptions, virtually all liquefaction sites in the Charleston area were discovered in existing excavations and staining and weathering on the excavated face requires scraping to reveal liquefaction features. However, a distinctive erosion pattern suggests the presence of SIL features in some exposures. In near-vertical exposures, mobilized sand often erodes or slumps in a fashion different from the adjacent clay-rich H_2 materials. An example is shown in Figure 7.3. This type of morphology is most likely related to: (1) the relative non-cohesive nature of the clean sands, resulting in more rapid erosion or slumping, and/or (2) their relatively high permeability, resulting in the development of characteristic "weeps".

7.3 Aerial Photography

Each of the SIL features identified was located on available aerial photographs. Black and white aerial photographs at a scale of 1:4800 was examined for each site. In addition, false color composite photographs were examined for approximately 80

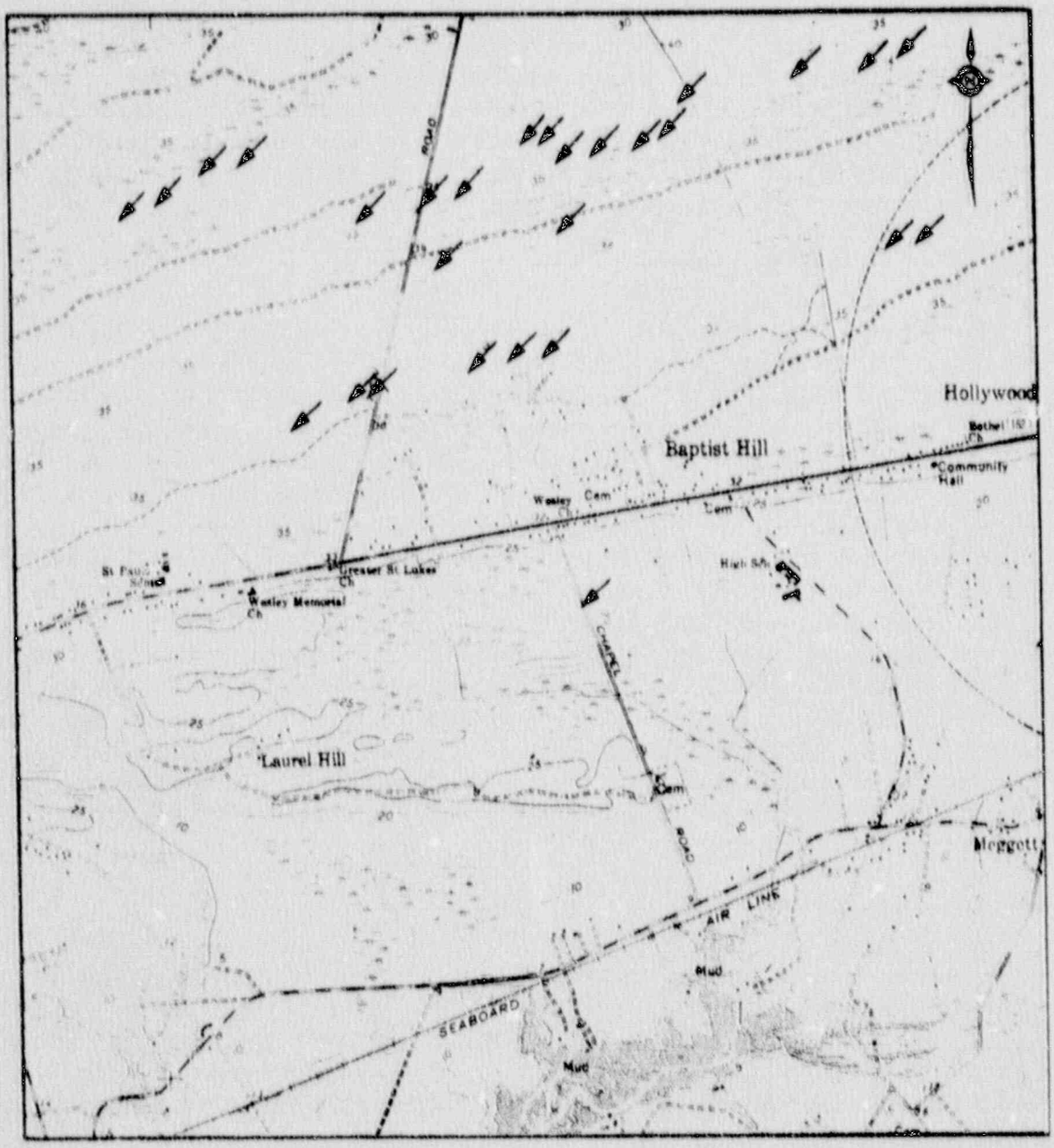

FIGURE 7.1: Example of depressions identified on 1:24,000 topographic maps. Arrows denote depressions identified in the vicinity of the Hollywood Ditch. These features are primarily associated with historical SIL sites located in mid to late Pleistocene beach complexes and take the form of a series of small circular to elliptical depressions along the old dune crests.

---

sites. Only about 10% of the sites were associated with probable expressions on the available imagery. An example of an 1886 SIL feature is shown in Figure 7.4. No pre-1886 SIL site was associated with recognizable expressions.

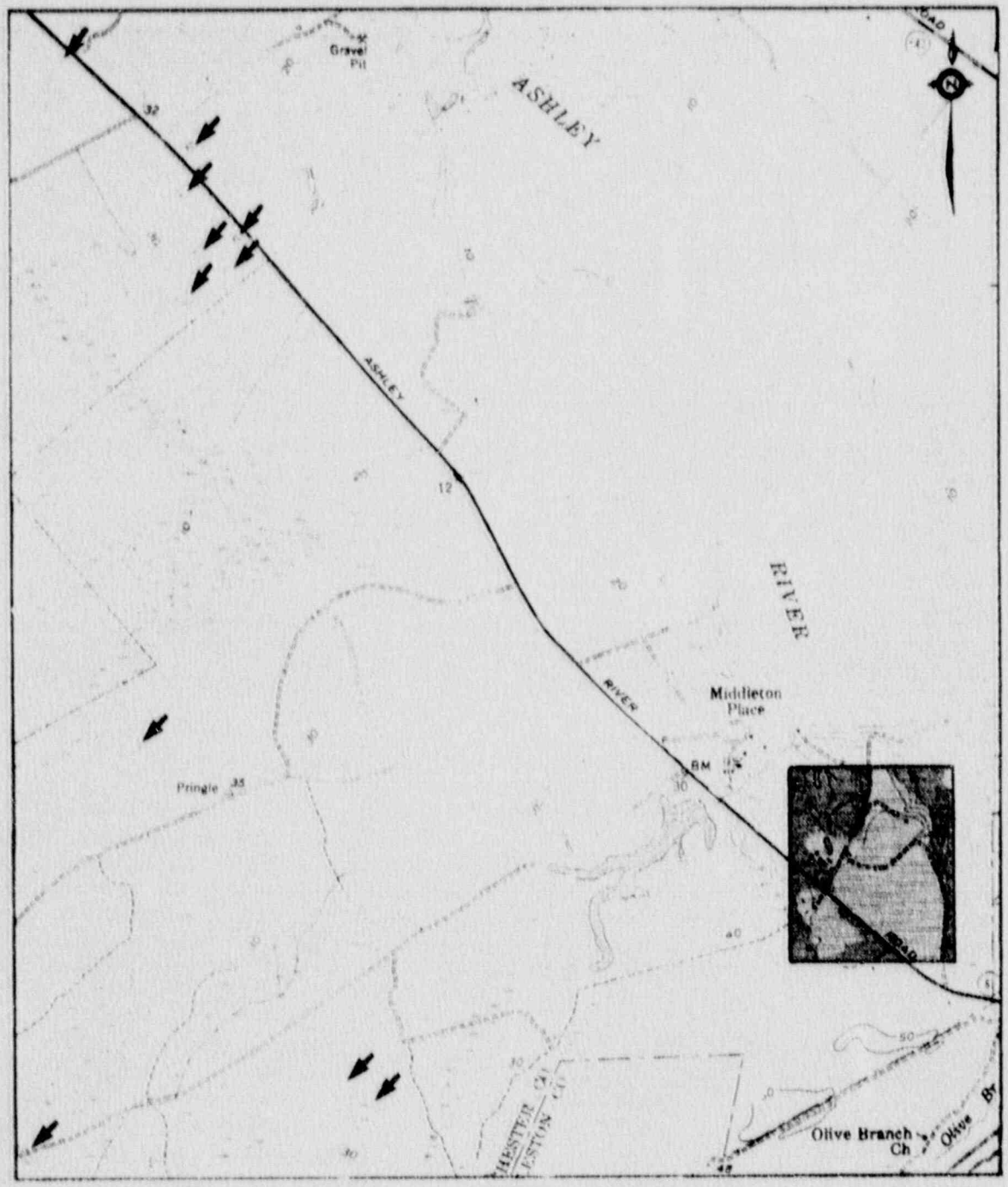

FIGURE 7.2: Another example of depressions identified on 1:24,000 topographic maps which are located in close proximity to SIL sites. Arrows denote depressions identified in the vicinity of Middleton Gardens. The shaded area identifies the area shown in detail on Figure 7.*. This is one of the few locations where these depressions were observed in fluvial deposits.

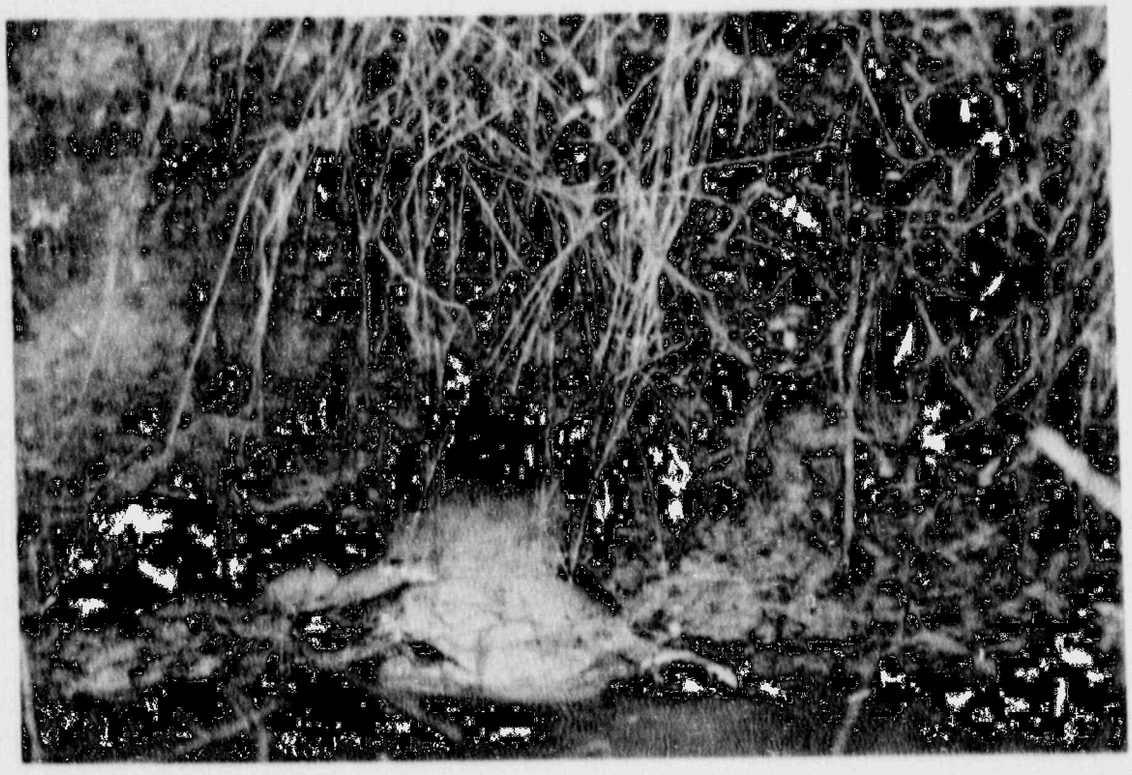

FIGURE 7.3: Example of distinctive "weep" feature. Similar features were noted at several SIL sites. In near vertical exposures such as ditches or the walls of other excavations, mobilized sands were often found to erode or slump in this manner. While not associated exclusively with SIL features, this morphology is usually indicative of sands adjacent to more clay rich materials. The formation of these features is due mostly to the relative non-cohesive nature of the clean sands, resulting in more rapid erosion or slumping, and/or their relatively high permeabilities, which result in the development of weeps. Excavation of this particular feature resulted in the identification of a lateral-spreading SIL site.

Next, low altitude overflights were carried out over many of the identified SIL sites and color and black-and-white infrared photographs were obtained. Again, while a few historical 1886 sites were associated with possible expressions on the infrared imagery, none of the pre-1886 locales showed a consistently recognizable expression.

The reason for the apparent lack of expression in remote sensing imagery is problematic. For example, Obermeier (1984) reported that many SIL sites in the New Madrid area could clearly be identified on available aerial photographs. But unlike the New Madrid area, most of the SIL sites in the Charleston area are located where sandy surface soils occur. Consequently, extruded sands would not

contrast sharply with the original surface materials. Conversely, many of the areas in the New Madrid region where the liquefaction features have been identified are where sands have been brought from depth and extruded onto extensive deposits of fluvial clays and silts. Further, and perhaps most importantly, many of the locales in the New Madrid area where evidence of liquefaction has been observed on aerial photographs are located in agricultural settings, where the land is cleared. In contrast, many of the liquefaction locales in the Charleston area are where the land is presently covered with timber or has been extensively urbanized.

7.4 Ground Penetrating Radar

Ground Penetrating Radar (GPR) was also tested at known liquefaction sites located in the Charleston area, to determine if this technique could be used as a reconnaissance tool in the search for liquefaction features outside the Charleston area (especially where exposure was limited or nonexistent). More detailed results of this aspect of these studies is presented in Appendix B. However, to summarize, field tests at control liquefaction sites in the Charleston area found that in interbedded depositional settings where an identifiable fine-grained cap (H_2) was present over the source sands, GPR anomalies were associated with the known SIL features (Figure 7.5). As noted previously, this type of depositional setting is most conducive to the formation of vent/fissure types of liquefaction features. At these sites, the near-surface materials are silts and clayey sands, which due to their relatively high conductivities, tend to attenuate the GPR signal. In areas where underlying sands have experienced liquefaction and moved upward resulting in the rupture or disruption of the overlying cap a distinctive GPR anomaly is observed. GPR tests at liquefaction sites located in beach/near-shore settings (where the sand-blow explosion crater type of SIL features predominate) were largely unsuccessful, probably due to the lack of a sufficient contrast between the H_2 and H_1 materials.

GPR data were next collected in several areas where local conditions appeared suitable for liquefaction, but where no liquefaction features had been identi ed. Five potential liquefaction sites in the Charleston area were identified solely on this basis. Trenches were excavated across two of these anomalies and liquefaction features were observed (Figure 7.6). These results suggest that in some geologic settings GPR may be a valuable reconnaissance tool in the search for paleoliquefaction features, especially in fluvial deposits such as along the James River in the Central Virginia Seismic Zone, or in the New Madrid region.

FIGURE 7.4: Aerial photograph of Middleton Place. This site is located near the center of the meizoseismal area of the 1886 earthquake and was reported as a site of liquefaction. The arrow denotes one of several light colored circular features identified in this pasture. These features may be associated with sands ejected during the 1886 vent. This site is one of the very few where any hint of SIL features could be identified on aerial photographs.

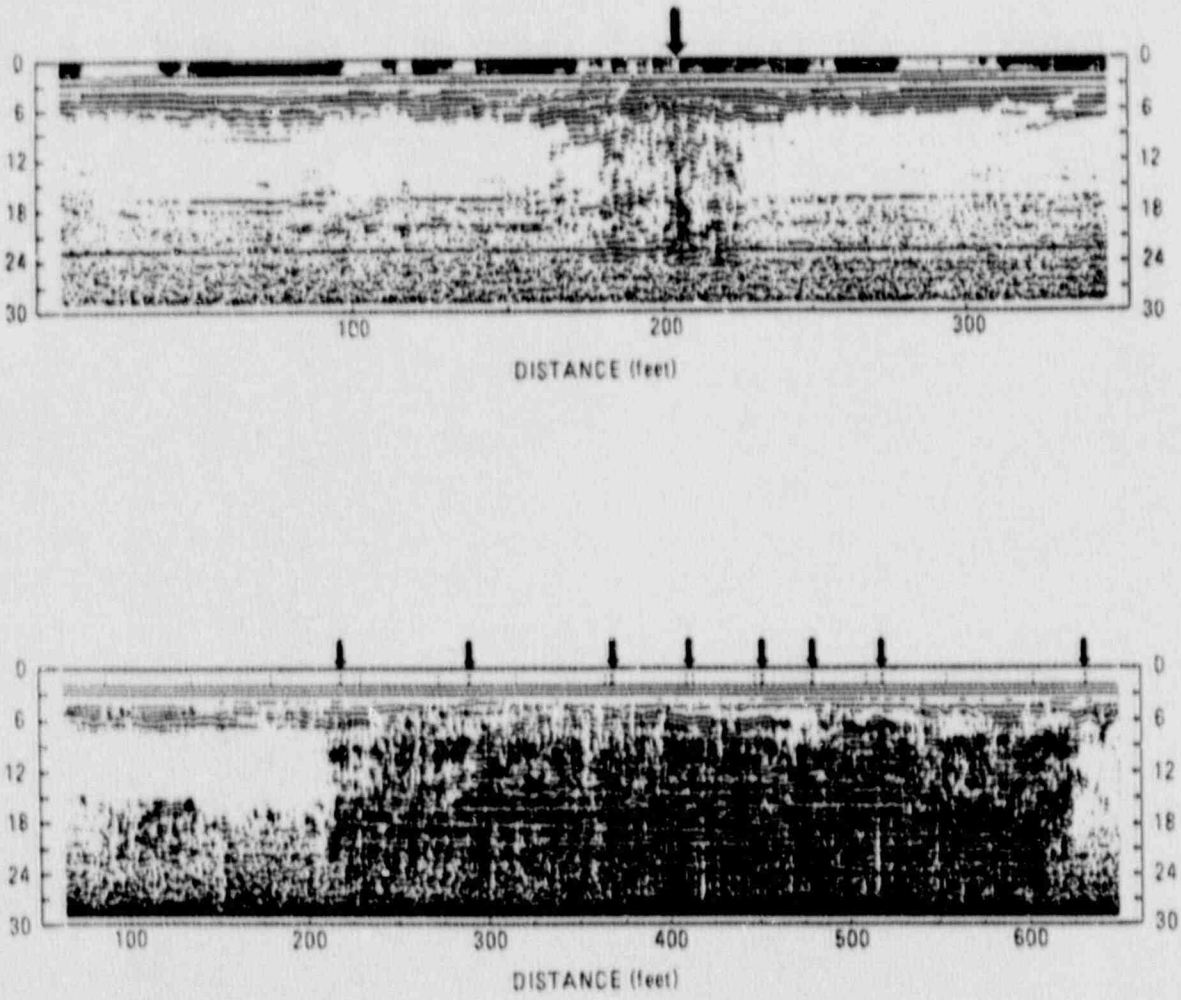

FIGURE 7.5: Two examples of Ground Penetrating Radar traverses over a known liquefaction locale located in the Charleston, S.C. area. Arrows identifies the location of large liquefaction features previously mapped in a drainage ditch running parallel to the GPR traverse. At each locale mapping within the ditch identified a series of sand vents that have disrupted the overlying silts and clays throughout wide zones.

FIGURE 7.6: Example of sand vent/fissure located in fluvial deposits. No pre-existing exposure was present at this site. It was discovered solely on the basis of a Ground Penetrating Radar (GPR) anomaly. Trenches were excavated across this and several other GPR anomalies. In each trench, vents/fissures similar to this were unearthed. At this site a layer of gray silty clay approximately 0.5 m thick acts as H_2. Based on site borings, the source bed (H_1) for the vent materials is at a depth of about two meters.

8.0 REVISED EARTHQUAKE CHRONOLOGY FOR THE CHARLESTON AREA

During the study of "control" SIL sites located in the Charleston area, samples of organic materials were recovered from within many SIL features. Based on the morphology of each features, as well as the type, size, and location of each sample, fifteen were identified as having a high probability of providing reliable age constraints on the timing of prehistoric liquefaction episodes. These were submitted for Carbon-14 age dating. Results have been obtained for ten of the samples collected at the Ten Mile Hill SIL site (site #3 in Figure 1.3). As part of this study, published radiometric age data for Charleston SIL features were also compiled and evaluated. Most of these data come from SIL features located at the Hollywood Site (site #2 on Figure 1.3) and have been reported in Obermeier and others (1985), Talwani and Cox (1985), Weems and others (1986), Weems and others (1988) and Weems and Obermeier (1990).

Collectively, these data were used to prepare a revised and updated prehistoric earthquake chronology for the Charleston meizoseismal area. Appendix B provides background information on Carbon-14 dating and discusses the techniques used during this study. Detailed information on the samples collected and dated during this study are also presented in that Appendix. An overview of our approach to dating SIL features is provided in subchapter 8.1. The relevant information used to identify and date liquefaction episodes in the Charleston meizoseismal area is discussed in subchapter 8.2 and summarized in Table 8.1.

8.1 Approach to Dating Paleoliquefaction Episodes

Qualitatively, the relative age of SIL features can often be determined by comparing the thickness of overlying soil profiles and the degree of staining and weathering of sands within the feature (Figure 8.1). Older SIL episodes are generally associated with more heavily stained sands within the feature and a thicker overlying soil profile. In contrast, younger SIL episodes are often associated with minimal staining and thinner overlying soil profiles. The relative age of liquefaction episodes can also be established based on the cross cutting relations of one feature to another (i.e. younger features truncating or intruding older features).

On a more quantitative basis, the age of liquefaction episodes can be determined by radiometric dating of organic materials contained within or cut by liquefaction features (Figure 8.2). For example, the Carbon-14 determined age of roots which have grown into a SIL feature provides a minimum age constraint on the liquefaction episode. Maximum age constraints can be obtained by dating roots cut by the feature, or by dating organic materials recovered from within soil clasts which collapsed into the deeper part of the crater during the SIL episode. Maximum age constraints can also be obtained by dating forest fire-derived charcoal which was washed or blown into the crater after its formation. Since charcoal is biologically inert and can reside at or near the ground surface for hundreds or even thousands of years following a forest fire, this type of sample only provides a maximum age

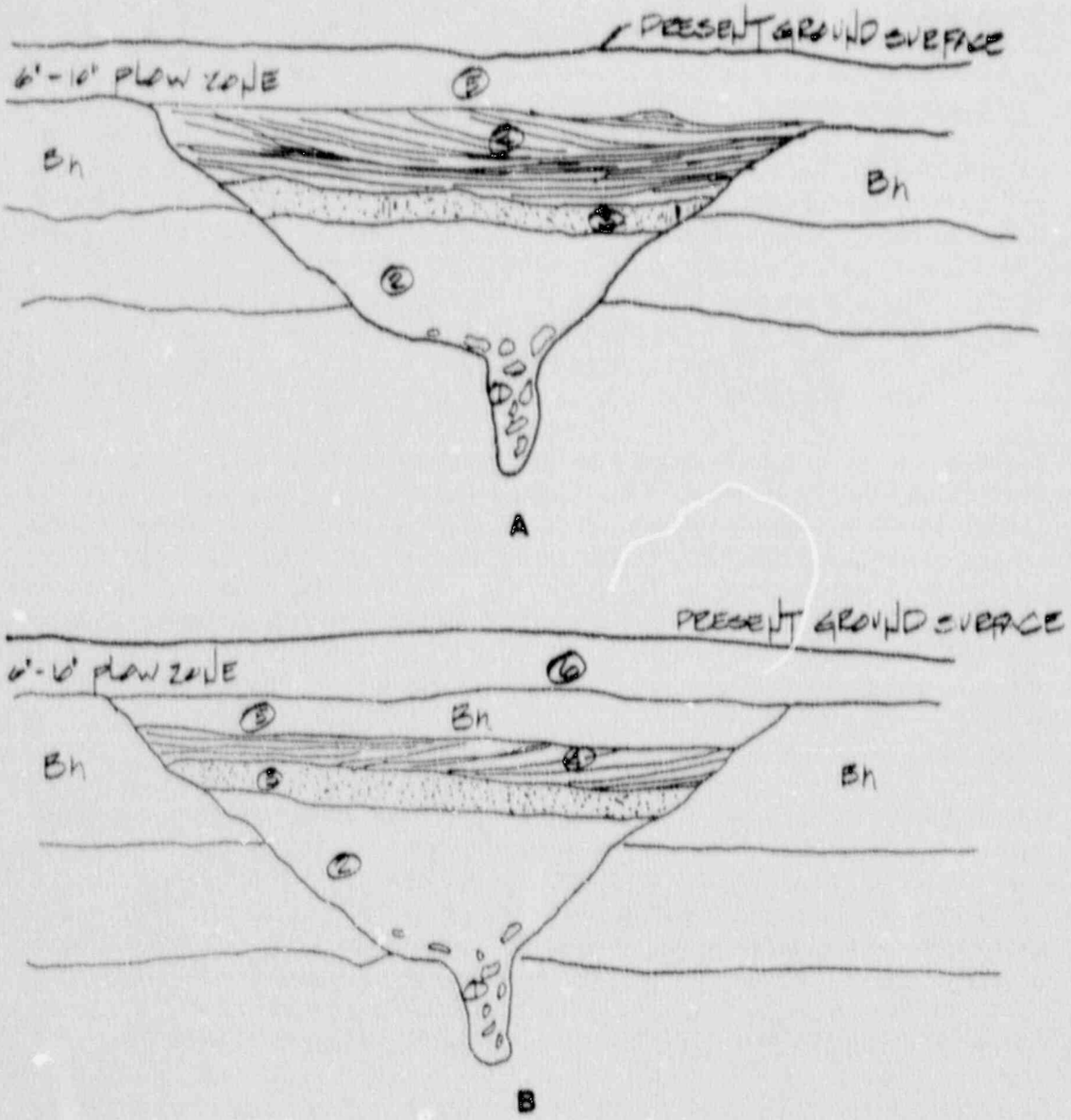

FIGURE 8.1: Qualitatively, the relative age of SIL features can often be determined by comparing the thickness of overlying soil profiles and the degree of staining and weathering of sands within the feature. This is illustrated schematically in Figures A and B. In both cases the feature is fed by a central vent filled with large clasts (#1). Overlying the large clast zone are massive sands (#2), a small clast zone (#3) and a bedded sequence (#4). In some older features these may be obscured due to stained and the development of soil profiles within them. Other factors equal, the older the feature the "deeper" the staining and soil development has progressed. In contrast, as illustrated in Figure A, very young (i.e. 1886) features have little of no soil profile developed over them and the overlying materials are often limited to only a 6 to 10 inch thick "plow zone" which is the result of cultivation over the past 100 years (#5). As illustrated in Figure B, "youngest" prehistoric features are often overlain by a newly developed Bh soil profile (#5) which is limited to the uppermost portions of the bedded sequence.

constraint on the time of liquefaction. The most accurate estimates for the age of a liquefaction episode are obtained by the radiometric dating of organic debris such as leaves, pine needles, bark or small branches that were washed or blown into the liquefaction crater following its formation.

8.2 Number and Ages of Paleoliquefaction Episodes

Collectively the Carbon-14 dating studies conducted by previous investigators and those carried out as part of this study suggest that in addition to liquefaction resulting from the 1886 earthquake, as many as five other liquefaction episodes may have occurred in the Charleston meizoseismal area during Holocene times. Including the 1886 event these are referred to from youngest to oldest as liquefaction episodes **CH-1** through **CH-6** (Table 8.1).

CH-1: The 1886 earthquake is designated as liquefaction episode **CH-1**. As reported by 19th century investigators, it resulted in the formation of numerous SIL features within 40 km of Charleston. Historical accounts also suggest that isolated occurrences of liquefaction associated with the 1886 earthquake may have occurred up to 125 km from Charleston as far north as Georgetown, South Carolina and as far south as Beaufort, South Carolina (Seeber and Armbruster, 1981).

CH-2: Liquefaction episode **CH-2** is based on data from the Hollywood site as reported in Weems and Obermeier (1990). They noted that some of the liquefaction features at this site have a distinctive soil profile which, although relatively thin, is still better developed than those overlying a typical 1886 liquefaction feature. Further, they note that this soil profile is less well developed than **CH-3** features (see following discussions). The age of **CH-2** has been quantified by the dating of a tree branch recovered from the base of the cross-bedded zone within one of these features (Table 8.1). The branch was probably deposited within the liquefaction feature as surface water and wind filled the depression with forest debris and has been dated at 640$\pm$60 YBP (Beta 20186). Note that the sample identifiers shown in parenthesis following each date represent laboratory reference numbers. The term "YBP" refers to years before present and is radiocarbon age relative to the year 1950. Its age should be nearly identical to the age of SIL formation. A photograph of this feature and the dated branch is presented as Figure 15 of Weems and Obermeier (1990). These investigators also noted that a root which had subsequently grown into this liquefaction feature was dated at 435$\pm$60 YBP (Beta 27733), confirming that it was not an 1886 SIL feature.

CH-3: Episode **CH-3** is based on data collected at the Hollywood site as reported by Talwani and Cox (1985) and Weems and others (1986). Figure 8.3 is taken from Talwani and Cox (1985) and illustrates an SIL feature that they studied at their Hollywood #2 site. Radiometric data collected by these investigators yielded modern ages for "new burn" charcoal recovered from the overlying soil profile and provided no constraints on the age of this feature. However, they suggested a pre-1886 origin on the basis of the overlying soil profile. Subsequent studies (see Figure 5 of Weems and others, 1986) excavated deeper into the trench wall and recovered

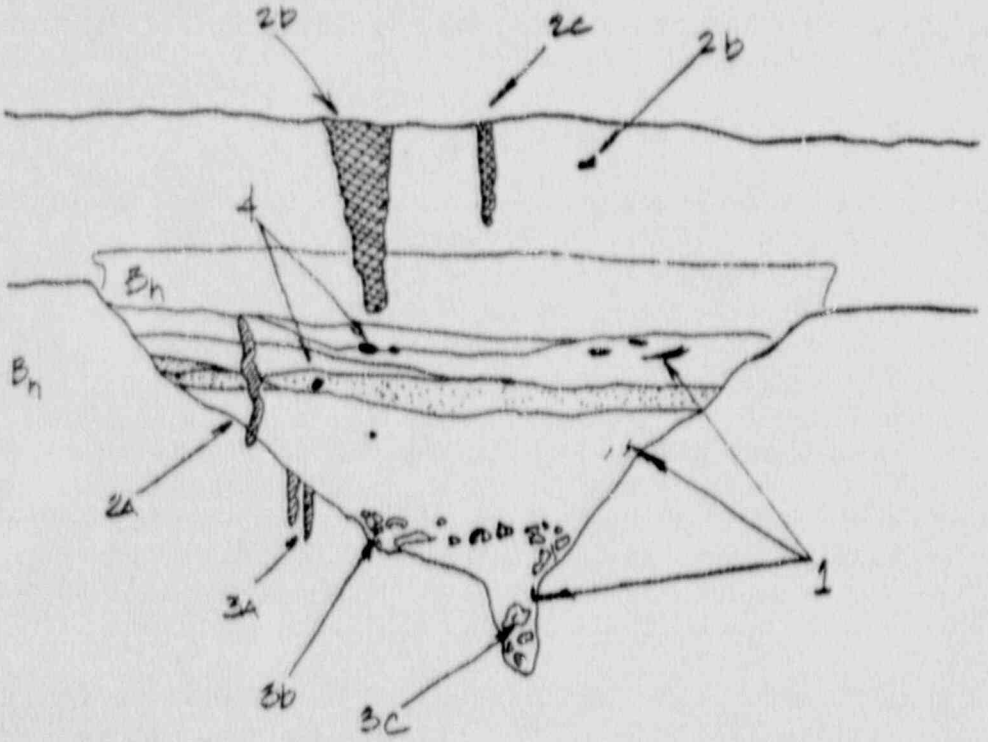

FIGURE 8.2: The age of liquefaction episodes can be determined by radiometric dating of organic materials contained within or cut by liquefaction features. The most accurate estimates for the age of a liquefaction episode are obtained by the radiometric dating of organic debris such as leaves, pine needles, bark or small branches that were washed or blown into the liquefaction crater following its formation (#1). The Carbon-14 determined ages of roots which have grown into a SIL feature (#2a) or into the overlying soil profile (#2b and #2c) provide minimum age constraints on the time of the liquefaction episode. Minimum age constraints can also be obtained by dating forest-fire derived charcoal from the shallow soil profile overlying the feature. To provide useful information, this "new burn" charcoal must clearly be within the overlying soils which post date feature formation. Maximum age constraints can be obtained by dating roots cut by the feature (#3a), humate materials recovered from soil clasts which are isolated from recharge due to their at depth in the feature (#3b), or by dating organic materials recovered from within soil clasts which collapsed into the deeper part of the crater during the SIL episode (#3c). Maximum age constraints can also be obtained by dating forest fire-derived charcoal which was washed or blown into the crater after its formation (#4). While wood recovered from within the feature, especially the bedded sequence, provides a very accurate age constraint on the timing of feature formation, charcoal is biologically inert and before being washed into the bedded sequence can reside at or near the ground surface for hundreds or even thousands of years following a forest fire. Consequently, this type of sampie only provides a maximum age constraint on the time of liquefaction.

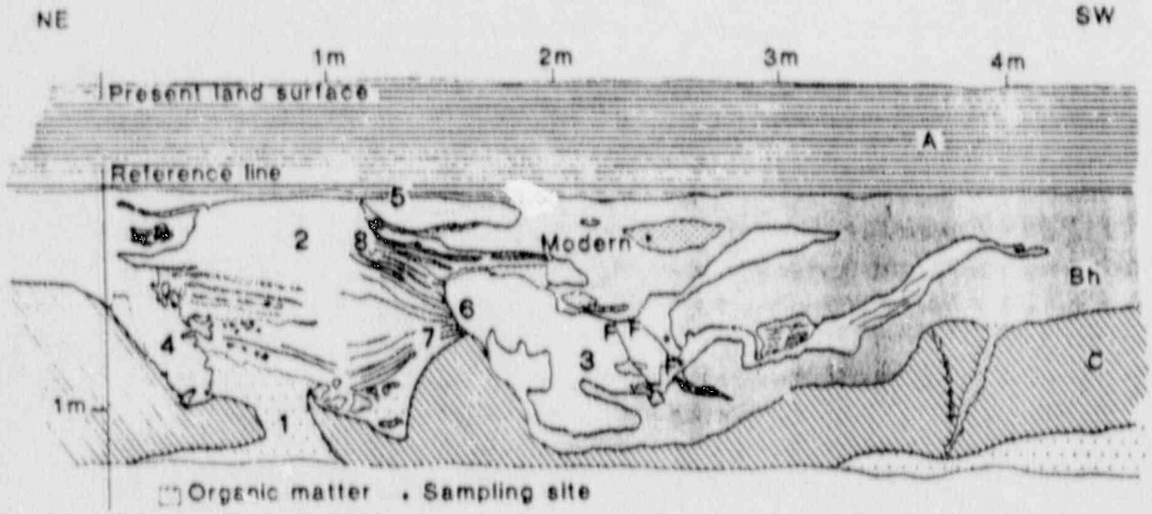

FIGURE 8.3: Trench log showing structures at Site 2 of Talwani and Cox (1985). The local soil profile has been disturbed by two liquefaction events. The structure to the northeast has been interpreted by these authors as an infilled crater. A preserved central vent (1) just below the crater differs markedly from the internal bedding present within the crater (2). A large block of Bh material (4) slumped along the northeast margin of the crater. A Bh horizon (5) that has developed since the emplacement of the crater overlies the crater, suggesting that this feature was not associated with the 1886 earthquake. The undisturbed Bh horizon at this locale typically attains a thickness of 60 cm. Southwest of the crater is another preserved conduit (3) which has been interpreted by these investigators as being associated with a later event - it truncates the internal bedding of the crater along its southwest margin (6). Subsequent studies (see Figure 5 of Weems and others, 1986) excavated deeper into the trench wall and recovered a stump (#7) that had apparently collapsed into the older feature during venting and a stick (#8) with rounded ends that also fell or was washed into the same feature shortly after its formation. Carbon-14 ages of these samples are included in Table 8.1. The stump was dated at 1290±90 YBP (W 5664) and 1070±200 YBP (W 5669). The stick was dated at 1230±85 YBP (Beta 12886) and 1230±90 YBP (W 5664). These data suggest that the older of the liquefaction features occurred about 1200 YBP. The age of the younger feature has not been determined but based on the overlying soil profile it probably was not associated with the 1886 earthquake. Modified from Talwani and Cox (1985).

a stump that had collapsed into the feature during venting and a stick with rounded ends that also fell or was washed into the feature shortly after its formation. Carbon-14 ages of these samples are included in Table 8.1. The stump was dated at 1290±90 YBP (W 5664) and 1070±200 YBP (W 5669). The stick was dated at 1230±85 YBP (Beta 12886) and 1230±90 YBP (W 5664).

Weems and others (1986) also recovered a stick from within the central vent of a second feature located at the Hollywood site (Figure 8.4). This feature had an overlying soil profile similar to that at Site 2 of Talwani and Cox (1985) and the radiometric age of the stick was very similar (1230±75 YBP - Beta 12885) to the age

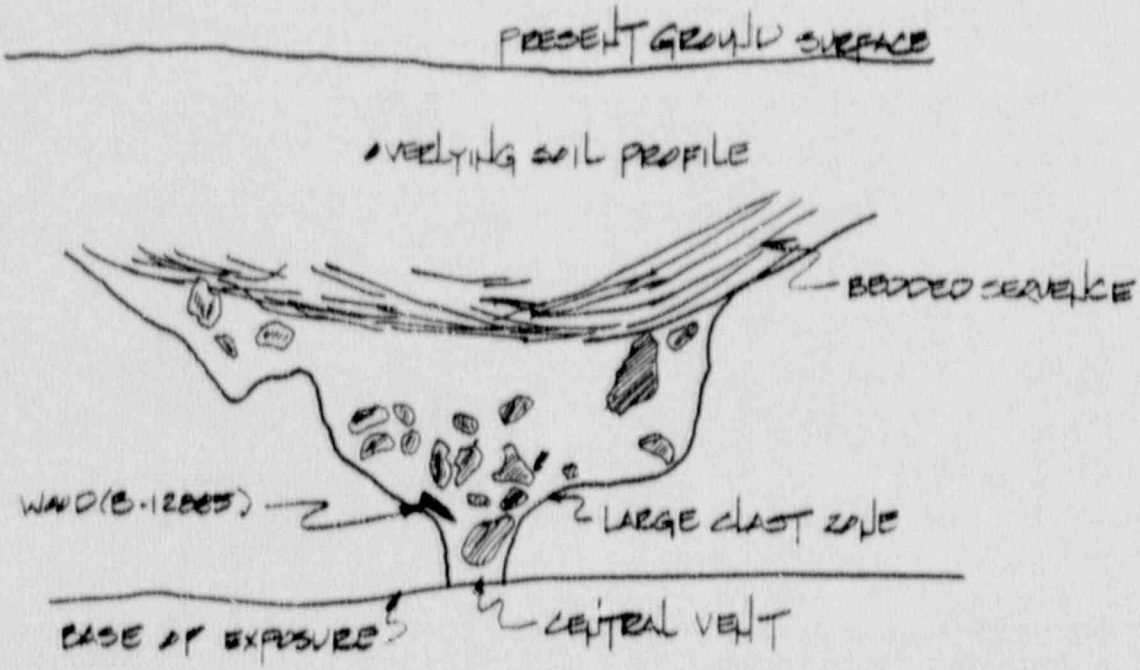

FIGURE 8.4: Sketch of sand-blow explosion crater at the Hollywood site (modified from Figure 4 of Weems and others, 1986). These investigators recovered a stick from within the central vent of this feature. The radiometric age of the stick was very similar (1230±75 YBP - Beta 12885). Weems and others (1986) and Obermeier (1989) note that many liquefaction features at the Hollywood Site exhibit very similar overlying soil profiles. They suggest that these features formed at approximately the same time as this feature.

---

determined for the liquefaction episode observed there. Weems and others (1986) and Obermeier (personal communication, 1989) noted that many liquefaction features at the Hollywood Site exhibit very similar overlying soil profiles. They suggested that these features formed at approximately the same time as the two SIL features discussed above.

CH-4: Episode **CH-4** is based on data collected at the Hollywood site as reported by Talwani and Cox (1985), and Weems and others (1986) in addition to data collected during this study at the Ten Mile Hill site and a radiometric date reported in Weems and others (1988). It is the best documented of the prehistoric Charleston liquefaction episodes.

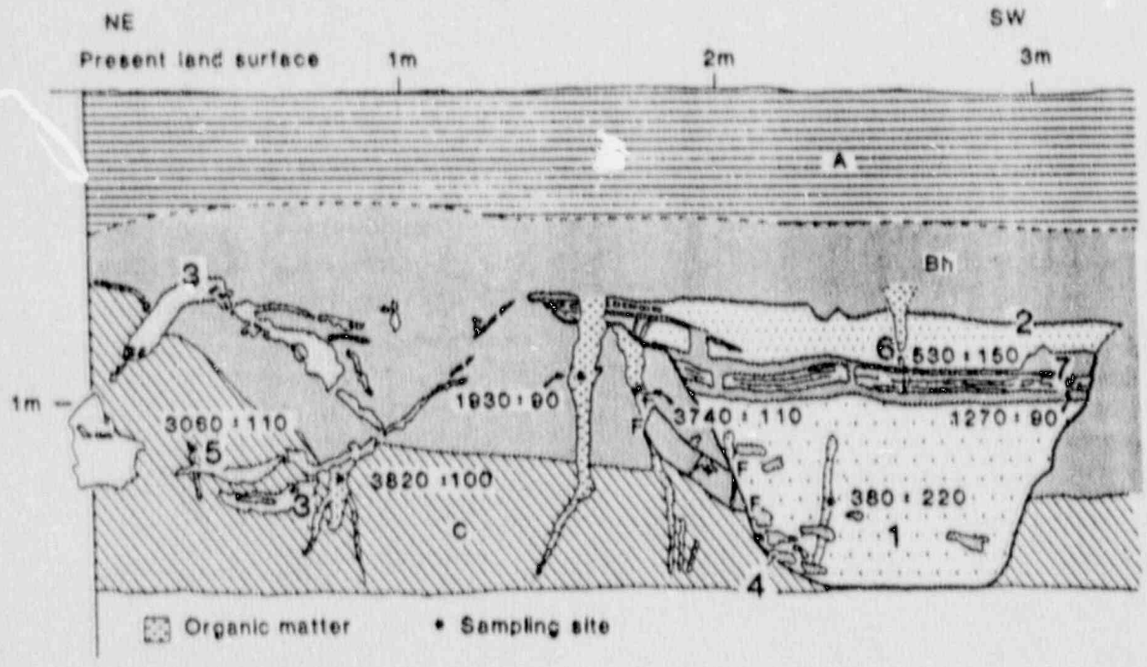

FIGURE 8.5: Cross-sectional trench log at site 1 of Talwani and Cox (1985). This feature is located approximately 50 m southwest of site 2 discussed in Figure 8.3. The preserved crater (1) has the same internal grading and bedding (2) and slumped clasts of Bh material (4) as were observed at Site 2. A preserved central vent (3) is northeast of the crater. Faulting (F) associated with formation of the crater offsets roots dated at 3740±110 years before present. Dates obtained from roots crosscutting the infilled crater yielded ages of 530±150 years (6), 380±220 years, and 1270±90 years (7). The oldest root is not shown because it was covered at the time the outcrop was mapped. Dates from the infilled crater indicate that it was emplaced after 3740±110 but before 1270±90 years before present. An age of 1930±90 years for a root provided no useful data on the timing of events. Subsequent studies (see Table 1 of Weems and others, 1986) excavated deeper into the trench wall and discovered an even older root that had grown into the crater. This root was dated at 1660±100 (Beta 11836). Collectively these data suggest that the feature formed more than about 1660 YBP and less than about 3740 YBP.

Figure 8.5 taken from Talwani and Cox (1985) shows a CH-4 feature that they evaluated at the Hollywood Site. At this locale, (referred to as Site 1 by these authors) a maximum age constraint of 3740±110 YBP was obtained by dating roots which were cut by this feature. Talwani and Cox also reported a minimum age constraint of 1270±90 YBP based on the dating of a root that had grown into the crater. Subsequent studies (see Table 1 of Weems and others, 1986) excavated deeper into the trench wall and discovered an even older root that had grown into the crater. This root was dated at 1660±100 (Beta 11836). Collectively these data suggest that the feature formed more than about 1660 YBP and less than about 3740 YBP. The overlying soil profile of this feature is thicker than that observed over the

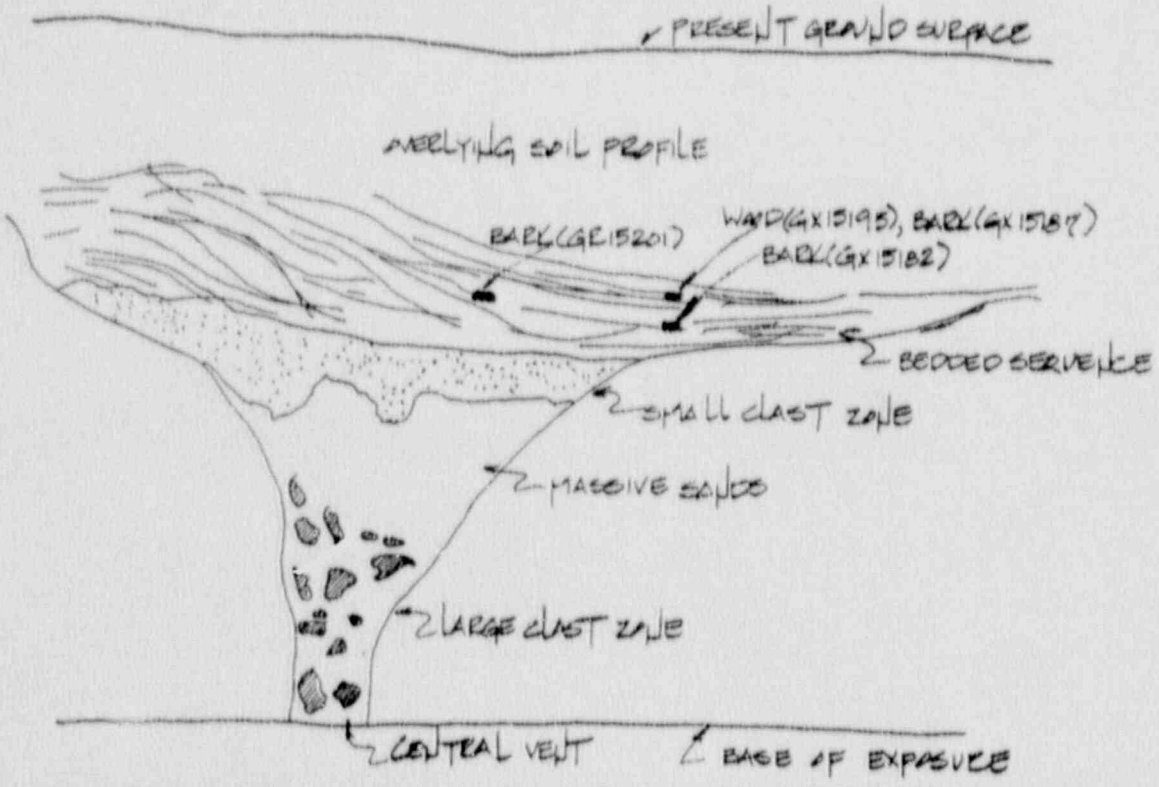

FIGURE 8.6: Sketch of sand-blow explosion crater discovered during this study. This feature is located at the Ten Mile Hill SIL site, near the 1886 SIL features shown in Figure 3.1. At this site several large SIL features were studied in detail. The bedded sequence of this feature is approximately 11 ft in width. The Carbon-14 determined ages of bark and wood recovered from the bedded sequence of this feature yielded dates that are approximately 3400 YBP (see Table 8.1).

1230 YBP **CH-2** (see previous discussion), consistent with an older origin. For comparison review the thickness of the soil profiles shown in Figures 8.4 and 8.5. Obermeier (personal communication, 1989) noted that many liquefaction features at the Hollywood Site exhibit very similar overlying soil profiles, and suggested that they probably formed at approximately the same time as this SIL feature.

The timing of episode **CH-4** is better constrained by data collected at a site evaluated during this investigation (Ten Mile Hill). It is located in the vicinity of the present day Charleston airport, near the 1886 SIL features shown in Figure 3.1. At this site several large SIL features were studied in detail. Sketches of two of these features are presented as Figure 8.6 and 8.7. A photograph of one of these features is presented as Figure 8.8. The Carbon-14 determined ages of bark and wood recovered from the bedded sequence of two craters were 3438$\pm$87 YBP (GX15201), 3405$\pm$255 YBP (GX15182), 3450$\pm$120 YBP (GX15185), and 2675$\pm$310 YBP

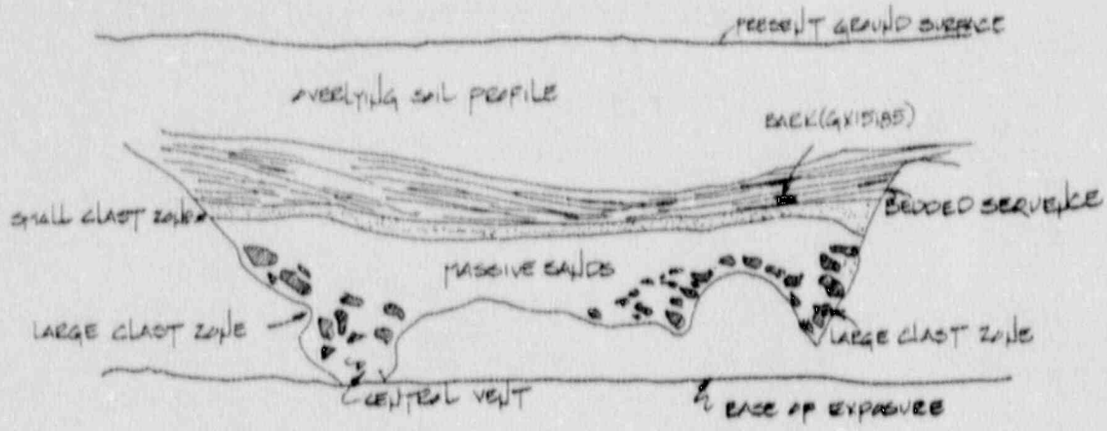

FIGURE 8.7: Sketch of sand-blow explosion crater discovered during this study. This feature is also located at the Ten Mile Hill SIL site, near the 1886 SIL features shown in Figure 3.1. The bedded sequence of this feature is approximately 14 ft in width. The Carbon-14 determined age of bark recovered from the bedded sequence of this feature was approximately 3400 YBP date (see Table 8.1).

(GX15196). As discussed previously, this type of sample is thought to provide a very good estimate on the timing of the liquefaction episode. A minimum age constraint of 2865±190 YBP (GX15186) was obtained from a tree root which had grown into one of the features after its formation. Weems and others (1988) report an age of 3280±130 YBP for tree bark recovered from the bedded sequence of a SIL feature located at their site ARP (Table 8.1). This site is located adjacent to the Ten Mile Hill site.

CH-5: Episode **CH-5** is based primarily on data obtained during this study at the Ten Mile Hill site. Several liquefaction features with extremely thick overlying soil profiles were observed there. The thickness of these overlying profiles suggest a very "old" age. The Carbon-14 derived age of a root that had grown into one of these features after its formation and subsequent filling provided a minimum age constraint of 4730±265 YBP (GX 15194). This clearly distinguishes these features from episode **CH-4** features. A maximum age constraint of 5790±650 YBP (GX 15184) was obtained from the Carbon-14 derived age of charcoal recovered from within the bedded sequence of one of these features (Figure 8.9).

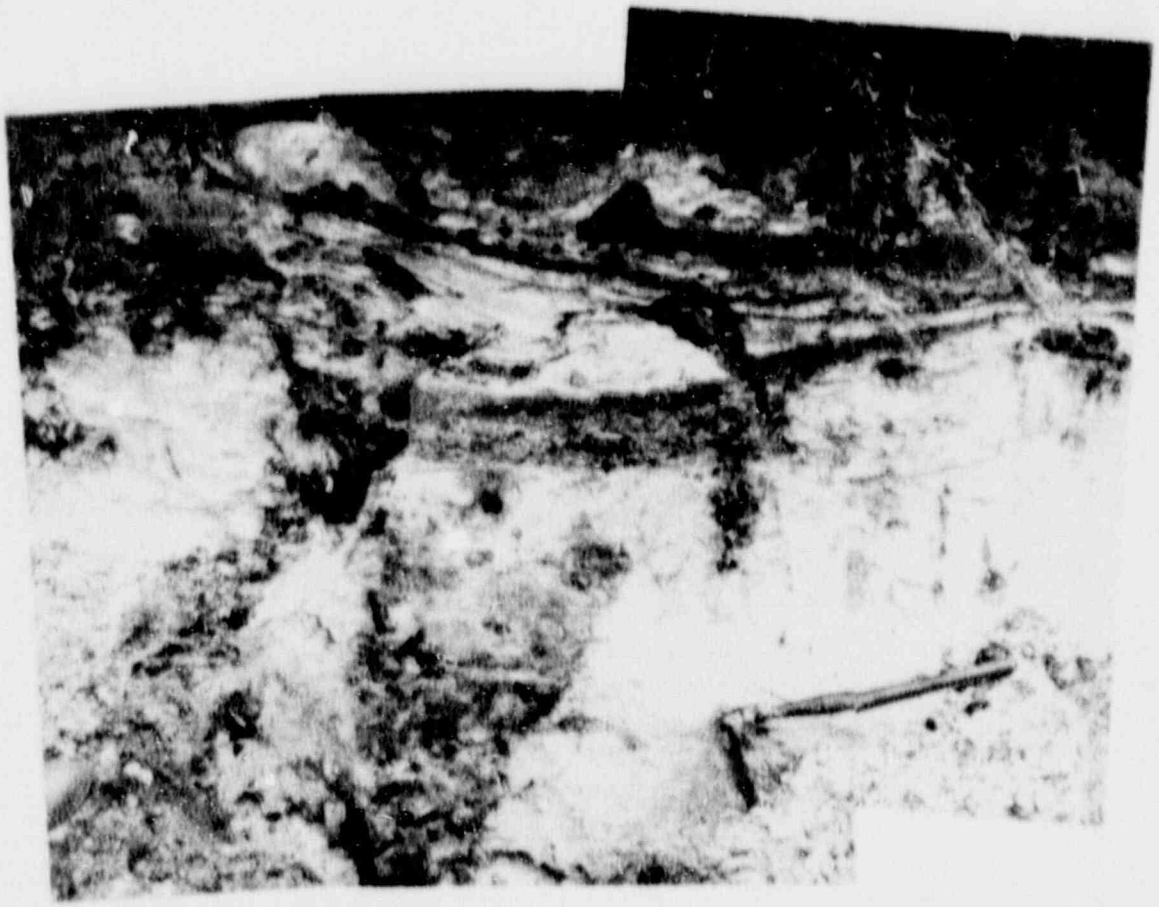

FIGURE 8.8: Photograph of large sand-blow explosion crater discovered during this study. This feature is also located at the Ten Mile Hill SIL site, near the 1886 SIL features shown in Figure 3.1. Note the central vent and associated large clast zone, the overlying massive sands, small clast zone and the bedded sequence.

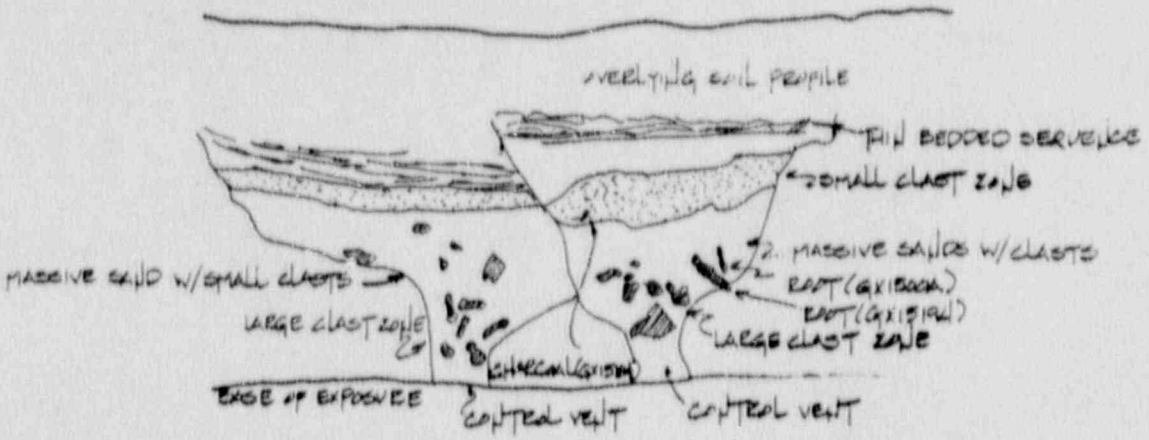

FIGURE 8.9: Sketch of cross cutting liquefaction features observed at the Ten Mile Site. The Carbon-14 derived age of a root that had grown into the feature on the right after its formation and subsequent filling provided a minimum age constraint of 4730 + 265 YBP (GX 15194). A maximum age constraint of 5790 + 650 YBP was obtained from the Carbon-14 derived age of charcoal recovered from within the bedded sequence of this same feature. This episode **CH-5** feature clearly cuts the margins of an even older liquefaction feature and the relative thickness of the soil profiles overlying these two liquefaction features suggest that their formation was separated by at least several hundred years.

CH-6: Episode **CH-6** is also based primarily on data collected during this study at the Ten Mile Hill site. The **CH-5** feature described above clearly cuts the margins of an even older liquefaction feature (Figure 8.9). The relative thickness of the soil profiles overlying these two liquefaction features suggest that their formation was separated by at least several hundred years.

Other Data: Data from SIL features at the Hollywood site (Weems and others, 1986) suggest at least one liquefaction episode which falls in the age range 4160$\pm$100 (Beta 11825) to 7060$\pm$110 YBP (Beta 11824). The estimated age of these features is consistent with their formation during either or both liquefaction episode **CH-5** or **CH-6**.

8.3 Summary

Collectively the data discussed above suggest that in addition to the 1886 liquefaction episode, five other earthquakes associated with liquefaction may have occurred near Charleston during Holocene times. The inferred age of each liquefaction episode is shown in Table 8.1. Episodes **CH-1**, **CH-3**, and **CH-4** are strongly supported by the available data and have been documented through the dating of several features at two different sites. Episodes **CH-2**, **CH-5**, and **CH-6** are based on reliable but more limited information.

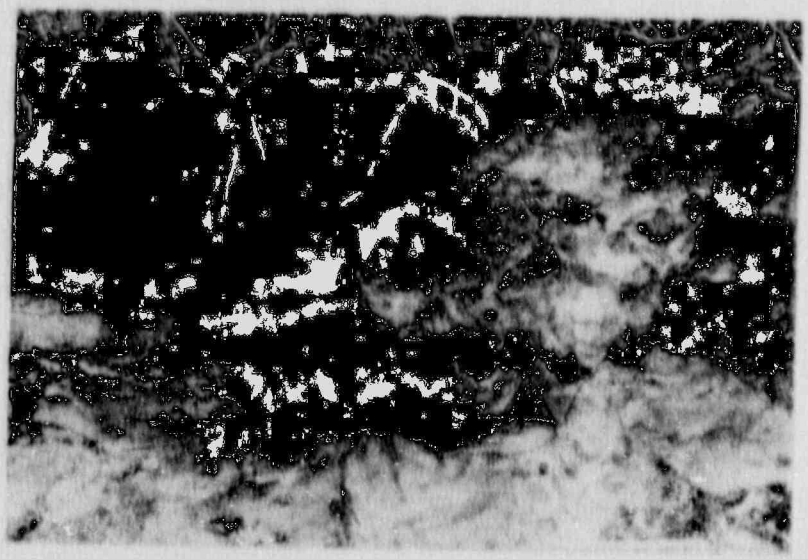

A

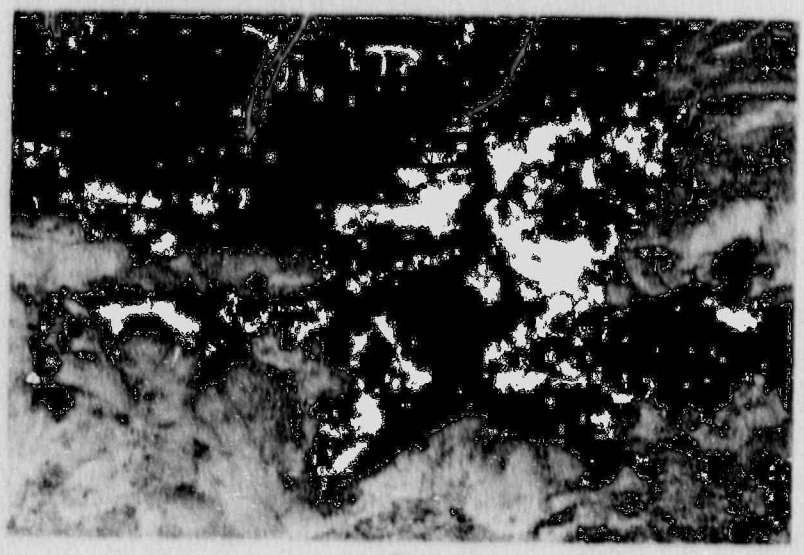

B

FIGURE 8.10: Photographs of CH-5 and CH-6 features. Also see Figure 8.9 for sketch. The feature on the right has been dated at 5150±500 YBP. Note that it truncates the bedded sequence of the feature on the left, suggesting that it is younger in age. Also note the thicker soil profile over the (CH-6) feature on the left, consistent with it being at least several hundred years older than the CH-5 feature on the right.

TABLE 8.1
CHARLESTON LIQUEFACTION EPISODES

LIQUEFACTION EPISODE CH-1 (AGE 104 YBP)				
SITE	AGE (YBP) MINIMUM	CONTEMP	MAXIMUM	SOURCE
MANY		104		1886 EQ-Historical Record

LIQUEFACTION EPISODE CH-2 (AGE 600±100 YBP)				
SITE	AGE (YBP) MINIMUM	CONTEMP	MAXIMUM	SOURCE
HOLLYWOOD		640± 60		Weems and Obermeier (1990)

LIQUEFACTION EPISODE CH-3 (AGE 1200±100 YBP)				
SITE	MINIMUM	AGE (YBP) CONTEMP	MAXIMUM	SOURCE
HOLLYWOOD		1230± 75		Weems and Others (1986)
		1230± 85		Weems and Others (1986)
		1070±200		Weems and Others (1986)
		1290±200		Weems and Others (1986)
		1230± 90		Weems and Others (1986)

TABLE 8.1 (Continued)
CHARLESTON LIQUEFACTION EPISODES

LIQUEFACTION EPISODE CH-4 (AGE 3200±200 YBP)				
SITE	AGE (YBP) MINIMUM	CONTEMP	MAXIMUM	SOURCE
HOLLYWOOD	380±220			Talwani and Cox (1985)
	530±150			Talwani and Cox (1985)
	1270±90			Talwani and Cox (1985)
			3740±110	Talwani and Cox (1985)
	1660±100			Weems and others (1986)
AIRPORT		3280±130		Weems and others (1988)
TEN MILE		3438± 87		This study
		3405±255		This study
	2865±260			This study
		2675±310		This study
		3450±120		This study

LIQUEFACTION EPISODE CH-5 (AGE 5150±500 YBP)				
SITE	AGE (YBP) MINIMUM	CONTEMP	MAXIMUM	SOURCE
TEN MILE	4730±265			This study
			5790±710	This study
HOLLYWOOD	4160±100			Weems and others (1986)
			7060±110	Weems and others (1986)

LIQUEFACTION EPISODE CH-6 (AGE >5150 YBP)				
SITE	AGE (YBP) MINIMUM	CONTEMP	MAXIMUM	SOURCE
TEN MILE	5790±710			This study

9.0 STUDIES IN THE CENTRAL VIRGINIA AREA AND WILMINGTON, DELAWARE AREAS

Along the Atlantic seaboard, intensity VII earthquakes have occurred at two other locales where potentially liquefiable deposits are present (Central Virginia and Wilmington, Delaware). The levels of ground motion resulting in MM intensity VII effects are generally not sufficient to generate liquefaction features (Russ, 1983). However, if the return periods between large rare events are greater than several hundred years, Charleston-like earthquakes may have occurred in these areas prior to colonization. Consequently, reconnaissance searches for paleoliquefaction evidence of prehistoric earthquakes were initiated in both areas.

9.1 Studies in the Central Virginia Area

The central Virginia area has been the locale of low level seismicity for the past two hundred years. Over 20 intensity V events are reported for the years 1770 through 1969 (Bollinger, 1973). Frequency magnitude relations developed for this area (Bollinger and others, 1989) suggest that if the area is capable of generating large events the return period between events similar to the 1886 Charleston earthquake would possibly be on the order of 600 to 5000 years.

The largest historical event in the central Virginia area occurred in December of 1875. It was felt over approximately 130,000 km^2 and was associated with intensity VII levels of ground motion in and west of Richmond. Maximum intensities were observed on river terrace deposits located along the James River. Based on a recent reevaluation of intensity data (Bollinger and Oaks, 1986), the epicenter of this event has been placed about 40 km west of Richmond, in Gouchland county (Figure 9.1). An earlier intensity VII event occurred in 1774. This event was felt over approximately 150,000 km^2 (Bollinger, 1975). Maximum intensities were reported on fluvial deposits about 10 km north of Petersburg.

Potentially liquefiable deposits in the central Virginia area are primarily fluvial in origin (see Figure 9.1 explanation for key references). They include alluvial sands and gravels of late Pleistocene age and more recent Holocene floodplain and overbank units along the James, the Appomattox, Mattaponi, Pamunkey, and Raphahannock Rivers. In general, the water table was found to be one to three meters deep and given their looseness and composition, their liquefaction potential was judged to be very high.

The distribution of potential liquefaction sites evaluated during this reconnaissance study is presented in Figure 9.1. The proximity of these sites to the two intensity VII historical earthquakes are shown in Figure 9.2. Extensive exposures were evaluated along the James River near Richmond, Virginia where numerous sand and gravel quarries are present. Sand and gravel operations are present to a much lesser degree along the Mattaponi and Raphannock rivers and only a limited number of existing exposures were identified along the portion of the James River west of Richmond.

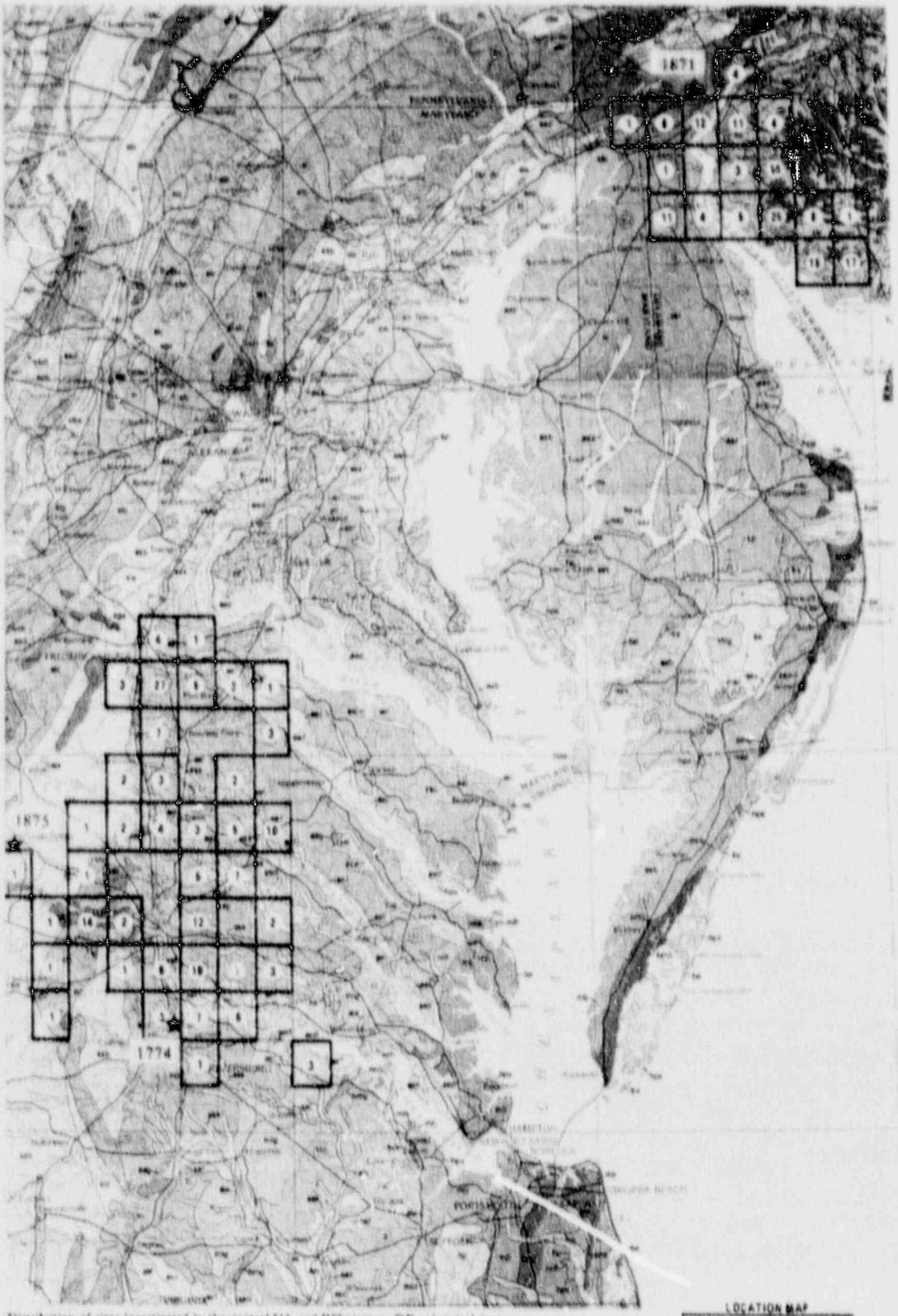

Distribution of sites investigated in the central VA and Wilmington, DE epicentral areas.

★ = Earthquake Location
See Text for discussion

2

Black outlines on geologic map represent USGS 7.5 minute topographic quadrangles which were used for all site reconnaissance work. The number of evaluated locations per quadrangle is shown in the circle.

25 0 25 50
SCALE IN KILOMETERS

LOCATION MAP

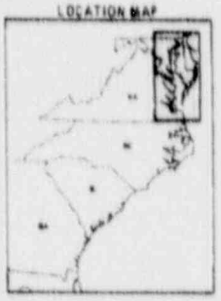

N

Modified after Cleaves and others, 1987 Quaternary Geology, Chesapeake Bay 4°x6° Quad., US, 1:1,000,000

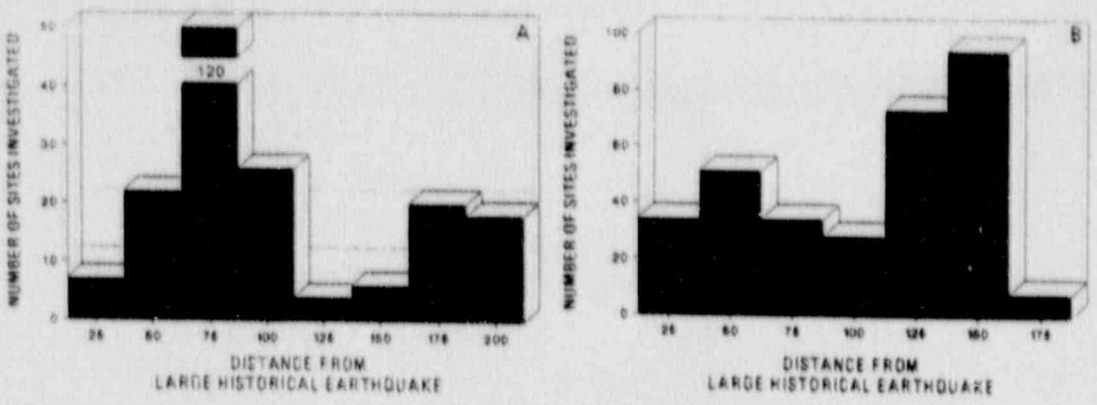

FIGURE 9.2: Distribution of potential liquefaction sites investigated in the Central Virginia study area. Figure A illustrates the proximity of sites (expressed in km) evaluated with respect to the epicenter of the December 1875 intensity VII earthquake. Figure B illustrates the proximity of sites evaluated with respect to the epicenter of the 1774 intensity VII event.

9.2 Studies in the Wilmington, Delaware Area

A historical intensity VII earthquake occurred in October, 1871, in the Wilmington, Delaware area, and caused minor structural damage in Wilmington (Jordan and others, 1972). Low-level activity has been recorded since 1971 in northeastern Delaware, near the Delaware River. The epicenter of the 1871 event is thought to be in the same general area as these instrumentally located earthquakes.

The sediments in northern Delaware have been described as Quaternary age deposits of the Columbia Formation. During field studies they were observed in many exposures to consist primarily of yellow and reddish brown quartz sand with some gravel. However, in general the water table was found to be deeper than anticipated, and was rarely observed to be within two to three meters from the surface. Further, the degree of weathering observed in the upper several meters of the Columbia formation suggests that it has a low potential for liquefaction.

The deposits along the Delaware River are late Pleistocene to Holocene age alluvial and estuary sediments. Most are members of the Pensauken and Cape May Formations. These deposits consist of sands, gravels, silts and marsh deposits. In general, the water table was found to be very shallow. The liquefaction potential of the sands was judged to be very high. Although, exposures are limited, several large sand and gravel operations were evaluated. At higher elevations than the alluvial and estuary sands discussed above, the Pensauken Formation is present. These deposits are thought to be Pleistocene in age and are found on high terraces and capping hills and drainage divides. They consist primarily of sands and gravels. Numerous pre-existing exposures of Pensaukin were identified and visited. In

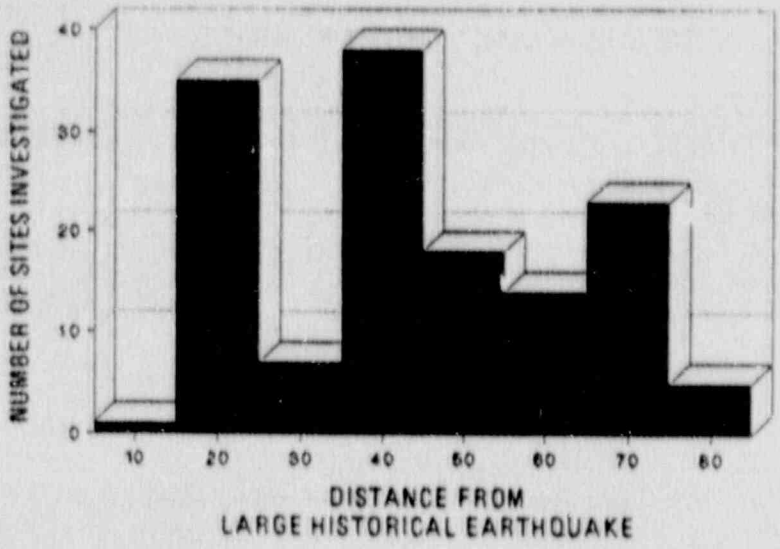

FIGURE 9.3: Proximity of potential liquefaction sites investigated in the Wilmington, Delaware study area with respect to the location of the October, 1871 MM intensity VII earthquake.

general, the depth to the water table within Pensaukin deposits was found to be more than 3 meters and given the composition and relative looseness of these materials the liquefaction potential of the sands was judged to be moderate to low. The distribution of potential liquefaction sites evaluated during this reconnaissance study is presented in Figure 9.1. The proximity of these sites to the intensity VII historical earthquake of October 1871 is shown in Figure 9.3.

9.3 Results of Reconnaissance Search

To date, no evidence of SIL has been found in either the central Virginia or Wilmington, Delaware areas. However, it must be stressed that potentially liquefiable deposits are not pervasive in these areas and existing exposures are somewhat limited, especially within 40 km of the larger historical events. Further, while the results of control studies as well as the work of Obermeier and others (1986) found that beach and near-shore marine deposits are most favorable for the generation and preservation of liquefaction features, most of the potentially liquefiable deposits in the central Virginia area are fluvial in origin, and the sources of those in the Wilmington area are fluvial and estuary. Furthermore, many of the deposits closest to the historical earthquakes are recent overbank deposits that are geologically very young (probably less than several thousand years in age). Given their age these units could not provide SIL data on early to mid Holocene seismicity which could have occurred prior to their deposition. The negative results of our search for SIL features in this area must be viewed with these limitations in mind.

10.0 ATLANTIC SEABOARD SEARCH AREA

A detailed search for evidence of prehistoric earthquakes has been implemented along the Atlantic seaboard. This search focused on late Quaternary beach and near-shore marine deposits. These units are most similar to the deposits in which, the great majority of SIL features in the Charleston area have been identified. Although no large earthquakes (other than the 1886 Charleston event) have been reported along this 1000 km stretch of the Atlantic seaboard, the potential for the generation and preservation of SIL evidence of large prehistoric earthquakes is very high. Furthermore, the extent of exposures, such as drainage ditches, sand and gravel quarries and borrow pits, allows for a fairly uniform search throughout this region, thus increasing the chance of discovering SIL features.

Investigations have been completed at over 1000 potential liquefaction sites, extending from the margins of the 1886 meizoseismal area southward to the Georgia/Florida state line, and northward to the Cape May peninsula of New Jersey (see Figure 10.1 for overview and Figures 10.2 through 10.5 for details). For ease in discussion the search region has been broken into four areas. The correlation of units between the four areas and how they relate to the control sites studies in the Charleston area is illustrated on Figures 10.6 and 10.7 (key references are listed in the explanation to this Figure). Also shown on Figure 10.7 is a breakdown of the number of potential liquefaction sites evaluated in each area. An overview of the number of sites evaluated and the distribution of sites with respect to their distance from the Charleston, S.C. area is presented in Figure 10.8. As illustrated, with the exception of the Delmarva and Cape May peninsulas (Area 4) where exposures are limited, a fairly uniform search has been completed throughout the region.

10.1 Area 1

Area 1 extends southward from the southern margin of the meizoseismal area of the 1886 earthquake to the Georgia/Florida state line. Over 350 sites were evaluated in this area. A breakdown by age is presented in Figure 10.9. The primary units studied were the Silver Bluff, Princess Anne, and Pamlico formations. SIL features have been identified at seven sites in Area 1. All are located within South Carolina, most near Bluffton and Hilton Head.

Historical accounts of the 1886 earthquake suggest that MM intensity VII to IX levels of ground motion occurred in the vicinity of these SIL sites (Figure 10.10). Although the exact locations were not noted, historical accounts suggest that during the 1886 event some scattered liquefaction associated with this earthquake may have occurred in the vicinity of the seven SIL sites identified (Seeber and Armbruster, 1981).

10.2 Area 2

Area 2 extends northward from the northern margin of the meizoseismal area of the 1886 earthquake to the Cape Fear Arch. Over 320 sites were evaluated in this

FIGURE 10.1: Distribution of potential liquefaction sites evaluated along the southeastern Atlantic Seaboard (dark shading). The lightly shaded regions lie within about 40 km of sites evaluated during this study. As noted in chapter 4, the great majority of the SIL features discovered in the Charleston area lie within 40 km of earthquake activity. Consequently, large prehistoric earthquakes within the lightly shaded regions could reasonably be expected to result in SIL in the dark shaded regions. However, it must be stressed that large earthquakes similar to the 1886 earthquake could have occurred in the unshaded regions without leaving their record in the unconsolidated deposits evaluated during this study.

---

area. The primary units studied included the Wando, Socassee and Talbot formations. A breakdown by age is presented in Figure 10.11. SIL features have been identified at seven sites in Area 2. Two additional sites in Area 2 have been reported by Obermeier and others (1987). However, these have not been independently confirmed during this study and will not be discussed further. Six of the seven SIL sites discovered are located in South Carolina, three in the general vicinity of Georgetown and three in the Myrtle Beach area. The seventh SIL site is located about 2 miles north of the SC/NC state line.

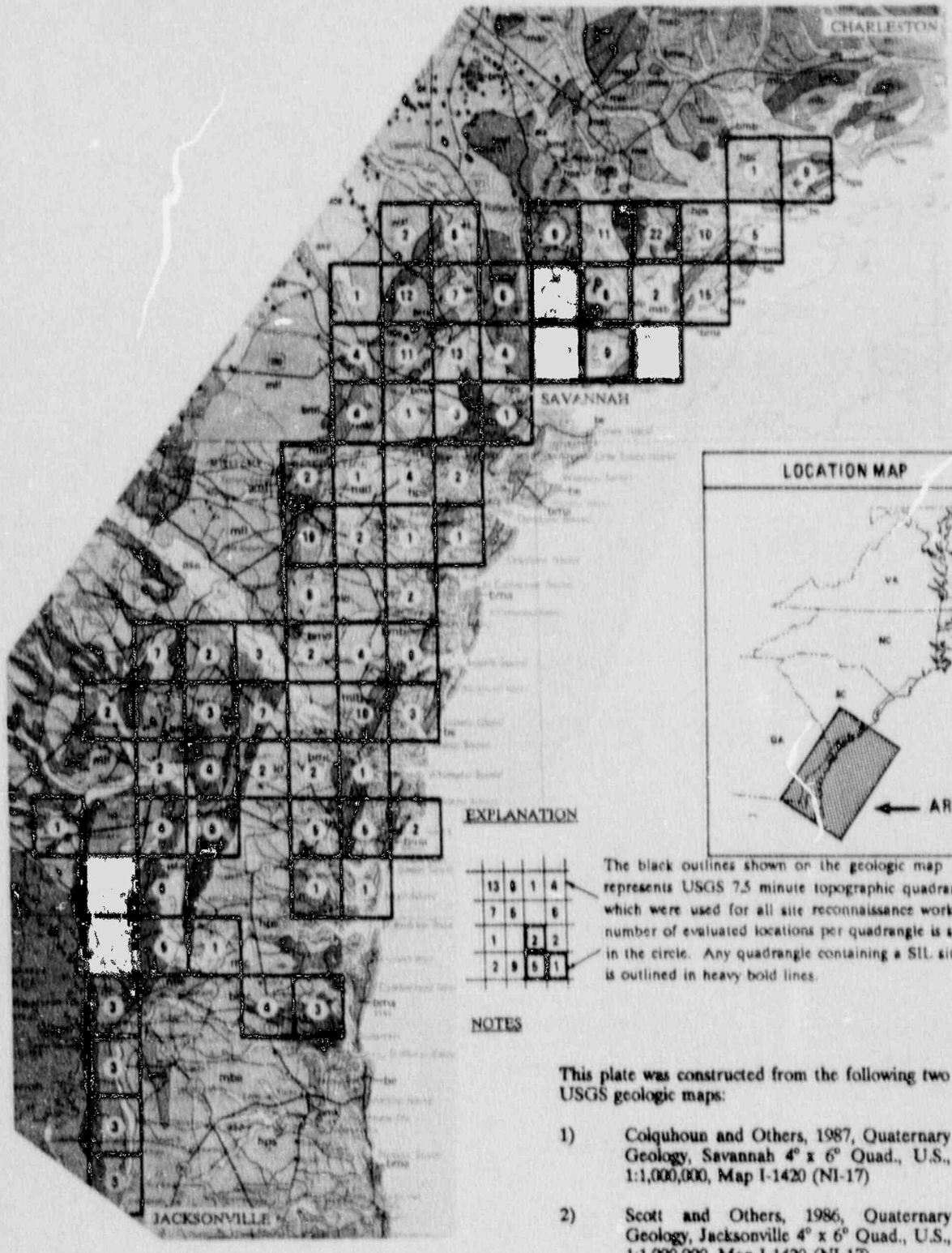
CHARLESTON
SAVANNAH
JACKSONVILLE
LOCATION MAP
VA
NC
SC
GA
AREA 1
EXPLANATION
13 0 1 4
7 6 6
1 2 2
2 9 5 1
The black outlines shown on the geologic map represents USGS 7.5 minute topographic quadrangles which were used for all site reconnaissance work. The number of evaluated locations per quadrangle is shown in the circle. Any quadrangle containing a SIL site is outlined in heavy bold lines.
NOTES
This plate was constructed from the following two USGS geologic maps:
1) Colquhoun and Others, 1987, Quaternary Geology, Savannah 4° x 6° Quad., U.S., 1:1,000,000, Map I-1420 (NI-17)
2) Scott and Others, 1986, Quaternary Geology, Jacksonville 4° x 6° Quad., U.S., 1:1,000,000, Map I-1420 (NI-17)
25 0 25 50
SCALE IN KILOMETERS

FIGURE 10.2

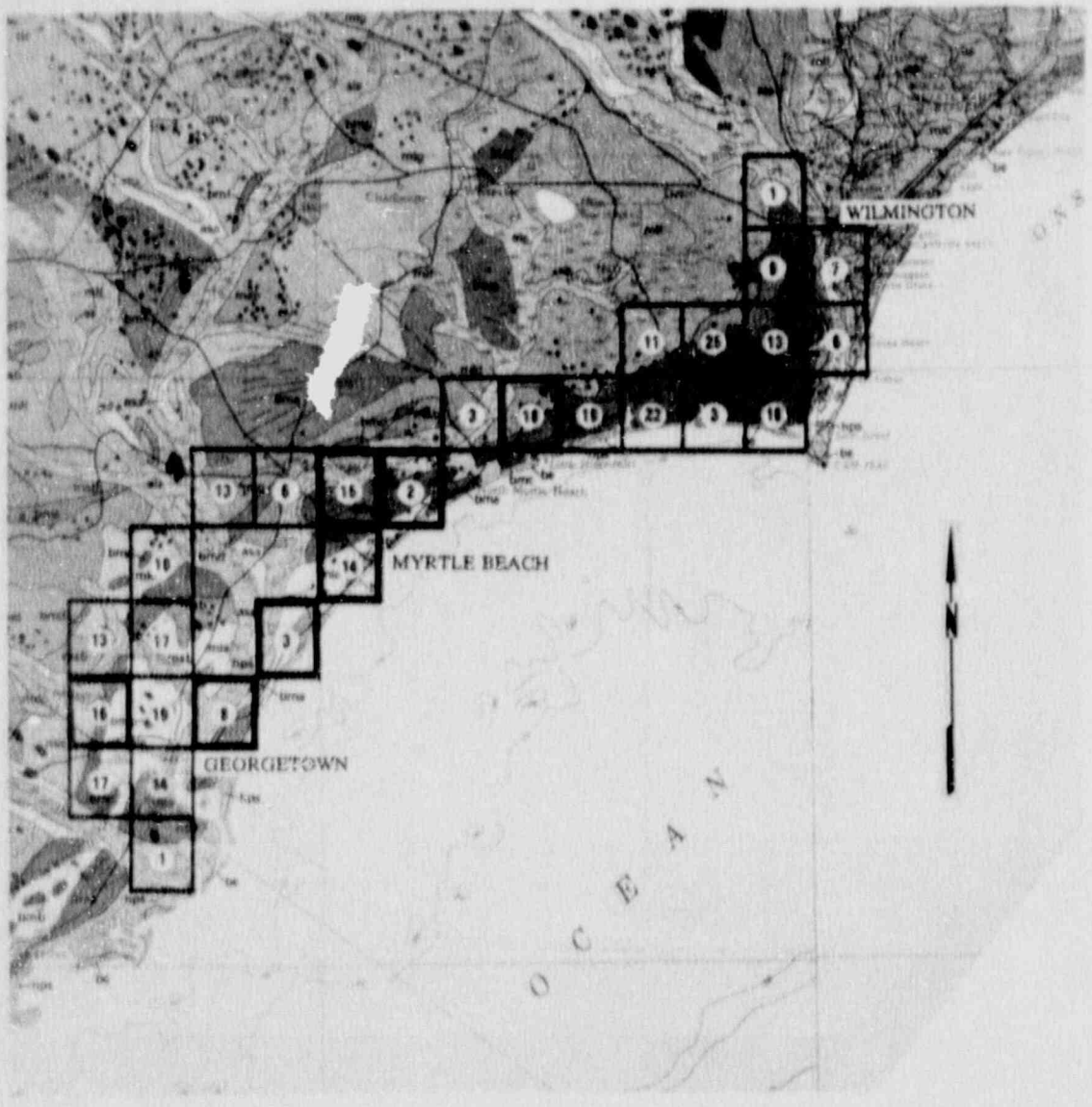

25 0 25 50
SCALE IN KILOMETERS

LOCATION MAP

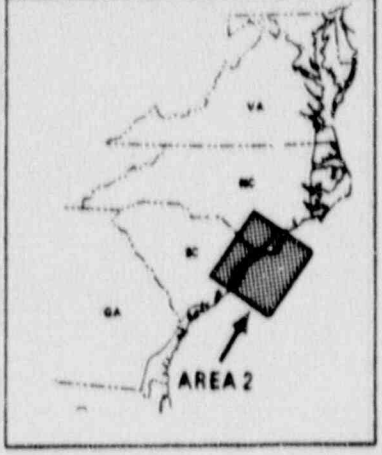

EXPLANATION

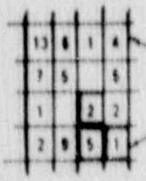

The black outlines shown on the geologic map represents USGS 7.5 minute topographic quadrangles which were used for all site reconnaissance work. The number of evaluated locations per quadrangle is shown in the circle. Any quadrangle containing a SIL site is outlined in heavy bold lines.

This plate was constructed from the following two USGS geologic maps:

1) Johnson and Peebles, 1986, Quaternary Geology, Hatteras 4° x 6° Quad., U.S., 1:1,000,000, Map I-1420 (NI-18).

2) Colquhoun and Others, 1987, Quaternary Geology, Savannah 4° x 6° Quad., U.S., 1:1,000,000, Map I-1420 (NI-17)

FIGURE 10.3

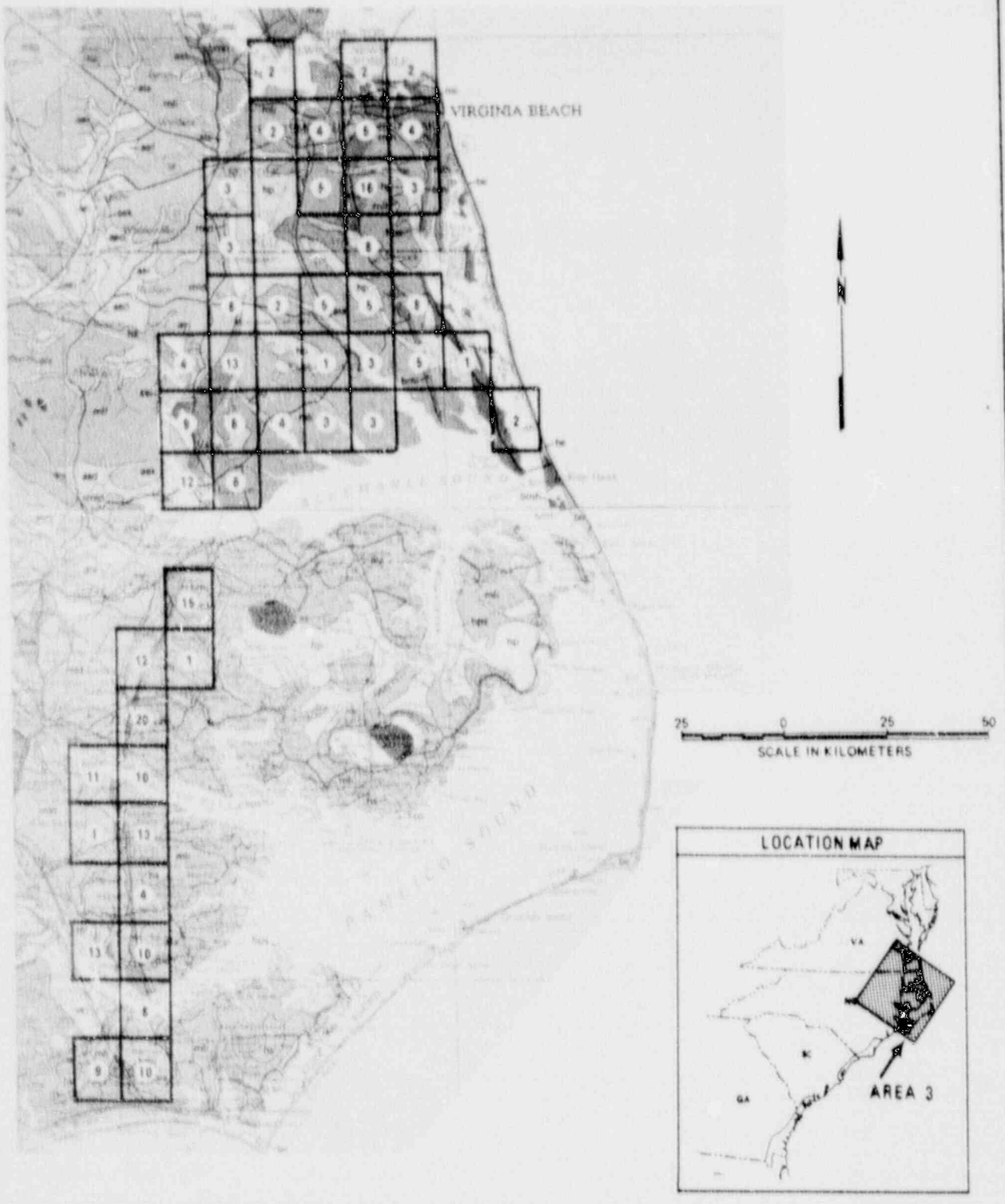

This plate was constructed from the following two USGS geologic maps:

1) Cleaves and Others, 1987, Quaternary Geology, Chesapeake Bay 4° x 6° Quad., U.S., 1:1,000,000, Map I-1420 (NJ-18)

2) Johnson and Peebles, 1986, Quaternary Geology, Hatteras 4° x 6° Quad., U.S., 1:1,000,000, Map I-1420 (NI-18)

EXPLANATION

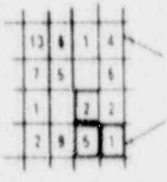

The black outlines shown on the geologic map represents USGS 7.5 minute topographic quadrangles which were used for all site reconnaissance work. The number of evaluated locations per quadrangle is shown in the circle. Any quadrangle containing a SIL site is outlined in heavy bold lines.

FIGURE 10.4

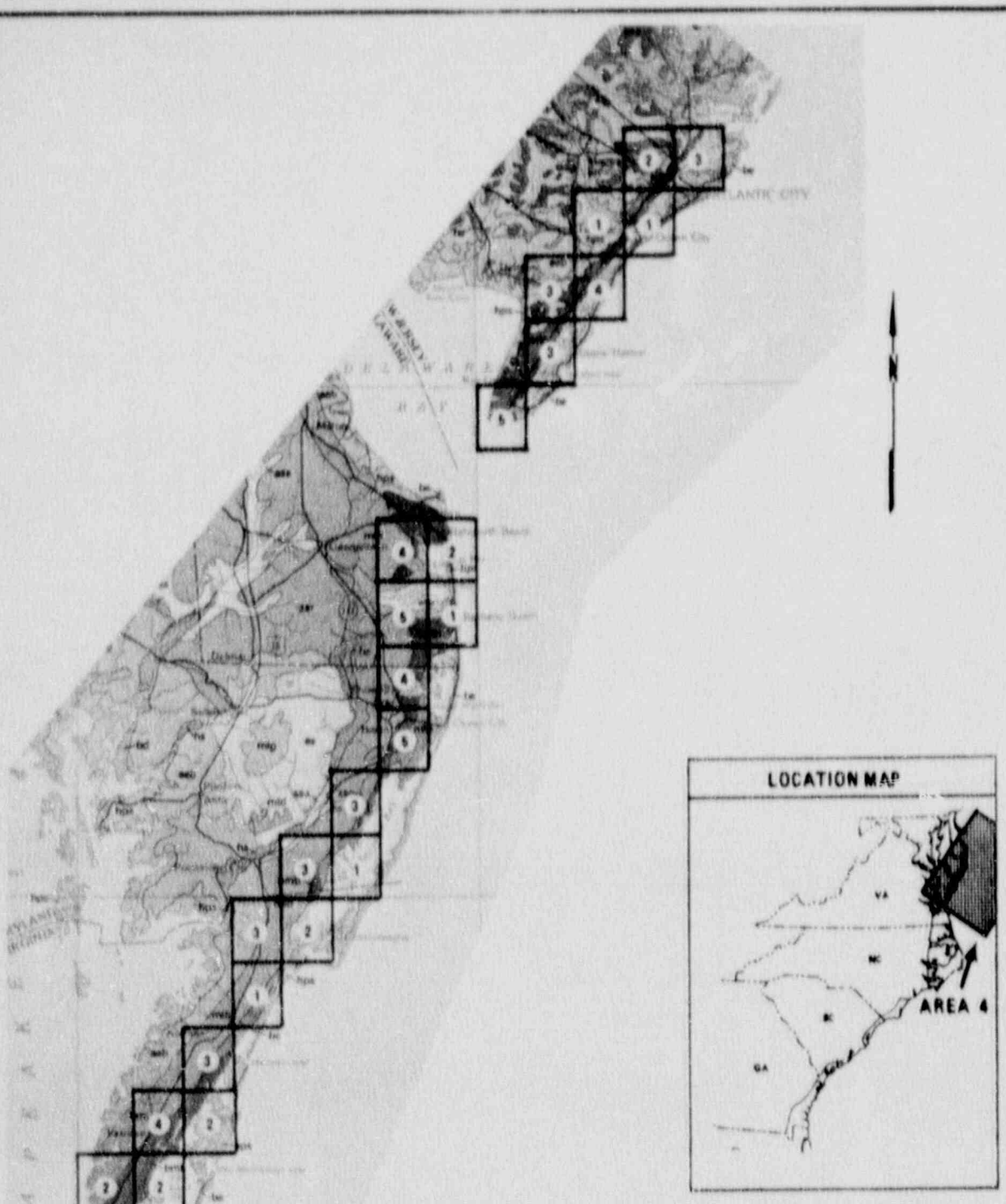

This plate was constructed from the following USGS geologic map:

1) Cleaves and Others, 1987, quaternary Geology, Chesapeake Bay 4° x 6° Quad., U.S., 1:1,000,000, Map I-1420 (NJ-18)

The black outlines shown on the geologic map represents USGS 7.5 minute topographic quadrangles which were used for all site reconnaissance work. The number of evaluated locations per quadrangle is shown in the circle. Any quadrangle containing a SIL site is outlined in heavy bold lines.

FIGURE 10.5

FLORIDA AND GEORGIA
SOUTH CAROLINA
NORTH CAROLINA
VIRGINIA, MARYLAND, DELAWARE AND NEW JERSEY

FIGURE 10.6

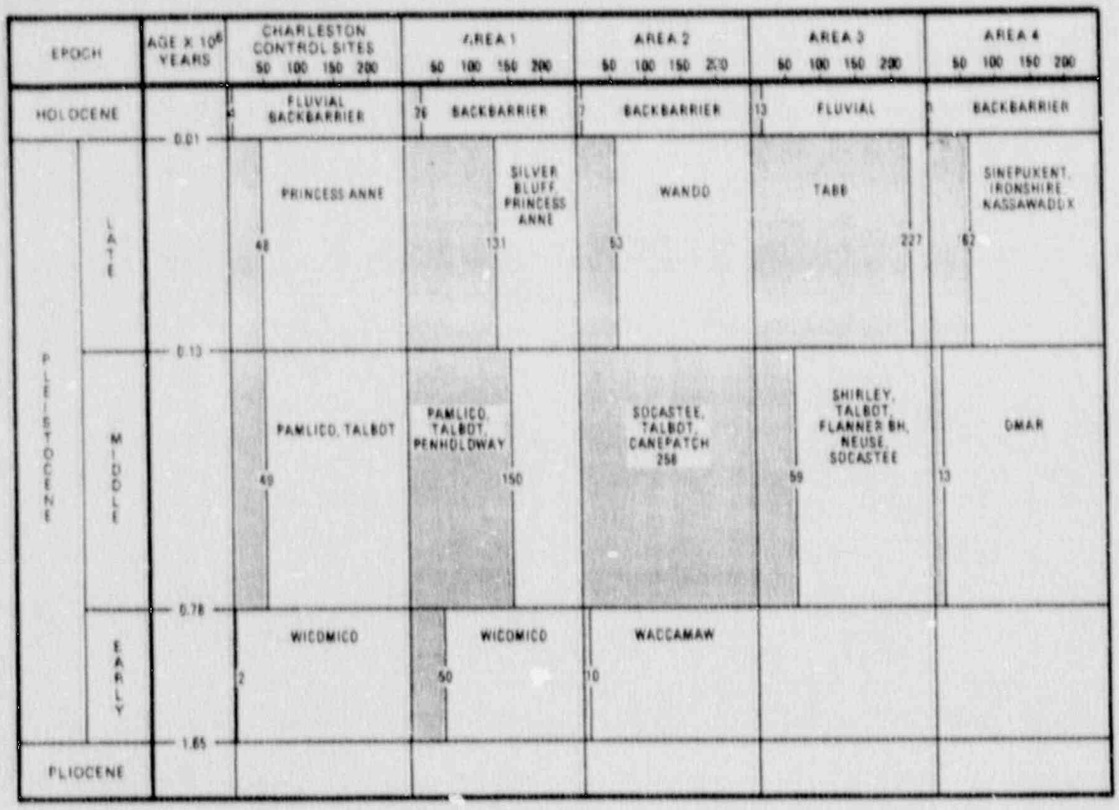

FIGURE 10.7: Correlation of units studied in the Charleston meizoseismal area and the four study areas evaluated along the Atlantic seaboard. Over 1000 potential liquefaction sites were evaluated. The search focused on mid to late Pleistocene beach deposits, which are most similar to those where SIL features occur in the Charleston area. Principal references include Colquhoun and others 1968, 1971, and 1981, Cooke (1943), Duban and others (1974, 1980), Johnson (1976), Johnson and Berquist (1984), Luddicoat and others (1982), McCartan and others (1982), Mixon and others (1982), Owens and Denny (1979), Peebles and others (1984), as reported in Richmond and others (1986a, 1986b, 1987a, and 1987b).

Historical accounts of the 1886 earthquake suggest that MM intensity VI to VIII levels of ground motion occurred in the vicinity of these SIL sites (Figure 10.5). Although their exact locations were not noted, historical accounts suggest that during the 1886 event some scattered liquefaction associated with this earthquake may have occurred in the vicinity of the three SIL sites identified in the Georgetown area (Seeber and Armbruster. 1981).

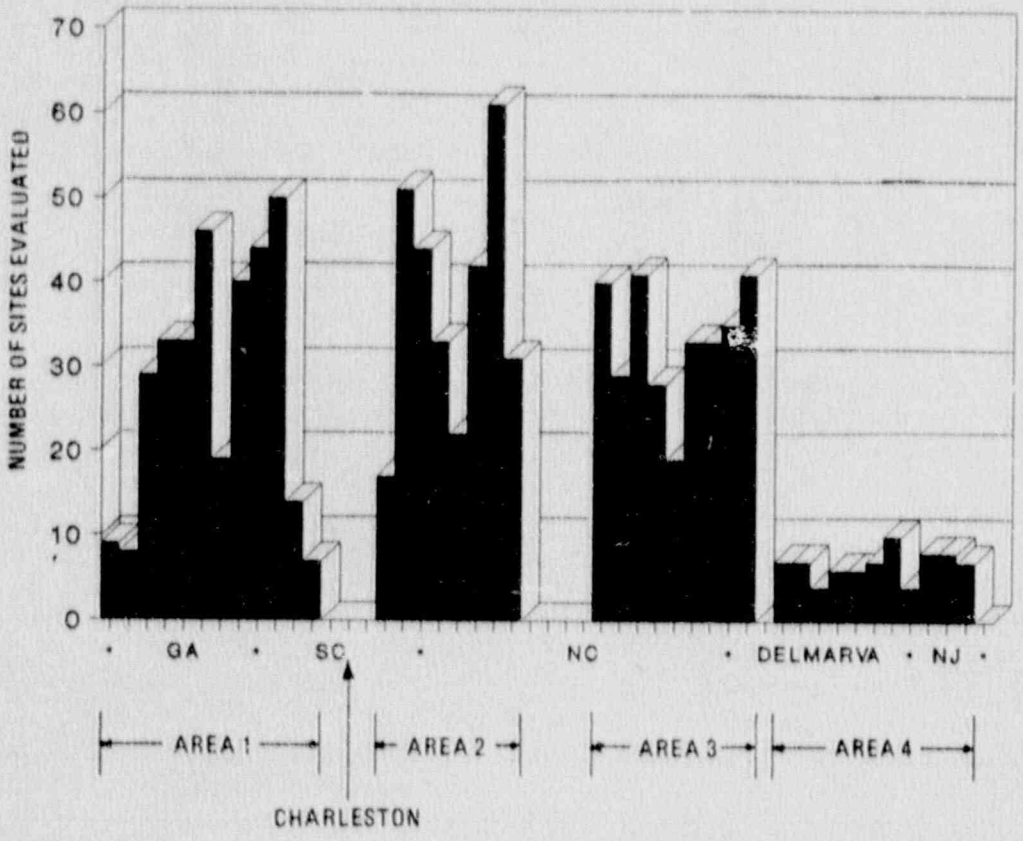

FIGURE 10.8: Distribution of potential liquefaction sites evaluated along the southeastern Atlantic Seaboard.

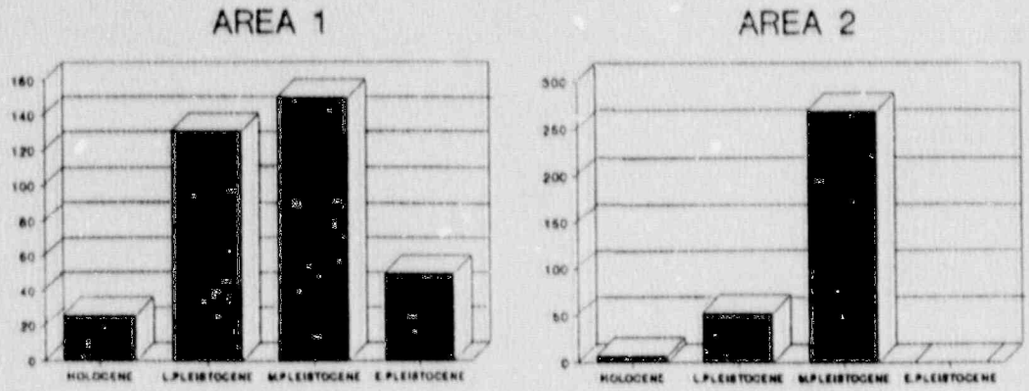

FIGURE 10.9: Number of potential liquefaction sites evaluated in Areas 1 and 2 broken down by age of deposits. A total of 357 sites were evaluated in Area 1. A total of 321 sites were evaluated in Area 2.

10.3 Area 3

Area 3 extends northward from the Cape Fear Arch to Chesapeake Bay. Approximately 300 sites were evaluated in this area. The primary units studies included the Tabb, Shirley and Flanner beach formations. A breakdown by age is presented in Figure 10.6. No SIL features have been identified in Area 3. Historical accounts of the 1886 earthquake suggest that MM intensity V to VI levels of ground motion occurred in this area during the 1886 Charleston earthquake.

10.4 Area 4

Area 4 extends northward from the Chesapeake Bay to an area just north of Atlantic City, N.J. The width of the Pleistocene beach complex in this area is much narrower than in Areas 1-3 and the total number of sites evaluated was limited to 76. Most of the sites evaluated are located in the late Pleistocene Sinnepuxent, Ironshire, Nassawadox, and Cape May formations. A breakdown by age is presented in Figure 10.11. Historical accounts of the 1886 earthquake suggest that MM intensity IV levels of ground motion occurred in this area during the Charleston earthquake.

While no SIL features have been identified in Area 4, unusual soil deformation structures were discovered on the Cape May peninsula. Although these features are similar in morphology to those found and described as SIL features at the Hain quarry in Connecticut (Thorson et al., 1986), evidence from this study would suggest that they are not the result of past earthquake activity.

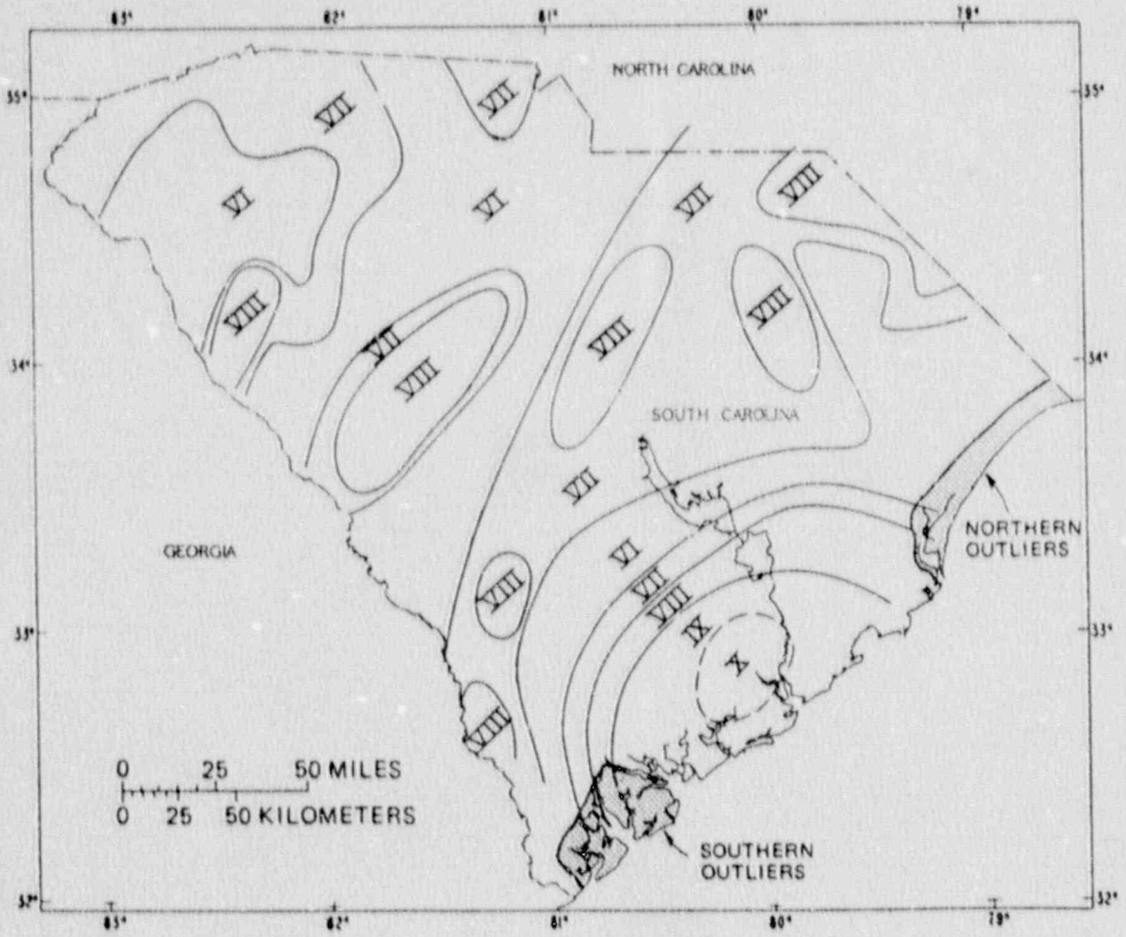

FIGURE 10.10: Isoseismal data for the 1886 earthquake within South Carolina. The general location of both northern and southern outlying liquefaction sites are also shown (modified from Bollinger, 1977).

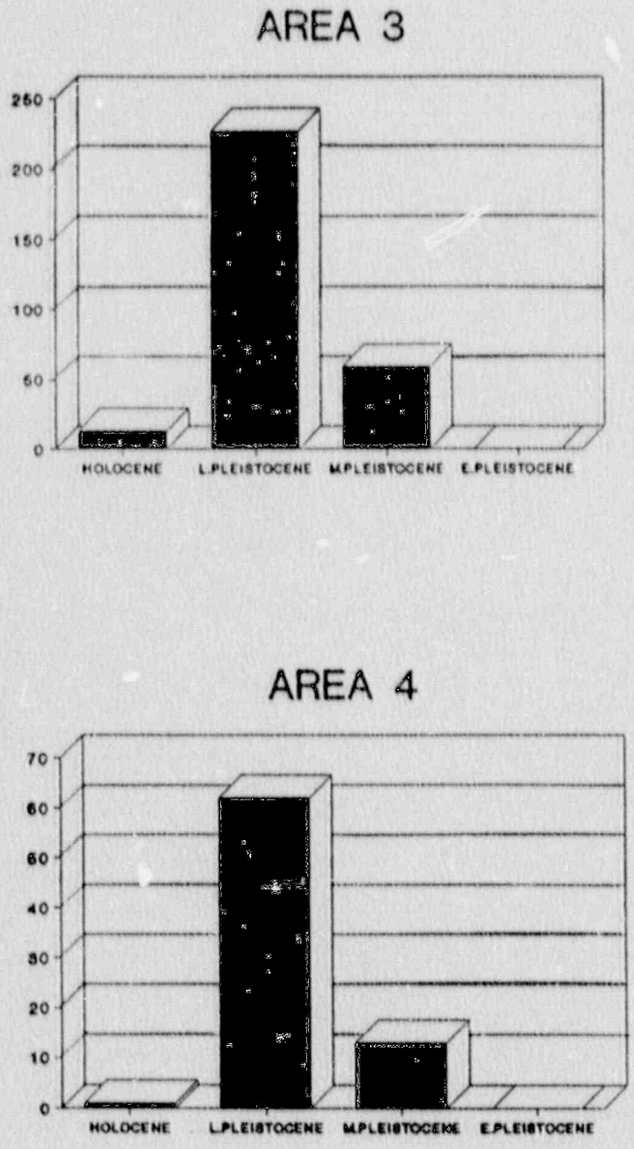

FIGURE 10.11: Number of potential liquefaction sites evaluated in Areas 3 and 4 broken down by age of deposits. A total of 299 sites were evaluated in Area 3. Only 76 sites were evaluated in Area 4 due to limited exposures in the beach ridge deposits in this area.

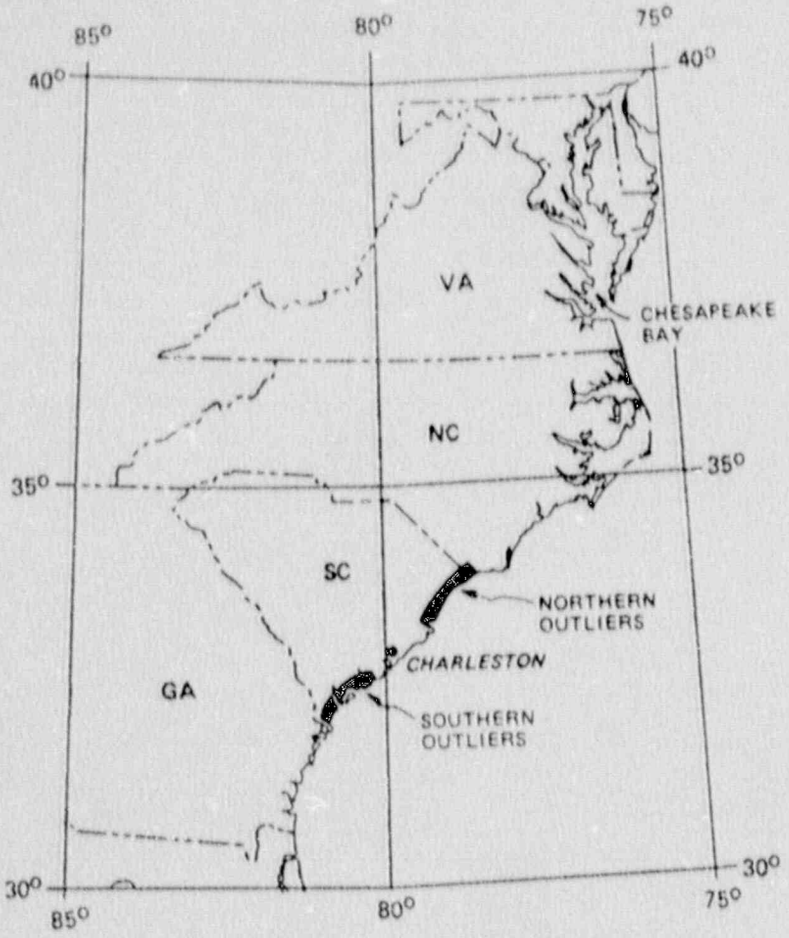

FIGURE 10.12: General location of outlying liquefaction sites discovered during this study. See Figure 11.1 for detailed locations.

10.5 Summary of Findings

Although suitable sites have been investigated throughout the region, liquefaction features have been found almost exclusively in South Carolina (Figure 10.12). These sites are located well to the south and north of the 1886 meizoseismal area and are referred to as "outliers". At most outlying sites, multiple liquefaction features representing two or more liquefaction episodes have been identified. The results of detailed studies at selected outlying sites are discussed in Chapter 11.

11.0 EVALUATION OF OUTLYING LIQUEFACTION SITES

As discussed in Chapter 10, liquefaction features were found almost exclusively in South Carolina (the lone exception discovered during this investigation is located just north of the S.C./N.C. state line). Of these, a total of 15 liquefaction sites were discovered well outside the meizoseismal area of the 1886 earthquake. At most of these "outlying sites", multiple liquefaction features representing two or more liquefaction episodes were identified. The locations of these outlying sites are presented on Figure 11.1. As shown, they occur both north and south of the Charleston, S.C. area. Also shown for reference purposes on Figure 11.1 are the Hollywood and Ten Mile Hill sites which were previously discussed in Chapter 8.

Detailed studies were conducted at selected northern and southern outlying liquefaction sites. Organic samples were collected and analyzed using radiocarbon dating techniques to determine the age of these outlying liquefaction features and to allow for comparison with the ages of paleoliquefaction episodes identified in the Charleston area. The results of radiocarbon age dating are presented in Tables 11.1 and 11.2 for the northern and southern sites respectively.

11.1 Northern Outlying Liquefaction Sites

A total of eight liquefaction sites were identified north of the Charleston meizoseismal area. From north to south they are referred to as: Calabash, Henry Road, Myrtle, Martin Marietta, Harbor, Georgetown, Olin, and Sampit. Three of these sites (Myrtle, Georgetown, and Olin) were originally discovered by investigators from the U.S. Geologic Survey (Obermeier and others, 1987). During this study these same general locales were reinvestigated and at each site additional liquefaction features were discovered. It should be noted that subsequent discussions have not addressed the reported liquefaction sites located farther from Charleston near Conway, S.C. and Southport, N.C. These sites were also reported by Obermeier and others (1987), however, they were not independently confirmed during this study.

Detailed investigations were conducted at five northern liquefaction sites. These included the Myrtle, Martin Marietta, Georgetown, Olin, and Sampit sites. The results of these field activities are presented below.

Myrtle: This is the northernmost of the sites evaluated in detail and covers several thousand acres. Within these lands, liquefaction features were identified at three different locales. Most features exhibit many of the morphological characteristics of sand-blow explosion craters, but are smaller - about one meter or less in width. Based on the degree of staining and the thickness of the overlying soil profiles, none are thought to have been associated with the 1886 earthquake. Radiocarbon data as well as the qualitative assessment of features based on relative degree of staining and thickness of overlying soil profiles suggest at least two liquefaction episodes.

TABLE 11.1
NORTHERN LIQUEFACTION EPISODES

LIQUEFACTION EPISODE N-1 (AGE 500 ±100 YBP)				
SITE	AGE (YBP) MINIMUM	CONTEMP	MAXIMUM	SOURCE
SAMPIT		504±97		This study

LIQUEFACTION EPISODE N-2 (AGE 1100±200 YBP)				
SITE	AGE (YBP) MINIMUM	CONTEMP	MAXIMUM	SOURCE
SAMPIT		940±80		This study
		907±79		This study
		1380±175		This study
		969±80		This study

LIQUEFACTION EPISODE N-3 (AGE 1800±200 YBP)				
SITE	AGE (YBP) MINIMUM	CONTEMP	MAXIMUM	SOURCE
SAMPIT	1232± 75			This study
	1955± 75			This study
	1690±220			This study
			2385±170	This study
			2355±250	This study
MYRTLE			1465±290	This study
		1700±250		Weems and Obermeier (1990)
MARIETTA		1820±180		This study
			1860±200	This study
GEORGETOWN				
	210±170			This study
	1200±110			This study
	1360±110			This study
	1050±190			This study
			2570±100	Weems and Obermeier (1990)
OLIN	1360±110			This study
	1150±190			This study
		1647±390		
			1600±100	Weems and Obermeier (1990)
			2197±200	This study
			2697± 84	This study

LIQUEFACTION EPISODE N-4 (AGE >4575 YBP)				
SITE	AGE (YBP) MINIMUM	CONTEMP	MAXIMUM	SOURCE
MYRTLE	4575±350			This study

TABLE 11.2
SOUTHERN LIQUEFACTION EPISODES

LIQUEFACTION EPISODE S-1 (104 YBP)				
SITE	AGE (YBP) MINIMUM	CONTEMP	MAXIMUM	SOURCE
BLUFA		100 <200 107±61		This study This study This study

Based on Soil profiles also present at Colony Garden and Classie.

LIQUEFACTION EPISODE S-2 (AGE 600±100 YBP)				
SITE	AGE (YBP) MINIMUM	CONTEMP	MAXIMUM	SOURCE
BLUFA	275±105	605±160 570±100		This study This study Weems and Obermeier (1990)

LIQUEFACTION EPISODE S-3 (AGE 1100±200 YBP)				
SITE	AGE (YBP) MINIMUM	CONTEMP	MAXIMUM	SOURCE
COLONY		1066±75	1305±87	This study This study

LIQUEFACTION EPISODE S-4 (AGE 5100±500 YBP)				
SITE	AGE (YBP) MINIMUM	CONTEMP	MAXIMUM	SOURCE
MALPHEROUS	4620±195		5520±370	This study This study

Henry Road (several pre-1886 features)
Myrtle (N-3 and older)
Martin Marietta (N-3)
Georgetown (N-3 and others)
Otis (N-3, others)
Calabash (several pre-1886 features)
MYRTLE BEACH
Harbor (pre-1886)
GEORGETOWN
Sampit (N-1, N-2, N-3)
CHARLESTON
Ten Mile Hill (CH-1, CH-4, CH-5, CH-6, and others)
Hollywood Ditch (CH-1, CH-2, CH-3, CH-4, and others)
Colony Garden (S-1, S-3)
Bluffton G (several pre-1886)
Classic (S-1)
Malpherons (S-4 and others)
SAVANNAH
Bluffton A (S-1, S-2, others)
Bluffton B (several pre-1886)
Bluffton C (several pre-1886)
LOCATION MAP
25 0 25 50
SCALE IN KILOMETERS

FIGURE 11.1

Weems and Obermeier (1990) reported the recovery of a stem from one of the features located at this site. It was dated at 1700±250 YBP (W 5799). As discussed previously, the age of this type of sample is interpreted to be very close to the actual age of the liquefaction episode. At this same site, a humate clast was recovered from an adjacent feature. It yielded a radiocarbon age of 1465±290 (GX14996). This sample is interpreted to provide a maximum age constraint for this second feature. Given the resolution of these radiocarbon dates, these two samples could represent the same liquefaction episode. Alternately the 1465 YBP age could represent a later, albeit pre-1886 liquefaction episode.

A piece of "new burn" charcoal was recovered from the soil profile overlying a third liquefaction feature located at the Myrtle site. This sample yielded an age of 4575±350 YBP (GX15575) and based on its position in the soil profile above and overlying the feature it provides a minimum age constraint on the age of the liquefaction episode, and confirms that two or more liquefaction episodes are present at this site.

Martin Marietta: This site is located several kilometers south of the Myrtle site. At this locale, three liquefaction features were identified. A photograph of the largest and best defined is shown in Figure 11.2. The central vent is approximately 30 centimeters wide and could be traced to more than three meters below the present ground surface. The bedded sequence is about two meters wide.

Two organic samples were recovered from this feature. A piece of tree bark was collected from within the central vent. This sample was dated at 1820±180 YBP (GX14994), and is interpreted to provide an estimate of the actual age of the liquefaction episode. The second sample was a soil clast recovered from above the small clast zone. This clast was very rich in organic materials and yielded an age of 1860±200 YBP (GX15004). This sample is thought to provide a maximum age constraint on the age of liquefaction.

Georgetown: This site is located several tens of kilometers south of the Myrtle and Martin Marietta sites. At this locale at least four liquefaction features were identified. Each is associated with similar staining and overlying soil profiles. The features are generally larger than those observed at the two sites previously discussed. Weems and Obermeier (1990) report the recovery of charcoal from within one of these features. This sample was dated at 2570±100 YBP (W 5830) and is interpreted to provide a maximum age constraint on the age of liquefaction at this site. Three tree roots which cut the feature were recovered and dated during this study. These samples provide minimum age constraints on the time of liquefaction and yielded ages of 210±170 YBP (GX15192), 1200±110 YBP (14995), and 1360±110 YBP (15003).

Olin: This site is located about 50 kilometers southwest of the Myrtle site and about 20 kilometers southwest of the Georgetown site. During this study, several liquefaction features were evaluated at this site, including one previously studied by the USGS. The features at this site were comparable in size to those observed at

FIGURE 11.2: Photograph of SIL feature discovered at the Martin Marietta site. See ruler for scale. Note the staining of the sands within the feature and the overlying soil profile. Also note the fracture that runs from the upper left to lower right portions of the photograph and recall the discussions in Chapter 5 about heaving of H_2 materials. Two organic samples were recovered from this feature - their location are identified by the arrows. A piece of tree bark was collected from the central vent (lower right). This sample was dated at 1820$\pm$180 YBP (GX14994), and is interpreted to provide an estimate of the actual age of the liquefaction episode. The second sample was soil clast recovered from above the small clast zone (upper left). This clast was very rich in organic materials and yielded an age of 1860$\pm$200 YBP (GX15004). This sample is thought to provide a maximum age constraint on the age of liquefaction.

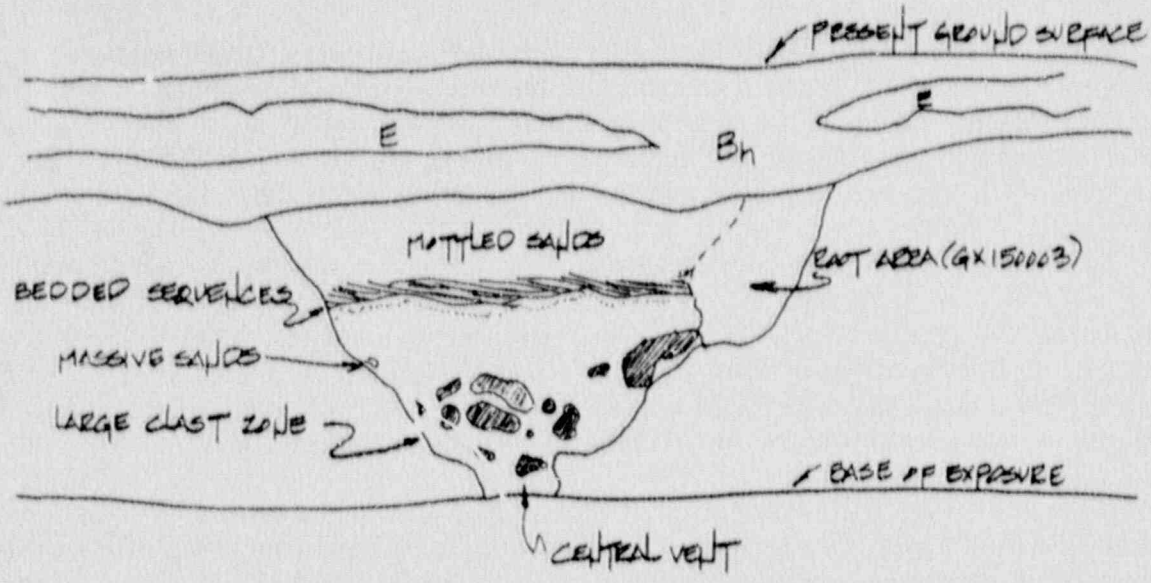

FIGURE 11.3: Sketch of SIL feature discovered at the Georgetown site. At this locale at least four liquefaction features were identified. Each is associated with similar staining and extensive overlying Bh and E soil profiles. Weems and Obermeier (1990) report the recovery of charcoal from within one of these features. This sample was dated at 2570±100 YBP (W 5830) and is interpreted to provide a maximum age constraint on the age of liquefaction at this site. Three tree roots which cut the feature were recovered and dated during this study. These samples provide minimum age constraints on the time of liquefaction and yielded ages of 210±170 YBP (GX15192), 1200±110 YBP (14995), and 1360±110 YBP (15003).

---

the Georgetown site. The bedding sequences of the larger features are about two meters in width. Based on the degree of staining and the thickness of the overlying soil profiles none were associated with the 1886 earthquake.

Weems and Obermeier (1990) reported the recovery of a piece of charcoal from one of these features that was dated at 1600±100 (W 5827). As discussed previously unless "new burn", the age of charcoal is interpreted to provide a maximum age constraint on the age of the liquefaction episode. At this same site, five additional samples were collected from a single liquefaction feature. Two samples were from a tap root of a tree which cut and disrupted the right side of a crater, clearly postdating its formation. These two samples yielded ages of 1150+190 YBP (GX15006) and 1360±110 YBP (GX14992) and provide a minimum age constraint on the age of liquefaction. A sample of tree bark was recovered from within the feature. This sample was dated at 1647±390 YBP (GX15199) and provides an estimate of the actual age of liquefaction. Two samples of charcoal were also recovered from within the feature and yielded dates of 2197±200 YBP (GX15005) and 2697±84 YBP (GX14993). They were not new burn and thus provide maximum age constraints on the age of the liquefaction episode. Given the resolution of the dates, the five samples collected during this study and the charcoal sample collected by Weems and Obermeier (1990) probably represent the same liquefaction episode.

Sampit: This site is the southernmost of the northern outlying liquefaction sites. It is located adjacent to and south of the Olin site, about 100 kilometers northeast of Charleston. Based on the degree of staining and the thickness of overlying soil profiles, several generations of liquefaction features are present at this site. They are similar in size to those observed at the Georgetown and Olin sites.

The feature with the thinnest overlying soil profile at the Sampit site is shown in Figure 11.4. Note the light color of the sands within the feature and the very thin overlying soil profile. Qualitatively, these observations suggest a relatively young age. Tree bark recovered from within this feature yielded an age of 507±97 YBP (GX15206), consistent with these observations. This type of sample is interpreted to give a very good estimate on the age of the liquefaction episode.

Two other liquefaction features at the Sampit site are shown on Figure 11.5. Based on the degree of staining and the thickness of the overlying soil profiles, both features appear to be older than the feature shown on Figure 11.4. However, of the two liquefaction features shown on this figure, the feature on the right has a thinner overlying soil profile and less staining than the feature on the left, suggesting that it may be the younger of the two. Three samples of tree bark were recovered from the feature on the right, two from near the base of the main crater and one from the smaller crater that is contained within the main crater. The bark taken from the base of the large crater yielded an AMS age of 940±80 YBP (GX15202) and an adjacent sample yielded a Beta age of 1380±175 YBP (GX15579). The differences in AMS vs Beta dates is discussed further in Appendix B. The bark recovered from the smaller crater-like feature yielded an AMS age of 907±79 YBP (GX15200). This type of sample is interpreted to give a very good estimate on the age of the liquefaction episode.

Whether the small crater within the main crater represents liquefaction associated with an aftershock, an earthquake occurring several decades later, or merely represents a small slump feature associated with dewatering of the large feature can not be determined on the basis of these radiocarbon data. However, field studies tend to support the latter hypothesis.

A small root was cut by the feature shown on the left side of Figure 11.5. It yielded an age of 1232±77 YBP (GX15000). Given the resolution of age constraints established for the feature on the right and the dark staining and thicker overlying soil profile of this feature, the feature on the left is thought to represent an older liquefaction episode.

The feature with the thickest overlying soil profile discovered at this site is shown in Figure 11.6. This feature is also extremely stained, suggesting that is older than the feature shown on Figure 11.4 and the feature shown on the right of Figure 11.5. Four organic samples were collected and dated from this feature. One sample was a root which had grown into the feature after its formation. This sample yielded an age of 1955±75 YBP (GX15189) and provides a minimum age constraint on the age of liquefaction. A sample of wood recovered from the bedded sequence was

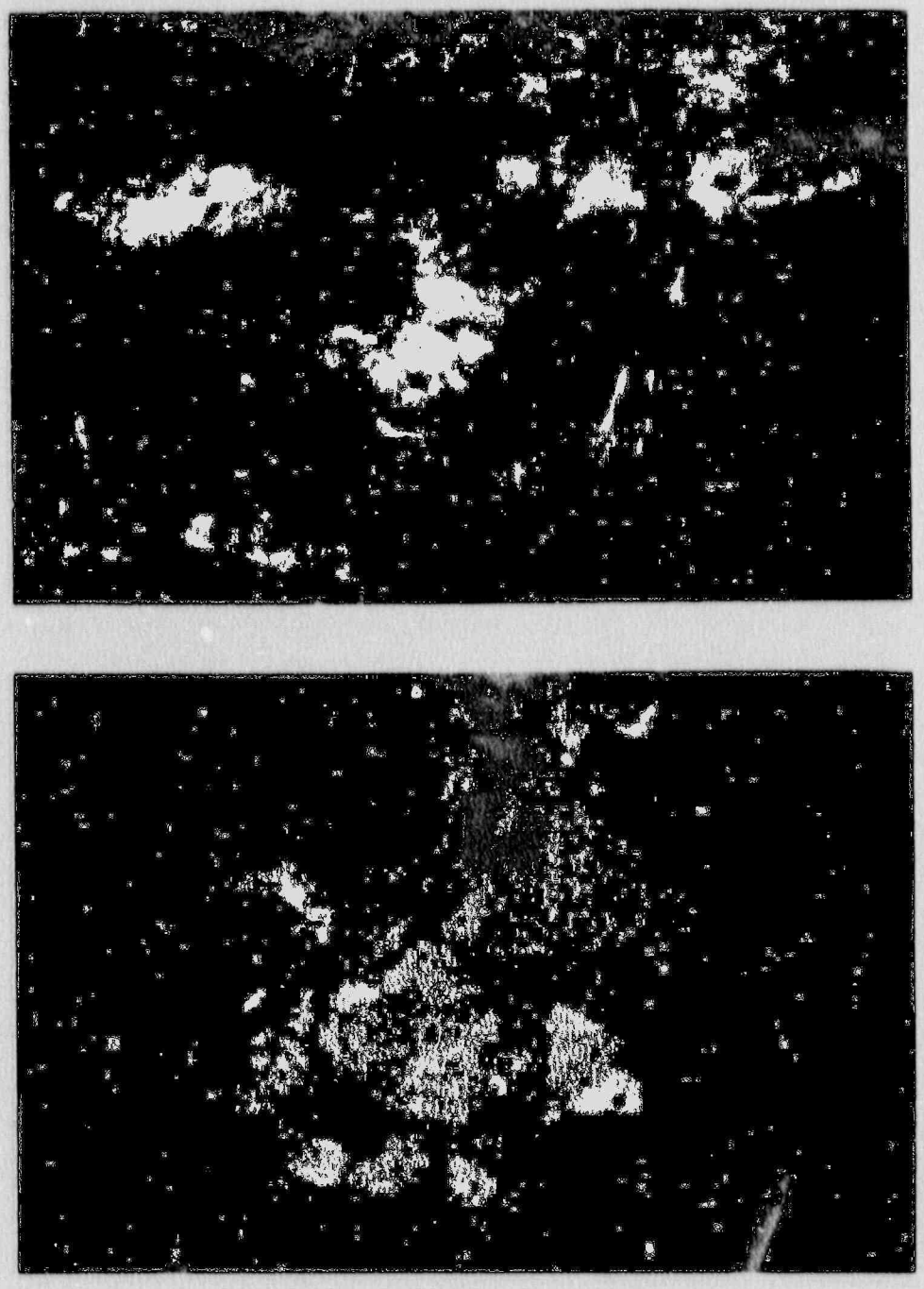

B

FIGURE 11.4: Photograph of very "young" SIL feature located at the Sampit site. Note the thin overlying soil profile and the light color of the sands within the feature. The arrow in photograph B shows the location of a small piece of tree bark that was recovered from within this feature. It yielded a radiocarbon age of 507±97 YBP (GX15206).

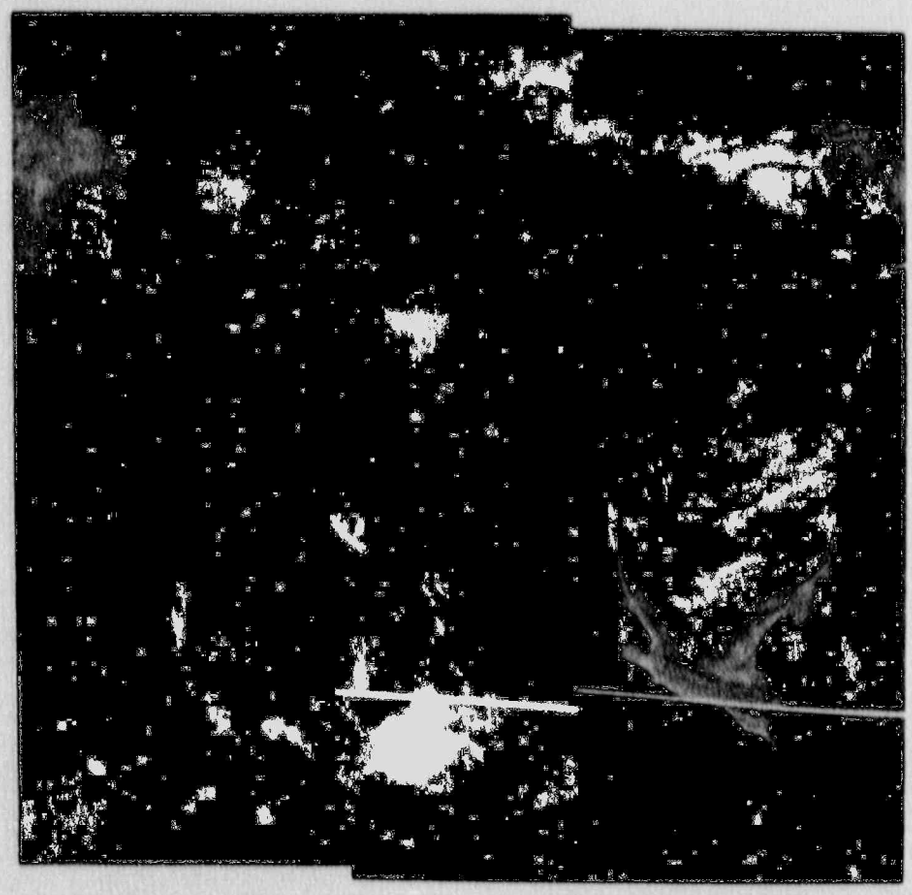

FIGURE 11.5: Photograph of two SIL features located at the Sampit site. Both features appear to be older than the feature shown on Figure 11.4. Arrows show the location of samples collected for radiocarbon dating. Three samples of tree bark were recovered from the feature on the right, two near the base of the main crater and one from the smaller crater that is contained within the larger crater. The bark taken from the base of the large crater yielded an AMS age of 940±80 YBP (GX15202) and an adjacent sample yielded a Beta age of 1380±175 YBP (GX15000). The bark recovered from the smaller crater-like feature yielded an AMS age of 907±79 YBP (GX15200). This type of sample is interpreted to give a very good estimate on the age of the liquefaction episode. A small root cut by the feature on the left yielded an age of 1232±77 YBP (GX15000). Given the resolution of age constraints established for the feature on the right and the dark staining and thicker overlying soil profile of the feature on the left, it is thought that they represent two different liquefaction episodes. Also note that the feature on the right includes a small crater contained within a larger crater. Whether the small crater represents liquefaction associated with an aftershock, an earthquake occurring several decades later, or merely represents a small slump feature associated with dewatering of the large feature can not be determined on the basis of these radiocarbon data. However, field studies tend to support the later hypothesis.

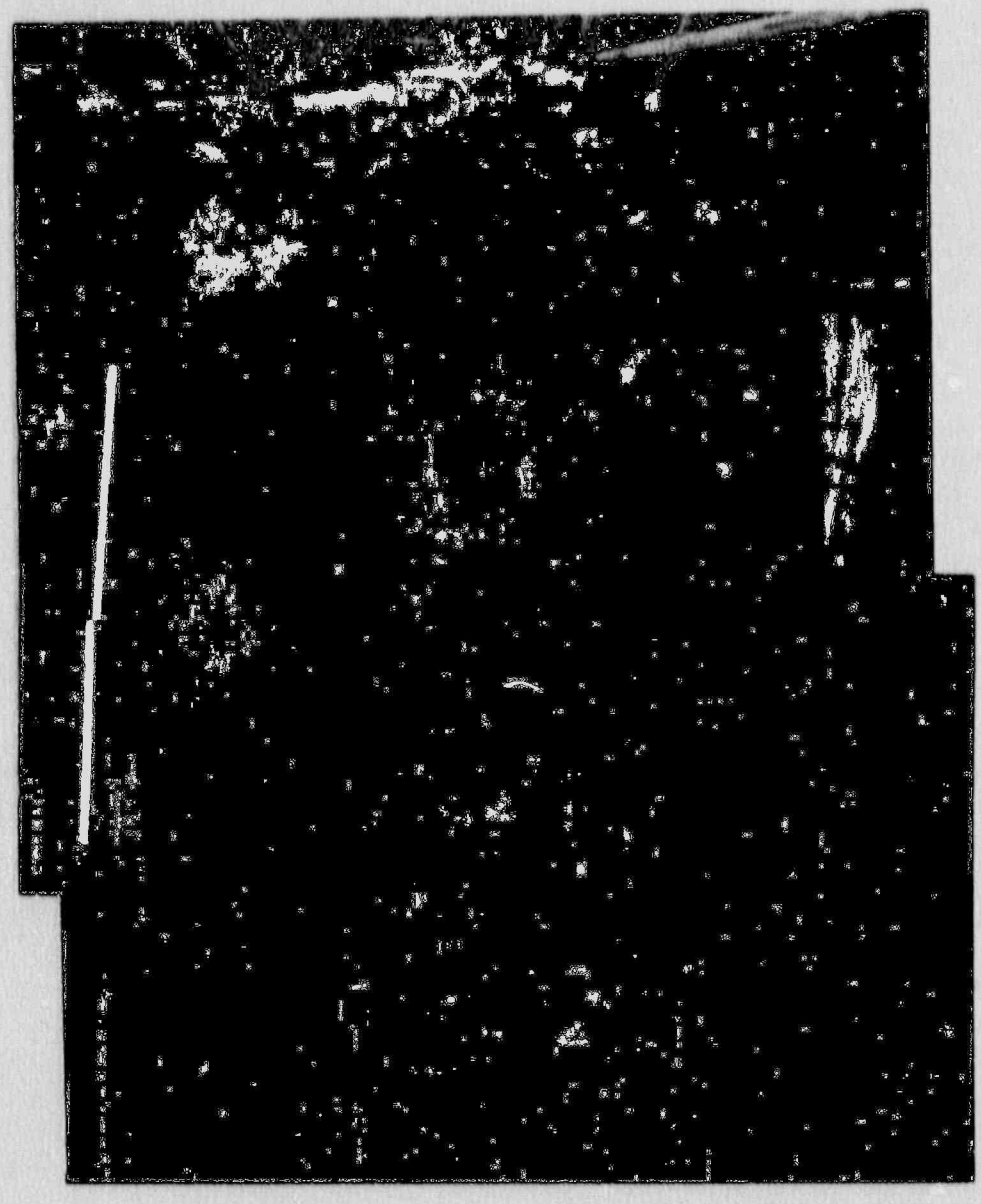

FIGURE 11.6: Based on the degree of staining and the thickness of the overlying soil profile this is a photograph of the "oldest" SIL feature discovered at the Sampit site. Four organic samples were collected and dated from this feature. One sample taken from the lower portion of the feature was a root which had grown into the feature after its formation. This sample yielded an age of 1955±75 YBP (GX15189) and provides a minimum age constraint on the age of liquefaction. A sample of wood recovered from the bedded sequence was dated at 1690±220 YBP (GX15199) and provides an estimate of the actual age of liquefaction. Two samples of charcoal were also recovered from within the feature and yielded dates of 2285±170 YBP (GX14998) and 2455±250 YBP (GX15001). They were not new burn and thus provide maximum age constraints on the age of the liquefaction episode.

dated at 1690±220 YBP (GX15199) and provides an estimate of the actual age of liquefaction. Two samples of charcoal were also recovered from within the feature and yielded dates of 2285±170 YBP (GX14998) and 2455±250 YBP (GX15001). They were not new burn and thus provide maximum age constraints on the age of the liquefaction episode.

Summary for Northern Sites: Based on the ages of organic samples collected from five northern outlying liquefaction sites, four liquefaction episodes may have occurred in this area during Holocene times. From youngest to oldest they are referred to as episodes N-1 through N-4. Liquefaction episodes N-1 and N-2 are based on the ages of liquefaction features discovered exclusively at the Sampit site. It is the southernmost of the northern outlying liquefaction sites and therefore is closest to the Charleston source area. Liquefaction episodes N-1 and N-2 have not been identified at any of the other northern liquefaction sites. In contrast, liquefaction episode N-3 is based on data from these five widely dispersed northern outlying liquefaction sites, and is dated at 1800±200 YBP. Liquefaction episode N-4 is based on limited radiocarbon data from the Myrtle site. Some of the features at this site are extremely stained and have very thick overlying soil profiles. A minimum age of about 4520±250 YBP has been determined for one such feature (Table 11.1). To date, no features of this age have been found at any of the northern outlying liquefaction sites located between this site and Charleston. Of the four northern liquefaction episodes proposed it is the least constrained.

11.2 Southern Liquefaction Locales

A total of seven liquefaction sites were identified south of the Charleston meizoseismal area. From north to south they have been named: Colony Gardens, Bluffton Golf, Bluffton A, Bluffton B, Bluffton C, Malpherous, and Classie. Two of these sites (Bluffton A and Bluffton B) were originally discovered by investigators from the U.S. Geological Survey (Obermeier and others, 1987).

Detailed investigations were conducted at five of these southern liquefaction sites. These included from north to south: Colony Garden, Bluffton A, Bluffton B, Malpherous, and Classie. The results of these field activities are presented below.

Colony Gardens: This is the closest of the southern liquefaction sites to Charleston. Several liquefaction features were identified at this site. The largest is approximately three meters in width, comparable in size to some of the larger SIL features discovered at the Ten Mile Hill site. Based on the degree of staining and the thickness of the overlying soil profile, at least two generations of liquefaction are present.

One feature at this site was virtually unstained and associated with only a very thin overlying soil profile. A sketch of this feature is presented as Figure 11.7. Leaves recovered from within this feature yielded a modern radiocarbon date. However, the sample came from an exposed face and could have washed into the

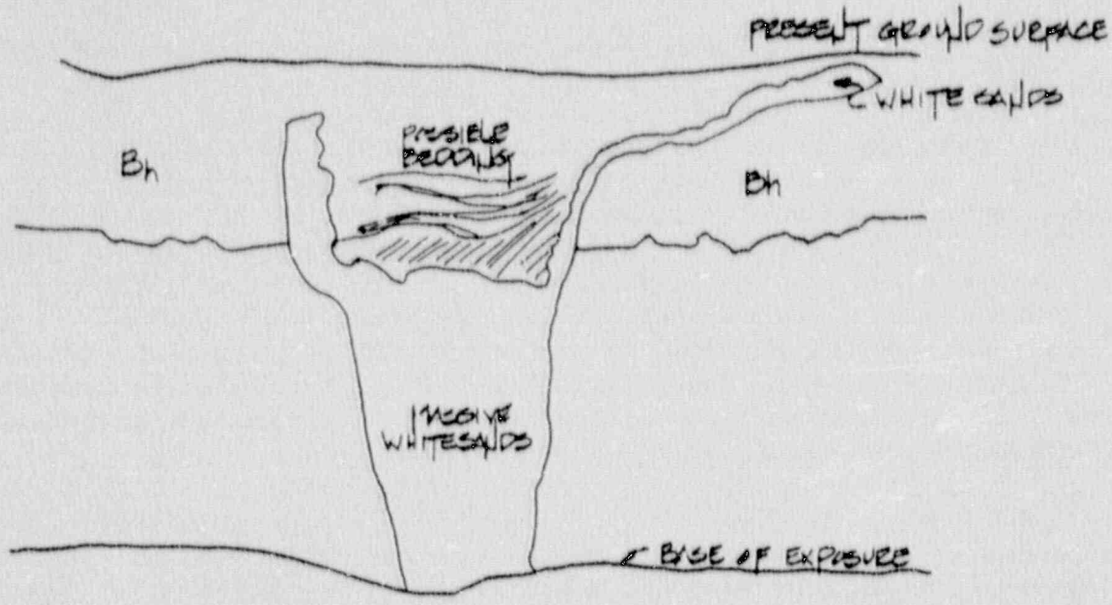

Figure 11.7: Sketch of "young" SIL feature discovered at the Colony Gardens site. This feature exhibits little or no staining of the vented sands and has only a very thin overlying soil profile. Qualitatively, these observations suggest a relatively young age.

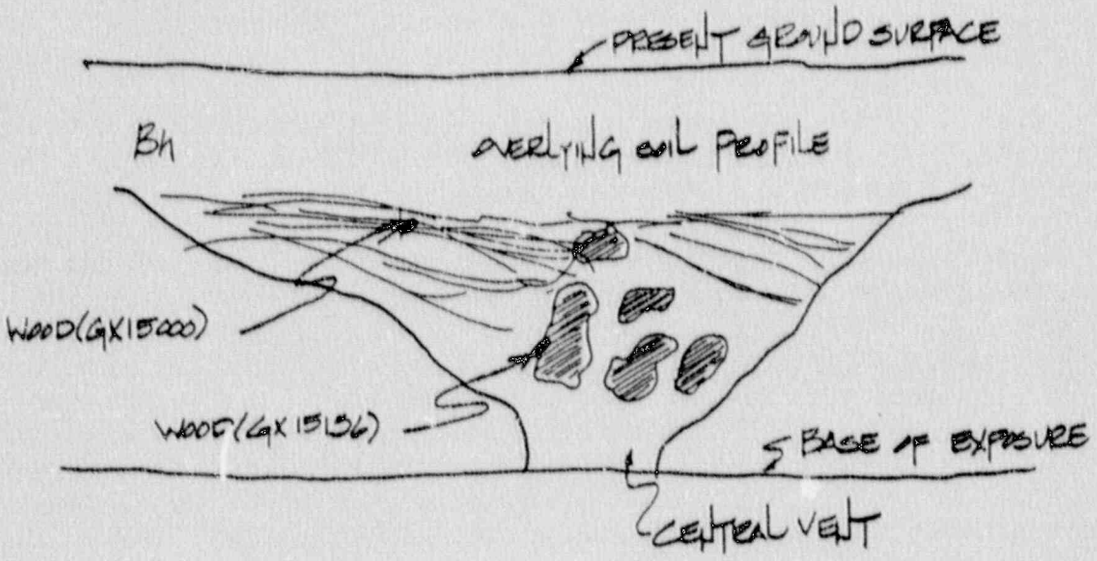

FIGURE 11.8: Sketch of "older" SIL feature discovered at the Colony Gardens site. Two organic samples were recovered from this feature. A piece of wood was recovered from the bedding sequence and yielded an age of 1066±75 YBP (GX15136). Its age is interpreted to be very close to the actual age of the liquefaction episode. A second piece of wood was recovered from within a soil clast which had collapsed into the feature. It yielded an age of 1305±87 YBP (GX15100) and provides a maximum age constraint.

feature after the ditch was excavated. Qualitatively, these observations suggest a relatively young age.

Two organic materials were recovered from a second "older" feature located at this site. A sketch of this feature is present as Figure 11.8. A piece of wood was recovered from the bedding sequence of this feature and yielded an age of 1066±75 YBP (GX15586). The age of this type of sample is interpreted to be very close to the actual age of the liquefaction episode. A second piece of wood was recovered from within a soil clast which had collapsed into the feature. It yielded an age of 1305±87 YBP (GX15136) and provides a maximum age constraint. Since this second sample was wood rather than charcoal, its residence time in the shallow soil prior to liquefaction was probably limited and it should provide tight control on the maximum age of liquefaction.

Bluffton A: At this site several generations of liquefaction features were discovered. Many were associated with very thin overlying soil profiles, suggesting a very young age. A photograph and sketch of one such feature is presented as Figure 11.9. Leaves were recovered from the bedding sequence of this liquefaction feature. They yielded a radiocarbon age older than 40 YBP and less than 200 YBP (GX15183).

A sketch of another "young" liquefaction feature discovered at the Bluffton A site is presented as Figure 11.10. Tree bark recovered from the bedding sequence of this feature yielded a radiocarbon age of 107±61 YBP (GX15582). A piece of wood recovered from a third feature was dated at older than 40 YBP but less than 100 YBP (GX15581).

Several "older" features associated with thicker overlying soil profiles were also discovered at this site. Figure 11.11 is a sketch of one of these older features. New burn charcoal recovered from the soils overlying this feature was dated at 275±105 YBP (GX15132), confirming that it is older than the features discussed previously. A tap root of a tree is located along the left margin of this feature. The bedded sequence of the crater does not appear to have been disrupted by the penetrative growth of this root. Rather, the bedding appears to have been laid down against and around the root, suggesting that the root was in place at the time of the liquefaction episode. It yielded a radiocarbon age of 605±160 YBP (GX15130). Based on flagging and sampling markers present at this feature, members of the USGS are thought to have also sampled this same feature. Weems and Obermeier (1990) reported a root dated at 570±100 (W 5804) that "was found with a crater developed along its side". They suggested that the root "predates the crater and may have been killed by the disruption due to the crater's formation".

Bluffton B: This site is located about a kilometer from Bluffton A. Based on the relative thickness of overlying soil profiles and their degree of staining, most of the liquefaction features discovered here are older than the young features discovered at Bluffton A. An example of one of these "older" features is shown in Figure 11.2.

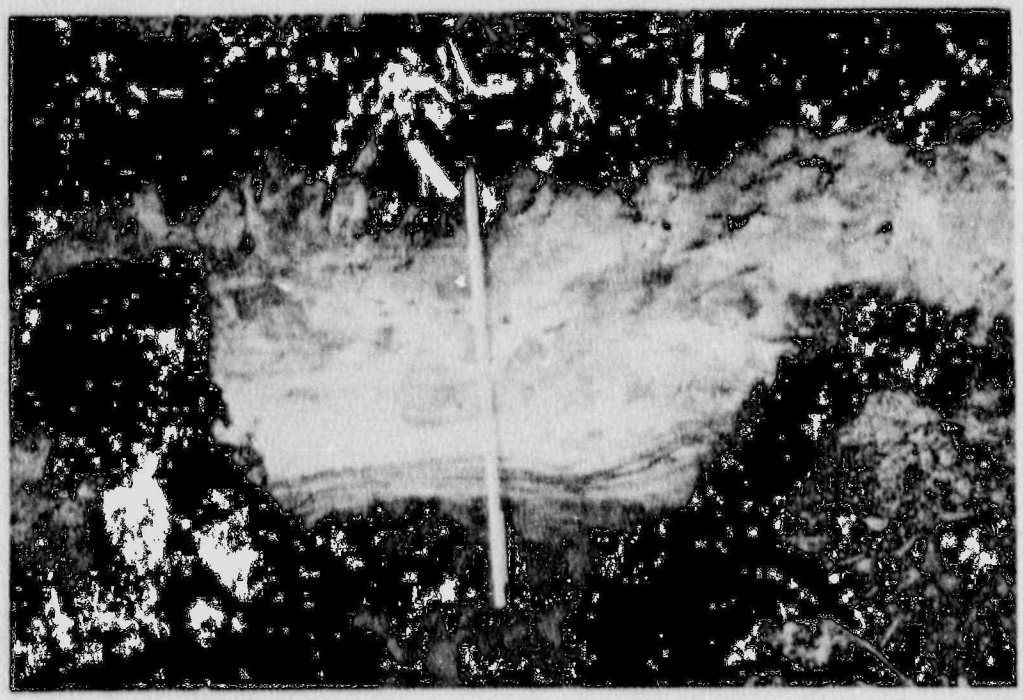

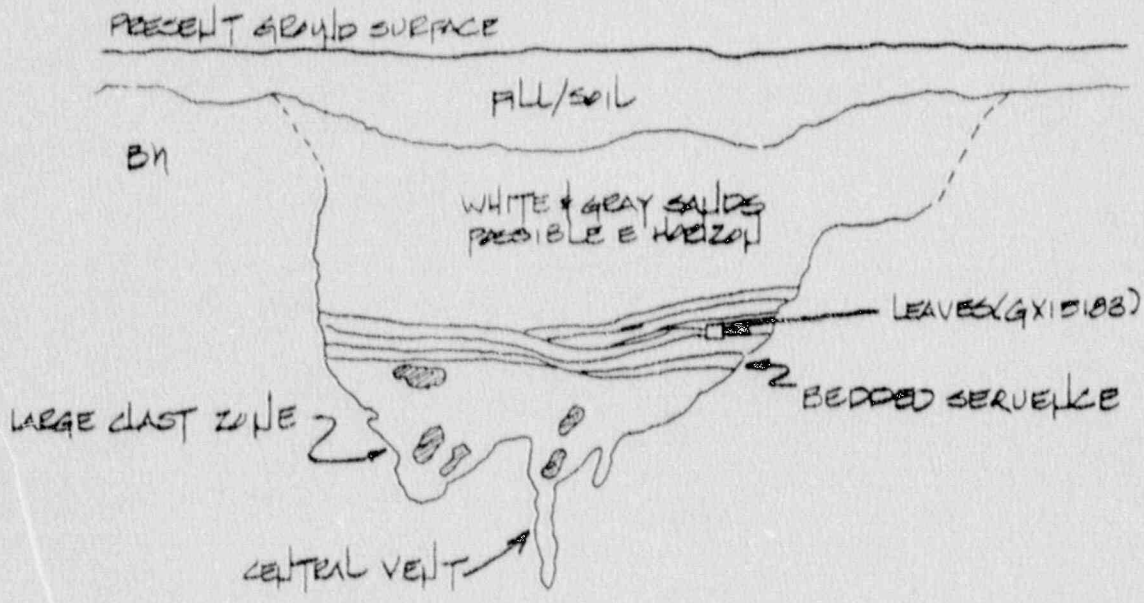

FIGURE 11.9: A) Photograph of young SIL feature discovered at the Bluffton A site. Note the light colored sands within the feature and the associated ejection blanket. A sketch of this same feature showing the sampling locale is presented in B. Leaves were recovered from the bedding sequence of this liquefaction feature. They yielded a radiocarbon age older than 40 YBP and less than 200 YBP (GX15183), and confirm that this is a very young feature.

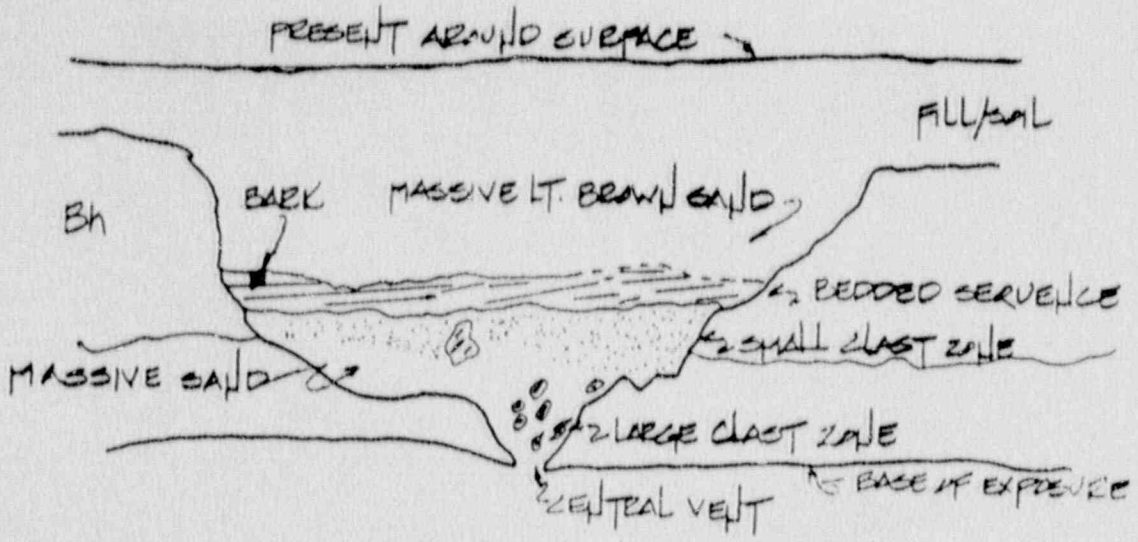

FIGURE 11.10: Sketch of another "young" liquefaction feature discovered at the Bluffton A site. Tree bark recovered from the bedding sequence of this feature yielded a radiocarbon age of 107±61 YBP (GX15000).

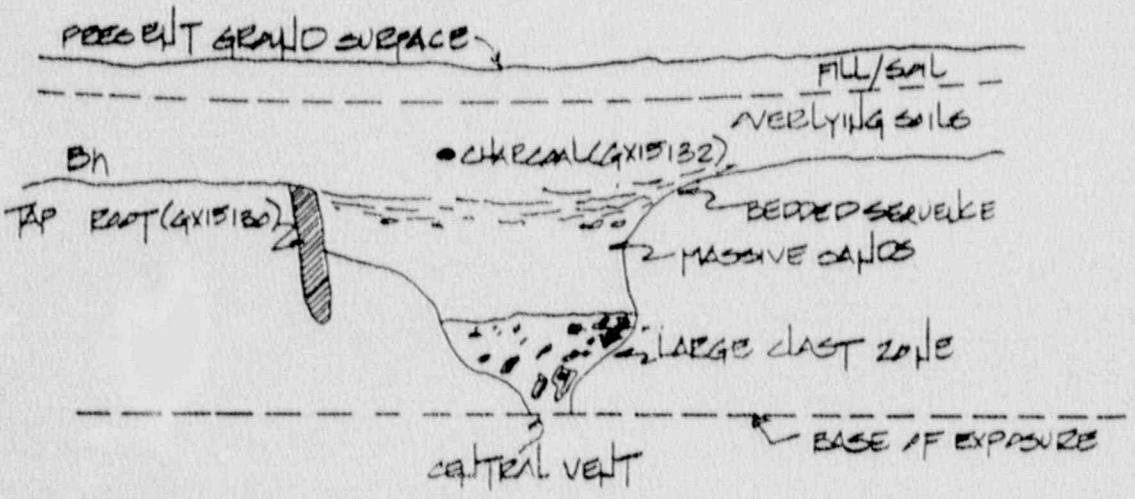

FIGURE 11.11: Sketch of an "older" SIL feature discovered at the Bluffton A site. Note the overlying soil profile. New burn charcoal recovered from the soils overlying this feature was dated at 275±105 YBP (GX15132), confirming that it is older than the feature shown in Figure 11.9. The tap root of a tree is located along the left margin of this feature. The bedded sequence of the crater does not appear to have been disrupted by the penetrative growth of this root. Instead, the bedding appears to have been laid down against and around the root, suggesting that it was in place at the time of the liquefaction episode. This root yielded a radiocarbon age of 605±160 YBP (GX15000).

To date, datable materials have been recovered from only one of these older features (Figure 11.3). Small pieces of new burn charcoal were recovered from overlying soils. Their distribution and the discoloration of the adjacent soils suggest that they originated from a tap root which burned in place. A composite sample yielded a radiocarbon age of 1850±80 YBP (GX15585). This date provides a minimum constraint on the age of liquefaction and distinguishes this older liquefaction episode from the younger episodes identified at Bluffton A.

Additional charcoal was recovered from this same feature near the top of the bedding sequence, immediately below the tap root charcoal samples discussed above. It could not be established conclusively whether this charcoal was actually from within the bedding sequence (in which case it would provide a maximum age constraint) or was part of the new burn tap root (in which case it provides a minimum age constraint). It yielded a radiocarbon age of 2164±68 YBP (GX15584).

Malpherous: Several liquefaction features were located at this site. Although differences in the thickness of overlying soil profiles and the degree of staining were noted, none were associated with very thin overlying soil profiles. Organic samples were recovered from one heavily stained liquefaction feature (Figure 11.14). A large root which had grown into the feature after its formation yielded a radiocarbon age of 4620±195 YBP (GX15131). This sample provides a minimum age constraint. A small charcoal sample recovered from within a soil clast that had collapsed into this same feature was dated at 5520±370 YBP (GX15190). It provides a maximum age constraint on the age of liquefaction.

Summary of Southern Liquefaction Sites: Based on the ages of organic samples collected from southern outlying liquefaction sites, four liquefaction episodes may have occurred in this area during Holocene times. They are referred to from youngest to oldest as episodes **S-1** through **S-4**.

Liquefaction episode **S-1** is based on data from the Colony Gardens, and Bluffton A sites. At both of these sites, several liquefaction features are present that have very thin overlying soil profiles, suggesting relatively recent origins. Radiocarbon data confirm that these features formed within the past two hundred years but are not modern in age (this generally represents the resolution of this technique for relatively young samples). The absence of a large earthquake in this southern area during historical times suggests that these features were most likely the result of the 1886 earthquake.

At both the Colony Gardens and Bluffton A sites, additional liquefaction features with well-developed overlying soil profiles were also observed. These are inferred to represent older liquefaction episodes. Similar "older" liquefaction features have been observed at each of the other southern sites studied. Liquefaction episode **S-2** is dated at 600±100 YBP and is based on the age of a tap root which may have been killed by the liquefaction episode.

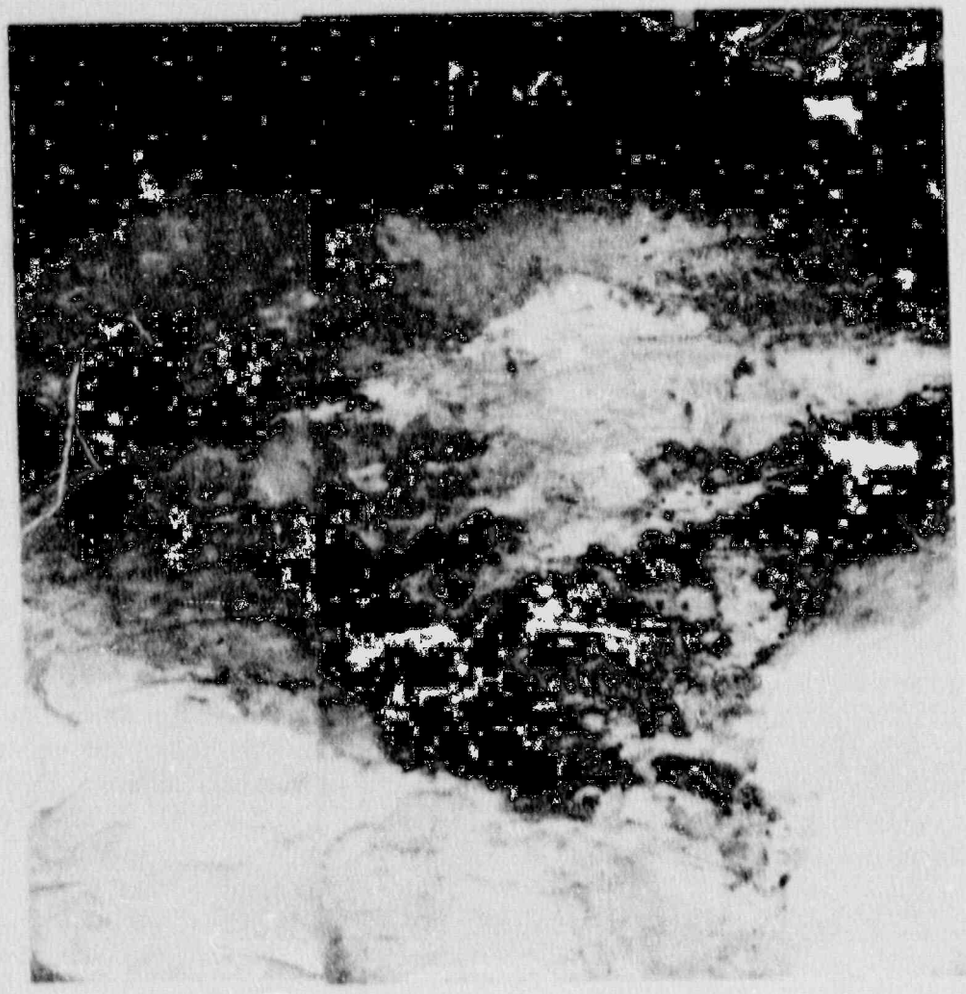

FIGURE 11.12: Photograph of "older" SIL feature discovered at the Bluffton B site. Note the degree of staining of the crater sands and the relatively thick overlying soil profile.

Liquefaction episode **S-3** is based on radiometric dates obtained from one of the "older" craters located at the Colony Gardens site and is estimated at 1066±75 YBP. The age of this episode is based on wood fragments recovered from within the bedded sequence of the sand-blow explosion crater and is further constrained by a maximum age of 1305±87 YBP.

Liquefaction episode **S-4** is based on data from the Malpherous site. Its age is estimated at 4620±195 to 5520±375 YBP. The minimum age constraint is based on the age of roots which had grown into the sand-filled crater after it formed. The maximum age constraint is based on the age of charcoal recovered from within a soil clast which had collapsed into the liquefaction feature during its formation.

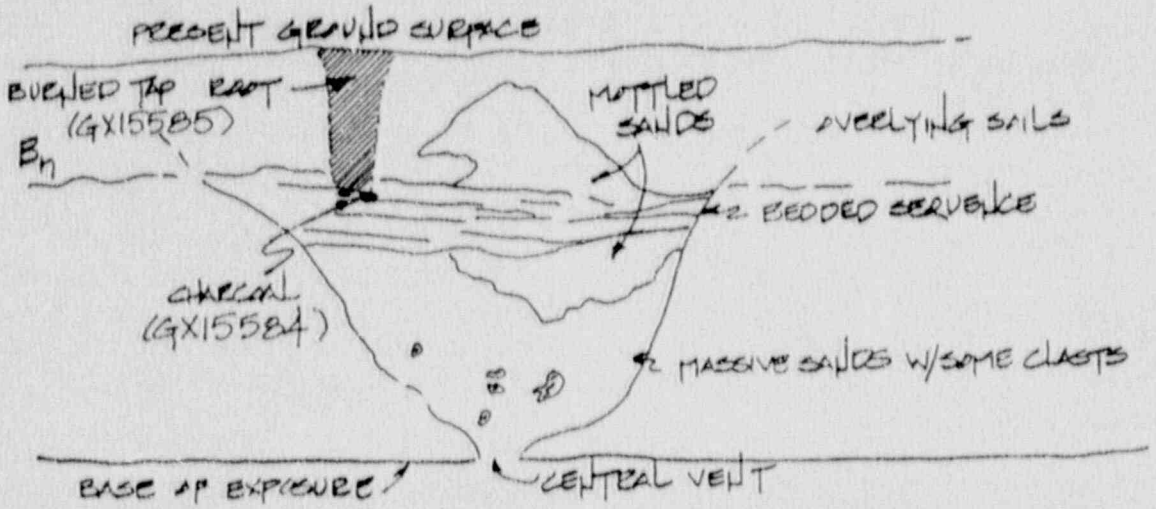

FIGURE 11.13: Sketch of "older" SIL feature discovered at the Bluffton B site. Small pieces of new burn charcoal were recovered from overlying soils. Their distribution and the discoloration of the adjacent soils suggest that they originated from a tap root which burned in place. A composite sample yielded a radiocarbon age of 1850±80 YBP (GX15000). This date provides a minimum age constraint on the age of liquefaction and distinguishes this older liquefaction episode from the younger episodes identified at Bluffton A. Additional charcoal was recovered from near the top of the bedding sequence, immediately below the tap root charcoal samples. It could not be established conclusively whether this charcoal was from within the bedding sequence (in which case it would provide a maximum age constraint) or was part of the new burn tap root (in which case it provides a minimum age constraint). It yielded a radiocarbon age of 2164±68 YBP (GX15000).

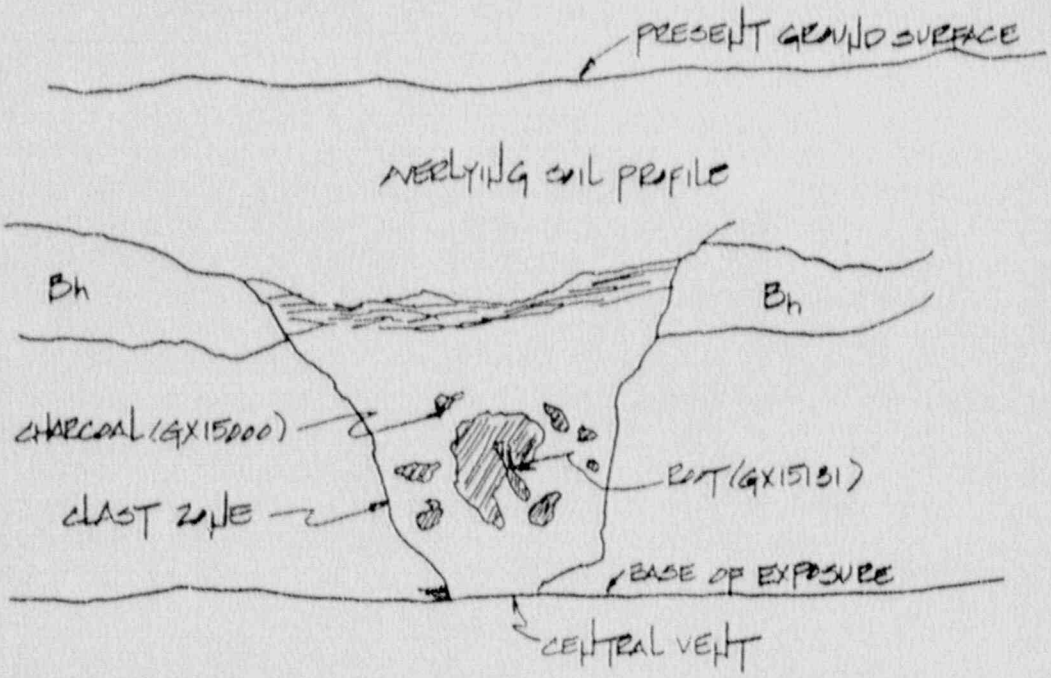

FIGURE 11.14: Sketch of SIL feature discovered at the Malpherous site. A large root which had grown into the feature after its formation yielded a radiocarbon age of 4620±195 YBP (GX15131). This sample provides a minimum age constraint. A small charcoal sample recovered from within a soil clast located within this same feature was dated at 5520±370 YBP (GX15000) and provides a maximum age constraint on the age of liquefaction.

12.0 CHARACTERIZATION OF EARTHQUAKE SOURCE, MAGNITUDE AND FREQUENCY

The morphology of paleoliquefaction features found both within the Charleston meizoseismal area and at outlying sites located both to the north and south are similar to features which clearly formed as a result of the 1886 earthquake. They have been interpreted to be the result of similar prehistoric earthquakes. If this interpretation is correct, then the spacial and temporal distribution of these liquefaction features can be used to: 1) broadly define the epicentral area of past earthquakes, 2) estimate the size of the earthquake generating these features, and 3) estimate the return period between earthquakes large enough to produce liquefaction features.

12.1 Epicentral Areas of Past Large Earthquakes in South Carolina

The outlying liquefaction sites are located well outside the meizoseismal area of the 1886 Charleston Earthquake. Their existence can be explained by three possible scenarios: 1) they could be outlying liquefaction sites resulting from ground motion associated with the 1886 Charleston event and/or prehistoric Charleston earthquake(s) comparable in size to the 1886 event, 2) they could be related to a pre-1886 Charleston earthquake larger than the 1886 event (which resulted in the generation of liquefaction features over a larger area), or 3) they could be the result of liquefaction associated with seismic events originating outside the Charleston epicentral area. Further, the potential the temporal and spacial distribution of impact that climatic and/or sea level changes could have on SIL features must also be considered.

Scenarios 1 and 2 predict that the ages of the outlying liquefaction features would be the same as the age of prehistoric Charleston earthquakes. Conversely, model 3 predicts different ages at the outlying sites (assuming that the seismogenic sources of the causative events do not act in unison). Any combination of these three models is also possible. For example, some outlying liquefaction features could be the result of a much larger prehistoric Charleston event, while others could be due to a second earthquake source.

The spacial and temporal distribution of the liquefaction episodes discussed in Chapters 8 and 11 is illustrated in Figure 12.1. As shown, data suggest that all of the liquefaction episodes observed at southern outlying liquefaction sites and at least two of the liquefaction episodes observed at the northern liquefaction sites can be attributed to earthquakes originating in the established Charleston epicentral area. The age of **N-4** is generally consistent with episodes **CH-5** or **CH-6**, but is poorly constrained.

However, liquefaction episode **N-3** has no clear parallel liquefaction episode in the Charleston epicentral area and the data collected to date suggest that its causative event may have originated in a different area. Alternately, the earthquake associated with liquefaction episode **N-3** may have originated near Charleston but

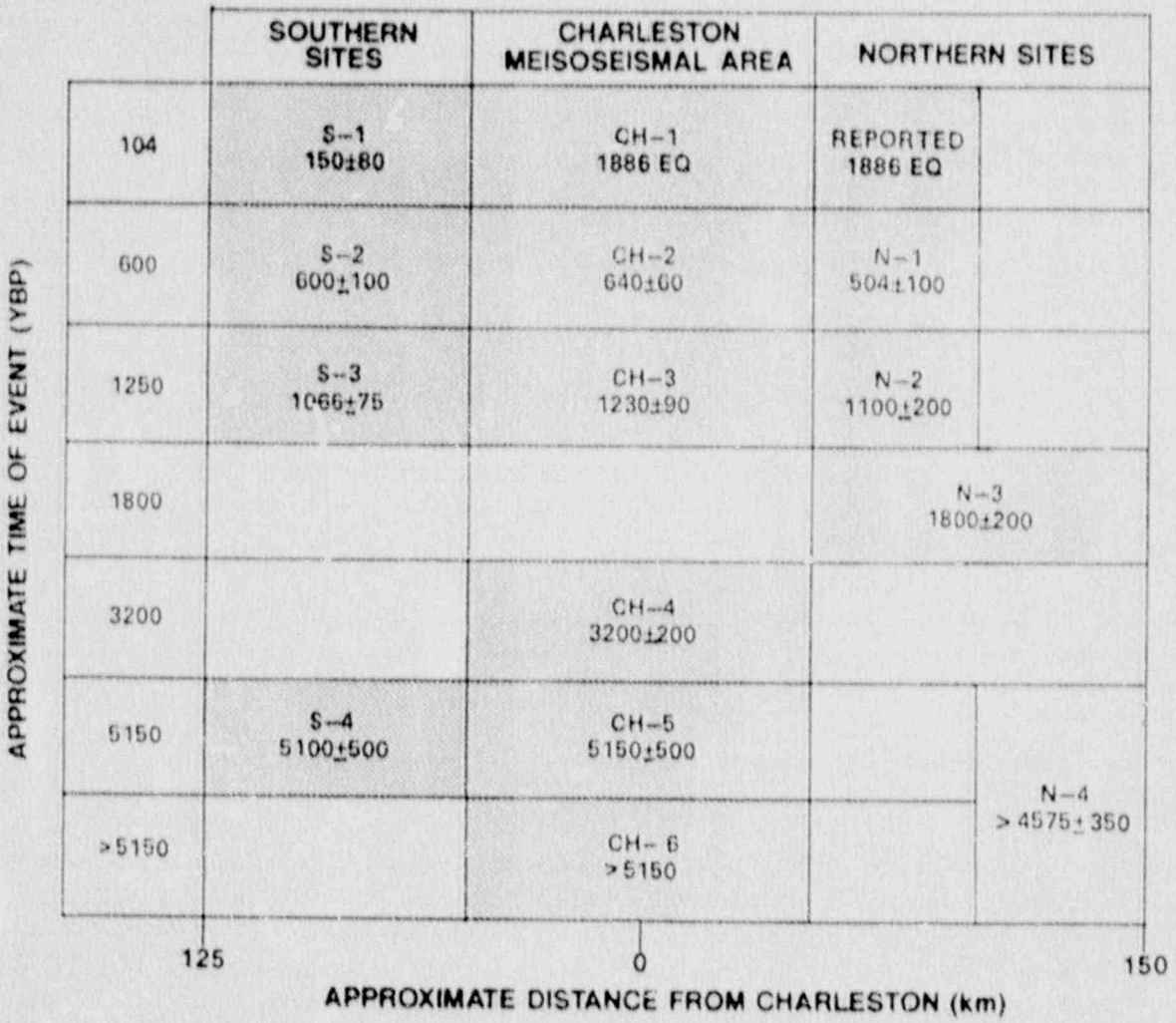

FIGURE 12.1: Temporal and spacial distribution of liquefaction and paleoliquefaction features at the southern and northern outlying liquefaction sites as well as in the meisoseismal area of the 1886 earthquake. Shading denotes events which are thought to correlate. Note that while the past three episodes (S-1/CH-1; S-2/CH-2/N-1; and S-3/CH-3/N-2) seem to correlate, the N-3 episode has no companion in the Charleston area and it is suggested that a different epicentral area was the source of the earthquake which caused these features.

it has not yet been identified in the paleoliquefaction record there. Additional studies would be needed to confirm the existence of this postulated northern liquefaction episode.

12.2 Impact of Climate and Sea Level on the Spacial and Temporal Distribution of SIL Features

As noted in Chapter 2, saturated conditions are required for SIL to occur. Further, the level of local ground-waters can play a significant role in determining the liquefaction potential of nearsurface sediments. In turn, ground-water tables rise and fall in response to changes in climatic conditions, and in coastal areas, regional

changes in ground-water levels often mimic changes in sea level. Consequently, variations in Holocene climatic conditions and sea levels may have played a significant role in determining the spacial and temporal distribution of paleoliquefaction features.

Brooks and others (1989) report that in the Southeastern U.S. sea level has been at or near its present elevation for about the past 2000 years and that climatic conditions have been relatively stable. Consequently, the paleoliquefaction record is probably most complete for this period. These same investigators note that during the period 2000 YBP to about 5000 YBP sea level was generally about one to four meters below present levels and fluctuated widely within this range. Consequently, the paleoliquefaction record for this interval probably includes only those earthquakes which occurred during periodic transgressive seas and/or wet climatic periods. Finally, there is abundant data to suggest that before about 5000 YBP the climate in the southeastern U.S. was drier and that sea level was more than four meters lower than present (Watts, 1971; Brown, 1981; and Brooks and other, 1989). Such conditions would severely reduce or eliminate the potential for SIL and may explain the absence of early Holocene paleoliquefaction features (before about 6000 YBP) in the paleoliquefaction record.

12.3 Size of Past Earthquakes

Work within the New Madrid Region (Russ, 1983) and worldwide empirical data (Youd, 1973; Seed and Idriss, 1982) the smallest earthquake which could reasonably be expected to generate significant SIL features is estimated to be in the magnitude range of m_b 5.8$\pm$.4. Each of the seven earthquakes postulated (**CH-1** to **CH-6**; and [illegible]) would be expected to have exceeded this threshold magnitude. The M_s 7.1 [illegible] earthquake (**CH-1**) generated liquefaction features over the same general area as episodes **CH-2** and **CH-3**, suggesting that these two older earthquakes were of similar magnitude. At this time, data are inconclusive regarding distribution of liquefaction features associated with older Charleston liquefaction episodes. This is especially true given that the impact of increases and decreases in liquefaction potential due to climatic and/or other factors is not fully understood.

For example, episode **CH-4** has been identified only at a few sites located in close proximity to Charleston, suggesting (all other factors being equal) that it may have been caused by an earthquake smaller than the 1886 event. However, the work of Brooks and others (1989) suggests that at the time of the CH-4 liquefaction episode (about 3200 YBP) sea level was three meters lower than present. If this resulted in lower ground-water tables, the liquefaction potential of shallow sediments along the South Carolina coast would have been greatly reduced. Consequently, an 1886-like earthquake occurring 3200 YBP would have generated SIL features over a smaller area than the 1886 event. Similarly, Brooks and others (1989) noted that about 1750 YBP sea level may have been slightly higher than at the present. If this resulted in higher regional ground-water tables, the liquefaction potential of shallow sediments would have been increased. Consequently, an 1886-like earthquake

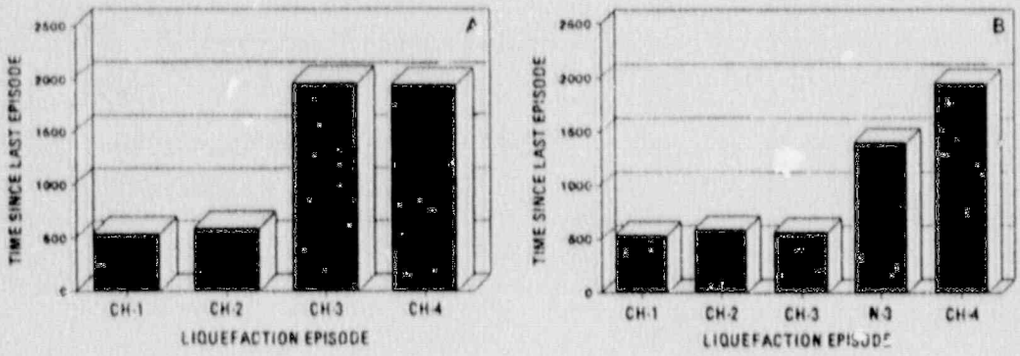

FIGURE 12.2: Variability of earthquake return period with time. Figure A illustrates the time elapsed since last liquefaction episode for only the CH series of liquefaction episodes. Figure B illustrates the elapsed since last liquefaction episode for all S.C. data (including episode N-3). Note that in either case the time between episodes appears to have decreased from about 2000 years in the mid holocene to about 500 to 600 years in more recent times.

---

occurring about 1750 YBP could have generated SIL features over a much larger area. This may explain the observed N-3 outlying SIL features. However, this hypothesis could only be confirmed if SIL features of similar ages are subsequently found in the Charleston area.

12.4 The 1886 Earthquake - A Characteristic Event?

Over the past decade several investigators have noted that the total rupture length and the amount of displacement at a given point along a fault are often very similar during successive surface-faulting earthquakes. Schwartz and Coppersmith (1984) reported this to be the case along many segments of the Wasatch fault. They also noted similar observations along the south central segment of the San Andreas fault, where location-specific slip during the 1857 earthquake appears to repeat the amount of displacement of at least the two prior prehistoric events.

The fault responsible for the 1983 Borah Peak, Idaho earthquake also appears to exhibit similar behavior. Mapping of the surface rupture (Crone and Machette, 1985; Crone et al., 1987) and trenching (Schwartz and Crone, 1985) showed that the distribution of slip during the 1983 event repeated, both in location and amount, the slip distribution of the one pre-1983 earthquake that had occurred on this segment of the Lost River fault zone during the past 12,000-15,000 years. Given similar rupture lengths for the 1983 and the prehistoric earthquake and similar amounts of slip at most locales along the fault, the magnitudes of these two earthquakes were inferred to be essentially the same. These observations as well as others have led to the development of the "characteristic earthquake model". This model proposes that many individual faults and fault segments tend to generate a characteristic maximum earthquake that is related to the geometry, mechanical properties, and state of stress of that fault or fault segment. Consequently, the characteristics of

large prehistoric earthquakes should provide a good estimate of the maximum magnitude earthquake that a specific fault can reasonably be expected to generate.

As noted in previous discussions, paleoliquefaction data suggests that the 1886 earthquake (**CH-1**) generated liquefaction features over the same general area as episodes **CH-2** and **CH-3**. Given sea level and climatic conditions are thought to have been relatively stable during these times, this observation could be interpreted to indicate that the $M_s = 7.1$ 1886 event may represent the "characteristic earthquake" for the Charleston source area.

12.5 Earthquake Return Periods

The mean return period between liquefaction episodes identified in the geologic record (including both those originating in the Charleston area and the single event to the north) is about 1000 years. However, as illustrated in Figure 12.2, data suggest that the time between episodes has varied from about 2000 years during mid-Holocene times to about 600 years in more recent times. The observed differences may reflect variability in the causative process. However, it is more probable that the **apparent** decrease in return periods is related to "gaps" in the paleoliquefaction record due to the absence of SIL features associated with earthquakes that occurred during times of decreased liquefaction potential. Since sea level has been at or near its present level over about the past 2000 years and climatic conditions have been relatively stable, the paleoliquefaction record is thought to be most complete for this period. Earlier, the record is thought to be incomplete and probably includes only those earthquakes which occurred during periodic transgressive seas and/or wetter climatic periods. The absence of early Holocene paleoliquefaction features is probably related to generally drier climatic conditions and much lower sea levels which greatly reduced the liquefaction potential of near surface sediments.

13.0 IMPLICATIONS FOR LONG-TERM SEISMIC HAZARD

When viewed in a statistical perspective, information presented in Chapter 12 can be used to estimate the likelihood of future large earthquakes. In this chapter paleoseismic data are used to estimate the probability of an earthquake similar to the 1886 event occurring within the next century. In addition, two recently published frequency-magnitude relations (Amick and Talwani, 1986; Bollinger and others, 1989) have been used to assess the probability of a smaller but still potentially damaging earthquake occurring during the next 15, 50, and 100 years.

13.1 The Time-Predictable Model

How uniform the time interval between successive characteristic earthquakes is a key to understanding long-term seismic hazard. Worldwide data exhibit a range of behavior, from time predictable to highly irregular patterns (Shimazaki and Nakata, 1980). Some investigators have suggested that along major plate boundaries where the rate and source of stress are relatively constant and the rate of strain accumulation is high, seismicity may tend to act in a more time predictable fashion with the variation between the actual and average times between large earthquakes being about 20 percent (Nishenko and Buland, 1987). In contrast, data for intraplate regions suggest that the times between characteristic earthquakes are highly variable and can differ by as much as factor of five. For example, Cluff and others (1980) and Wallace and others (1984) showed that on a regional scale intraplate recurrence of earthquake activity is often characterized by episodic seismicity characterized by clusters of events that are concentrated in small areas or zones and that these bursts of activity can be separated by long periods (tens to hundreds of thousands of years of quiescence).

Paleoliquefaction data collected as part of this study suggests that unlike some intraplate earthquake sources, prehistoric seismicity in S.C. has behaved in a generally time-predictable manner during late Holocene times. This concept of regular recurrence intervals appears to be most valid for the last four events (1800, 1230, 640 and 104 YBP) which give a mean return period of 566 years. Assuming a time-predictable model, it is possible to estimate the likelihood of a liquefaction-inducing earthquake similar in size to the 1886 event occurring in the future.

To apply a time-predictable earthquake model, the mean recurrence time and the variability about this mean must be estimated. A common approach is to model the variability about the mean using an appropriate probability distribution function (for additional background information see, Johnston and Nava, 1985). For illustrative purposes an arbitrary probability distribution function is shown on Figure 13.1. Given a mean recurrence interval and a standard deviation about this mean, the cumulative probability is simply the probability that an earthquake would have occurred in a given time since the last event. Of more importance than the cumulative probability is the probability that an earthquake will occur in the future, given the time passed since the last occurrence is known. This is referred to as the conditional probability of occurrence (Figure 13.1).

Different types of probability density functions have been used in time-predictable studies, including Gaussian, Weibull, and log normal. Both the Gaussian and log normal have been used more extensively in modeling earth sciences phenomena. Using the techniques outlined in Johnston and Nava (1985), they have been used in this investigation to evaluate the conditional probability of several possible cases.

13.2 Paleoseismic Data - The Probability of a Characteristic Charleston Earthquake

Given that 104 years have passed since the last characteristic earthquake (1886) the conditional probability has been evaluated using both Gaussian and log-normal distributions for the following three cases:

Case 1: All seven liquefaction associated South Carolina earthquakes (six paleoseismic, one historic) were used to calculate a mean recurrence interval of 1009 years and an associated standard deviation of 57%. The conditional probabilities for the occurrence of a similar large earthquake were then estimated for a time window of 100 years (Figure 13.2).

Case 2: Only the six earthquakes inferred to have originated within the Charleston source area were considered. These data were used to calculate a mean recurrence interval of 1262 years and an associated standard deviation of 55%. The conditional probabilities for the occurrence of a similar large earthquake were then estimated for a time window of 100 years (Figure 13.3).

Case 3: Assuming that the four most recent events (**CH-1, CH-2, CH-3,** and **N-3**) represent the current earthquake process, a mean recurrence time of 566 years and an associated standard deviation of 4% were calculated. Although the inferred variability is very low, given the resolution of the paleoseismic data conditional probabilities were estimated using standard deviations of 10% and 33%. The time windows under consideration were 15, 50, and 100 years (Figures 13.4 and 13.5).

As illustrated in Figures 13.2 to 13.5, the probability of an earthquake similar to the 1886 event occurring over the next 100 years is estimated as less than five percent for all three cases considered.

13.3 Historical Seismicity

While this statistical evaluation based on paleoliquefaction data suggests that the potential for a liquefaction-inducing earthquake is very low in the Charleston area, the hazard presented by smaller more frequent earthquakes cannot be overlooked. For example, empirical data suggest that earthquakes as large as about m_b 5.8$\pm$.4 do not usually generate liquefaction features, and therefore would not be represented in the paleoliquefaction record. Although smaller, these moderate events could still cause damage to structures in the epicentral area.

The frequency-intensity relations developed for historical seismicity in Charleston area developed by Amick and Talwani (1986) and Bollinger and others (1986) were used to estimate the probability of the occurrence of this smaller yet potentially damaging earthquake.

It should be stressed that two underlying assumptions were made to estimate the probability of future events. First, it was assumed that the Charleston source is capable of producing magnitude 5 to 6 earthquakes during the intervals between rare characteristic earthquakes. This may or may not be the case. Second, it was assumed that the frequency-intensity relation of low-level seismicity occurring in the Charleston area can be used to estimate the recurrence interval of these moderate magnitude earthquakes.

The two frequency-intensity relations used were derived using slightly different techniques. For a complete description, see the referred articles. To briefly summarize, the relation derived by Amick and Talwani (1986) was based on a linear least squares fit to historical seismicity for the ninety year period 1893 through 1983. This time window was chosen to exclude both the 1886 earthquake and its aftershocks from consideration and was designed to provide an estimate of the frequency-distribution of background seismicity occurring within in the Charleston area between characteristic earthquakes. The frequency-magnitude relation derived by Bollinger and others (1989) is based on the evaluation of a 215 year historical record for the Charleston source, including the 1886 earthquake but excluding all dependant events. The maximum likelihood method was used to fit the observed data in this later study (Bender, 1983).

These two published frequency-intensity relations have been used to evaluate the conditional probability of an MM intensity VII earthquake occurring assuming several time windows and associated distribution functions and variabilities (Figures 13.6 through 13.9). The results suggest that the probability of a moderate earthquake of epicentral MM intensity VII occurring within the next 15 years is between 30% and 75%. For a 50 year window the probability is 60% to 99%. The probability of the occurrence of an MM intensity VII earthquake over the next 100 years is even higher. Such an event would be similar to the Charleston-Summerville earthquake of June 12th, 1912. This event produced ground motions levels of MM intensity IV to V in the South Carolina Piedmont and eastern coastal plain of Georgia and some structural damage in the epicentral area (Taber, 1914).

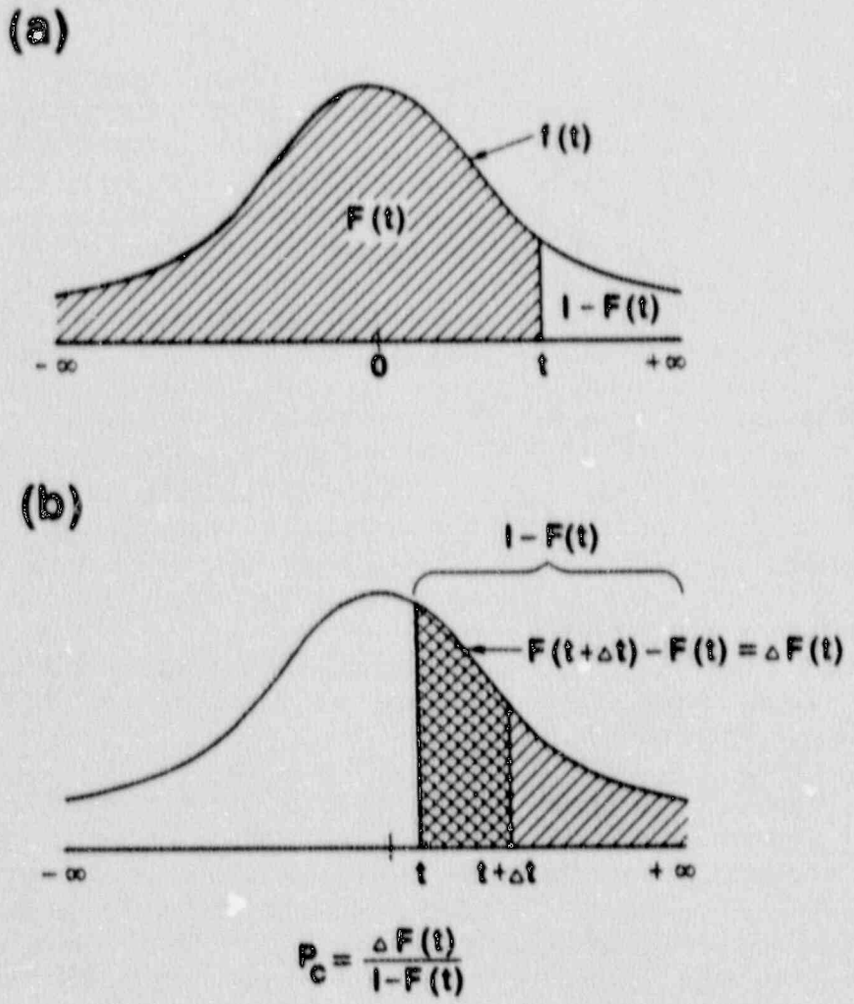

FIGURE 13.1: A) An arbitrary distribution function illustrating the concept of f(t), the probability density function, and F(t), the cumulative probability function. The variable t denotes time. B) Formulation of conditional probability Pc in terms of the ratio of two areas of cumulative probability. (From Johnston and Nava, 1985).

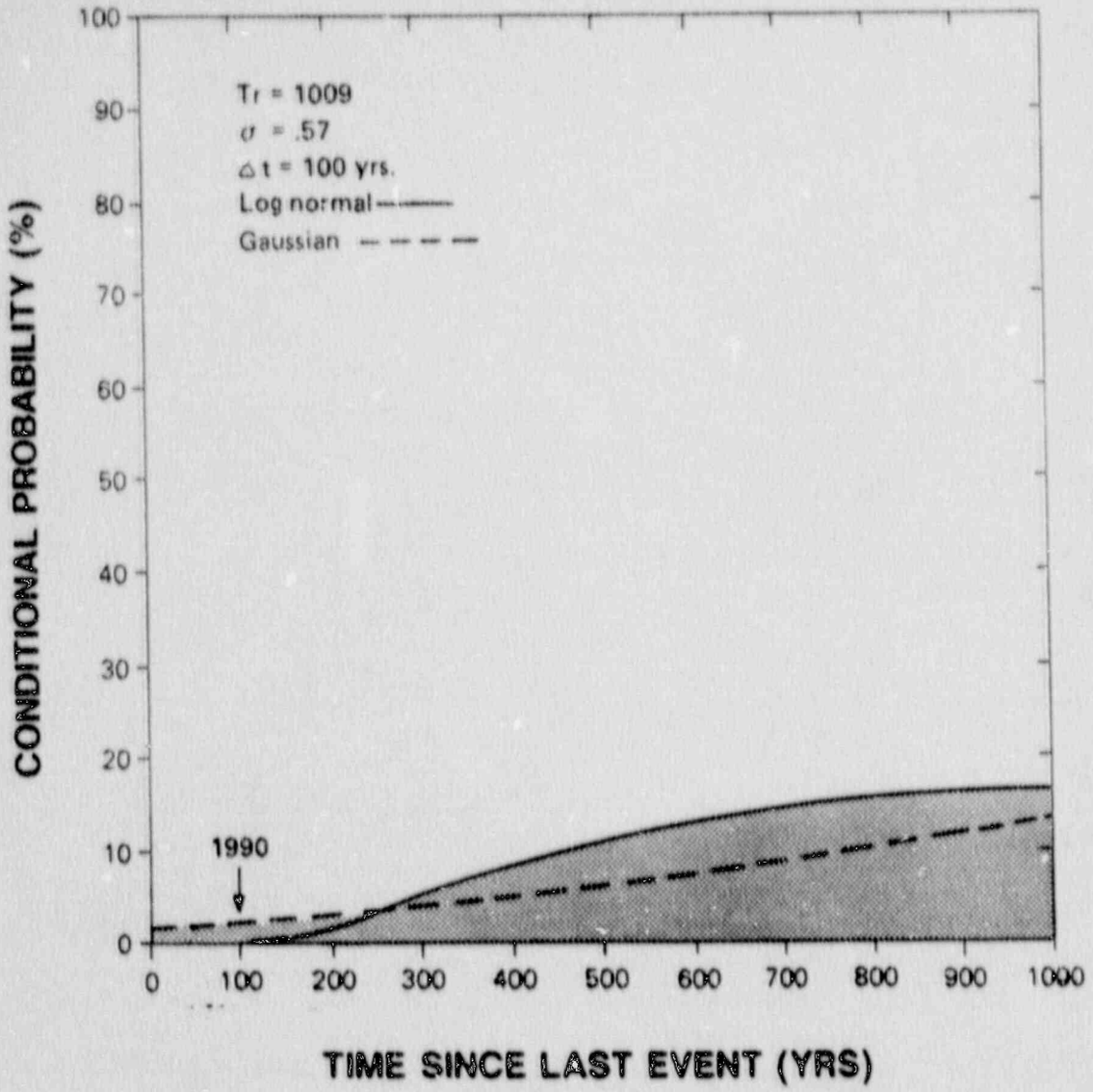

FIGURE 13.2: Gaussian and log normal derived conditional probability curves for Case 1. The mean recurrence interval (Tr) is 1009 years with an associated standard deviation (σ) of 57%. At present (1990), there is about a 3% probability of an event in the next 100 years. Gaussian values were derived from equation (1) using values of $G(z + \Delta z)$ and $G(z)$ taken from National Bureau of Standards (1953).

$$G_c(t, \Delta t) = G_c(z, \Delta z) = \frac{G(z + \Delta z) - G(z)}{1 - G(z)} \qquad (1)$$

Log normal values were derived from equation (2)

$$z = \frac{\ln(t) - T_r^*}{\sigma^*} \qquad \sigma^* = \left[\ln\left(\frac{\sigma^2 + T_r^2}{T_r^2}\right)\right]^{1/2} \qquad (2)$$

$$T_r^* = \ln(T_r) - \frac{\sigma^{*2}}{2}$$

where T_r^* and σ^* are the mean and standard deviation of the log normal distribution. For background discussions and more detailed information of the techniques used see Johnston and Nava (1985).

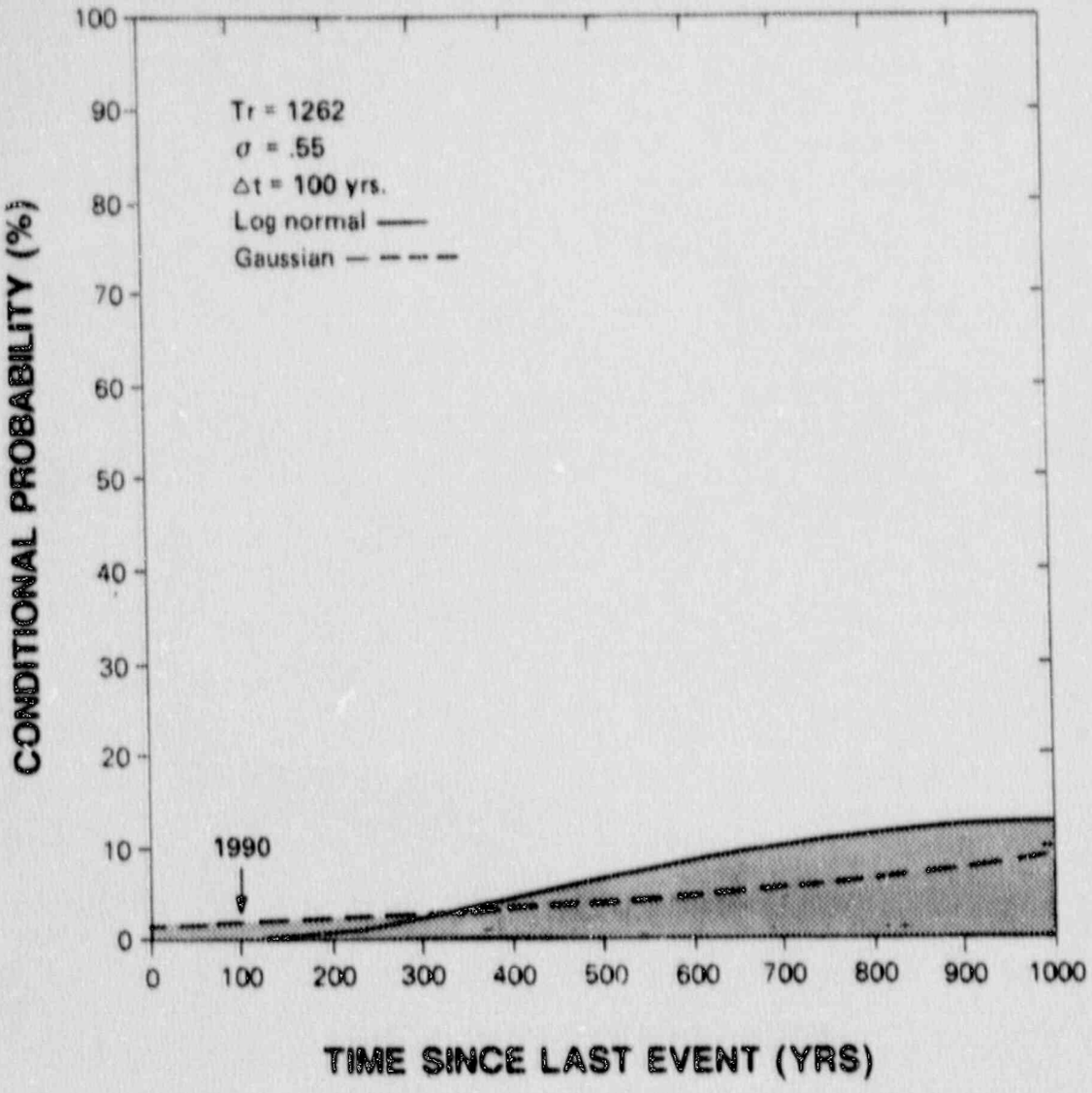

FIGURE 13.3: Gaussian and log normal derived conditional probability curves for Case 2. The mean recurrence interval (Tr) is 1262 years with an associated standard deviation (σ) of 55%. At present (1990), there is about a 3% probability of an event in the next 100 years.

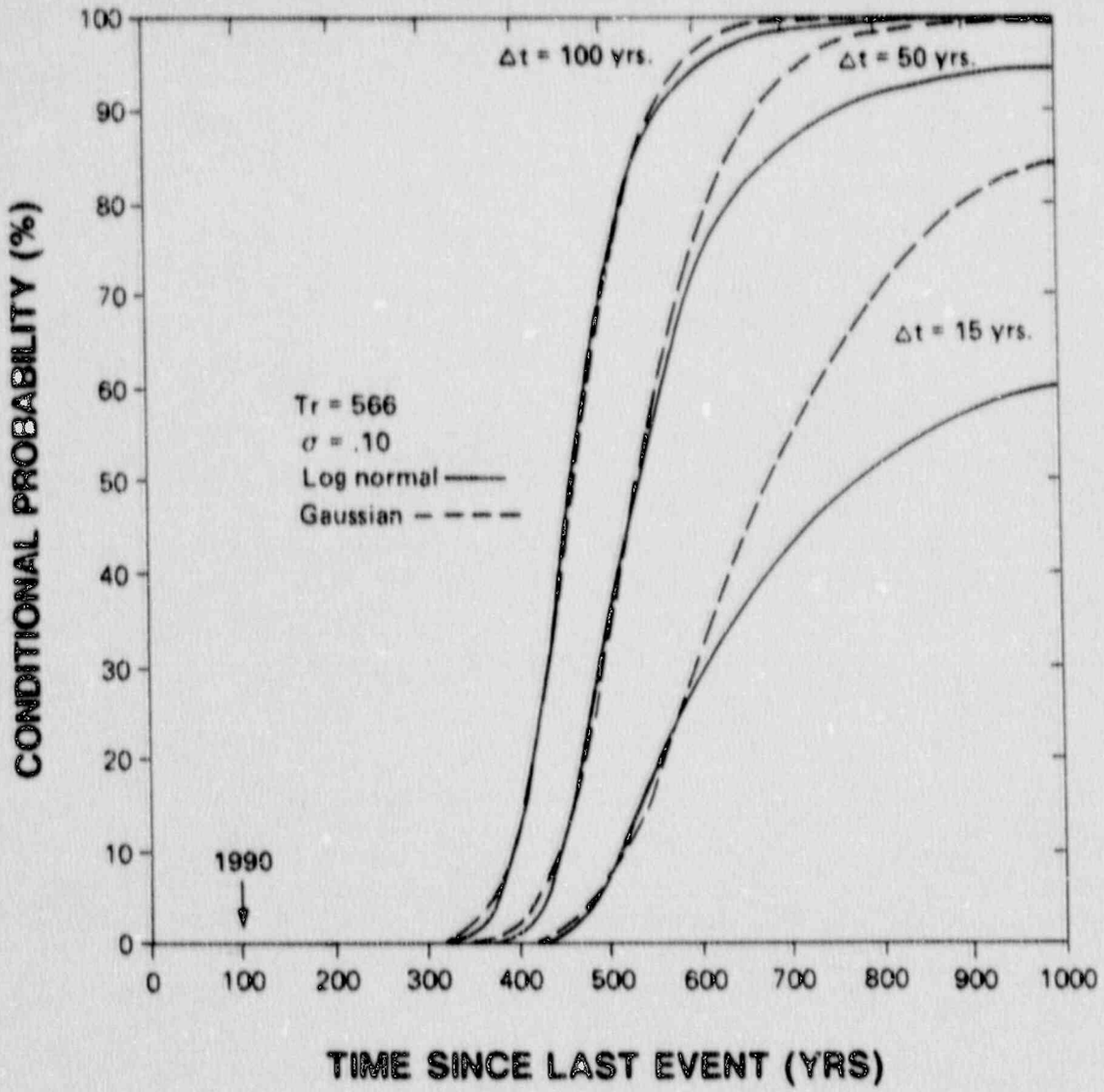

FIGURE 13.4: Gaussian and log normal derived conditional probability curves for Case 3. The mean recurrence interval (Tr) is 566 years with an associated standard deviation (σ) of 4%. Given the nature of the paleoliquefaction data a standard deviation of 10% was assumed. At present (1990), there is virtually no probability of an event in the next 100 years.

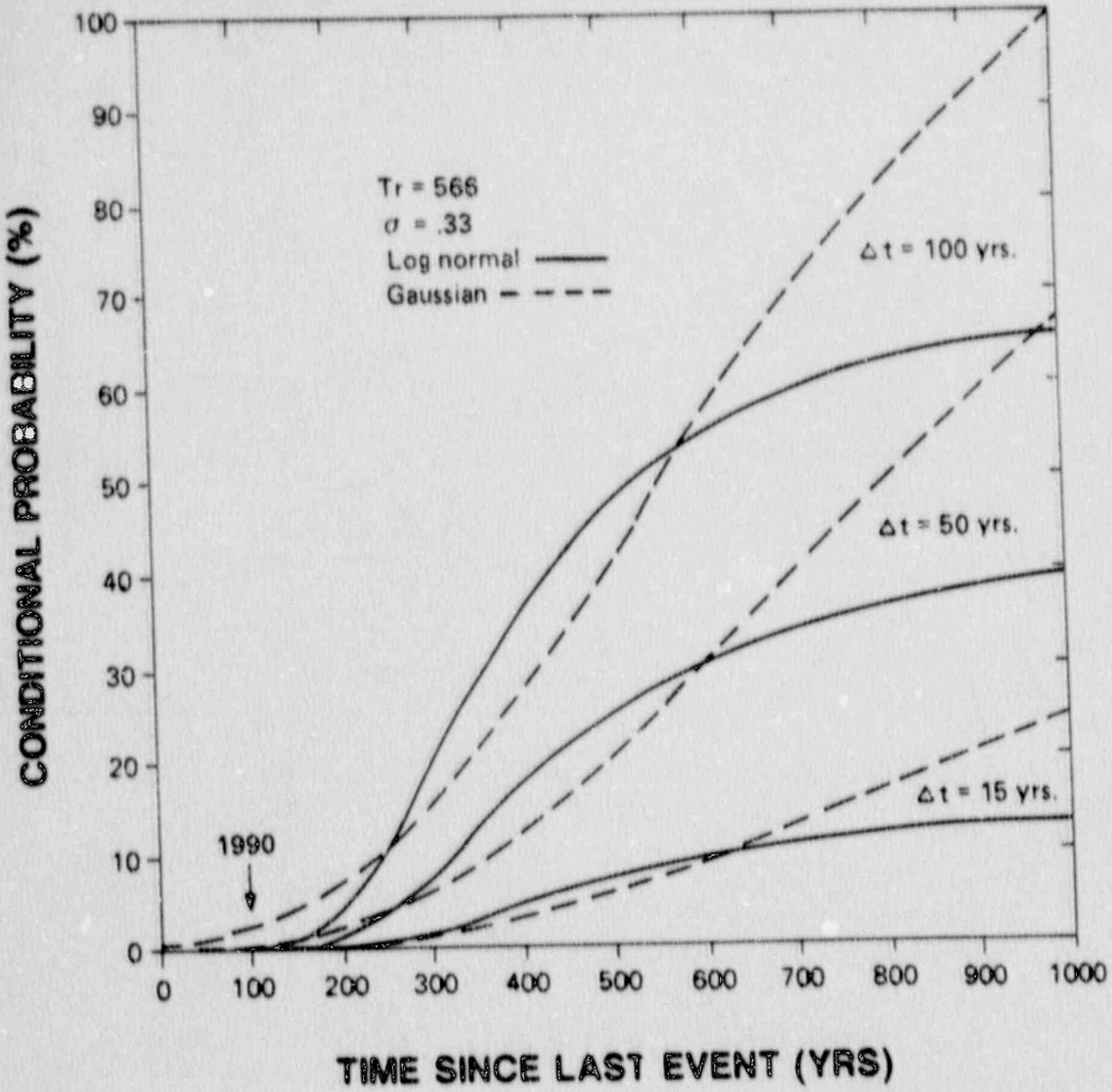

FIGURE 13.5: Gaussian and log normal derived conditional probability curves for Case 3. The mean recurrence interval (Tr) is 566 years with an associated standard deviation (σ) of 4%. Given the nature of the paleoliquefaction data a standard deviation of 33% was assumed. At present (1990), there is less than a 3% probability of an event in the next 100 years.

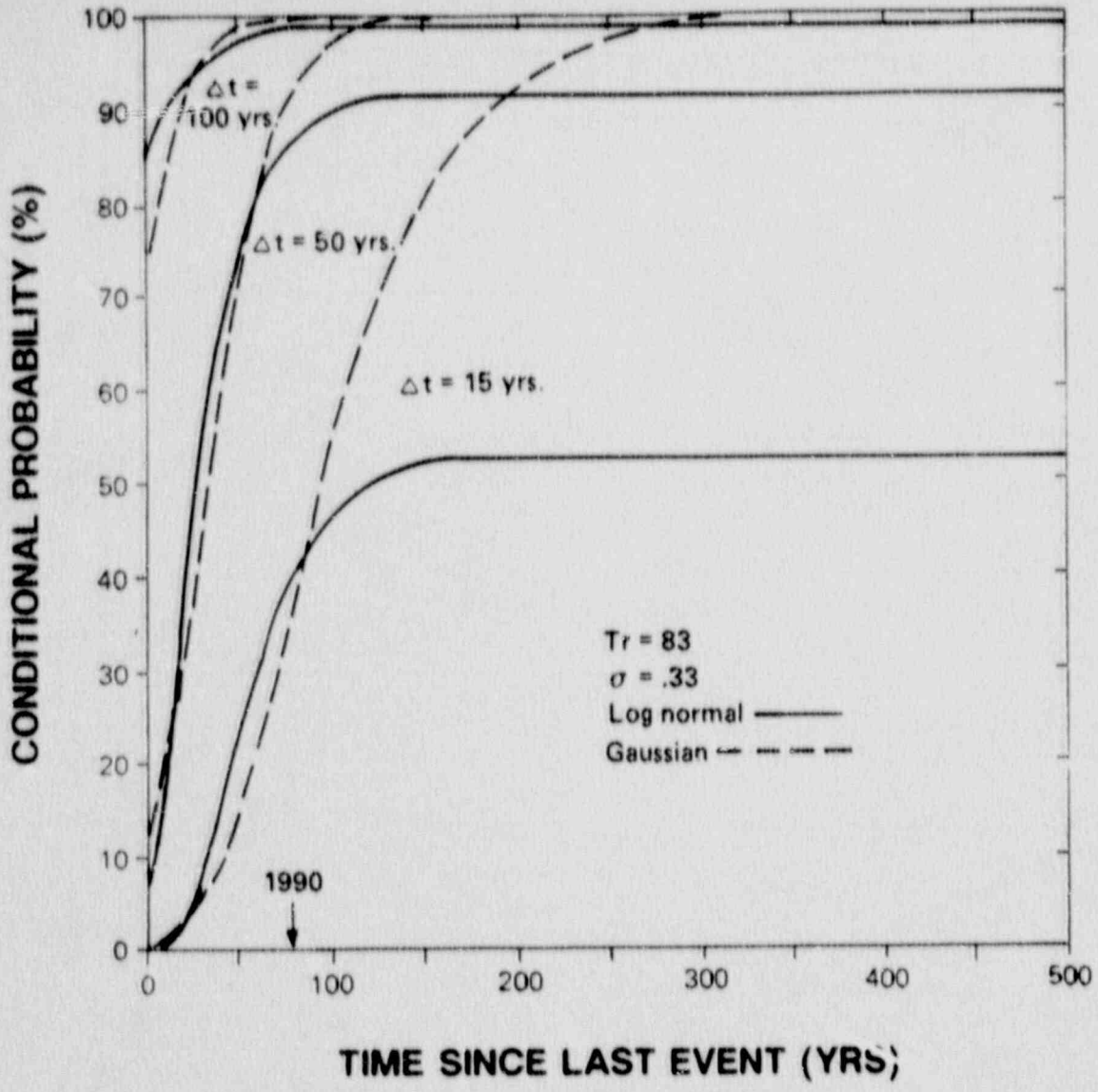

FIGURE 13.6: The frequency-magnitude relation derived by Amick and Talwani (1986) suggests that the recurrence interval for a MM intensity VII earthquake is 83 years (T_r). The last such earthquake occurred in 1912, 78 years ago. Using these values the conditional probabilities for the occurrence of an MM intensity VII earthquake were then estimated for time windows of 15, 50, and 100 years and an assumed standard deviation of 33%.

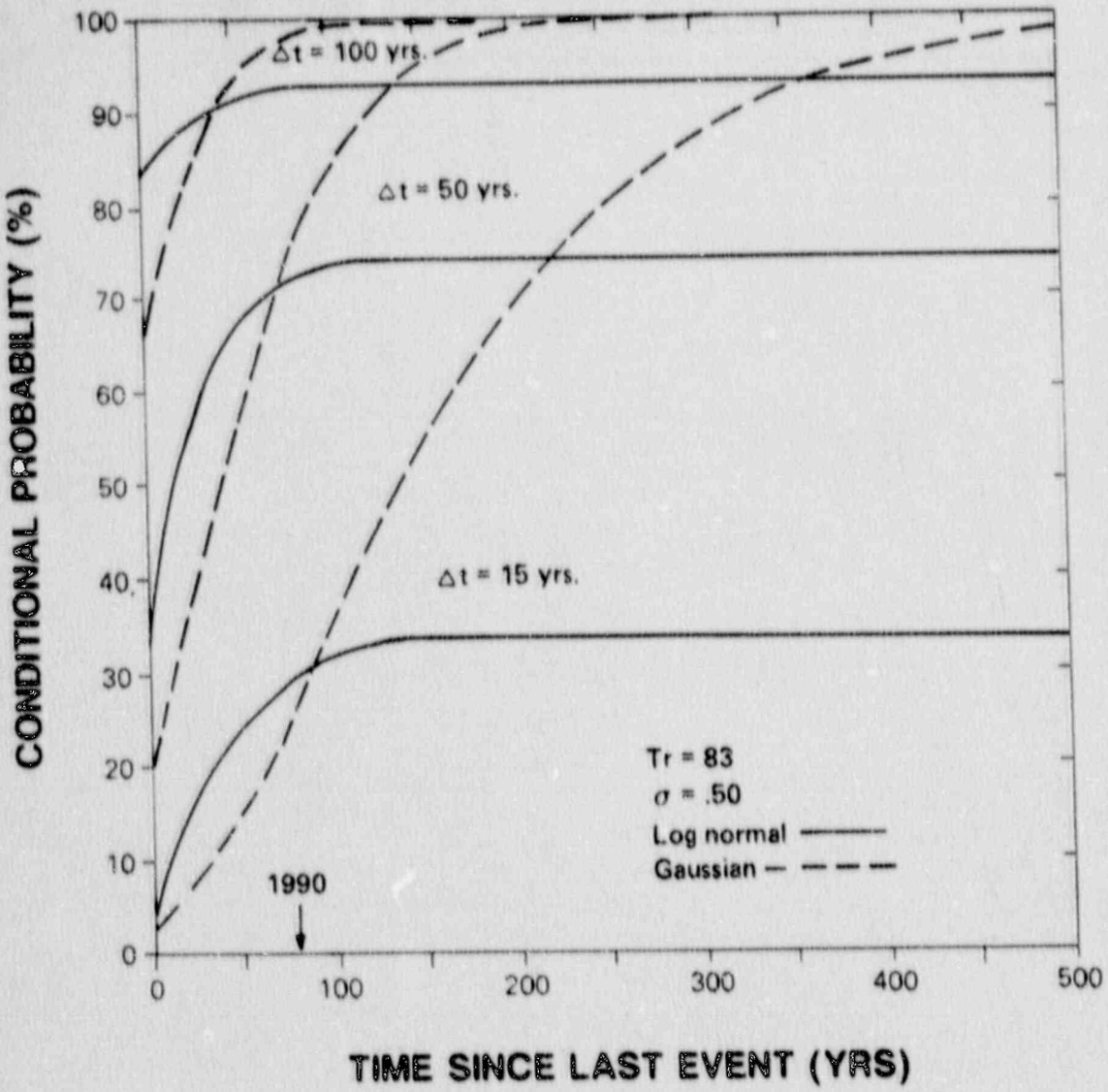

FIGURE 13.7: The frequency-magnitude relation derived by Amick and Talwani (1986) suggests that the recurrence interval for a MM intensity VII earthquake is 83 years (T_r). The last such earthquake occurred in 1912, 78 years ago. Using these values the conditional probabilities for the occurrence of an MM intensity VII earthquake were then estimated for time windows of 15, 50, and 100 years and an assumed standard deviation of 50%.

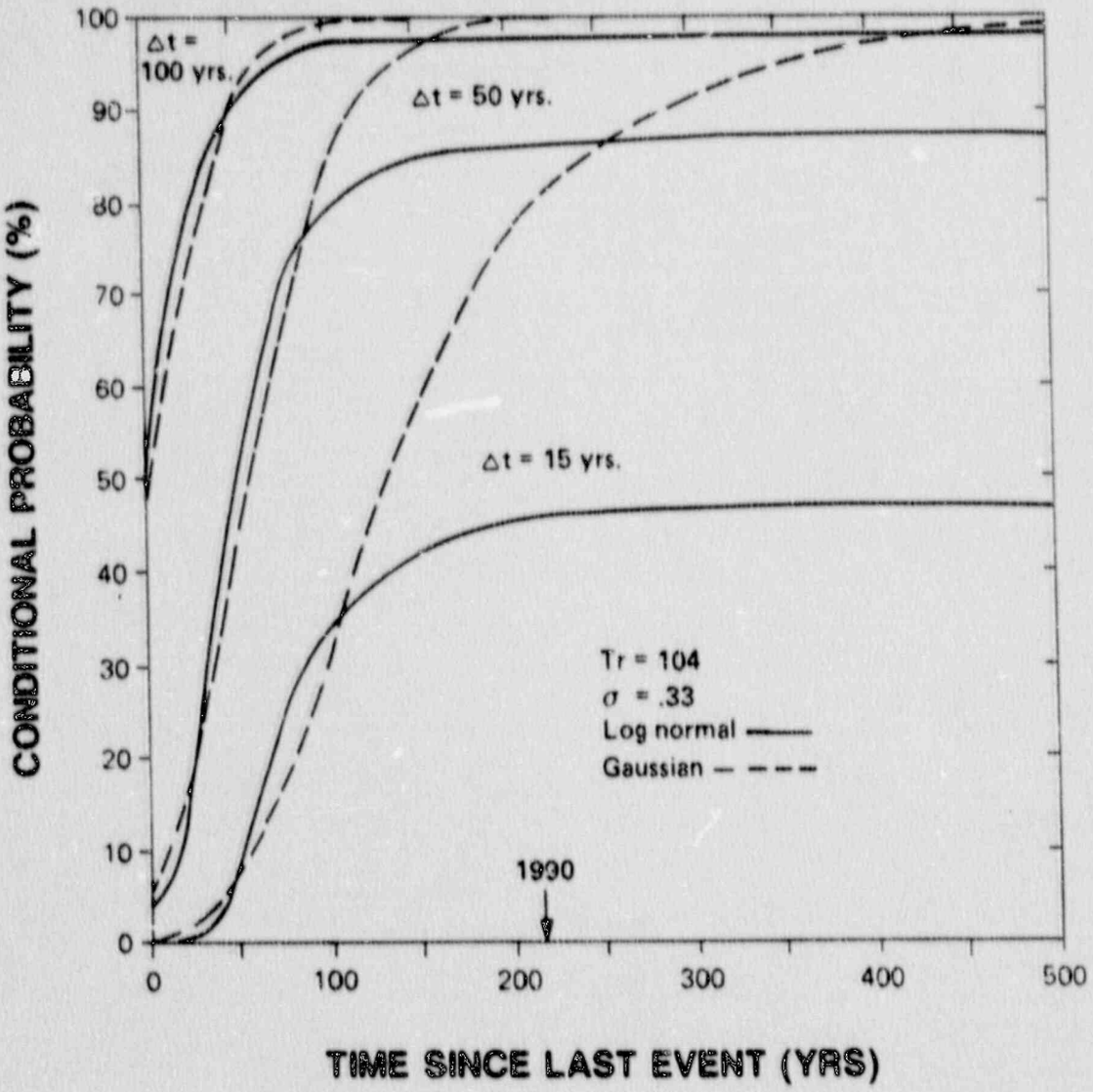

FIGURE 13.8: The frequency-magnitude relation derived by Bollinger and others (1989) suggests that the recurrence interval for an MM intensity VII earthquake is 104 years (T_r). These investigators modeled the MM intensity VII of 1912 as an aftershock of the 1886 earthquake and no other MM intensity VII events have been reported in their catalog. Consequently the time passed since the last such event is not known, However, these same authors suggest that the historical seismic record in the Charleston area is only complete for MM intensity VII earthquakes for the past 215 years. For Tr = 104 years and at assumed time since last event of 215 years, the conditional probabilities for the occurrence of an MM intensity VII earthquake were then estimated for time windows of 15, 50, and 100 years for an assumed standard deviation of 33%.

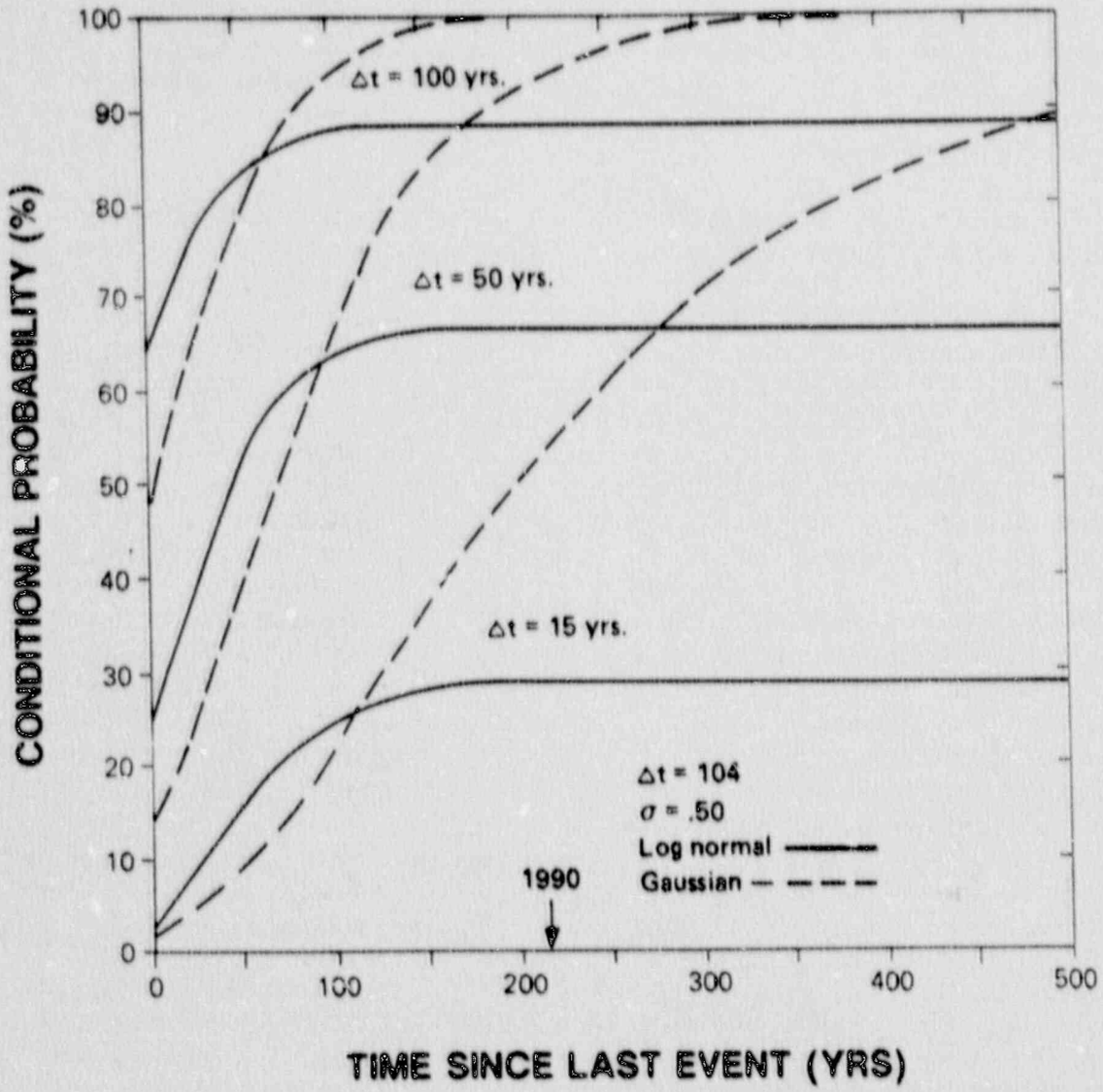

FIGURE 13.9: Conditional probabilities for the occurrence of an MM intensity VII earthquake for time windows of 15, 50, and 100 years. The recurrence interval (104) years is based on frequency-intensity relation of Bollinger and others (1989), time since last event assumed to be 215 years. A standard deviation of 50% was assumed for these calculations.

14.0 DISCUSSION

Over the past decade, three groups of investigators identified paleoliquefaction features located in the vicinity of the 1886 Charleston, S.C. earthquake. The morphology of these features were similar to liquefaction features which clearly formed as a result of the 1886 earthquake, and they were interpreted to represent prehistoric seismic events.

The characteristics of over 100 "control" seismically induced liquefaction sites and features located in the epicentral area of the 1886 Charleston, S.C., earthquake were evaluated during this study. The great majority of SIL sites were found to be located in the vicinity of the 1886 Charleston, SC earthquake occur in deposits which are either Holocene or mid to late Pleistocene in age (4,000 to about 250,000 years old). Materials older than about 250,000 years were found to be significantly less susceptible to liquefaction than these younger deposits (Figure 4.2). Beach settings were found to be the most favorable depositional environment for the generation and preservation of seismically-induced liquefaction features (Figure 4.3). Virtually all liquefaction sites for which local stratigraphic information was available are underlain by at least three meters of sand, or by at least three meters of alternating sand, silt, and clay beds. The depth to the probable source beds at these liquefaction sites is in virtually every case less than six to seven meters and the ground-water table is characteristically less than three meters beneath the present ground surface. Finally, all of the seismically induced liquefaction sites identified on the basis of historical accounts of the 1886 earthquake and most of the seismically induced liquefaction sites associated with pre-historic earthquakes were located within 40 kilometers of an epicentra of the 1886 earthquake or the epicenter of more recent instrumentally located seismicity.

The two most common seismically induced liquefaction features observed during these studies were sand-blow explosion craters and sand vents/fissures. Sand-blow explosion craters formed as a result of the explosive upward movement of pore fluids and liquefied materials and were associated with a concave upwards bowl shaped "craters". They were roughly circular to elliptical in plan view. In section, their most distinguishing characteristics were a central "feeder vent" and two separate clast zones, which form near the bottom and top of the crater as a result of differential settlement following the initial explosive excavation of the crater (Figure 5.2). This type of SIL feature occurs almost exclusively where no significant confining layer other than a soil profile is present over liquefiable sands and where the source beds are relatively thick and loose (Figure 5.3). In the Charleston area this local stratigraphic setting is most commonly found in old beach and near-shore marine depositional environments. Significantly, this type of SIL liquefaction feature is virtually absent in fluvial sites, where thinly bedded silts, sands and clays are common.

In addition, sand vents/fissures were also found in the Charleston area. At almost all locales where sand vents/fissures were found, a non-liquefiable confining layer or "cap" was present over the source bed of liquefied sands. At some sites the

cap appeared to have been transported short distances down slope due to a loss of friction along the boundary between the cap and the underlying sand resulting from the formation of water interlayers. During transport, the cap apparently failed under laterally directed tension, resulting in the ejection of the underlying liquefied sands into tabular fissures in the cap materials. The fissures at these sites were generally oriented normal to the direction of lateral transport (Figure 5.5). At other sand vent sites, the cap appeared to have been shattered in place due to heaving associated with elevated pore pressures within the underlying water interlayer and/or oscillatory motion between the cap and the underlying liquefied sands. At these sites the cap was often broken in polygons rather than along distinct tabular fissures. In the Charleston area, the local stratigraphic setting most commonly associated with sand vents/fissures are interbedded river terrace or back-barrier deposits (Figure 5.7). Although liquefiable these deposits are generally thinner and not as loose as materials at locales where explosion craters were found.

A systematic evaluation of remote sensing imagery including black and white, color and infrared photographs was conducted during this study. Low altitude aerial surveys were also carried out. Unfortunately, no consistently recognizable expressions for either liquefaction sites associated with the 1886 earthquake or liquefaction sites associated with older, pre-historic earthquakes was found. Most importantly from the point of view of finding prehistoric liquefaction events in other areas of the Atlantic Seaboard, none of the pre-1886 liquefaction structures was found to be associated with recognizable expressions on the available imagery.

About one third of the sites in the Charleston area were found to be associated with characteristic topographic depressions identified on 1:24,000 scale topographic maps (Figure 7.1). These features were primarily associated with historical SIL sites located in beach complexes and took the form of a series of small circular to elliptical depressions along the dune crests. The preferred model for the development of these features suggests that they indicate loose, thick sand deposits, which were especially susceptible to liquefaction when saturated. Consequently, this distinctive morphology could possibly be used to identify areas where thick deposits of loose liquefiable sands are present and/or areas where liquefaction may have occurred in the recent geologic past.

During this study, Ground Penetrating Radar (GPR) was also tested at known liquefaction sites located in the Charleston area, to determine if this technique could be used as a reconnaissance tool in the search for paleoliquefaction features outside the Charleston area. The results of these tests at control liquefaction sites found that in interbedded depositional settings where an identifiable fine grained "cap" was present over the source sands, GPR anomalies were associated with the known liquefaction features (Figure 7.6).

Based on the findings of these control studies, a systematic search for similar seismically induced paleoliquefaction features in other parts of the Atlantic Coastal Plain was implemented. The search has focused on late Quaternary beach and near shore deposits in Virginia, North Carolina, South Carolina, and Georgia. These

deposits are most similar to the units where the great majority of liquefaction features have been identified in the Charleston area. In addition, limited studies have also been conducted along the James River in Central Virginia and near Wilmington, Delaware (locales of moderate seismicity in the 1800's). Limited studies were also conducted on the Delmarva Peninsula, northward to the Delaware Bay (Figure 9.1 and Plate 1).

To date, no conclusive paleoliquefaction evidence of large prehistoric earthquakes originating outside of South Carolina has been found (Figure 11.1). Given the caveats expressed in earlier chapters, these findings suggest that over the past several thousand years coastal South Carolina has been more seismically active than the other areas studied.

Based on the results of paleoliquefaction studies within South Carolina, several important observations can be made. In addition to SIL resulting from the 1886 earthquake, radiocarbon dates indicate that perhaps as many as six other earthquakes associated with liquefaction occurred in coastal South Carolina during Holocene times (Figure 12.1). Each of these earthquakes is inferred to have been greater than magnitude 5.8$\pm$.4 (the threshold required to generate SIL features). The M, 7.1 1886 earthquake generated liquefaction features over the same general area as the two most recent prehistoric liquefaction episodes and it is inferred that they were caused by earthquakes of similar magnitude. This suggests that the 1886 could be viewed as the "characteristic event" for the Charleston source area. At this time, data are inconclusive regarding distribution of liquefaction features associated with older Charleston liquefaction episodes and additional studies would be required to provide more definitive information regarding the size of these older Charleston earthquakes.

Paleoliquefaction data also suggested that past large earthquakes within coastal S.C. may not have been limited exclusively to the established Charleston epicentral area. In addition to the six large earthquakes originating near Charleston, an earthquake located within a different epicentral area may have occurred about 1800$\pm$200 years ago. This earthquake could have originated in the Georgetown/Myrtle Beach area. Alternately, the outlying paleoliquefaction features used to identify this new source area may be a result of the increased liquefaction potential of shallow sediments due to elevated ground-water levels resulting from a slightly higher sea level stand. If this was the case, an 1886-like earthquake occurring in the Charleston area could have generated the observed SIL features. However, this hypothesis could only be confirmed if SIL features of similar ages are subsequently found in the Charleston area. To date, no such features have been discovered. Additional studies would be required to confirm the existence of this postulated northern source and to better quantify its seismic potential and associated return periods.

The mean return period between liquefaction episodes identified in South Carolina is 1009 years. If only those earthquakes located in Charleston are considered the mean return period is approximately 1250 years. The

paleoliquefaction data suggest that the apparent interval between liquefaction episodes has decreased from as much as 2000 years during mid-Holocene times to about 600 years in more recent times. However, since sea level has been at or near its present level over the past 2000 years and climatic conditions have been relatively stable, the paleoliquefaction record is probably most complete for this period. The return period between large earthquakes during this time probably is more representative of the overall seismic process acting in the area than the overall mean.

During the period 2000 YBP to about 5000 YBP sea level was generally one to four meters below present levels and fluctuated widely. Consequently, the paleoliquefaction record for this time interval probably includes only those earthquakes which occurred during periodic transgressive seas and/or wet climatic periods. Further, before about 5000 YBP the climate in the southeastern United States was drier and sea level was more than four meters lower than present. Such conditions would severely reduce or eliminate the potential for SIL and may explain the absence of early Holocene paleoliquefaction features in the paleoliquefaction record.

With respect to long-term seismic hazard, paleoliquefaction seismic data suggest that the probability of an earthquake similar to the 1886 event occurring within the next several decades is less than 5%. While the potential for an earthquake large enough to produce significant liquefaction features is very low, the hazard presented by smaller earthquakes should not be overlooked. Frequency-magnitude relations derived from historical data suggest that the probability of a event similar to the intensity VII 1912 Charleston-Summerville earthquake occurring during the next few decades is relatively high (over 60%). Although smaller than the 1886 earthquake, such an event could be in the magnitude m_b 5.0 to 6.0 range. Given the low attenuation characteristics of the region such an event would be felt throughout the Southeastern U.S. and would be of engineering concern in the epicentral region.

BIBLIOGRAPHY

Amick, D. and P. Talwani (1986). Earthquake recurrence rates and probability estimates for the occurrence of significant seismic activity in the Charleston area: The next 100 years, Third U.S. National Conference on Earthquake Engineering, Vol. 1, (1986) p. 55-64.

Amick, D., R. Gelinas, G. Maurath, and R. Cannon (1990). Paleoliquefaction Studies along the Atlantic Seaboard-Implications for Long-Term Seismic Hazard Proceedings of the 17th Water Reactor Safety Information Meeting, Nuclear Regulatory Commission, Rockville, Maryland, October 23-25, 1989. (in press).

Amick, D., G. Maurath, and R. Gelinas (1990). Characteristics of Seismically-Induced Liquefaction Sites and Features Located in the Vicinity of the 1886 Charleston, South Carolina Earthquake, in press, Seismological Research Letters.

Amick, D.C., and P. Talwani (1991). The Use of Paleoliquefaction Features to Estimate Prehistoric Levels of Ground Motion. Proceedings of the Second International Conference on Recent Advances in Geotechnical Earthquake Engineering and Soil Dynamics, St. Louis, Missouri, March 11-15, 1991.

Armbruster and L. Seeber (1983). 1886-1889 "Aftershocks" of the Charleston, South Carolina, Earthquake: A regional burst of seismicity, U.S.G.S. Proc. of Conference XX, p. 107-116.

Bender, B. (1983). Maximum likelihood estimation of b values for magnitude grouped data, Bull. Seismol. Soc. Am., 73, 831-851.

Bollinger, G.A. (1973). Seismicity of the Southeastern United States, Bulletin of the Seismological Society of America, Vol. 63, No. 5, p. 1785-1808.

Bollinger, G.A. (1975). A catalog of Southern United States earthquake-1754 through 1974: Virginia Polytech. Inst. and State Univ. Research Div. Bull. 101, 68 p.

Bollinger, G.A. (1977). Reinterpretation of the intensity data for the 1886 Charleston, South Carolina, earthquake, in Studies related to the Charleston, South Carolina, earthquake of 1886 - A preliminary report, D.W. Rankin, ed., U.S. Geol. Survey Prof. Paper 1028, p. 17-32.

Bollinger, G.A. (1986). The epicenter of the m_b 5, December 22, 1875 Virginia Earthquake: New findings from documentary sources. EQ Note (SSA) Vol. 52., No. 3.

Bollinger, G.A., F.C. Davison, Jr., and M.S. Sibol (1990). Magnitude recurrence relations for the southeastern United States and its subdivisions, Journal of Geophysical Research, Vol. 94, No. 83, p. 2857-2873.

Bolt, B.A. (1978). Earthquake Hazards Transactions of the American Geophysical Union, Vol. 59, p. 946-962.

Brooks, M.J., P.A. Stone, D.J. Colquhoun, and J.G. Brown (1989). Sea Level Change, Estuarine Development and Temporal Variability in Woodland Period Subsistence-Settlement Patterning on the Lower Coastal Plain of South Carolina. Chapter 5 in Studies in South Carolina Archaeology: Essays In Honor of Robert L. Stephenson, edited by Albert C. Goodyear, III, and Glen T. Hanson, Anthropological Studies 9, Occasional Papers of the South Carolina Institute of Archaeology and Anthropology.

Brown, J.G. (1981). Palynologic and Petrographic Analyses of Bayhead Hammock and Marsh Peats at Little Salt Spring Archaeological Site (8-So-18), Florida. M.S. thesis, Department of Geology, University of South Carolina, Columbia.

Castro, G. (1975). Liquefaction and cyclic mobility of saturated sands, ASCE J. Geotech. Engin. Div., 101, GT6, p. 551-569.

Cleaves, E.T., J.D. Glaser, A.D. Howard, G.H. Johnson, W.H. Wheeler, W.D. Sevon, S. Judson, J.P. Owens, and P.C. Peebles (1987). Quaternary geologic map of the Chesapeake Bay 4° x 6° quadrangle, United States: U.S. Geologic Survey Miscellaneous Investigations Map I-1420 (NJ-18), Scale 1:1,000,000.

Cluff, L.S., A.S. Patwardhan, and K.J. Coppersmith (1980). Estimating the probability of occurrences of surface faulting earthquakes on the Wasatch fault zone, Utah, Bull. Seismol. Soc. Am., 70, p. 1463-1478.

Colquhoun, D.J. (1965). Terrace sediment complexes in South Carolina, Atlantic Coastal Plain Geological Association Field Conference, Univ. of South Carolina Press, Columbia.

Colquhoun, D.J. (1969). Geomorphology of the Lower Coastal Plain of South Carolina, Div. of Geology, State Development Board, Columbia, SC, MS-15.

Colquhoun, D.J., M.J. Brooks, W.H. Abbott, F.W. Stapor, W.S. Newman, and R.R. Pardi (1980). Principles and Problems in Establishing a Holocene Sea-level Curve for South Carolina. In Excursions in Southeastern Geology, Geological Society of America, Guidebook 20:143-159. Edited by Howard et al.

Colquhoun, D.J. (1981). Variation in sea level on the South Carolina Coastal Plain, in volume of same title published by Department of Geology, University of South Carolina for meeting of UNESCO-IGCP Project 61, Columbia, South Carolina, p. 1-44.

Colquhoun, D.J., L. Campbell, S. Campbell, J. Ernissee and W. Abbott (1977). Significant age revisions of Atlantic coastal terraces, eastern North America [abs.]: International Union for Quaternary Research, 10th Congress, Birmingham, United Kingdom, Abstracts, p. 94.

Colquhoun, D.J., S.M. Herrick, H.G. Richards, (1968). A fossil assemblage from the Wicomico Formation in Berkeley County, South Carolina: Geological Society of America Bulletin, v. 79, no. 9, p. 1211-1220.

Colquhoun, D.J., M.S. Friddell, W.H. Wheeler, R.B. Daniels, J. P. Gregory, R.A. Miller, and A.K Van Nostrand, (1987). Quaternary geologic map of the Savannah 4° x 6° quadrangle, United States: U.S. Geologic Survey Miscellaneous Investigations Map I-1420 (NI-17), Scale 1:1,000,000.

Cooke, C.W. (1936). Geology of the coastal plain of South Carolina: U.S. Geological Survey Bulletin 867, 196 p.

Cooke, C.W. (1943). Geology of the coastal plain of Georgia: U.S. Geological Survey Bulletin 941, 121 p.

Cox, J. and P. Talwani (1983). Paleoseismic studies in the 1886 Charleston earthquake meizoseismal area, Geol. Soc. Am. Abstracts with Programs, 16, 130.

Cox, J.H.M. (1984). Paleoseismology studies in South Carolina: M.S. thesis, Univ. of South Carolina, Columbia, 75 p.

Dewey, J.W. (1985). A review of recent research on the seismotectonics of the Southeastern seaboard and an evaluation of hypotheses on the source of the 1886 Charleston, South Carolina, earthquake. NUREG/CR-4439: 1-44. U.S. Nuclear Regulatory Commission. Washington, D.C., 44 p.

Dobry, R., R.S. Ladd, F.Y. Yoke., R.M. Chung, and D. Powell (1982). Prediction of pore water pressure buildup and liquefaction of sands during earthquakes by the cyclic strain method, National Bureau of Standards, Washington DC, NBS Building Science Series 138.

DuBar, J.R., and J.R. Solliday (1963). Stratigraphy of the Neogene deposits, lower Neuse Estuary, North Carolina: Southeastern Geology, v. 4, no. 4, p. 213-233.

DuBar, J.R., J.R. Solliday, and J.F. Howard, (1974). Stratigraphy and morphology of Neogene deposits, Neuse River Estuary, North Carolina, in Oaks, R.Q., Jr., and DuBar, J.R., eds., Post-Miocene stratigraphy, central and southern Atlantic Coastal Plain: Logan, Utah, Utah State University Press, p. 102-122.

DuBar, J.R., S.S. DuBar, L.W. Ward and B.W. Blackwelder with contributions by W.H. Abbott and P.F. Huddlestone (1980). Cenozoic biostratigraphy of the Carolina outer Coastal Plain, in R.W., Frey and T.L. Neathery, editors, Excursions in Southeastern Geology, v. 1, Geological Society of America 1980 Annual Meeting Atlanta, Georgia: American Geological Institute, p. 179-236.

Dutton, C.E. (1889). The Charleston earthquake of August 31, 1886, U.S. Geol. Survey Annual Rpt. 1887-1888, p. 203-528.

Fallaw, W.C. and W. H. Wheeler (1969). Marine fossiliferous Pleistocene deposits in southeastern North Carolina: Southeastern Geology, v. 10, no. 1, p. 35-54.

Gelinas, R.L. (1986). Mineral alterations as a guide to the age of sediments vented by prehistoric earthquakes in the vicinity of Charleston, South Carolina: M.S. Thesis, Univ. of N.C., 304 p.

Gelinas, R., D. Amick, and G. Maurath (1990). The search for seismically induced paleoliquefaction features outside the Charleston, SC area, 4th US Conference on Earthquake Engineering, Palm Springs, CA, May, 1990.

Gohn, G.S., R.E. Weems, S.F. Obermeier, and R.L. Gelinas (1984). Field studies of earthquake-induced, liquefaction-flowage features in the Charleston, South Carolina, area--preliminary report U.S. Geol. Survey Open File Rpt. 84-670, 26 p.

Gutenberg, B., and C.F. Richter (1956). Magnitude and energy of earthquakes, Ann. Geof., 9, p. 1-15.

Hoyt, J.H., R.J. Weimer, V.J., Henry (1965). Age of late Pleistocene coastal deposits, central Georgia: Abstracts, International Association for Quaternary Research 7th Congress, p. 228.

Hoyt, J.H. and J.R. Hails (1967). Pleistocene shoreline sediments in coastal Georgia-Deposition and modification: Science, v. 155, p. 1541-1543.

Hoyt, J.H. and J.R. Hails (1974). Pleistocene stratigraphy of southeast Georgia, in Oaks, R.W., Jr., and DuBar, J.R., editors, Post-Miocene stratigraphy, central and southern Atlantic coastal plain: Logan, Utah State University Press, p. 191-201.

Ishihara, K. (1985). Stability of Natural Deposits During Earthquakes, Proceedings of the Eleventh International Conference on Soil Mechanics and Foundation Engineering, San Francisco, VOl. 1, 1985, pp. 321-376.

Johnson, G.H. and P.C. Peebles (1986). Quaternary geologic map of the Hatteras 4° x 6° quadrange, United States: U.S. Geologic Survey Miscellaneous Investigations Map I-1420 (NI-18), Scale 1:1,000,000.

Johnston, A.C. (1981). On the use of the frequency-magnitude relation in earthquake risk assessment, in Earthquakes and Earthquake Engineering-Eastern United States, vol. 1, edited by J.E. Beavers, pp. 161-181, Ann Arbor Science, Ann Arbor, Mich.

Johnston, Arch C., and Susan J. Nava (1985). Recurrence Rates and Probability Estimates for the New Madrid Seismic Zone, Journal of Geophysical Research, v. 90, p. 6737-6753.

Jordan, R.R., T.E. Pickett and K.D. Woodruff (1972). Delaware Geological Survey, Preliminary Report on Seismic Events in Northern Delaware, Open File Report No. 2.

Liddicoat, J.C., D.F. Belknap, J.F. Wehmiller (1982). Pleomagnetic and amino acid dating of sediment in the Atlantic Coastal Plain: Geological Society of America Abstracts with Programs, v. 14, no. 7, p. 546.

Liu, H., and T. Qiao (1984). Liquefaction potential of saturated sand deposits underlying foundation of structure: Proceedings of the 8th World Conference on Earthquake Engineering III, San Francisco, 199-206.

Maurath, G., and D. Amick (1988). Characterization of liquefaction sites/ features in the Charleston, S.C. area: Proceedings of the second international conference on case histories in geotechnical engineering, June 1-5, 1988.

McCartan, Lucy, R.E. Weems, E.M. Lemon, Jr. (1980). The Wando Formation (Upper Pleistocene) in the Charleston, South Carolina, area: U.S. Geological Survey Bulletin 1502-A, p. A110-A116.

McCartan, Lucy, E.M. Lemon, Jr. and R.E. Weems (1982). Generalized geologic map of the Charleston, South Carolina, area: U.S. Geological Survey Open-File Report 82-187, scale 1:575,000.

McCartan, Lucy, J.P. Owens, B.W. Blackwelder, B.J. Szabo, D.F. Belknap, D.F. Kriausakul, R.M. Mitterer and J.F. Wehmiller (1982). Comparison of amino acid racemization geochronometry with lithostratigraphy, biostratigraphy, uranium-series coral dating, and magnetostratigraphy in the Atlantic Coastal Plain of the southeastern united States: Quaternary Research, v. 18, p. 337-359.

McCartan, L., E.M. Lemon, and R.E. Weems (1984). Geologic map of the area between Charleston and Orangeburg, South Carolina, U.S. Geol. Survey Misc. Invest. Map I-1472.

McCulloch, D.S., and M.G. Bonilla (1970). Effects of the earthquake of March 27, 1964, on the Alaska railroad, U.S. Geol. Survey Prof. Paper 545-D.

Mixon, R.B., B.J. Szabo, J.P. Owens (1982). Uranium-series dating of mollusks and corals, and age of Pleistocene deposits, Chesapeake Bay area, Virginia and Maryland: U.S. Geological Survey Professional Paper 1067-E, 18 p.

National Bureau of Standards, (1953). Tables of Normal Probability Functions, NBS Appl. Math. Ser., vol. 23, 344 pp., U.S. Government Printing Office, Washington, D.C.

Nishenko, S.P. (1985). Seismic potential for large and great interplate earthquakes along the Chilean and southern Peruvian margins of South America: A quantitative reappraisal, J. Geophys. Res, 90, 3589-3615.

Nishenko, S.P. and R. Buland (1987). A Generic Recurrence Interval Distribution for Earthquake Forecasting, Bulletin of the Seismological Society of America, Vol. 77, No. 4, pp. 1382-1399.

Nuttli, O. W. (1983). 1885 Charleston, South Carolina, earthquake revisited: Proceedings of Conference XX, a workshop on "The 1886 Charleston, South Carolina, earthquake and its implications for today," W.W. Hays and P.L. Gori, eds., U.S. Geol. Surv. Open File Rpt. 83-843, p. 44-50.

Obermeier, S.F. (1984). Liquefaction potential in the Central Mississippi Valley, U.S. Geol. Survey Open-File Report 84-515.

Obermeier, S.F., G.S. Gohn, R.E. Weems, R.L. Gelinas, and M. Rubin, (1985). Geologic evidence for recurrent moderate to large earthquakes near Charleston, South Carolina, Science, 227, p. 408-411.

Obermeier, S.F., R.B. Jacobsen, D.S. Powers, R.E. Weems, D.C. Hallbick, G.S. Gohn, and H.W. Markenwich (1986). Holocene and Late Pleistocene (?) earthquake-induced sand blows in coastal South Carolina: Proceedings of the Third U.S. National Conference on Earthquake Engineering--Charleston, South Carolina, I, 197-208.

Obermeier, S., R.E. Weems, and R.B. Jacobson (1987). Earthquake-induced liquefaction features in the Coastal South Carolina Region, U.S. Geol. Survey Open-File Report 87-504.

Obermeier, S.F., R.E. Weems, R.B. Jacobson, and G.S. Gohn (1989). Liquefaction evidence for repeated Holocene earthquakes in the Coastal Region of South Carolina, Annuals of the N.Y. Academy of Sciences, 558, p. 183-195.

Obermeier, S.F., R.B. Jacobson, J.P. Smoot, R.E. Weems, G.S. Gohn, J.E. Monroe, and D.S. Powars (1990). Earthquake-induced liquefaction features in the coastal setting of South Carolina and in the fluvial setting of the New Madrid Zone, U.S. Geol. Survey Prof. Paper 1504.

Owens, J.P., C.S. Denny (1979)[1980]. Upper Cenozoic deposits of the central Delmarva Peninsula, Maryland and Delaware: U.S. Geological Survey Professional Paper 1067-A, p. A28.

Peters, K.E. and R.B. Herrmann (1986). First-hand observations of the Charleston earthquake of August 31, 1886, and other earthquake materials, S.C. Geol. Survey Bull. 41, p. 116.

Rankin, D.W. (ed.) (1977). Studies related to the Charleston, South Carolina, earthquake of 1886--A preliminary report: U.S. Geological Survey Professional Paper 1028, p. 1-204.

Richards, H.G. (1950). Geology of the Coastal Plain of North Carolina: American Philosophical Society Transactions, v. 40, pt. 1, 83 p.

Russ, D.P. (1979). Late Holocene faulting and earthquake recurrence in the Reelfoot Lake area, northwestern Tennessee, Geol. Soc. Am. Bull. 90 (Part 1), p.1013-1018.

Russ, D.P. (1982). Style and significance of surface deformation in the vicinity of New Madrid, Missouri, Investigations of the New Madrid, Missouri, Earthquake Region, U.S. Geological Survey Prof. Paper 1236, p. 95-114.

Schwartz, D.P. and K.J. Coppersmith (1984). Fault behavior and characteristic earthquakes: Example from the Wasatch and San Andreas faults, J. Geophys. Res., 89, p. 5681-5698.

Scott, T.M., M. S. Knapp, and D. L. Weide (1986). Quaternary geologic map of the Jacksonville 4° x 6° quadrangle, United States: U.S. Geologic Survey Miscellaneous Investigations Map I-1420 (NH-17), Scale 1:1,000,000.

Seeber, L., and J.G. Armbruster (1981). The 1886 Charleston, South Carolina earthquake and the Appalachian detachment: Journal of Geophysical Research, vol. 86, p. 7874-7894.

Seed, H.B. (1968). Landslides During Earthquakes due to Liquefaction, Journal Soil Mechanics and Foundations Div., ASCE, 94:SM5, pp. 1053-1122.

Seed, H.B. and I.M. Idriss (1971). Simplified Procedure for Evaluating Soil Liquefaction Potential, Journal of the Soil Mechanics and Foundations Division, ASCE, Vol. 97, No. SM9, pp. 1249-1277.

Seed, H.B. and I.M. Idriss (1982). Ground motions and soil liquefaction during earthquakes, EERI Monograph Series, p. 134.

Shimazaki, K., and T. Nakata (1980). Time-predictable recurrence model for large earthquakes, Geophys. Res. Lett., 7, p. 279-282.

Sieh, K.E. (1978). Prehistoric large earthquakes produced by slip on the San Andreas fault at Pallett Creek, California, J. Geophys. Res., 83, p. 3907-3939.

Stover, C.W., B.G. Reagor, S.T. Algermissan, L.T. Long (1979. Seismicity map of the State of Georgia, U.S. Geological Survey MF 1060.

Swan, F.H., III, D.P. Schwartz, and L.S. Cluff (1980). Recurrence of moderate to large magnitude earthquakes produced by surface faulting on the Wasatch fault zone, Utah, Bull. Seismol. Soc. Am., 70, p. 1431-1462.

Swan, F.H., Kelson, K.I., and Coppersmith, K.J. (1989). Paleoseismic History of the Meers Fault, southwestern Oklahoma and its implications to evaluations of earthquake hazards in the center and eastern United States, Transactions of the Seventeenth Water Reactor Safety Information Meeting, Oct. 1989.

Taber, S. (1914). Seismic activity in the Atlantic Coastal Plain near Charleston, South Carolina: Seismol. Soc. Bull., v. 4, no. 3, p. 108-160.

Talwani, Pradeep (1982). Internally consistent pattern of seismicity near Charleston, South Carolina: Geology, vol. 10, p. 654-658.

Talwani, P. (1985). Current thoughts on the cause of the Charleston, South Carolina earthquakes, South Carolina Geol. 29, p. 19-38.

Talwani, P., and J. Cox (1985). Paleoseismic evidence for recurrence of earthquakes near Charleston, South Carolina, Science, 229, p. 379-381.

Tarr, A.C., P. Talwani, S. Rhea, D. Carver, and D. Amick (1981). Results of recent South Carolina seismological studies: Seismological Society of America Bulletin, vol. 71, p. 1883-1902.

U.S. Geological Survey Staff (1990). The Loma Prieta, California, earthquake: An anticipated event, Science, Vol. 247 p. 286-293.

Wallace, R.E., J.F. Davis, and K.C. McNally (1984). Terms for expressing earthquake potential, prediction, and probability, Bull. Seism. Soc. Am. 74, p. 1819-1825.

Watts, W.A. (1971). Postglacial and Interglacial Vegetation History of Southern Georgia and Central Florida. Ecology 52: p. 676-690.

Watts, W.A. (1980). The Late-Quaternary Vegetation History of the Southeastern United States. Annual Review of Ecology and Systematics 11: p. 387-409.

Weems, R.E., S.F. Obermeier, M.J. Pavich, G.S. Gohn, M. Rubin, R.L. Phipps, and R.B. Jacobson (1986). Evidence for three moderate to large prehistoric Holocene earthquakes near Charleston, S.C.: Proceedings of the Third U.S. national conference on earthquake engineering, Charleston, South Carolina, I, p. 3-13.

Weems, R.E., R.B. Jacobson, S.F. Obermeier, G.S. Gohn and M. Rubin (1988). New radiocarbon ages from earthquake-induced liquefaction features in the lower Coastal Plain of the Carolinas: Geological Society of America Abstracts with Programs, vol. 20, no. 4.

Weems, R.E., S.F. Obermeier (1990). The 1886 Charleston Earthquake -- An Overview of Geological Studies, in press, in Proceedings of the 17th Water Reactor Safety Information Meeting (October 23-25, 1989).

Weibull, W.A. (1951). A statistical distribution function of wide application, J. Appl. Mech., 18, p. 293-297.

Youd, T.L. (1973). Liquefaction, flow and associated ground failure, U.S. Geol. Survey Cir. 688.

Youd, T.L. (1977). Packing changes and liquefaction susceptibility, J. of the Geotechnical Engr. Div., Proc. of the Am. Soc. of Civil Engr., 103, GT8, p. 918-922.

Youd, T.L. (1984). Recurrence of liquefaction at the same site: Proceedings of the Eighth World Conference on Earthquake Engineering, 3, p. 231-238.

APPENDIX A
THE APPLICATION OF GROUND PENETRATING RADAR IN THE SEARCH FOR PALEOLIQUEFACTION FEATURES

A.0 BACKGROUND

During this study Ground Penetrating Radar (GPR) was tested at known liquefaction sites located in the Charleston area, to determine if this technique could be used as a reconnaissance tool in the search for liquefaction features outside the Charleston area (especially where exposure was limited or nonexistent). Most of the discussion presented below is presented by Amick and others (1990).

A.1 Introduction

Over the past eighteen months we have tested Ground Penetrating Radar (GPR) GPR several controlled liquefaction sites located within the epicentral area of the 1886 Charleston, S.C. earthquake. This MM intensity X event resulted in the formation of numerous seismically induced liquefaction features throughout the southeastern coastal plain of S.C. However, one hundred years later, unless exposed in recent excavations, it is virtually impossible to find clear evidence at the ground surface of 1886 liquefaction features. This study was conducted to determine if the GPR technique could be used to identify and trace liquefaction features where no present day exposure exists.

Ultimately it is hoped that GPR can be used to aid in a search for paleoseismic evidence of large prehistoric earthquakes both within the Charleston, S.C. area, and elsewhere along the Atlantic Coastal Plain. In this Appendix, we present a background discussion of paleoseismicity as it relates to the Eastern United States, outline the need for developing remote sensing techniques to aid in the search for evidence of large prehistoric earthquakes, and discuss the results of GPR field tests in the Charleston area.

A.2 Paleoseismicity

Paleoseismicity is the search for evidence of prehistoric earthquakes as expressed in the geologic record. Previously, much of this work was centered in the western United States where numerous prehistoric earthquakes associated with surface faulting episodes have been documented. For example, paleoseismic investigations along portions of the San Andreas Fault have discovered geologic evidence which suggests that the recurrence times of large earthquakes to be on the order of several hundred years (Seih, 1978). Further, within the Basin and Range Province, far from the present plate boundary, paleoseismic investigations have clearly documented the repeated occurrence of characteristic large earthquakes with recurrence times on the order of several thousand years (Cluf and others, 1980).

In contrast, seismic sources within the eastern United States are still poorly defined and clear evidence of surface faulting (such as that found in the western U.S.) is generally lacking. In these areas paleoseismic studies have focused on the

identification and dating of secondary deformation features resulting from faulting or strong ground shaking, such as seismically induced liquefaction.

The two largest historical earthquake sequences to occur in the eastern United States (1811-1812, New Madrid, Mo. earthquakes and the 1886 Charleston, S.C. earthquake) each resulted in widespread liquefaction. Paleoseismic investigations in the New Madrid area have found sediments dated at about 2,250 BP which show evidence of liquefaction related to earthquakes that predated the 1811-1812 New Madrid events (Russ, 1979). These data suggest a recurrence interval of approximately 900 years for large potentially damaging earthquakes in the region. More recently, studies of seismically-induced liquefaction features associated with the 1886 Charleston, S.C. earthquake have revealed the existence of as many as three older liquefaction caused by similar large prehistoric earthquakes (see main text for discussion). Based on the ages of prehistoric liquefaction features, the time between these large Charleston earthquakes is estimated to be on the order of 500 to 1000 years.

While both the New Madrid and Charleston areas still exhibit higher levels of seismicity than most other areas in the eastern United States, recent studies of the Meers Fault have shown that structures responsible for large prehistoric earthquakes may be aseismic between large rare events (Swan and others, 1990). Most importantly from the stand point of seismic hazards, the results of many paleoseismic studies both in the eastern and western U.S. strongly suggest that the absence of moderate to large earthquakes during historical times and/or the lack of instrumental seismicity in a region does not in and of itself preclude the possible future occurrence of a large earthquake.

A.3 The Problem

Unlike many fault scarps in the western U.S, paleoliquefaction features such as those identified in the New Madrid and Charleston areas (as well as the small scale liquefaction features associated with the recent Saguenay earthquake in Quebec) are not generally associated with an identifiable geomorphologic expression. Virtually all prehistoric liquefaction features identified to date in the Charleston, S.C. and New Madrid areas have been discovered in existing excavations such as quarries, drainage ditches or borrow pits. Consequently, the search for such features is limited to areas where prior exposures are present, precluding an extensive search in most regions.

A.4 Ground Penetrating Radar

Ground penetrating radar (GPR) is a relatively recent addition to the remote sensing tools available for subsurface investigations. GPR uses a transducer to generate short-duration electromagnetic pulses (generally in the 80 to 500 Mhz range). The transmitted pulse travels through the subsurface until it reaches an interface where a portion of the transmitted pulse is reflected back to the surface and picked up by a receiver. The received signal is sent to the control unit where it

is processed and a real-time display of the information is presented on the systems graphic recorder.

Only interfaces associated with a change in the dielectric properties of the materials result in "reflections" on the GPR record. Dielectric properties are to a great extent related to the conductivity of the medium. Variations in dielectric and conductivity properties are most often the result of changes in the physical and chemical properties of the subsurface units. For example, changes in lithology, moisture content, and porosity are commonly associated with significant variations in the dielectric and conductivity values and result in identifiable "reflections" on GPR records.

The transmission and adsorption (attenuation) of GPR electromagnetic pulses is governed by two main factors. First, pulses generated using higher frequency transducers attenuate more rapidly than pulses generated using lower frequency transducers. While associated with less penetration, higher frequency signals do provide better resolution. Therefore, higher frequency sources/antennas are most effective at detecting variations in subsurface properties near the surface, while lower frequency sources/antennas have greater "penetration" power and are more effective at detecting deeper subsurface variations. Unfortunately, detailed information near the surface is lost in order to obtain the greater "penetration" power of lower frequency sources/antennas.

Secondly, and most importantly from the perspective of these discussions, the transmission and adsorption of the radar pulse is also controlled by the electrical properties of the material through which it is traveling. Generally, the higher the conductivity of a material the greater it attenuates the transmitted signal.

Based on this premise, GPR is sometimes used in hazardous waste site investigations to trace contaminant plumes which contain conductive pollutants such as solvents, salt compounds, acids, or metallic compounds. Often, the GPR signal is greatly attenuated by the highly conductive plume effectively masking any deeper horizons. This masking phenomena can also occur when highly conductive natural materials such as clays are present in the subsurface. In general, clays and to a lesser extent silts are associated with relatively higher conductivities than coarser grained materials such as sand. When these finer grained conductive materials are present they reflect and adsorb the GPR signal, resulting in a masking of underlying units.

A.5 Approach

As an initial test of the GPR technique, radar surveys were completed at seven known liquefaction sites located in the epicentral area of the 1886 Charleston earthquake. At each site where field tests were conducted, liquefaction features had already been identified in existing excavations during previous field studies. The results of these GPR surveys serve as control data to evaluate this technique as a means to locate and/or trace liquefaction features.

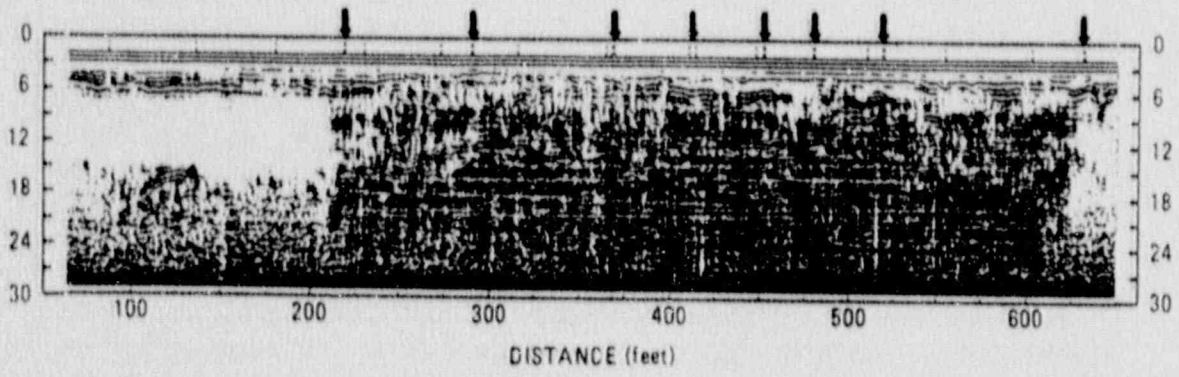

FIGURE A.1: Example of Ground Penetrating Radar traverse over a known liquefaction locale located in the Charleston, S.C. area. Arrows identify the location of larger liquefaction features previously mapped in a drainage ditch running parallel to the GPR traverse. As noted a series of sand vents have penetrated and disrupted the overlying silts and clays over a zone several hundred feet in width.

Of the seven control liquefaction sites evaluated, radar anomalies were noted at each of the four liquefaction sites located in fluvial depositional environments. Figures A.1 and A.2 provide examples of radar data from two of these previously identified seismically induced liquefaction locales. Note the distinct GPR anomaly associated with each of the previously identified zones of liquefaction. At all four fluvial sites the shallow units are clays and silts. In existing exposures these "cap" materials were observed to have been broken and disrupted by fluidized sand ejected from underlying units.

The GPR data from the three control liquefaction sites located in beach deposits failed to show any anomalies associated with the known liquefaction features. The absence of a GPR anomaly at liquefaction sites located in beach depositional settings is thought to be due to the similarity of the materials at these locales. Although sands from depth have been ejected into and through overlying sands and may be different in grain size, the conductivity of the overlying "host" sands and underlying "source" sands are essentially identical. Consequently, the GPR technique was unable to distinguish the liquefaction features.

A.6 Interpretation

As noted previously, in general the higher the conductivity of a material is the greater it attenuates the transmitted signal. Where the relatively high conductivity "cap" silts and clays are intact and have not been disrupted, the GPR signals have been attenuated greatly and fail to produce significant GPR returns from below

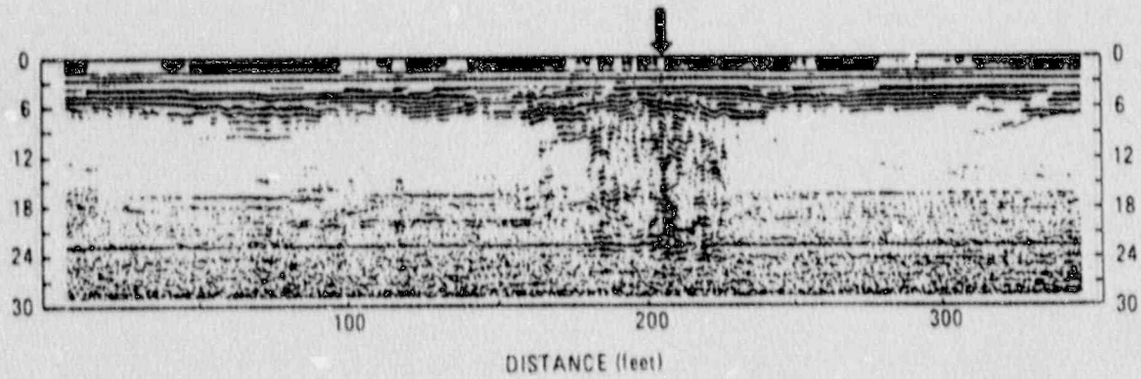

FIGURE A.2: Another example of a Ground Penetrating Radar traverse over a known liquefaction locale located in the Charleston, S.C. area. Arrow identifies the location of several large liquefaction features previously mapped in a drainage ditch running parallel to the GPR traverse. At this locale mapping within the ditch identified a series of sand vents that have disrupted the overlying silts and clays throughout a zone approximately 20 feet in width.

about 4 to 6 feet. In contrast where the "cap" has been broken by and/or incorporated into the liquefied underlying source sands, the attenuation of the GPR signal is much less and a "window" into the underlying materials is present.

A.7 Additional Field Tests

After initial studies established that GPR could be used as a reconnaissance tool to locate liquefaction features in favorable stratigraphic settings, additional GPR data was collected at a number of known liquefaction sites using a variety of instrument settings, data acquisition rates and transducer combinations to refine this exploratory method. This test confirmed that a 120 MHz transducer produced optimum results. Subsequently, as an additional field test of this technique, reconnaissance GPR data was then collected in several areas where local conditions appeared right for liquefaction, but where no liquefaction features have been identified previously.

Several potential liquefaction sites in the Charleston area were identified solely on the basis of this reconnaissance GPR survey. Figures A.3 and A.4 illustrate the GPR anomalies discovered along several of these profiles. Note the similarity of anomalies present on Figures A.3 and A.4 with those associated with known liquefaction features shown on Figures A.1 and A.2.

Trenches were subsequently excavated across the GPR anomalies shown. In each case, features interpreted to be the result of seismically induced liquefaction were observed. Figure 7.6 in the main text presents a photograph showing the disrupted cap materials and associated sands unearthed in one of these test trenches.

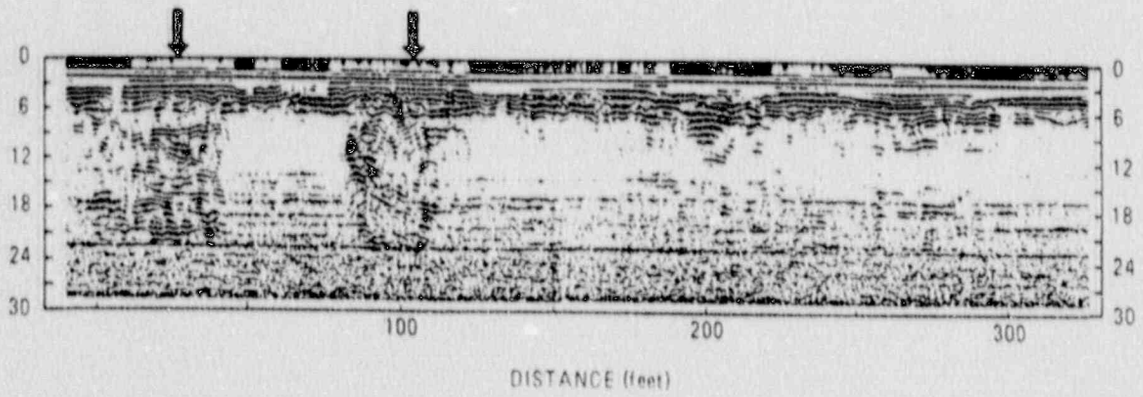

FIGURE A.3: Example of Ground Penetrating Radar traverse where no liquefaction features were known to be present. Note the similarity of these anomalies with that shown in Figure 2. Subsequent trenching confirmed the presence of liquefaction features in each area.

A.8 Summary

Over the past eighteen months, the authors have field tested Ground Penetrating Radar (GPR) as a method to identify and trace seismically induced liquefaction features in areas where no preexisting excavations are present. As the first step in this study, GPR surveys were completed at known liquefaction sites located in the epicentral area of the magnitude 6.7-7.1 Charleston earthquake of August, 1886. Liquefaction features had previously been identified in existing excavations at each of these control sites.

This field test found that in interbedded depositional settings where an identifiable fine grained "cap" was present over the source sands, GPR anomalies were associated with the known liquefaction features. At these sites the near surface materials are silts and clayey sands, which due to their relatively high conductivities, tend to attenuate the GPR signal. In areas where underlying sands have experienced liquefaction and moved upward resulting in the rupture or disruption of the overlying "cap" a distinctive GPR anomaly is observed.

Subsequently, as an additional field test of this technique, GPR data was then collected in several areas where local conditions appeared to be right for liquefaction, but where no liquefaction features have been identified previously. Several potential liquefaction sites in the Charleston area were identified solely on the basis of this reconnaissance GPR survey. Trenches were excavated across several of these GPR anomalies and, in each trench, liquefaction features were observed.

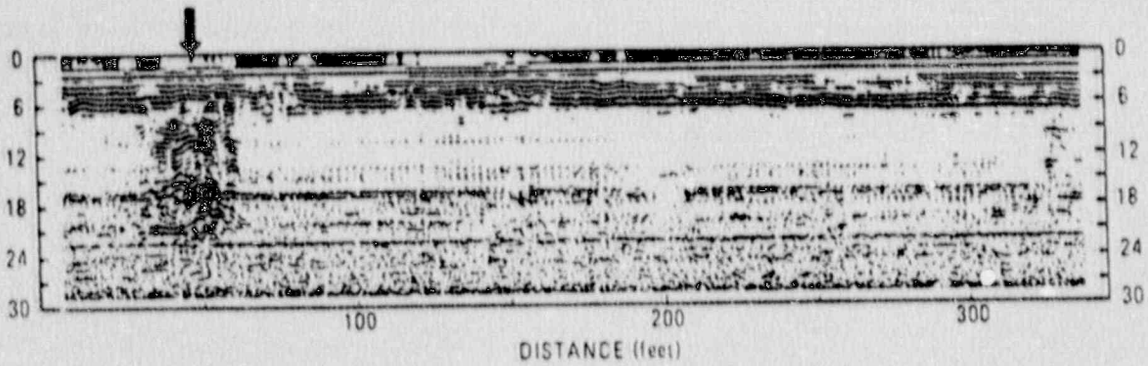

FIGURE A.4: Another example of Ground Penetrating Radar profile where no liquefaction features were known to be present. Again note the similarity of this anomaly with that shown in Figures 1, 2, and 3. Subsequent trenching confirmed the presence of liquefaction features over a zone 30 feet in width.

Based on this successful test, GPR is currently being used as a reconnaissance tool to aid in the search for paleoliquefaction features elsewhere along the Atlantic Seaboard. The ultimate goal of these investigations is to determine if prehistoric earthquakes similar to the 1886 Charleston, S.C. earthquake have occurred elsewhere in the region, and, if so, assess the potential for their occurrence in the future.

A.9 Recommended Additional Studies

The results of field tests conducted in the Charleston S.C. area suggest that where an identifiable silt or clay "cap" is present and/or where finer grained materials overly clean sands, GPR can be used to identify and trace liquefaction features. However, these tests have been limited to the Charleston region. To further test and refine this reconnaissance tool additional controlled studies should be conducted in other areas where seismically induced liquefaction features are known to be present. The goal of these recommended studies is to further test (GPR) as a method for locating and tracing paleoliquefaction sites. Subsequent trenching of radar anomalies (paleoliquefaction features) will also provide additional information on the characteristics of liquefaction features and their morphology. This data will enhance the understanding of how prehistoric liquefaction features are represented in the geologic record.

APPENDIX B
RADIOCARBON AGE DATING - BACKGROUND AND APPROACH

B.0 BACKGROUND

Radiocarbon dating is the principal method for determining the age of organic materials that are less than about 40,000 years old. This method uses the presence and established decay rate of a natural occurring radioactive isotope of carbon (C-14) to estimate the age of organic materials.

Carbon-14 is formed in the earth's upper atmosphere due to the interaction of cosmic ray neutrons with Nitrogen-14. The C-14 formed as a result of this interaction is oxidized in the earth's atmosphere into carbon dioxide, which is incorporated into plants during photosynthesis. Through plants, C-14 is introduced to the food chain. The ratio of C-14 to C-12 and C-13 in the cells of an organism is the same as the ratio of C-14 present in atmospheric carbon dioxide. However, once an organism dies, its C-14 is no longer "recharged" by flow from the atmosphere and the C-14 present in its structure gradually decays to N-14. The half life of C-14 is approximately 5730 years. By measuring the amount present in samples of ancient carbon compounds and comparing this with the amount in modern materials, it is possible to determine the time of cessation of carbon exchange with the atmosphere and the approximate age of the death of the organism.

B.1 Dating Techniques

There are two techniques available for dating radiocarbon: Beta-decay and accelerator mass spectrometry (AMS). Each technique has associated advantages and disadvantages. The beta-decay technique determines the relative C-14 content of an organic sample by counting the beta-decay events which occur when C-14 atoms decay to N-14. This technique is more economical and has a relatively short processing time of about one month. However, relatively large samples which yield more than about 50 milligrams of carbon are needed to maximize the results using this technique.

The AMS technique uses an accelerator ion source and mass spectrometry to determine the relative amount of C-14, C-13, and C-12 in an organic sample and can determine the age of samples which yield as little as 5 to 10 milligrams of carbon. However, it is more costly (about 2-3 times the cost of beta-decay) and requires two to four months for processing. Both techniques were used during this study, with the most costly AMS technique being used to date key samples which were too small for conventional beta-decay dating. Information regarding the samples dated using radiocarbon methods is included in Table B.1.

The initial pretreatment of all samples evaluated during this study was conducted by Kruger Enterprises Inc. Geochron Enterprises Division. This same group performed all of the Beta-decay radiocarbon dates reported in the study. The

accelerator mass spectrometry work was performed by the Institute of Nuclear Sciences (INS) within the Department of Scientific and Industrial Research of New Zealand.

B.2 Sample Identification

During this investigation the location of each sample within an SIL feature was noted in the field prior to its collection. In each instance a sketch was prepared illustrating the spacial relationship of the sample to the feature and a photograph was taken. The type of sample (root, charcoal, wood, etc) was also noted as was the potential age constraint that the sample could potentially provide with respect to the timing of the SIL episode.

The approach used during this study to determine the age of liquefaction episodes was based on the radiocarbon dating of various types of organic materials contained within or cut by SIL liquefaction features. The most accurate estimates for the age of a liquefaction episode were obtained from the radiocarbon age of organic debris such as leaves, pine needles, bark or small branches that were washed or blown into the liquefaction crater following its formation. These samples were given the highest priority for radiocarbon dating.

The Carbon-14 determined ages of roots which had grown into a SIL feature or into the overlying soil profile provided minimum age constraints on the time of the liquefaction episode. Minimum age constraints were also obtained by dating forest-fire derived charcoal recovered from the shallow soil profile overlying the feature. Maximum age constraints were obtained by dating roots cut by the feature and by dating forest fire-derived charcoal which was washed or blown into the crater after its formation. During this study, these types of samples were given the second highest priority for radiocarbon dating. Finally, maximum age constraints were also obtained by dating humate materials recovered from soil clasts which were isolated from surface recharge due to their isolation at depth in the feature, or by dating organic materials recovered from within soil clasts which collapsed into the deeper part of the crater during the SIL episode. These types of samples were given a lower priority for radiocarbon dating.

B.3 Sample Preparation and Pretreatment

Upon returning from the field, the samples were cleaned of dirt and any clearly recent organic materials. They were then weighted, reinspected and dissected to better determine the type of organic material. For example, many samples which were thought to be "charcoal" in the field were found after cleaning to be wood. (In this study only those materials which have clearly been burned are referred to as charcoal.) The sample was then shipped to Geochron Laboratory for further processing.

The first step at the laboratory was a second cleaning followed by pretreatment of the sample to remove possible contaminants. All samples were sequentially

treated with dilute acid and dilute base solutions in order to remove, respectively, contaminant carbonates and humates which could recharge C-14 levels. Next, samples were converted to carbon dioxide by combustion in pure oxygen or by acid hydrolysis. The carbon dioxide was purified and collected by passing it through a series of cryogenically cooled traps.

B.4 Analysis

For samples analyzed using the Beta-decay technique, methane was prepared by reacting the carbon dioxide with hydrogen at 475° C in the presence of a ruthenium catalyst. The methane was then purified and separated from excess hydrogen and water of reaction by passing it through a series of cryogenic traps. The methane was then transferred to a vacuum flask from which it was loaded into one of several proportional counters which are especially designed for the detection of C-14 decay events. The counters were shielded in lead and surrounded by annular guard counters operating in anticoincidence with the sample counters in order to reduce external radiation background to very low levels. Each sample was counted for C-14 beta-decay activity for at least 1200 minutes, longer if activity is very low or if the results were unstable.

Standard activity is determined by periodic counting of methane prepared from the original NBS oxalic acid standard (SRM-4990) or the newly issued replacement standard, NBS Research Material RM-49. Isotopic fractionization was corrected for by measuring the C13/C12 ratio and correcting the C-14 content accordingly. The fractionation of C-14 relative to C-12 is considered to be twice that of C-13 relative to C-12.

Reported radiocarbon ages were calculated by comparing the beta-decay activity of each sample to that of the international standard, NBS oxalic acid (SRM-4990). Calculations were identical to those outlined in Stuvier and Polach (1977). The error assigned to the calculated radiocarbon age assessment included potential errors associated with: 1) the uncertainty due to the random nature of C14 decay in the sample, 2) the error due to background count fluctuations in the proportional counters, and 3) the precision with which the activity of the standard is known. The reported error expressed in Table B.1 and in the main text represents a one standard deviation aggregate of these three potential errors. (Note, many labs report an error which is only based on the uncertainty due to the random nature in the decay of the sample. To provide a general qualitative comparison to this type of reported error, the values in Table B.1 should be reduced by a factor of approximately 2 - H. Kruger, personal communication 1990).

For samples analyzed using accelerator mass spectrometry, the Carbon dioxide gas prepared by Kruger was shipped to INS. There it was converted to graphite by reaction with hydrogen over an iron catalyst in a sealed reaction vessel at 700°C. The graphite was deposited onto a copper target that was then mounted into the accelerator ion source along with a NBS oxalic standard, sucrose standard, and

background target that is 44,000 years before present in age. Each target was measured for five two-minute counting periods.

The resulting radiocarbon age was calculated using the techniques and definitions of Stuvier and Polach (1977). The stated experimental error is calculated from counting the statistics for each run and include the three potential errors discussed previously. A chi-square test was applied to all runs on each sample to identify non-statistical error components and apply a scaling factors to the assigned error.

The data collected during this study provided several cases where a rough comparison could be made between radiocarbon ages determined using Beta-decay vs AMS techniques. For three potential sample pairs in the age range 500 YBP to 1500 YBP, the AMS ages were found to be 10% to 20% lower than the Beta-decay ages. In two of these three cases the values, although different, were within the stated errors. In the third case the values differed by just over the stated errors. For a single potential sample pair in the age range of 3000 YBP to 3500 YBP the AMS age was found to be about approximately 5% older, but the difference in ages were within the stated errors. As a follow-up to this observation two split samples were recently submitted for both Beta-decay and AMS dating.

TABLE B.1
TEN MILE HILL SITE

Feature	Geochron ID	Field ID	Sample Wt.	Carbon Wt.	Type	Sample Location	Significance/Observation	Age(YBP)	Episode
A	GX15201 AMS	TMHA3	118	<50	tree bark	horizontal layer within bedded sequence	contemporary to slightly older than liquefaction episode	3438±87	CH-4
A	GX15182 Beta	TMHA4	6770	190	tree bark	horizontal layer within bedded sequence	contemporary to slightly older than liquefaction episode	3405±255	CH-4
A	GX15187 Beta	TMHA5	530	110	tree bark	within organic layer of bedded sequence	contemporary to slightly older than liquefaction episode.	2165±260	-
A	GX15196 Beta	TMHA5C	150	70	carbonized wood	from bedded sequence	contemporary to slightly older than liquefaction	2675±310	CH-4
B	GX15188 Beta	TMHB8	2150	625	tree root	vertical root cutting right margin of feature	minimum age of liquefaction episode	155±150	-
B	GX15186 Beta	TMHB10	9730	1000	tree root	large root cutting central portion of crater	minimum age of liquefaction episode	2865±90(2)	CH-4
C	GX15185 AMS	TMHCBARK	6300	<50	tree bark	organic rich layer of the bedded sequence	contemporary to slightly older than liquefaction episode	3450±120	CH-4
D	GX15184 Beta	TMHDCHAR	1300	45	charcoal	from bedded sequence	maximum age of liquefaction episode	5790±710	CH-5
D	GX15194 Beta	TMHD15	5080	280	tree root	grown into right portion of clast/zone	minimum age of liquefaction episode	4730±265	CH-5
D	GX15578 Beta	TMHD17	17790	800	tree root	grown into clast zone	minimum age of liquefaction	1165±125	-

TABLE B.1 (cont.)

MYRTLE BEACH

Feature	Geochron ID	Field ID	Sample Wt.	Carbon Wt.	Type	Sample Location	Significance/Observation	Age(YBP)	Episode
1	GX14996 AMS	MYRBAE	14000	85	humate rich clast	base of clast zone matrix of large clast zone	maximum age of liquefaction episode	1465±290	M-3
2	GX15575 Beta	MYRBBS	6350	130	charcoal	overlying in soil profile "new burn"	minimum age of liquefaction episode	4575±350	M-4

MARTIN MARIETTA

Feature	Geochron ID	Field ID	Sample Wt.[1]	Carbon Wt.[2]	Type[3]	Sample Location[4]	Significance/Observation	Age(YBP)	Episode
1	GX14994	CMM	4000	400	tree bark	recovered from matrix of large clast zone	contemporary to slightly older than liquefaction episode	1860±180	M-3
	GX15004	XMM	31000	370	organic rich clast	top of small clast zone	maximum age of liquefaction episode	1880±200	M-3

TABLE B.1 (cont.)
GEORGETOWN

Feature	Geochron ID	Field ID	Sample Wt.	Carbon Wt.	Type	Sample Location	Significance/Observation	Age(TBP)	Episode
A	GX15192 Beta	GTA5	5620	180	root	grown into feature	minimum age of liquefaction episode	210±170	-
	GX14995 Beta	GTAD	7000	1000	charcoal	within overlying soil profile (recent burn)	minimum age of liquefaction episode	1200±110	B-3
	GX15003 Beta	GTAW	6000	1000	charcoal	within overlying soil profile (recent burn)	minimum age of liquefaction episode	1360±110	B-3
	GX15587 AMS	GE01A		<50	wood	in feature	contemporary age or possibly root	104±190	B-3
B	GX15198 AMS	GTB7	1730	<50	root	grown into feature	minimum age of liquefaction episode	modern	-
	GX15577 Beta	GETBB	1000	350	top root	cutting right margin of feature	minimum age of liquefaction episode	2820±220	B-4

TABLE B.1 (CONT.)

QLIP

Feature	Geochron ID	Field ID	Sample Wt.(1)	Carbon Wt.(2)	Type(3)	Sample Location(4)	Significance/Observation	Age(YBP)	Episode
A	GX-14992 Beta	A	10000	1000	tap root	cutting right side of feature	minimum age of liquefaction	1360±110	W-3
	GX-15006 Beta	Z	3000	375	tap root	cutting right side	minimum age of liquefaction	1150±190	W-3
	GX-15199 Beta	CB-1	1800	110	bark	recovered from within the central vent of feature	contemporary to slightly older than liquefaction episode	1647±390	W-3
	GX-15005 Beta	Y	19800	520	humate clast	from base of large chert zone	maximum age of liquefaction episode	2655±200	W-3
	GX-14993 AMS	B	1300	<50	humate clast	from base of large clast zone	maximum age of liquefaction episode	2197±84	W-3

TABLE B.1 (cont.)
SAMPIT

Feature	Geochron ID	Field ID	Sample Wt.	Carbon Wt.	Type	Sample Location	Significance/Observation	Age(YBP)	Episode
SPW	GX15206 AMS	SPW2	520	<50	bark	within matrix of large clast zone	contemporary to slightly older than liquefaction episode	504±97	W-2
SPWR	GX15202 AMS	SPW2	1000	<50	bark	within matrix of clast zone of feature	contemporary to slightly older than liquefaction episode	940±80	W-2
	GX15200 AMS	SPW5	800	<50	bark	within bedded sequence	contemporary to slightly older than liquefaction episode	907±79	W-2
	GX15579 Beta	SPW5A	2350	375	bark	within matrix of chart zone of feature	contemporary to slightly older than liquefaction episode	1380±175	W-2
SPWL	GX15000 AMS	SPW7	8460	<50	root	cut by feature	minimum age of liquefaction episode	1232±77	W-3
SPS	GX15189 Beta	SPS-3	15400	1000	root	grown into feature	minimum age of liquefaction episode	1955±75	W-3
SPS	GX14997 Beta	F	6000	125	carbonized wood	recovered from within bedded sequence	contemporary to slightly older than liquefaction episode	1690±220	W-3
SPS	GX14998 Beta	G	10000	600	charcoal	recovered from within bedded sequence	older than liquefaction episode	2385±170	W-3
SPS	GX15001 Beta	U	8800	125	charcoal	recovered from within bedded sequence	older than liquefaction episode	2455±250	W-3

TABLE B.1 (cont.)
COLONY GARDEN

Feature	Geochron ID	Field ID	Sample Wt.	Carbon Wt.	Type	Sample Location	Significance/Observation	Age(YBP)	Episode
1	GX-15136 AMS	CGard1	1500	100	Wood	within large θ_h clast	maximum age of liquefaction episode	1305±87	S-3
1	GX-15586 AMS	CGard5	<50	1000	Wood	recovered from bedded sequence	contemporary to slightly older than liquefaction episode	1066±78	S-3

HALPHEROUS

Feature	Geochron ID	Field ID	Sample Wt.	Carbon Wt.	Type	Sample Location	Significance/Conservation	Age(YBP)	Episode
1	GX15131 Beta	HcR	13000	700	root	cutting massive zone and soil clast	minimum age of liquefaction episode	4620±195	S-4
	GX15190 AMS	HAL2	10560	95	charcoal	in massive zone	maximum age of liquefaction episode	5520±370	S-4

TABLE B.1 (cont.)
BLUFFTON SIL SITES

Feature	Geochron ID	Field ID	Sample Wt.	Carbon Wt.	Type	Sample Location	Significance/Observation	Age(YBP)	Episode
AA	GX15581 AMS	BLUFAA2	1400	<50	carbonized wood	at contact between large clast zone and massive zone	contemporatory to stightly older than liquefaction episode	100	S-1
AB	GX15183 AMS	BLUBA6	6040	<50	leaves and organics	within bedded sequence	contemporary to liquefaction episode	<200	S-1
AC	GX15582 AMS	BLUFC7	900	<50	tree bark	tree bark within small clast zone	contemporary to slightly older than liquefaction episode	107±61	S-1
AD	GX15132 Beta	BLUFCARB	6200	1200	charcoal	charcoal in overlying soil profile	recent "burn" of forest debris-minimum age of liquefaction episode	275±105	S-2
AD	GX15130 Beta	Blufroot	14000	500	tap root	forming left margin of crater-in growth position	may provide contemporary to older age constraint	605±160	S-2
BD	GX15584 AMS	BLUFBD8	1400	<50	Charcoal	top of bedded sequence	possible maximum age of liquefaction episode	2164±68	-
BD	GX15585 AMS	BLUFBD9	600	<50	Charcoal	burned tap root grown into feature	minimum age of liquefaction episode	1850±80	>S-3

NRC FORM 335 (2-89) NRCM 1102, 3201, 3202

U.S. NUCLEAR REGULATORY COMMISSION

BIBLIOGRAPHIC DATA SHEET

(See instructions on the reverse)

1. REPORT NUMBER (Assigned by NRC, Add Vol., Supp., Rev., and Addendum Numbers, if any.)

NUREG/CR-5613

2. TITLE AND SUBTITLE

Paleoliquefaction Features Along the Atlantic Seaboard

3. DATE REPORT PUBLISHED

MONTH: October YEAR: 1990

4. FIN OR GRANT NUMBER

D1682

5. AUTHOR(S)

D. Amick, R. Gelinas, G. Maurath, R. Cannon, D. Moore, E. Billington, H. Kemppinen

6. TYPE OF REPORT

Technical

7. PERIOD COVERED (Inclusive Dates)

September 30, 1986 to June 30, 1990

8. PERFORMING ORGANIZATION – NAME AND ADDRESS (If NRC, provide Division, Office or Region, U.S. Nuclear Regulatory Commission, and mailing address; if contractor, provide name and mailing address.)

Ebasco Services Incorporated
2211 West Meadowview
Greensboro, NC 27407

9. SPONSORING ORGANIZATION – NAME AND ADDRESS (If NRC, type "Same as above"; if contractor, provide NRC Division, Office or Region, U.S. Nuclear Regulatory Commission, and mailing address.)

Division of Engineering
Office of Nuclear Regulatory Research
U.S. Nuclear Regulatory Commission
Washington, DC 20555

10. SUPPLEMENTARY NOTES

11. ABSTRACT (200 words or less)

This study is a phased investigation to determine in a systematic fashion, whether or not seismcally induced paleoliquefaction features such as those observed in the Charleston, S.C., area are present elsewhere in young sediments of the Atlantic Coastal Plain. The discovery of similar liquefaction features in other areas could indicate that large, potentially damaging, earthquakes have not been restricted to the Charleston area in the recent geologic past. Conversely, if no evidence of similar liquefaction features is found, the uniqueness of the Charleston area in the context of eastern United States seismicity would tend to be confirmed.

Phase 1 of this study centered on documenting the ages and characteristics of control liquefaction sites and features located in the Charleston area, and identifying the criteria by which similar sites and features, which may be located elsewhere, could be identified. Phase 2 investigations built on the results of these control studies and centered on the search for seismically induced paleoliquefaction features outside the epicentral area of the 1886 Charleston earthquake.

12. KEY WORDS/DESCRIPTORS (List words or phrases that will assist researchers in locating the report.)

Charleston Earthquake or Seismicity
Paleoliquefaction
Paleoseismicity
Seismically Induced Liquefaction
Eastern U.S. seismic hazard

13. AVAILABILITY STATEMENT

Unlimited

14. SECURITY CLASSIFICATION

(This Page) Unclassified

(This Report) Unclassified

15. NUMBER OF PAGES

16. PRICE

THIS DOCUMENT WAS PRINTED USING RECYCLED PAPER.

UNITED STATES
NUCLEAR REGULATORY COMMISSION
WASHINGTON, D.C. 20555

OFFICIAL BUSINESS
PENALTY FOR PRIVATE USE, $300

SPECIAL FOURTH-CLASS RATE
POSTAGE & FEES PAID
USNRC
PERMIT No. G-67

120555139531 1 1AN1RA
US NRC-OADM
DIV FOIA & PUBLICATIONS SVCS
TPS PDR-NUREG
P-223
WASHINGTON DC 20555